Influences of PEGylated Emulsifiers on Skin Barrier and Skin Penetration Behaviors

Dissertation

der Mathematisch-Naturwissenschaftlichen Fakultät

der Eberhard Karls Universität Tübingen

zur Erlangung des Grades eines

Doktors der Naturwissenschaften

(Dr. rer. nat.)

vorgelegt von

Yali Liu

aus Hunan, China

Tübingen

2022

Gedruckt mit Genehmigung der Mathematisch-Naturwissenschaftlichen Fakultät der Eberhard Karls Universität Tübingen.

Acknowledgments

First and foremost, I would like to express my deepest gratitude to my extraordinary supervisor, Prof. Dr. Dominique Jasmin Lunter, for providing me with an invaluable chance to write this dissertation. I sincerely thank her for devoting so much time and effort to mentoring me. I am fortunate that I have received unwavering respect, encouragement, and incalculable support. I appreciate her exceptional help in putting me on the proper track, entrusting me with cooperative projects and exchange programs, and giving me concerns in life and work when I had difficulties. I am indebted to her for her unlimited patience and assistance in proofreading all of my publications and posters and for familiarizing me with new devices. Additionally, she aided me in developing my confidence and knowledge base. I express my highest appreciation to her.

Sincere appreciation is given to Prof. Dr. Rolf Daniels, who has been my second supervisor and discovered me from the ocean of emails. I am incredibly grateful for the opportunity to receive various constructive recommendations and engage in interesting discussions during each of my progress reports. His enthusiasm and optimism have motivated me to achieve goals. Furthermore, I would also like to express my appreciation to him for revising and evaluating this work.

Great thanks to the technicians, Klaus Weyhing, Jutta Bloschies, and Boguslawa Adamek, who take care of many duties in the lab. Special thanks to Klaus for assisting me with learning new instruments and resolving various issues. I'd like to express my gratitude to Ingrid Straub, the secretary of our laboratory, for her kind attention to all of the materials I handed over.

I would like to thank my current and former colleagues. I am grateful for the time and experiences we shared in the lab, at conferences, and social activities. In particular, I'd like to thank everyone for assisting me in learning German, familiarizing me with new instruments, and sharing the local culture with me. It was a wonderful trip and experience to meet all of you

here in Germany. I'd like to extend my gratitude to Ziwei Zhang, who was not only a colleague but also a close friend.

Thanks to my close friends in Tuebingen, Junjing Jiao, Huanlei Zhang, Liunan Song, and Yi Wang, for their kind assistance and enjoyable time. Many thanks to Siyao Liu for sharing her job-hunting experiences and offering me valuable advice. I especially appreciate my best friend, Menglin Yu, in China, who offered me help and comfort whenever we crossed paths.

My sincere thanks go to my partner and friend, Peng Li, who has provided me with invaluable assistance and concern throughout the years. I've always believed that we are both more fortunate than we realize. Without him, I would never have reached this milestone. I am grateful for all the valuable life lessons he has given me. I am thankful for his encouragement and love, which provided me with strength and motivation. I cherish every moment we spend together, and I am so ready to walk with him on the path of life.

I want to express my deep gratitude to my beloved parents and grandparents, who have always been missing and concerned about me. I appreciate them taking the time to video chat with me and sharing their joy in life. My mother deserves special recognition for staying up many nights taking care of my grandfather when he was in the hospital. I am also sorry that I could not take responsibility and alleviate the strain. I truly express my deepest love to my family and appreciate having the best and kindest parents and grandparents ever.

I give my sincere appreciation to my motherland China for providing me with the opportunity to expand my knowledge and to meet a bigger world.

The final acknowledgment is to me. I am so grateful that I never stopped striving for a better me and a better life during these four years. This particular experience has altered my perception of the mind and cognition.

My second youth will awaken on the next journey. I am excited to begin new chapters in my life! Proceed with calmness, authenticity, and courage to explore the higher world!

To my parents, Qingxin Liu and Fen Zhou, for their unconditional and unwavering support and love;

To Peng Li, for being with me for every step of this journey

谨以此文，献给我的父母刘庆新、周芬

献给我的伴侣李鹏

Table of Contents

Abbreviations

%	Percentage
°C	Celsius degree
µg/mL	Microgram per milliliter
µl	Microliter
µm	Micrometer
a.u.	Arbitrary unit
Alu	Aluminum
ANOVA	Analysis of variance
AUC	Area under the curve
BCC	Basal cell carcinoma
C=O	Carbon oxygen double bond
CA	Cluster analysis
C-C	Carbon-carbon bond
CCD	Charge-coupled device
CERs	Ceramides
C10	PEG-10 cetyl ether
C2	PEG-2 cetyl ether
C20	PEG-20 cetyl ether
CD_3OD	Deuterated methanol
CH_2	Methylene group
CH_2, CH_3	Ethyl group
CH_3	Methyl group
CH_3OH	Methanol
CHOL	Cholesterol
cm	Centimeter
cm^{-1}	Per centimeters
CMC	Critical micelle concentration
CPEs	Chemical penetration enhancers
CRS	Confocal Raman spectroscopy
D_2O	Heavy water
DA	Single donor-single acceptor

DAA	Single donor-double acceptor
DDA	Double donor-single acceptor
DDAA	Double donor-double acceptor
DNA	Deoxyribonucleic acid
DPH	1,6-diphenyl-hexatriene
DSC	Differential scanning calorimetry
EO	Ethylene oxide
EP	Eppendorf
et al.	Et alia, and others
FFAs	Free fatty acids
Fluo-Na	Fluorescein sodium salt
FTIR	Fourier transform infrared spectroscopy
FWHM	Full width of half maximum
g	Gram
g/cm^2	Gram per square centimeter
g/cm^3	Gram per cubic centimeter
g/mL	Gram per milliliter
g/mm	Grooves per millimeter
h	Hour
HCl	Hydrochloric acid
HLB	Hydrophilic-lipophilic balance
HPLC-UV	Liquid chromatography-ultraviolet spectroscopy
HPTLC	High-performance thin-layer chromatography
HWN	High wavenumber
IR	Infrared spectroscopy
kg	Kilogram
LC-MS	Liquid chromatography-mass spectrometry
LDA	Linear discriminant analysis
LPP	Long periodicity phase
min	Minute
min.	Minimum
Mix1	50 mM C20 mixed with 50 mM O2
Mix2	50 mM C20 mixed with 50 mM S20

MLR	Multiple linear regression
mm	Millimeter
mM	Millimole
MS	Mass spectroscopy
mW	Milliwatt
n	Number
NA	Numerical aperture
NH	Nitrogen-hydrogen bond
nm	Nanometer
NMF	Natural moisturizing factor
NMR	Nuclear magnetic resonance
O/W	Oil-in-water
O10	PEG-10 oleyl ether
O2	PEG-2 oleyl ether
O20	PEG-20 oleyl ether
OH	Hydroxyl group
PA	Palmitic acid
PBS	Phosphate buffer saline
PCA	Principal component analysis
PCs	Principal components
PEG	Polyethylene glycol
PEGylated	Polyoxyethylated
pH	Negative log of activity of hydrogen ions
Polysorbate 40, PS40	PEG-20 sorbitan monopalmitate
Polysorbate 60, PS60	PEG-20 sorbitan monostearate
Polysorbate 80, PS80	PEG-20 sorbitan monooleate
R^2	Correlation coefficients
ref.	Reference
rpm	Revolutions per minute
SAXD	Small-angle X-ray diffraction
SB	Stratum basale
SC	Stratum corneum
SCC	Squamous cell carcinoma

SD	Standard deviations
SG	Stratum granulosum
SLS	Sodium lauryl sulfate
SNK	Student-Newman-Keuls
SNR	Signal-to-noise ratio
SPP	Short periodicity phase
SS	Stratum spinosum
S10	PEG-10 stearyl ether
S2	PEG-2 stearyl ether
S20	PEG-20 stearyl ether
TEWL	Trans-epidermal water loss
UV	Ultraviolet
W/O	Water-in-oil
XRD	X-ray diffraction analysis

Zusammenfassung

In Bereich der dermalen Verabreichung von Arzneimitteln wurden in den letzten Jahren Ansätze und Technologien entwickelt, um die Penetration von Arzneimitteln durch die Haut zu verbessern, wobei chemische Penetrationsverstärker als einfachste Strategie am häufigsten eingesetzt werden. In dieser Arbeit werden polyoxyethylierte (PEGylierte) Emulgatoren als eine interessante Klasse von nichtionischen Emulgatoren untersucht. Ziel ist es, ihre genaue Rolle beim Transport von Arzneistoffen und den Mechanismus der Interaktion mit Hautbestandteilen in den unterschiedlichen Hautschichten beleuchten. Der ungeordnete und lockere Zustand der Stratum corneum (SC) Lipide wird als Indikator für das Eindringen von Emulgatoren und die Extraktion von Hautlipiden während Waschprozessen angesehen. Die Analysen in dieser Arbeit wurden mit konfokaler Raman-Spektroskopie (CRS) als markerfreiem, nicht-invasivem und zeiteffizientem Instrument durchgeführt, um mehrere Funktionen für diese Messungen zu erfüllen. Parallel dazu wurden verschiedene Instrumentenkonfigurationen evaluiert, um optimale Ergebnisse bei der Analyse von Hautproben zu erzielen.

Es wurden charakteristische CRS-Signale bestimmt, um die verschiedenen Lipideigenschaften zu bewerten und die selektivsten und empfindlichsten Parameter zur Unterscheidung der verschiedenen Auswirkungenen der Emulgatoren zu erhalten. Es wurden Analysen von mit zwischen Wasser und Natriumlaurylsulfat (SLS) behandelten Hautproben in Bezug auf den Lipidgehalt, die SC-Dicke und die Eigenschaften des Ordnungszustands der Lipide durchgeführt. Zudem wurde festgestellt, dass die spektralen Signale im Fingerprintbereich empfindlicher waren als die im Bereich der hohen Wellenzahlen (HWN). Diese erste Studie dieser Arbeit filterte effektivere spektrale Merkmale für die Hautanalyse heraus und bildete die Grundlage für nachfolgende Untersuchungen (Kapitel 3).

Anschließend wurden geeignete Spektralsignale ausgewählt, um die Auswirkungen von PEGylierten Emulgatoren mit unterschiedlichen hydrophilen und lipophilen Kettenlängen und Sättigungsgraden auf die

Haut zu analysieren. Der Gehalt an SC-Lipiden und die Veränderungen von deren Ordnungszustand wurden untersucht, um potenzielle Regeln für die Störung der Struktur der SC-Lipide durch die untersuchten Emulgatoren zu ermitteln. Die Ergebnisse deuteten darauf hin, dass die hydrophilen Kettenlängen eine wichtige Rolle bei der Ausbildung der Fähigkeit der verwendeten Emulgatoren zur Interaktion mit den SC-Komponenten spielten. Dies führte dazu, dass PEGylierte Emulgatoren mit einer längeren hydrophilen Kette eingehender untersucht wurden. Die Ergebnisse könnten auch bei der Suche nach geeigneten Emulgatoren für die Formulierungsentwicklung hilfreich sein (Kapitel 4).

Eine weitere Untersuchung wurde durchgeführt, um die Auswirkungen von PEGylierten Emulgatoren auf die Barrierefunktion der Haut zu überprüfen. Schweres Wasser (D_2O) wurde als Markiersubstanz verwendet.. Die Verteilung von D_2O in SC wurde mit Hilfe von CRSuntersucht. Gleichzeitig wurden die Auswirkungen der Emulgatoren auf den Lipidgehalt der Haut, die Lipidorganisation, den relativen Wassergehalt und die Wasserstoffbrückenbindungsstruktur analysiert. Die erzielten Ergebnisse spiegeln die größte Barriereschädigung durch PEG-20-Ether wider. Ebenso führten sie zu einer erhöhten Penetration von D_2O in das SC. Diese Studie bestätigte die stärkere Schädigung der Hautbarriere durch PEG-ylierte Emulgatoren mit einer längeren hydrophilen Kette bei dermaler Anwendung und zeigte die Möglichkeit auf, D_2O als geeignete Markiersubstanz zur Bewertung der Hautbarrierefunktion zu verwenden (Kapitel 5).

Im Anschluss an die Studie sollte die verlängerte hydrophile Kettenlänge von PEGylierten Emulgatoren untersucht werden. Die Dicke des SC wurde als Indikator für die reduzierte und aufgelockerte Struktur der SC-Komponenten verwendet. Parallel dazu wurde die Konfiguration der CRS mit verschiedenen Objektiven und Blendengrößen optimiert. Die Ergebnisse zeigten, dass ab einer Länge von etwa 40 Oxyethylengruppen zu eine geringere Barriereschädigung auftritt. Die Korrelation von chemischem Aufbau der Emulgatoren und ihrer Wirkung auf die SC Lipide kann dazu beitragen, mögliche Mechanismen der Wechselwirkungen

zwischen Emulgatoren und der Haut aufzudecken. In der Zwischenzeit hat sich die Kombination aus Wasserimmersionsobjektiv und 50-μm-Blende als optimale CRS-Konfiguration erwiesen, um präzisere Daten zur Dicke des SC zu erhalten (Kapitel 6).

Um die Rolle von PEGylierten Emulgatoren als Penetrationsverstärker zu bestimmen, wurden Fluorescein-Natriumsalz (Fluo-Na) und Procain-HCl separat als Modellarzneistoffe verwendet und ihre Penetrationsverstärkungswirkung mit der herkömmlichen Tape-Stripping-Methode und CRS untersucht. Die Ergebnisse zeigten, dass die Penetrationsprofile im Allgemeinen korreliert waren, was CRS zu einer leistungsfähigen Alternative für die Bewertung der dermalen Arzneistoffabgabe macht. Darüber hinaus wurde die penetrationsfördernde Wirkung von PEGylierten Emulgatoren mit der Störung von SC Lipiden in Verbindung gebracht, was auf den zugrunde liegenden Mechanismus der Arzneistoffpenetration hindeutet (Kapitel 7).

Im letzten Teil der Arbeit wurde versucht, einen tieferen Einblick in die Wechselwirkungen zwischen Emulgatoren und dem SC zu gewinnen. Mischungen von PEGylierten Emulgatoren wurden unter den Aspekten der molekularen Eigenschaften des SC und der Penetrationsverstärkung untersucht. Gleichzeitig wurden verschiedene CRS-Laserwellenlängen verwendet, um ihre Eignung und Anwendbarkeit in systematischen SC-Analysen zu bewerten. Die Ergebnisse zeigten, dass die gemischten Emulgatorsysteme das Potenzial zur Verringerung von Wechselwirkungen mit den SC-Lipiden hatten. Dies schien auch mit den CMC-Werten (kritische Mizellenkonzentration) zusammenzuhängen, was darauf hindeutet, dass die vorhandenen Monomere die Hauptursache für die Verbesserung der Arzneistoffpenetration und die Störung des Ordnungszustands der Lipide des SC waren. Außerdem konnte nachgewiesen werden, dass sowohl 532-nm- als auch 785-nm-Laser für Hautanalysen geeignet sind. Darauf basierend wurden Vor- und Nachteile der verschiedenen Anregungswellenlängen diskutiert, um eine Auswahl auf der Grundlage unterschiedlicher experimenteller Anforderungen zu ermöglichen (Kapitel 8).

Summary

In dermal drug delivery studies, approaches and technologies have recently been advanced to enhance drug penetration through the skin, with chemical enhancers being the most widely used as the simplest strategy. Within their uses, polyoxyethylated (PEGylated) emulsifiers are focused on in this thesis as an interesting class of nonionic emulsifiers. It aims to determine their exact role in transporting drugs and their mechanism of action in skin layers to interact with the skin components. Herein, the disordered and loose state of stratum corneum (SC) lipids are used as indicators of emulsifiers' penetration and lipids' extraction during the washing process. The analyses were conducted with confocal Raman spectroscopy (CRS) as a label-free, non-invasive and time-efficient instrument to exploit multiple functions for the needs. Different instrumental configurations were evaluated to achieve optimal performance in skin analyses.

Characteristic CRS signals were determined to evaluate lipid properties and obtain the most selective and sensitive parameters for differentiating different samples applied to the skins. Analyses were performed between water and sodium lauryl sulfate (SLS)-treated skin samples regarding lipid content, SC thickness, and lipid molecular structure properties. It was found that the spectral signals in the fingerprint region were more sensitive than those in the high wavenumber (HWN) region. This initial study in this thesis filtered out more effective spectral features for skin analysis and formed the basis for subsequent studies (Chapter 3).

Suitable spectral signals were then selected to analyze the effects of PEGylated emulsifiers with different hydrophilic and lipophilic chain lengths and degrees of saturation on skin samples. The SC lipid content and organizational changes were examined to study the potential rules of disruptions of SC lipids by the studied emulsifiers. The results indicated that the hydrophilic chain lengths played an important role in governing the ability of applied emulsifiers to interact with the SC components. This led to a deeper investigation concerning PEGylated emulsifiers with a longer

hydrophilic chain. The results could also help find suitable emulsifiers for formulation development (Chapter 4).

Another investigation was carried out to verify the effects of PEGylated emulsifiers on the skin. Heavy water (D_2O) was used as a probe. The distribution of D_2O was tracked using CRS. Simultaneously, the emulsifiers' effects on skin lipid content, lipid organization, relative water content, and hydrogen bonding structure were monitored. The obtained results reflected the higher penetration ability of PEG-20 ethers in skin. The penetration of $D_2O$was also enhanced. This study verified the increased barrier disruption of PEGylated emulsifiers with longer hydrophilic chains. It demonstrated the possibility of using D_2O as an appropriate probe to evaluate the skin barrier function (Chapter 5).

Following the study, the extended hydrophilic chain length of PEGylated emulsifiers was investigated. The SC thickness was used to reflect the reduced and loosened structure of SC components. In parallel, the configurations of CRS, including different objectives and pinhole sizes, were optimized. The results revealed the limit of oxyethylene groups of around 40 to cause lower interruptions of the SC lipids, which may help to reveal possible mechanisms that determine the interactions between emulsifiers and skin. Meanwhile, the combination of water immersion objective and 50 µm pinhole was the optimal CRS configuration for obtaining more precise data on SC thickness (Chapter 6).

To determine the role of PEGylated emulsifiers as penetration enhancers, fluorescein sodium salt (Fluo-Na) and procaine HCl were used separately as model drugs. The penetration enhancement efficacy was investigated using the conventional tape-stripping method and CRS. The results showed that the penetration performances were generally correlated, making CRS a powerful alternative for evaluating dermal drug delivery. Moreover, the penetration-enhancing effect of PEGylated emulsifiers has been associated with the disruption of SC components, suggesting the underlying mechanism of drug penetration (Chapter 7).

The final part of the thesis aims to gain a deeper insight into the interactions between emulsifiers and SC. Mixtures of PEGylated emulsifiers were investigated from the aspects of SC molecular properties and penetration enhancement. Simultaneously, different CRS laser wavelengths were used to evaluate their suitability and applicability in systematic SC analyses. The results showed that the mixed emulsifier systems had the potential to reduce their interaction with SC. This was also related to the CMC (critical micelle concentration) values, suggesting that the monomers present were the main cause of enhancing drug penetration and triggering skin disruption. Meanwhile, both 532 nm and 785 nm lasers were suitable for skin analyses. Benefits and pitfalls were addressed to allow selection based on different experimental needs (Chapter 8).

List of publications

The work presented in the thesis has been published in international peer-reviewed journals. Six research papers were published to fulfill the requirement of this cumulative dissertation.

Publications related to the dissertation

Publication 1

Liu Y, Lunter D J*. Selective and sensitive spectral signals on confocal Raman spectroscopy for detection of ex vivo skin lipid properties [J]. *Translational Biophotonics*, 2020, 2(3): e202000003. doi: 10.1002/tbio.202000003

Publication 2

Liu Y, Lunter D J*. Systematic Investigation of the Effect of Non-Ionic Emulsifiers on Skin by Confocal Raman Spectroscopy—A Comprehensive Lipid Analysis [J]. *Pharmaceutics*, 2020, 12(3): 223. doi: 10.3390/pharmaceutics12030223

Publication 3

Liu Y, Lunter D J*. Tracking heavy‑water‑incorporated confocal Raman spectroscopy for evaluating the effects of PEGylated emulsifiers on skin barrier [J]. *Journal of Biophotonics*, 2020, 13: 1-12. doi: 10.1002/jbio.202000286

Publication 4

Liu Y, Lunter D J*. Optimal configuration of confocal Raman spectroscopy for precisely determining stratum corneum thickness: Evaluation of the effects of polyoxyethylene stearyl ethers on skin [J]. *International Journal of Pharmaceutics*, 2021, 597: 120308. doi: 10.1016/j.ijpharm.2021.120308

Publication 5

Liu Y, Lunter D J*. Profiling skin penetration using PEGylated emulsifiers as penetration enhancers via confocal Raman spectroscopy and fluorescence spectroscopy [J]. *European Journal of Pharmaceutics and Biopharmaceutics*, 2021, 166: 1-9. doi: 10.1016/j.ejpb.2021.04.027

Publication 6

Liu Y, Lunter D J*. Confocal Raman spectroscopy at different laser wavelengths in analyzing stratum corneum and skin penetration properties of mixed PEGylated emulsifier systems [J]. *International Journal of Pharmaceutics*, 2022, 616: 121561-121570. doi: 10.1016/j.ijpharm.2022.121561

Other publications

Publication 1

Liu Y, Krombholz R, Lunter D J*. Critical parameters for accurate monitoring of caffeine penetration in porcine skin using confocal Raman spectroscopy [J]. *International Journal of Pharmaceutics*, 2021, 607: 121055. doi: 10.1016/j.ijpharm.2021.121055

Publication 2

Krombholz R[#], Liu Y[#], Lunter D J*. In-Line and Off-Line Monitoring of Skin Penetration Profiles Using Confocal Raman Spectroscopy [J]. *Pharmaceutics*, 2021, 13(1): 67. doi: 10.3390/pharmaceutics13010067.

[#] Co-first author

* Corresponding author

Personal contribution

Publications related to the thesis

Publication 1

Selective and sensitive spectral signals on confocal Raman spectroscopy for detection of ex vivo skin lipid properties

Yali Liu, Dominique Lunter*

Idea: Dominique Lunter and Yali Liu

Study design: Yali Liu and Dominique Lunter

Experiment: Yali Liu

Evaluation: Yali Liu and Dominique Lunter

Manuscript: Yali Liu and Dominique Lunter

Publication 2

Systematic Investigation of the Effect of Non-Ionic Emulsifiers on Skin by Confocal Raman Spectroscopy—A Comprehensive Lipid Analysis

Yali Liu, Dominique Lunter*

Idea: Dominique Lunter and Yali Liu

Study design: Yali Liu and Dominique Lunter

Experiment: Yali Liu

Evaluation: Yali Liu and Dominique Lunter

Manuscript: Yali Liu and Dominique Lunter

Publication 3

Tracking heavy ‑ water ‑ incorporated confocal Raman spectroscopy for evaluating the effects of PEGylated emulsifiers on skin barrier

Yali Liu, Dominique Lunter*

Idea: Dominique Lunter and Yali Liu

Study design: Yali Liu and Dominique Lunter

Experiment: Yali Liu

Evaluation: Yali Liu and Dominique Lunter

Manuscript: Yali Liu and Dominique Lunter

Publication 4

Optimal configuration of confocal Raman spectroscopy for precisely determining stratum corneum thickness: Evaluation of the effects of polyoxyethylene stearyl ethers on skin

Yali Liu, Dominique Lunter*

Idea: Dominique Lunter and Yali Liu

Study design: Yali Liu and Dominique Lunter

Experiment: Yali Liu

Evaluation: Yali Liu and Dominique Lunter

Manuscript: Yali Liu and Dominique Lunter

Publication 5

Profiling skin penetration using PEGylated emulsifiers as penetration enhancers via confocal Raman spectroscopy and fluorescence spectroscopy

Yali Liu, Dominique Lunter*

Idea: Dominique Lunter and Yali Liu

Study design: Yali Liu and Dominique Lunter

Experiment: Yali Liu

Evaluation: Yali Liu and Dominique Lunter

Manuscript: Yali Liu and Dominique Lunter

Publication 6

Confocal Raman spectroscopy at different laser wavelengths in analyzing stratum corneum and skin penetration properties of mixed PEGylated emulsifier systems

Yali Liu, Dominique Lunter*

Idea: Dominique Lunter and Yali Liu

Study design: Yali Liu and Dominique Lunter

Experiment: Yali Liu

Evaluation: Yali Liu and Dominique Lunter

Manuscript: Yali Liu and Dominique Lunter

Other publications

Publication 1

Critical parameters for accurate monitoring of caffeine penetration in porcine skin using confocal Raman spectroscopy

Yali Liu, Richard Krombholz, Dominique Lunter*

Idea: Dominique Lunter and Yali Liu

Study design: Yali Liu and Dominique Lunter

Experiment: Yali Liu

Evaluation: Yali Liu, Richard Krombholz and Dominique Lunter

Manuscript: Yali Liu and Dominique Lunter

Publication 2

In-Line and Off-Line Monitoring of Skin Penetration Profiles Using Confocal Raman Spectroscopy

Richard Krombholz[#], Yali Liu[#], Dominique Lunter*

Idea: Dominique Lunter, Richard Krombholz and Yali Liu

Study design: Dominique Lunter, Richard Krombholz and Yali Liu

Experiment: Richard Krombholz and Yali Liu

Evaluation: Richard Krombholz, Yali Liu and Dominique Lunter

Manuscript: Richard Krombholz, Yali Liu and Dominique Lunter

[#] Co-first author

* Corresponding author

List of poster presentations

Poster presentations in academic conferences during the period of this thesis are listed as follows.

Poster presentation 1

13th World Meeting on Pharmaceutics, Biopharmaceutics and Pharmaceutical Technology (PBP), March 2022, Rotterdam.

Raman spectroscopy at different laser wavelengths in analyzing skin properties of mixed PEGylated emulsifier systems.

Yali Liu and Dominique Lunter*

Poster presentation 2

12th World Meeting on Pharmaceutics, Biopharmaceutics and Pharmaceutical Technology (PBP), May 2021, online.

Monitoring drug penetration with PEGylated emulsifiers as penetration enhancers by confocal Raman spectroscopy.

Yali Liu and Dominique Lunter*

Poster presentation 3

WITec Raman Imaging Summit, September 2020, online.

Tracking heavy water incorporated confocal Raman spectroscopy for evaluating the effects of PEGylated emulsifiers on skin barrier.

Yali Liu and Dominique Lunter*

* Corresponding author

1. Introduction

1.1 The skin

The skin is the largest and heaviest organ in the human body, covering about 2 m^2 of the surface body area and accounting for around 10 % of total body mass [1]. The skin, which acts as a barrier between the human body and the outside world, is the most critical barrier because of its vital functions in maintaining and regulating the body's health [2,3]. The transfer of active compounds over the skin has been a persistent challenge in pharmaceutical research owing to the skin's effective barrier function [4,5]. By deepening the insights into the physicochemical properties of the skin barrier, the mechanisms of pathways through the skin for topical and dermal drug delivery are gradually explored [6–8]. Besides, *ex-vivo* skin models in preclinical studies are also entering a more mature phase [9–11]. Based on the main subject of this thesis concerning the skin barrier and skin penetration properties, this introductory chapter covers the fundamentals of skin structure and stratum corneum properties, and recent advances in dermal drug delivery and *ex-vivo* skin models.

1.1.1 Structure and function of the skin

The skin has a complex structure composed of mainly three layers: the epidermis, dermis, and deeper subcutaneous tissue (*Fig. 1*). Each contains various cell types and performs diverse functions [5,12]. The outmost layer of the skin is the epidermis, which is divided into layers of stratum corneum (SC), stratum granulosum (SG), stratum spinosum (SS), and stratum basale (SB). This layer is the main barrier to protecting the skin from external stimuli, such as pathogens, microbes, mechanical injuries, and accidental contact with chemical irritants [13,14]. Besides, it also works on regulating the temperature and preventing water loss from the human body [15,16]. Despite the multilayered structure of the epidermis, it lacks blood vessels and hence must rely on nutrients given by the underlying dermis [17,18]. Keratinocytes are the predominant cell type in the epidermis, accounting for 95% of the total cell population, except for a few melanocytes,

Langerhans cells, and Merkel cells. They are in different stages of differentiation with the migration from the inner epidermal layer to the outer layers [19,20]. This transition process starts from the SB, where the keratinocytes proliferate and move upward through the SS and SG. As the keratinocytes go through differentiation, they become enucleated, dead, and flattened cells; they eventually reach the final stage of differentiation and are seen as the SC or horny layer [9,17,21].

The dermis is a layer of skin between the epidermis and the subcutaneous tissue filled with a fibrous structure comprised primarily of collagenous, elastic, and reticular fibers [22,23]. The dermis is further divided into papillary and reticular layers. The papillary dermis is the uppermost layer of the dermis, located 100 to 150 µm beneath the skin surface and composed of fine and loose connective tissue. The reticular dermis is the lower part of the dermis, highly vascular, and comprises a thicker layer of dense connective tissue [24,25]. The dermis also contains extracellular components such as vasculature, nerve endings, hair follicles, sebaceous, and sweat glands which also serve distinct functions. The primary elastic tissue supports the skin's regular structure and flexibility [20]. The abundant vascular network provides nutrients, facilitates waste elimination, and plays a critical role in regulating body temperature and wound healing. The huge network of nerve endings and various touch receptors perceive sensations in the human body and make up the somatosensory system [1]. The dermis contains various cell types, including fibroblasts, macrophages, adipocytes, mast cells, Schwann cells, and stem cells. The primary cell type of fibroblasts is responsible for the syntheses of extracellular matrix and different fibers, serving as a structural component of the immunological response to tissue injury [26,27].

The bottom layer of the skin is the subcutaneous tissue, composed of loose connective tissue and fat that provides the skin with main structural support, protects the body from rapid temperature changes, and absorbs shock from underlying tissues [28]. Throughout the layer, large numbers of blood vessels and nerves are interlaced, performing the functions of

thermoregulation and energy reserve. This layer is mostly composed of adipose cells from fat tissue and fibroblasts that release collagen [29,30].
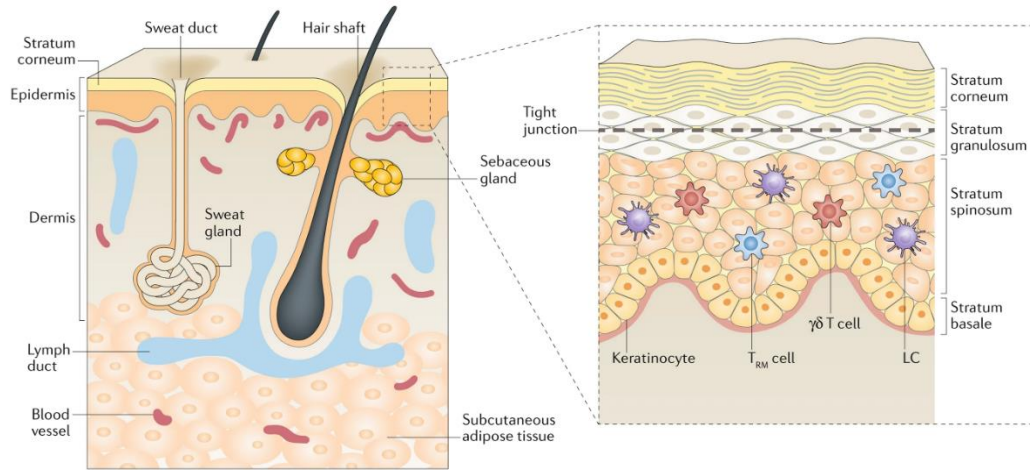
Fig. 1. Schematic overview of the structure of the skin in cross-section. The skin is broadly composed of three layers of the epidermis, dermis, and subcutaneous tissue. The layer of the epidermis was specifically displayed, which contains layers of stratum corneum, stratum granulosum, stratum spinosum, and stratum basale. This figure is modified from Kabashima et al. [12].

1.1.2 Stratum corneum properties

Many of the skin's vital functions, including its ability to form an effective barrier to the outside world, are highly dependent on the composition and structure of the SC located at the superficial layer of the epidermis [31,32]. SC serves as the most significant barrier resisting their entry into the body [33,34]. To develop strategies for improving dermal drug delivery, it is critical to thoroughly understand the various SC properties.

The SC comprises flattened anucleated cells surrounded by a highly organized and continuous lipid matrix that resembles a "brick and mortar wall" (*Fig. 2*). It contains 10-15 layers of corneocytes loaded with keratin filaments and low amounts of water which are separated by numerous densely-packed lipid bilayers [35,36]. The lipid matrix is primarily composed of the three lipid classes of cholesterol (CHOL), free fatty acids (FFAs), and ceramides (CERs) in an approximately equimolar ratio [4,37]. Plenty of studies has demonstrated their critical involvement in maintaining the skin

barrier function and explored their extensive links with skin lesions and diseases [38–40].

The normal SC holds two organized lamellar phases with a repeat distance of nearly 6 and 13 nm, termed the short periodicity phase (SPP) and the long periodicity phase (LPP). In the vertical plane of the lamellae, the lipids are organized in lateral packing. They retain orthorhombic, hexagonal, or liquid states as they transition from dense to less dense lateral organization [41,42]. Many analytics have been involved in different studies in understanding the relationship between lipid lateral packing order and skin barrier functions [43–45]. First observations verified the shift toward a disordered lipid packing state with increased temperature applied to the skin [46,47]. Simultaneously, it was shown that trans-epidermal water loss (TEWL), a frequently used indication of skin barrier functions, is related to the degree of lateral packing order in the human SC [48,49]. Increased permeability of actives has also been observed with the change from orthorhombic to hexagonal packing of SC lipid structures [42,50]. Besides, in plenty of diseased skin samples, such as atopic dermatitis, psoriasis, and lamellar ichthyosis, an increase in the short-chain fraction of lipids (CERs) generates a less dense lateral packing state [21,41,51,52].

Along with the significance of the SC's lateral packing structure, the conformational order of lipid acyl chains is also a critical parameter. Their molecular vibration modes can be employed to characterize the trans and gauche conformer populations. The growing abundance of gauche conformers in chains indicates a trend toward disordered conformational states [53,54]. In addition, lipids with a greater degree of fluidity and disorder are more easily washed away via dermal treatments [55]. Thus, a decrease in lipid content and a reduction in the SC thickness can also be considered appropriate indicators of SC barrier disruption [56,57].
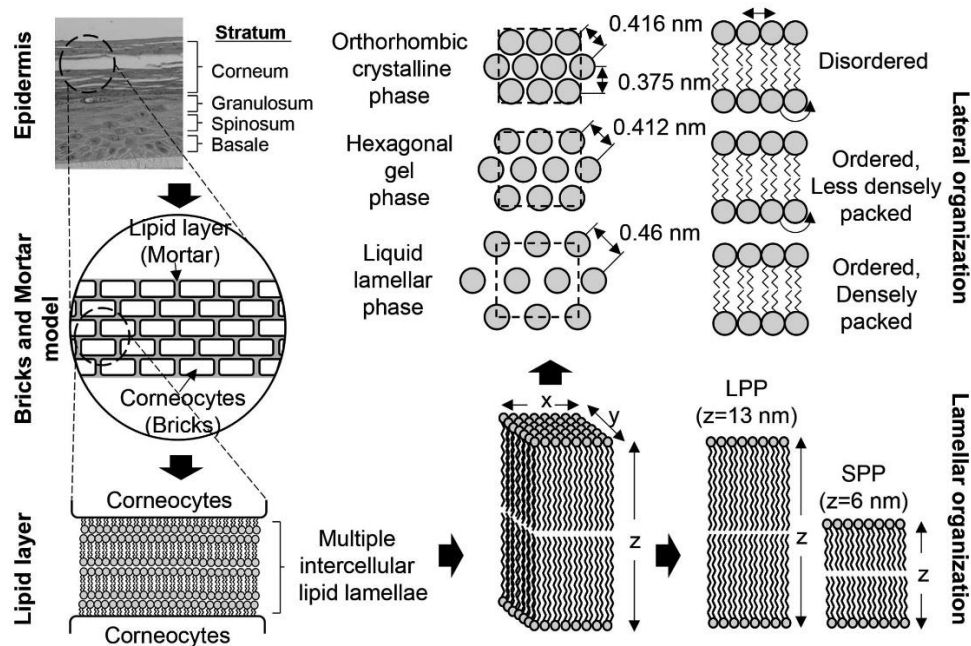
Fig. 2. Structure of the multiple lamellae, which have both lateral and lamellar levels of the organization. The lateral organization includes orthorhombic, hexagonal, and liquid lamellar. The lamellar organization is classified as long periodicity phase (LPP) and short periodicity phase (SPP) [58].

1.1.3 Dermal drug delivery

That the skin acts as an effective, selective barrier to the external environment has been discussed in detail in the preceding section. Simultaneously, it has also been recognized as an important drug delivery route due to its ease of access for pharmaceutical applications [2,59]. In this regard, the question of how effective therapeutic concentrations pass the skin to exert their effect has been raised. In dermal drug delivery, the first step involves passing through the SC and permeating the viable epidermis and dermis layer. Although the underlying skin can also limit drug penetration rates to a minor extent, the main function of blocking the drug absorption is attributed to the SC [41,60]. Three potential penetration routes through the SC are brought forward [61]. These include the intercellular, transcellular, and appendageal routes (*Fig. 3*) [62].

Typically, the intercellular route is considered the predominant pathway of drug molecules through the skin. It represents the diffusion of molecules through the lipid-rich 'mortar' area surrounding the 'brick' structure of corneocytes. The amphiphilic nature of intercellular lipids facilitates the

5

passage of a wide variety of molecules with different polarities while polar molecules diffuse through the polar part, and lipophilic molecules pass through the lipophilic part of lipids. However, their highly organized lamellar and lateral packing structures still reduce the penetration efficiency via this route. Penetration through the corneocytes is regarded as the transcellular route contributing less to the drug delivery process [63]. This pathway requires molecules to cross the hydrophilic but sparsely water-containing environment within the cells and the lipophilic domain of lipid lamellae. Thus, actives are still significantly hindered during the penetration despite its shortest distance. The appendageal route involves drug permeation via the hair follicles and sweat ducts, which is thought to contribute less to the drug delivery but might be important for ions and large polar molecules as well as nanoparticles that cannot penetrate the intact SC [64]. Due to the abundance of hair follicles on the skin surface, applying samples to the skin cannot avoid penetration through this route. However, the primary reason for poor drug uptake is the low density of hair follicles and glands, which reduces drug delivery efficiency [65].

Methods for circumventing the SC barrier have been developed to ensure the efficacy of dermal treatment, such as chemical and physical approaches to improve drug penetration [66,67]. Among these, chemical penetration enhancers (CPEs) have grown in popularity as a significant class of penetration enhancing techniques due to their advantages over physical approaches such as being painless [20]. Extensive studies have demonstrated their abundant applications in the pharmaceutical area [63,68]. However, it is critical to discover how they enter the SC and act on its components.

Researchers have confirmed different mechanisms that improve drug penetration for various CPEs [69,70]. Focusing on the principal intercellular route, CPEs can partition into the lamellae lipids, inducing a more disordered, fluid lipid state and further resulting in lower resistance of SC to drug molecules. On the other hand, their extraction of SC lipid components can also disrupt lipid organization and increase lipid fluidity, further inducing a higher absorption of drug molecules [42,71]. In transcellular delivery,

some studies have also described their interaction with keratin filaments within corneocytes as one of the factors inducing penetration enhancement [2,72]. Due to the complexity of CPEs' behavior within the skin, the mechanisms involved in dermal drug delivery remain poorly understood for many types and applications of them in drug formulations. Thus, using certain CPEs, their mechanism of action should be clearly understood as they may have adverse effects due to the interruption of the skin.
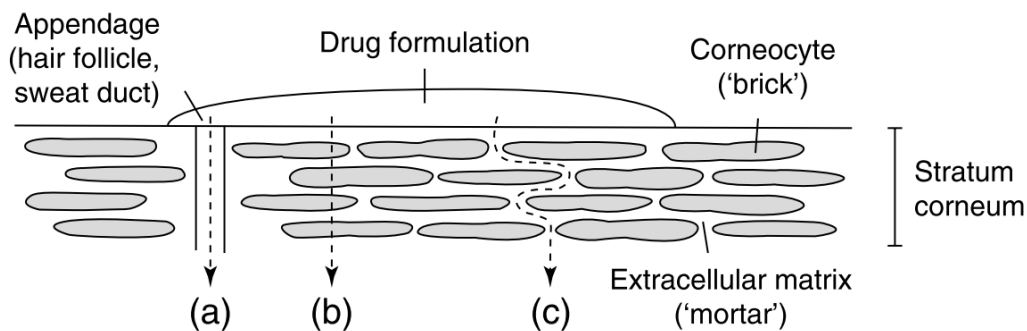
Fig. 3. Pathways of drug penetration across the skin include the (a) follicular route, (b) transcellular route, and (c) intercellular route. This figure is modified from [62].

1.1.4 *Ex-vivo* skin models

Skin barrier properties and dermal drug delivery are key parameters in pharmaceutical and dermatological developments. Although the application of *in-vivo* human skin is ideal for these experimental studies, availability and ethical considerations restrict the use. The *ex-vivo* human skin is usually obtained from plastic surgery and retains the biological properties of *in-vivo* skin. Comparative studies have demonstrated that the tissue viability, barrier function, and extracellular matrix composition remained comparable [73–75]. However, multiple factors still hold its widespread use back. The economic and ethical considerations are the main concerns, although *ex-vivo* human skin has been proven appropriate in penetration studies and evaluation of barrier disruption properties [76,77]. Together with the economic and ethical reasons, alternative skin models are essential through the early stages of pharmaceutical research.

So far, various skin models have been developed, including animal skin, artificial skin, and reconstructed skin models [11,78–80]. Animal skin finds

7

extensive use in most of the recent works. Alternatives, including porcine, rat, mouse, guinea pig, and snake models, involve the skin structural characteristics and transdermal delivery studies [17,19]. Based on their limited cost and comparability to human skin, porcine skin shows great benefits of easy-to-access and less ethical approval procedures [78,81]. Artificial membranes and reconstructed skin models have emerged as substitutes for animal experimentations. They are designed to have comparable skin structural and drug penetration properties. However, these models are typically composed of simple homogeneous polymer materials, which allows for studying fundamental molecular transportation mechanisms. However, due to the lack of complexity and nature of human skin, they cannot represent cellular interactions and *in-vivo* skin properties [36,82,83].

Concerning the application of porcine skin, the flank and ear are common sites to be used. The feasibility of using porcine skin to replace human skin has been demonstrated in percutaneous drug absorption, irritation, and toxicity studies [84–86]. In the early stage, porcine ear skin was evaluated for increasing TEWL with progressive SC removal, representing the same property variation as *in-vivo* human skin [87]. Porcine skin has also been analyzed by confocal laser scanning microscopy and multiphoton tomography confirming its suitability as a human skin model. Properties regarding the skin hydration, the shape and size of corneocytes and single cells, the nucleus size, the amount of cytoplasm, and the intracellular area are identical to those of human skin [25]. Besides, porcine skin features, including the hair follicle size, SC thickness, the number, size, and distribution of dermal vessels, are similar to those of human skin [88]. Numerous investigations have recently established a correlation between the porcine and human skin's penetration and permeation properties [89,90]. For instance, the skin penetration potential of curcumin and fluorescein sodium determined using porcine ear skin was highly representative of the *in-vivo* situation on human skin [91]. Apart from the discovered similarities, there are undoubtedly distinctions between porcine and human skin. The main variability refers to the lower

skin barrier functions. Previous research has mostly reported the differences in SC lipid lateral organization, showing that porcine skin has more hexagonal lateral packing order lipids and higher active permeability than human skin [92]. However, although porcine skin is not completely equivalent to human skin, it is still the most suitable substitute for preclinical studies of dermal drug delivery systems.

1.2 Nonionic emulsifiers: polyethylene glycol (PEG) modified emulsifiers

Nonionic emulsifiers have been used in different fields [93,94]. Within their categories, the initial syntheses of polyoxyethylated (PEGylated) emulsifiers in the early years facilitated the widespread usage of nonionic emulsifiers [95,96]. This section discusses the structural characteristics and emerging applications of PEGylated emulsifiers. The attention is mostly on their use as CPEs and the mechanism of action within the skin. Additionally, the application and potential behaviors of emulsifier mixtures in the skin area are also of interest to be included.

1.2.1 Structures of PEGylated emulsifiers

Polyoxyethylene is a synthetic polyether covering a wide range of molecular weights, which has the common formula of $H-(O-CH_2-CH_2)_n-OH$, where 'n' represents the number of oxyethylene groups. PEGylated emulsifiers are synthesized by forming addition compounds or complexes on their ether bridges [97]. In this way, PEG fatty acid esters, ethers, amine ethers, and other derivatives can be produced. PEG alkyl ethers are one of the largest categories of commercially available PEGylated emulsifiers [94,98]. They are usually prepared by the ethoxylation of alcohol, such as cetyl (C), stearyl (S), oleyl (O), lauryl (L), or cetearyl (CS), with a variable number of ethylene oxide units that corresponds to the length of the hydrophilic chain. Thus, they have the general formula of $R-(O-CH_2-CH_2)_n-OH$, where R denotes an alkyl chain with a certain number of carbons referring to the length of the hydrocarbon chain, which can exhibit a range of saturation degrees [99].

Based on varying developments through fields, PEG alkyl ethers are registered with different trademarks, such as the Brij series provided by Croda Europe Ltd. *Table. 1* summarizes the Brij emulsifiers used in this thesis, including the name, product name, alkyl chain length, and moles of EO. Since the series has varying lengths of hydrophilic and lipophilic chains, they exhibit varying values of hydrophilic-lipophilic balance (HLB) and solubility in aqueous solutions, which should be addressed for formulation development.

Table 1. Technical information of Brij series used in this thesis.

Name	Product name	Fatty alcohol	Alkyl chain length	Moles of EO
PEG-2 stearyl ether	Brij S2	Stearyl alcohol	C18	2
PEG-2 oleyl ether	Brij O2	Oleyl alcohol	C18	2
PEG-2 cetyl ether	Brij C2	Cetyl alcohol	C16	2
PEG-10 stearyl ether	Brij S10	Stearyl alcohol	C18	10
PEG-10 oleyl ether	Brij O10	Oleyl alcohol	C18	10
PEG-10 cetyl ether	Brij C10	Cetyl alcohol	C16	10
PEG-20 stearyl ether	Brij S20	Stearyl alcohol	C18	20
PEG-20 oleyl ether	Brij O20	Oleyl alcohol	C18	20
PEG-20 cetyl ether	Brij C20	Cetyl alcohol	C16	20
PEG-40 stearyl ether	Brij S40	Stearyl alcohol	C18	40
PEG-100 stearyl ether	Brij S100	Stearyl alcohol	C18	100

1.2.2 Applications of PEGylated emulsifiers

PEGylated emulsifiers are widely employed in the pharmaceutical, cosmetic, food, and biomedical industries [95,100,101]. In pharmaceutics and cosmetics, they are typical excipients in oral, ophthalmic, rectal, and cutaneous formulations [102–105]. Due to their lower toxicity, irritation, and hemolytic activity than other emulsifier types, this family of non-ionic emulsifiers performs various functions as solubilizers, wetting agents, cleansing agents, skin conditioners, humectants, and penetration enhancers [106–108]. They can also be useful in analytical chemistry, where they are frequently used for analytical separations requiring little

ultraviolet (UV) absorption, low sensitivity to ions, and a wide range of polarity differences [95].

PEGylated emulsifiers can be used in various dosage forms in the production of pharmaceutical and skincare products, including emulsions, suspensions, micellar solutions, noisomes, and cerasomes [109–111]. Depending on their HLB values, which represent their hydrophilic and lipophilic natures, they may perform a variety of activities, including the formation of oil-in-water (O/W) or water-in-oil (W/O) emulsions [112]. Additionally, Manconi et al. reported high entrapment efficiency of tretinoin in noisomes using PEG-4 lauryl ether [113]. PEG-23 lauryl ether, PEG-20 stearyl ether, and PEG-20 oleyl ether were used in micellar solution to improve the corneal permeability of atenolol, timolol, and betaxolol [114]. Albash et al. have shown that cerasomes prepared with PEG-2 cetyl ether and PEG-10 oleyl ether could be used to administer fenticonazole nitrate topically [115].

In recent decades, due to the thought that PEGylated emulsifiers have a lower risk of skin impairment and irritation, they have been widely explored as penetration enhancers in dermal drug delivery systems. Reports have been published on applying actives with a variety of physicochemical and biological properties [101,116,117]. For instance, it refers to the use of PEG-2 oleyl ether to enhance piroxicam permeation through rat skin and the decreasing order of PEG-5 cetyl/oleyl ether, PEG-2 lauryl ether, PEG-2 oleyl ether, and PEG-10 stearyl ether in promoting the transdermal flux of ibuprofen through excised rat skin [118,119]. With growing interest in PEGylated emulsifiers as penetration enhancers, it is critical to understand their interaction with the skin and the factors that may govern the interaction and potential to promote drug penetration. The comprehensive studies and principal experiments can help expand the application of this series of emulsifiers and provide guidance in further formulation development using this type of emulsifier and other emulsifiers with comparable chemical structures and biological properties.

Based on existing studies, the enhancing ability of PEGylated emulsifiers has been examined concerning their natures from multiple aspects. It is generally regulated by some variables, including the hydrophilic and hydrophobic chain length, the saturation degree, and the physicochemical properties of actives [99,117,120]. Some authors emphasized the importance of the polar head group of emulsifiers, stating that their bigger size may be the primary obstacle to passing through the skin [120]. Furthermore, reports indicated that PEGylated emulsifiers with fewer EO groups have a higher risk for skin irritation, as evidenced by the higher TEWL values of PEG-2 stearate and PEG-9 stearate compared to PEG-40 stearate [121]. However, Okuyama et al. proposed a debate in which they determined that the optimal PEG ethers or esters for penetration enhancement have EO chain lengths of 5 to 15 [122]. When evaluating the penetration enhancing the ability of PEGylated emulsifiers, the length of the hydrophobic alkyl chains was also considered. Kim et al. demonstrated that the penetration of ketoprofen was not dependent on different alkyl chain lengths when ketoprofen patches containing PEGylated emulsifiers were applied to excised hairless mouse skin [120].

Nevertheless, a double bond in the alkyl chain was suggested to play a significant role. Since PEG-2 oleyl ether had a greater enhancing effect than PEG-2 stearyl ether, considering the cumulative effects of these factors, one may expect that elucidating the penetration enhancing ability with a single cause would be challenging [119]. A systematic examination of a series of PEGylated emulsifiers is still required to establish a more precise underlying law.

1.2.3 Mechanistic action of PEGylated emulsifiers on skin

It is undeniable that skin treatment can have diverse impacts on the skin, particularly when emulsifiers are included in formulations. Generally, skin safety evaluation and skin irritation are determined by the changes in skin physical and biological properties generated by the interactions between emulsifiers and skin. It has been reported that the emulsifiers primarily interact with the SC, which serves as the skin's most functional

and critical barrier. Recent discoveries suggest that the interactions are mostly related to the denaturation of SC keratin and the alteration of structures and components of SC lipids [123–125].

The impact on SC keratin is often attributed to ionic emulsifiers, which can bind with the keratin filaments. This effect was observed when sodium lauryl sulfate (SLS) solution was applied to an SC model membrane, confirming keratin denaturation [126]. In principle, it could be explained that the keratin changes from a highly stable and less exposed α-helix structure to a more unstable and exposed β-sheet structure, leading to easier binding with surrounding biomolecules [92]. On the other hand, nonionic emulsifiers were shown to have a lower ability to cause keratin denaturation, which was commonly attributed to their relatively weak hydrogen and van der Waals bonds [114,127]. With this fact, the studies of elucidating the mechanisms of PEGylated emulsifier impact on the skin have been less focused or have revealed a less evident effect on denaturing the structure of SC keratin.

Research indicates that much emphasis is placed on the interactions between emulsifiers and SC lipid layers. SLS was used to evaluate SC lipid abnormalities to determine the reason for dry scaly skin. Significant changes in the composition of SC lipids have been observed, primarily in the CER species, and a decrease in long-chain (C22-28) FFAs [128,129]. Furthermore, Saad et al. demonstrated that when human skin is treated with SLS, the loss of orthorhombically packed SC lipids was compensated for by increasing a hexagonal phase [130]. Although nonionic emulsifiers generally have lower irritation potential than anionic emulsifiers, interactions with intercellular skin lipids are still found in some types. For example, PEG-20 sorbitan monooleate was investigated for its ability to alter the lipid arrangements in the SC, hence increasing lorazepam penetration [131]. When it was discovered that PEGylated emulsifiers have the penetration-enhancing ability and were widely used in commercially available dermal products, evaluation regarding their effects on skin lipid properties was frequently undertaken to gain insights into the mechanism of action. PEG-20 glycerol monostearate was previously examined for its ability to extract porcine SC lipids and modify their conformational order to

13

a more gauche state [132]. In addition, it was shown that treatment with PEG-23 lauryl ether disrupted the lipid structure rather than extracting lipids. Specifically, it can dissolve into the lipid matrix and fluidize the lipid chains [101]. The penetration of procaine HCl was enhanced by PEG-23 lauryl ether [133,134]. It has been assumed that when PEGylated emulsifiers interact with SC lipids, the emulsifiers partition into the intercellular lipids, disordering and fluidizing the lipid organization, thereby facilitating the removal of lipid components from applied solutions or formulations [132,135,136].

Apart from the interactions between emulsifiers and SC components, it is also interesting to understand how emulsifiers enter the skin and further disturb the skin structures. It is still debatable whether the emulsifiers enter the intercellular regions of SC as monomers or micelles. Certain research groups discovered that when the emulsifier concentration exceeds the CMC, the drug penetration is improved, and the SC is highly disrupted. In this case, the number of monomers was highly increased, and their smaller size was widely accepted to facilitate penetration into the skin and further disturb its barrier properties. On the other hand, micelles lack the surface activity to interact with the skin components and are too large to penetrate the skin [125,137]. However, this theory has been challenged by some experimental studies, which demonstrate that the lipids solubilization and washing from the SC only occur when the CMC of applied emulsifier concentrations is reached [138,139].

According to the facts described above, it is obvious that the penetration of PEGylated emulsifiers and their actions within the SC are complex courses working together. Thus, it is important to conduct a thorough evaluation of potential mechanisms and negative effects related to the interactions of PEGylated emulsifiers with SC.

1.2.4 Characteristics of emulsifier mixtures

Emulsifier mixtures are broadly used in commercially available cleansing and skincare products. They generally outperform single emulsifiers in improved interfacial behavior and lower consumption.

Additionally, literature reports highlight the use of emulsifier mixtures that show milder effects on skin barrier functions [140,141]. Anionic emulsifiers were focused since they cause the most damage to the skin. A study was conducted to determine the effect of SLS and dodecyl trimethylammonium bromide on skin barrier properties. The results indicated that using a mixed emulsifier system resulted in a more compact packing state of the mixed micelles, which are generally stable and difficult to penetrate the SC [140]. To test the penetration of mixed micelles into the epidermis, SLS was also combined with a nonionic emulsifier, PEG-6 lauryl ether. The inclusion of a nonionic emulsifier significantly reduced SLS penetration into the epidermis, hence lowering skin disturbance [142].

According to the findings above and several similar studies, the mixed emulsifier system has recently gained attention. Some authors have advanced theories on the CMC values of mixtures. A correlation was discovered between a drop in CMC values and a decrease in skin barrier disruption. According to Hall-Manning et al., SLS and dimethyl dodecyl amido betaine combinations have the lowest CMC value and the fewest skin interactions following a patch test [143]. Many researchers have described that the lower the CMC value of emulsifiers or their mixtures, the easier the emulsifier monomers penetrate the SC and interact with the inner skin components [49,144,145]. Due to the complexity of the interactions between emulsifiers and skin, the mechanism of action of emulsifier mixtures on skin requires better understanding. Furthermore, there is a lack of evidence about the behavior of PEGylated emulsifier mixtures on the SC. As a result, more exploration of their interactions with skin components and penetration enhancing behaviors are of interest to be carried out.

1.3 Confocal Raman spectroscopy (CRS) in skin analysis

CRS finds widespread applications in different fields, including pharmaceutics, cosmetics, geology, mineralogy, semiconductors, carbon materials, and life sciences. It can characterize samples' chemical composition and structure in any phase or state (solid, liquid, gas, gel, powder, etc.) [146–151]. Recently, the application of CRS has been

expanded in skin research, with plenty of advantages ranging from physiologically components characterization to dimensionally distribution assessment [152–154]. With diverse applications in skin research, ranging from physiological components characterization to dimensional distribution assessment, CRS is introduced here in terms of its fundamental principles, diverse application aspects, proper configurations, and comparisons to other relevant techniques.
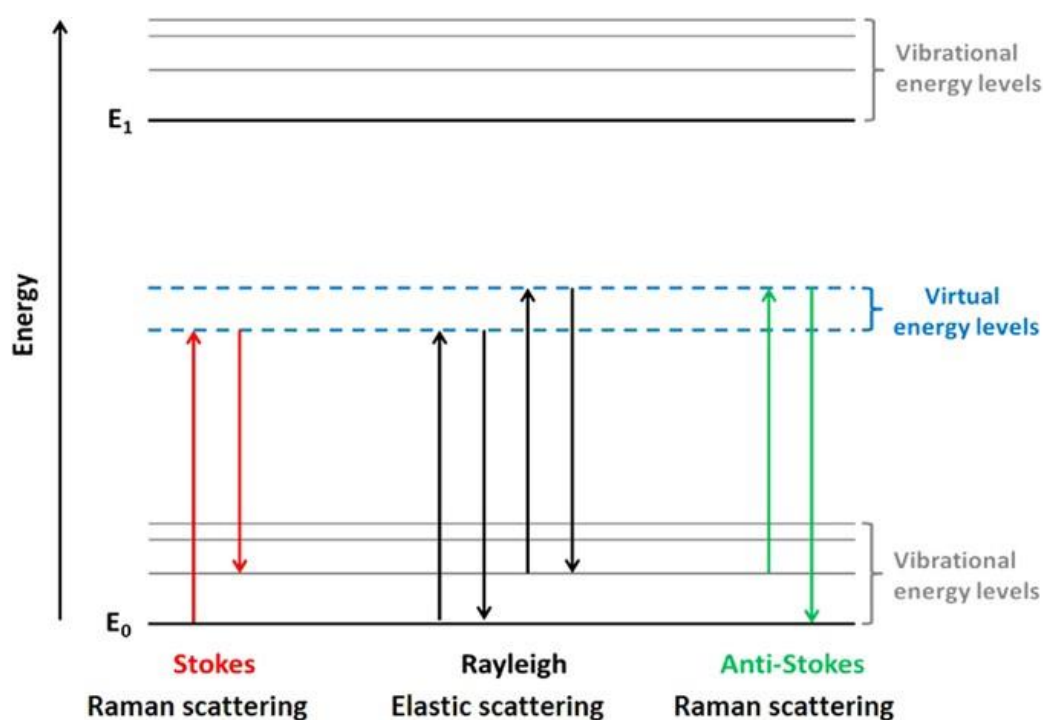
1.3.1 Principles of Raman spectroscopy

Different optical phenomena, including transmission, absorption, and scattering, occur when light interacts with a material. In the case of light scattering, photons are elastically and inelastically scattered. Elastic scattering, also known as Rayleigh scattering, is a mechanism in which the energy of the scattered photon remains constant, and the same frequency can be detected compared to the incident photon. The inelastic scattering is also known as the Raman effect, the observation of which was first published in 1928 by the Indian physicist Sir Chandrasekhara Venkata Raman, who was also later awarded the Nobel prize for this great discovery [155]. The Raman effect happens to only about one photon in a million (0.0001%), which involves both energy and frequency changes compared to the incident light. The inelastic scattering includes the Stokes scattering, where the sample molecule takes up energy from the photons; thus, Raman scattering has lower energy than the incident light. It also includes the anti-Stokes scattering, where the molecule gives energy to the photons, resulting in Raman scattering having higher energy than the incident light. The energy level changes correspond to the Raman frequency shifts and are related to transitions between the molecule's different rotational and vibrational states. These effects are depicted in *Fig. 4*, illustrating the energy levels of molecular vibrations and the scattered photons [156,157].

Raman spectroscopy is based on the principle of Raman scattering, which allows for the detection of scattered photons to create a spectrum according to the molecular vibrations and chemical structure of a sample. Raman spectroscopy accelerated its development in the 1960s, shortly

after the invention of the laser [158]. The modern laser-Raman spectroscopy includes coherent anti-Stokes Raman spectroscopy, surface-enhanced Raman spectroscopy, and tip-enhanced Raman spectroscopy [159–162]. In the 1990s, the Raman spectrometer was integrated for the first time with an optical microscope, enabling both visual and spectroscopic examinations. As a result of merging confocal microscopy and Raman spectroscopy, the confocal Raman microscope was developed, enabling the collection of the single spectrum from a single point on/in the sample. In principle, the analyzed volume within the sample can be spatially filtered with high resolution in both the lateral (XY) and axial (Z) axes using a confocal microscope. By combining the Raman spectroscopy with a moving stage, CRS can perform depth profiling and map multilayer samples [163,164].

Fig. 4. Energy level diagram illustrating different types of Raman scattering [157].

1.3.2 Applications of confocal Raman spectroscopy in skin research

CRS has been a vital technique in the food, biomedical, and pharmaceutical industries due to the continual advancement of Raman spectroscopy [165–167]. In skin research and dermal drug delivery, CRS

also receives considerable interest in investigating the drug penetration kinetics, skin compositional and structural properties, and skin diagnosis. CRS was first used in skin research in the late 1990s when the group of Pupples used it to explore the skin's hydration status. This strongly promoted the progress of skin studies such as assessing physiological skin status, comparing differing skin models, examining skin diseases, developments of dermal formulations, and evaluating skin disruption [168–173].

CRS is a valuable tool for evaluating physiological skin status. The skin hydration state can be determined by the variation of characteristic water peaks to provide depth information on the SC layer's water distribution. Caspers et al. performed rapid measurements of molecular concentration profiles by determining the water/protein ratios in the skin using the OH stretching band and the CH stretching band [16,174]. Besides, CRS can measure the SC thickness, which was commonly evaluated by the SC removal using tape stripping, cyanoacrylate biopsies, and trypsinization. In Raman analysis, SC thickness can be assessed using the specific keratin signal profile or the water concentration profile. The *in-vivo* SC thickness is often estimated using the skin's water content, which varies across SC and SG. The SC thickness can be defined at the intersection of two tangent lines in the increasing and constant regions by calculating the percentage of water within the SC and generating the water profile [175,176]. On the other hand, the separated *ex-vivo* SC is commonly determined by tracking the laser beam moving half in and out of the SC at the point where the specific keratin intensities of SC reach half their maximum intensities. The full width at half maximum (FWHM) can serve as the SC thickness [135]. Furthermore, CRS is available to characterize the surface properties of skin samples. Thanks to the function of the confocal microscope, the imaging and mapping of CRS of the skin surface can be suitable for visualizing histological features such as hair follicles, skin wrinkles, etc. [14,22,64,177].

CRS has been extensively used to compare various skin models. The characterization refers to the differences in the compositional and structural states of the skin [90,152,178]. As aforementioned, *in-vivo* or *ex-vivo*

human skin is considered the gold standard for determining the suitability of employing alternative skin models. The comparisons between *ex-vivo* porcine ear skin and human skin are mostly conducted. Choe et al. reported on relevant investigations comparing the barrier function of porcine skin *ex-vivo* with human skin *in-vivo* via CRS in terms of keratin structure, natural moisturizing factor concentrations, and intercellular lipid lateral organization [92]. Besides, as tissue engineering improves, reconstructed skin tissue and skin substitutes attract special attention compared to human skin [179–181]. Leroy et al. used CRS to compare human skin to human skin constructs composed of dermis and stratified epidermis. The experimental results verified that human skin had a higher lipid content and more organized lipid structures and revealed a similar protein secondary structure and protein content compared to the skin construct [54]. Similar findings can also be found in plenty of recent reports highlighting the application of CRS to the analysis of different skin models [182,183].

Recently, the focus has been placed on the use of CRS in histopathology, with evidence that it may be utilized to distinguish between diseased and healthy skin samples [184,185]. Most commonly, CRS is reported to diagnose skin cancers such as nonmelanoma, including basal cell carcinoma (BCC) and squamous cell carcinoma (SCC) as the most common skin cancers [186,187]. In this respect, Lieber et al. used CRS to investigate 39 skin tissue samples, including normal, BCC, SCC, and melanoma, from 39 patients. The tissue CRS spectra were classified into pathological states with maximal overall sensitivity and specificity for the disease of 100%, suggesting the potential use of CRS for skin cancer diagnosis [188,189]. In addition, various studies have reported the differences between normal skin and lesional skin as well as skin from patients with atopic dermatitis or xerosis when CRS was applied. These findings emphasized the importance of lipid-protein ratios and lipid structure in the skin barrier. Reduced lateral or conformational order of lipids and the rapid changes in lipid composition have been observed in various skin diseases, pointing out the acceptance of CRS in these fields [190–192].

CRS is extensively used in the development of dermal formulations in a similar fashion. Topically applied formulations are supposed to be non-irritating to the skin; thus, the ingredients included in the formulation are of interest for evaluating their potential effects on the skin for better selection. For this reason, emulsifiers have attracted attention as the most commonly used ingredients in dermal products. They have been analyzed via CRS in multiple aspects, such as the lipid lateral packing order and conformational order. In addition, when the active signal is differentiated from the skin signal, this analytical setup can offer data on skin penetration, enabling the evaluation of the effectiveness of topical and dermal formulations [133,152,153,191,193,194]. Zhang et al. examined the effects of different substances employed in formulations on SC thickness, lipid content, and lipid conformational order. [132,135]. The distribution of deuterated SLS in the skin was also visualized by CRS from the study of Mao et al., providing insight into the interaction between permeants and skin [195].

Furthermore, the route of actives through the skin has also been tracked in several studies. Mélot et al. evaluated the penetration enhancing ability of chemical penetration enhancers *in-vivo* by monitoring the distribution of trans-retinol into human skin using CRS [196]. In *ex-vivo* research, Franzen et al. developed a method for quantitatively detecting caffeine in human skin via CRS [197]. The active ingredients that have so far been investigated include retinol, lidocaine, procaine HCl, niacinamide, hyaluronic acid, flufenamic acid, Punica granatum seed oil hydroxy phenethyl esters, and Beta-carotene. They have all been targeted in dermal delivery studies using CRS [86,134,180,198–202].

1.3.3 Data processing and configuration of confocal Raman spectroscopy

In skin research, preprocessing of Raman spectra is critical for providing accurate and reliable information from CRS analysis. It refers to the method used to process Raman spectra before generating the final spectra and image presentation. In general, the first step is to remove cosmic rays from originally acquired spectra. Cosmic rays are high-energy

particles from outer space that produce a very sharp peak in the spectrum that is unrelated to the Raman signal. Various mathematical and computational methods exist for filtering the cosmic rays from the spectra without removing the real Raman peaks [133,203]. Second, the smoothing methods should be applied to eliminate noise from the true sample spectrum. Generally, algorithms can be employed to data to gradually replace the original value with the calculated value through various filters. This step is often carried out by selecting different filters, including the moving average, weighted average, median, and Savitzky-Golay filter. The latter has been extensively used in CRS skin analysis [193,204]. Following, the Raman spectrum is frequently obscured by the background signal from the charge-coupled device (CCD) camera, fluorescence or substrate signals. Thus, each Raman spectrum requires the elimination of the signal background. Several ways to subtract the background from the spectrum can be easily modified using the software. The most often used methods for baseline correction are polynomial fitting, median window, and asymmetric least squares, the frequency domain analysis. The appropriate selection of them empirically depends on the quality of the spectrum [166,177].

After preprocessing Raman data, it is important to apply multivariate techniques to achieve the desired results while working with a large dataset and aligning its informative features. Using multivariate analytical tools, patterns in the data can be modeled and routinely used to predict the acquired data of a similar type. The analyses of skin have experienced various multivariant methods, including principal component analysis (PCA), linear discriminant analysis (LDA), multiple linear regression (MLR), and cluster analysis (CA) [149,205,206]. Among them, PCA analysis has been widely used in the spectra of biological skin samples. In general, it is a method that extracts the principal components and uses them to build a predictive model to reduce noise and highlight the signals in the samples. It is obvious that PCA has been a useful tool; for example, Ascencio et al. used it to reconstruct the Raman spectra by selecting the first two components and highlighting the caffeine and propylene glycol peaks [86].

Choe et al. used the first three components to reconstruct the Raman spectrum of human skin and remove minor noise variations in the fingerprint region [207,208].

Apart from the data analysis, configurations of CRS also play a role in determining the efficiency and accuracy of Raman data. They have been optimized for various sample measurements, including laser power, objective, pinhole size, laser wavelength, etc. [209–211]. In biological sample analysis, laser power is extremely important and should be kept within a safe range to avoid burning and damaging the sample. Thus, it is also customary to reduce the laser power in skin measurements and consider the laser wavelengths, objectives, sample properties, and other imaging parameters [212,213]. The selection of objectives has been widely explored to achieve a higher spatial resolution and collection efficiency with a higher numerical aperture (NA) giving higher resolution. Meanwhile, objectives can affect the correct interpretation of depth profiling used to characterize skin depth and dermal drug penetration in skin analysis. Lunter demonstrated that the penetration profiles of procaine were altered by the use of a 40× 0.6 NA objective and a 100× 1.25 NA objective [214]. Likewise, Zou et al. discussed the accurate determination of layer thickness of a multilayer polymer film using CRS, highlighting the essential topic of precisely measuring skin thickness using a water immersion objective [215]. The size of the pinhole in front of the detector is critical for CRS depth resolution. While a smaller pinhole size theoretically improves depth resolution, it comes at the significant cost of low throughput, and a proper balance should be established based on the experimental needs [216,217].

The laser wavelength is another crucial aspect to consider while performing skin analysis. It refers to the increase of signal-to-noise ratio (SNR), elimination of fluorescence noise, and avoidance of photoluminescence at a longer wavelength. The selection of proper laser wavelength has been examined in a variety of biological samples, including cheek cells and the skin surface [210,218,219]. The comprehensive examination of appropriate laser wavelength for various skin sample types is one of the subjects of this thesis.

1.3.4 Instrumental comparisons in skin application

CRS is a useful tool for skin analysis compared to other analytics in different aspects, where its advantages and limitations were comprehensively elaborated.

In principle, CRS can yield information on the molecular vibrations of skin components similar to infrared (IR) spectroscopy in identifying functional groups. These spectroscopic tools are commonly used in skin research and are occasionally compared [220,221]. For instance, Mao et al. conducted a comparative study examining the distribution of deuterated SLS in the skin using Raman and IR spectroscopy [195]. Additionally, comparisons of drug and excipient penetration monitoring were carried out between CRS and ATR-FTIR spectroscopy combined with tape stripping [222]. Throughout these studies, it was shown that IR spectroscopy could provide information about skin molecular vibrations and track the spectral features of actives in skin samples. However, it has a lower resolution and lower penetration of the beam into the skin sample, indicating that depth profiling is limited. This explains why it is normally used with tape stripping to achieve skin depth profiles, which is minimally invasive but more time-consuming. By contrast, CRS provides the benefit of a non-invasive and time-efficient measuring process. It enables the laser spot to move in multiple directions including the depth, allowing depth profiling. On the other hand, CRS is more expensive and shows challenges, including fluorescence, noise, weaker signal intensity, and a slower data acquisition time [167,205,223–225]. Despite so, CRS still has more advantageous qualities and is, therefore, a preferable choice.

It has been mentioned that with CRS it is feasible to measure the skin lipid content, which is conventionally evaluated by high-performance thin-layer chromatography (HPTLC) or liquid chromatography-mass spectrometry (LC-MS) [83,226–228]. HPTLC methods were usually developed to assay the skin lipid classes, especially the various CERs found in SC. Ochalek et al. investigated the CER species found in lipid model membranes to determine their effect on drug diffusion and

penetration. The concentrations of CER AP, CER EOS, palmitic acid (PA), and CHOL in the membrane were evaluated with HPTLC [229]. The LC-MS method has been broadly used to identify and quantify different skin lipid types (specifically CERs, FFAs, and CHOL). Many comparisons of the lipid distribution in the skin were implemented between human skin and other skin models or between healthy and diseased skin. The significance and contribution of several lipid classes in maintaining the skin barrier function or regulating the repair of skin diseases were then highlighted [230,231]. Bouwstra's research group has performed plenty of such investigations; for example, when examining the SC in canine atopic dermatitis, Chermprapai et al. found lower FFA levels and a decreased ratio of CER NS C44/C34. The C44/C34 denotes the total numbers of carbon atoms in the sphingosine (S) and non-hydroxy (N) acyl chains, respectively [232]. Despite their widespread use, the limitations of HPTLC and LC-MS in comparison to CRS remain clear, as they involve invasive skin lipid extraction and complicate sample preparation. Furthermore, the feasibility of CRS for determining the SC lipid content was validated by the experimental results from HPTLC, which was investigated by Zhang et al. for analyzing the lipid extraction by emulsifiers and formulations [135]. Thus, CRS can be a suitable alternative for assessing the skin's lipid content due to its non-invasive and easy-to-handle nature, although the drawback is also clear that it cannot differentiate between types of lipids.

The structure and organization of the intercellular skin lipids are the primary focus of this thesis, which is intended to determine the effects of PEGylated emulsifiers. In other studies, the evaluation of lipid structure is often implemented by using differential scanning calorimetry (DSC), X-ray diffraction analysis (XRD), or nuclear magnetic resonance (NMR) spectroscopy [132,233,234]. The DSC analysis was used to identify phase transitions associated with lipid structural changes. As a conventional method, it has been utilized to validate the use of CRS to detect the SC lipid conformation before and after the skin treatment with emulsifiers and formulations [35]. In addition, Bouwstra's research group has largely employed small-angle X-ray diffraction (SAXD) to characterize biophysical

properties of SC, such as the existence, formation, repeat distance, and order of LPP and SPP, which are used to indicate lamellar lipid organization. With this application, Berkers et al. investigated the interactions between topically applied CERs and SC lipid matrix in compromised *ex-vivo* skin [235]. The characteristics of SC lipids can also be deduced from the molecular mobility of a small fraction of the lipid components as determined by NMR measurements. NMR has been used to demonstrate the importance of natural moisturizing factor (NMF) in SC and explore its effect on SC lipid molecular properties [236]. In general, each of these applications has distinct advantages for skin analysis. However, CRS can more effectively accomplish the goal of simultaneously assessing multiple skin properties without causing damage to the skin sample.

Thus, this thesis primarily focuses on the multifunctional approach of CRS, which is of special importance for usage in various skin analyses with optimization of critical aspects.

References

[1] K.A. Walters, M.S. Roberts, The structure and function of skin, Dermatological Transdermal Formul. CRC Press (2002) 19–58. doi:10.2307/j.ctt46nrzt.12.

[2] J. Bouwstra, Structure of the skin barrier and its modulation by vesicular formulations, Prog. Lipid Res. 42 (2003) 1–36. doi:10.1016/S0163-7827(02)00028-0.

[3] R.R. Wickett, M.O. Visscher, Structure and function of the epidermal barrier, Am. J. Infect. Control. 34 (2006) 98–110. doi:10.1016/j.ajic.2006.05.295.

[4] J.A. Bouwstra, P.L. Honeywell-Nguyen, Skin structure and mode of action of vesicles, Adv. Drug Deliv. Rev. 54 (2002) 41–55. doi:10.1016/S0169-409X(02)00114-X.

[5] S. Hansen, C.M. Lehr, U.F. Schaefer, Modeling the human skin barrier-Towards a better understanding of dermal absorption, Adv. Drug Deliv. Rev. 65 (2013) 149–151. doi:10.1016/j.addr.2012.12.002.

[6] A. Gillet, F. Lecomte, P. Hubert, E. Ducat, B. Evrard, G. Piel, Skin penetration behaviour of liposomes as a function of their composition, Eur. J. Pharm. Biopharm. 79 (2011) 43–53. doi:10.1016/j.ejpb.2011.01.011.

[7] Q. Tian, P. Quan, L. Fang, H. Xu, C. Liu, A molecular mechanism investigation of the transdermal/topical absorption classification system on the basis of drug skin permeation and skin retention, Int. J. Pharm. 608 (2021) 121082. doi:10.1016/j.ijpharm.2021.121082.

[8] S. Kumar, M. Zakrewsky, M. Chen, S. Menegatti, J.A. Muraski, S. Mitragotri, Peptides as skin penetration enhancers: Mechanisms of action, J. Control. Release. 199 (2015) 168–178. doi:10.1016/j.jconrel.2014.12.006.

[9] G.K. Menon, New insights into skin structure: Scratching the surface, Adv. Drug Deliv. Rev. 54 (2002) S3. doi:10.1016/S0169-409X(02)00121-7.

[10] L. Busch, Y. Keziban, L. Dähne, C.M. Keck, M.C. Meinke, J. Lademann, A. Patzelt, The impact of skin massage frequency on the intrafollicular transport of silica nanoparticles: Validation of the ratchet effect on an ex vivo porcine skin model, Eur. J. Pharm. Biopharm. 158 (2021) 266–272. doi:10.1016/j.ejpb.2020.11.018.

[11] S. Eberlin, G. Facchini, G.H. da Silva, S. Eberlin, A.R. Bragatto, A.L.T.A. Pinheiro, A. da Silva Pinheiro, Ex Vivo Human Skin: An

Alternative Test System for Skin Irritation and Corrosion Assays, Altern. Lab. Anim. 49 (2021) 137–146. doi:10.1177/02611929211038652.

[12] K. Kabashima, T. Honda, F. Ginhoux, G. Egawa, The immunological anatomy of the skin, Nat. Rev. Immunol. 19 (2019) 19–30. doi:10.1038/s41577-018-0084-5.

[13] S.H. Moghadam, E. Saliaj, S.D. Wettig, C. Dong, M. V Ivanova, J.T. Huzil, M. Foldvari, Effect of Chemical Permeation Enhancers on Stratum Corneum Barrier Lipid Organizational Structure and Interferon Alpha Permeability, Mol. Pharm. 10 (2013) 2248–2260. doi:10.1021/mp300441c.

[14] D. Falcone, N.E. Uzunbajakava, B. Varghese, G.R. De Aquino Santos, R.J.H. Richters, P.C.M. Van De Kerkhof, P.E.J. Van Erp, Microspectroscopic Confocal Raman and Macroscopic Biophysical Measurements in the in vivo Assessment of the Skin Barrier: Perspective for Dermatology and Cosmetic Sciences, Skin Pharmacol. Physiol. 28 (2015) 307–317. doi:10.1159/000439031.

[15] N.A. Belsey, N.L. Garrett, L.R. Contreras-Rojas, A.J. Pickup-Gerlaugh, G.J. Price, J. Moger, R.H. Guy, Evaluation of drug delivery to intact and porated skin by coherent Raman scattering and fluorescence microscopies, J. Control. Release. 174 (2014) 37–42. doi:10.1016/j.jconrel.2013.11.002.

[16] P.J. Caspers, G.W. Lucassen, H.A. Bruining, G.J. Puppels, Automated depth-scanning confocal Raman microspectrometer for rapid in vivo determination of water concentration profiles in human skin, J. Raman Spectrosc. 31 (2000) 813–818. doi:10.1002/1097-4555(200008/09)31:8/9<813::AID-JRS573>3.0.CO;2-7.

[17] J.A. Bouwstra, R.W.J. Helder, A. El Ghalbzouri, Human skin equivalents: Impaired barrier function in relation to the lipid and protein properties of the stratum corneum, Adv. Drug Deliv. Rev. 175 (2021) 113802. doi:10.1016/j.addr.2021.05.012.

[18] H. Thompson, J. North, R. Davenport, J. Williams, Matching the skin barrier to the skin type., Br. J. Nurs. 20 (2011) 29–32. doi:10.12968/bjon.2011.20.sup9.s27.

[19] E. Abd, S.A. Yousef, M.N. Pastore, K. Telaprolu, Y.H. Mohammed, S. Namjoshi, J.E. Grice, M.S. Roberts, Skin models for the testing of transdermal drugs, Clin. Pharmacol. Adv. Appl. 8 (2016) 163–176. doi:10.2147/CPAA.S64788.

[20] C. Vitorino, J. Sousa, A. Pais, Overcoming the Skin Permeation Barrier: Challenges and Opportunities, Curr. Pharm. Des. 21 (2015) 2698–2712. doi:10.2174/1381612821666150428124053.

[21] F.F. Sahle, T. Gebre-Mariam, B. Dobner, J. Wohlrab, R.H.H. Neubert, Skin diseases associated with the depletion of stratum corneum lipids and stratum corneum lipid substitution therapy, Skin Pharmacol. Physiol. 28 (2015) 42–55. doi:10.1159/000360009.

[22] T.T. Nguyen, T. Happillon, J. Feru, S. Brassart-Passco, J.F. Angiboust, M. Manfait, O. Piot, Raman comparison of skin dermis of different ages: Focus on spectral markers of collagen hydration, J. Raman Spectrosc. 44 (2013) 1230–1237. doi:10.1002/jrs.4355.

[23] D. Zhang, Q. Bian, Y. Zhou, Q. Huang, J. Gao, The application of label-free imaging technologies in transdermal research for deeper mechanism revealing, Asian J. Pharm. Sci. 16 (2021) 265–279. doi:10.1016/j.ajps.2020.07.004.

[24] A.M. Römgens, D.L. Bader, J.A. Bouwstra, F.P.T. Baaijens, C.W.J. Oomens, Diffusion profile of macromolecules within and between human skin layers for (trans)dermal drug delivery, J. Mech. Behav. Biomed. Mater. 50 (2015) 215–222. doi:10.1016/j.jmbbm.2015.06.019.

[25] M.E. Darvin, H. Richter, Y.J. Zhu, M.C. Meinke, F. Knorr, S.A. Gonchukov, K. Koenig, J. Lademann, Comparison of in vivo and ex vivo laser scanning microscopy and multiphoton tomography application for human and porcine skin imaging, Quantum Electron. 44 (2014) 646–651. doi:10.1070/qe2014v044n07abeh015488.

[26] M.A. Sallam, S. Prakash, V. Krishnan, K. Todorova, A. Mandinova, S. Mitragotri, Hyaluronic Acid Conjugates of Vorinostat and Bexarotene for Treatment of Cutaneous Malignancies, Adv. Ther. 3 (2020) 1–10. doi:10.1002/adtp.202000116.

[27] M. Donejko, A. Przylipiak, E. Rysiak, K. Głuszuk, A. Surażyński, Influence of caffeine and hyaluronic acid on collagen biosynthesis in human skin fibroblasts, Drug Des. Devel. Ther. 8 (2014) 1923–1928. doi:10.2147/DDDT.S69791.

[28] M.M. Sedky, S.M. Fawzy, N.A. El Baki, N.H. El Eishi, A.E.M.M. El Bohy, Systemic sclerosis: An ultrasonographic study of skin and subcutaneous tissue in relation to clinical findings, Ski. Res. Technol. 19 (2013) 78–84. doi:10.1111/j.1600-0846.2012.00612.x.

[29] H. Ye, S. De, Thermal injury of skin and subcutaneous tissues: A review of experimental approaches and numerical models, Burns. 43 (2017) 909–932. doi:10.1016/j.burns.2016.11.014.

[30] J.Z. Wu, R.G. Cutlip, M.E. Andrew, R.G. Dong, Simultaneous determination of the nonlinear-elastic properties of skin and subcutaneous tissue in unconfined compression tests, Ski. Res. Technol. 13 (2007) 34–42. doi:10.1111/j.1600-0846.2007.00182.x.

[31] J.M. Crowther, A. Sieg, P. Blenkiron, C. Marcott, P.J. Matts, J.R. Kaczvinsky, A. V. Rawlings, Measuring the effects of topical moisturizers on changes in stratum corneum thickness, water gradients and hydration in vivo, Br. J. Dermatol. 159 (2008) 567–577. doi:10.1111/j.1365-2133.2008.08703.x.

[32] C.L. Silva, D. Topgaard, V. Kocherbitov, J.J.S. Sousa, A.A.C.C. Pais, E. Sparr, Stratum corneum hydration: Phase transformations and mobility in stratum corneum, extracted lipids and isolated corneocytes, Biochim. Biophys. Acta - Biomembr. 1768 (2007) 2647–2659. doi:10.1016/j.bbamem.2007.05.028.

[33] D. Yang, C. Liu, D. Ding, P. Quan, L. Fang, The molecular design of drug-ionic liquids for transdermal drug delivery: Mechanistic study of counterions structure on complex formation and skin permeation, Int. J. Pharm. 602 (2021) 120560. doi:10.1016/j.ijpharm.2021.120560.

[34] M. Sochorová, P. Audrlická, M. Červená, A. Kováčik, M. Kopečná, L. Opálka, P. Pullmannová, K. Vávrová, Permeability and microstructure of cholesterol-depleted skin lipid membranes and human stratum corneum, J. Colloid Interface Sci. 535 (2019) 227–238. doi:10.1016/j.jcis.2018.09.104.

[35] S. Wartewig, R. Neubert, W. Rettig, K. Hesse, Structure of stratum corneum lipids characterized by FT-Raman spectroscopy and DSC. IV. Mixtures of ceramides and oleic acid, Chem. Phys. Lipids. 91 (1998) 145–152. doi:10.1016/S0009-3084(97)00105-9.

[36] A. Tfayli, F. Bonnier, Z. Farhane, D. Libong, H.J. Byrne, A. Baillet-Guffroy, Comparison of structure and organization of cutaneous lipids in a reconstructed skin model and human skin: Spectroscopic imaging and chromatographic profiling, Exp. Dermatol. 23 (2014) 441–443. doi:10.1111/exd.12423.

[37] D. Groen, G.S. Gooris, J.A. Bouwstra, Model membranes prepared with ceramide EOS, cholesterol and free fatty acids form a unique lamellar phase, Langmuir. 26 (2010) 4168–4175. doi:10.1021/la9047038.

[38] D. Gabriel, T. Mugnier, H. Courthion, K. Kranidioti, N. Karagianni, M.C. Denis, M. Lapteva, Y. Kalia, M. Möller, R. Gurny, Improved topical delivery of tacrolimus: A novel composite hydrogel formulation for the treatment of psoriasis, J. Control. Release. 242 (2016) 16–24. doi:10.1016/j.jconrel.2016.09.007.

[39] J. van Smeden, M. Janssens, E.C.J. Kaye, P.J. Caspers, A.P. Lavrijsen, R.J. Vreeken, J.A. Bouwstra, The importance of free fatty acid chain length for the skin barrier function in atopic eczema patients, Exp. Dermatol. 23 (2014) 45–52. doi:10.1111/exd.12293.

[40] C.L. Emson, S. Fitzmaurice, G. Lindwall, K.W. Li, M.K. Hellerstein, H.I. Maibach, W. Liao, S.M. Turner, A pilot study demonstrating a non-invasive method for the measurement of protein turnover in skin disorders: application to psoriasis, Clin. Transl. Med. 2 (2013) 12. doi:10.1186/2001-1326-2-12.

[41] J. Van Smeden, J.A. Bouwstra, Stratum Corneum Lipids: Their Role for the Skin Barrier Function in Healthy Subjects and Atopic Dermatitis Patients, Curr. Probl. Dermatology. 49 (2016) 8–26. doi:10.1159/000441540.

[42] S.H. Moghadam, E. Saliaj, S.D. Wettig, C. Dong, M. V. Ivanova, J.T. Huzil, M. Foldvari, Effect of Chemical Permeation Enhancers on Stratum Corneum Barrier Lipid Organizational Structure and Interferon Alpha Permeability, Mol. Pharm. 10 (2013) 2248–2260. doi:10.1021/mp300441c.

[43] D. Groen, D.S. Poole, G.S. Gooris, J.A. Bouwstra, Is an orthorhombic lateral packing and a proper lamellar organization important for the skin barrier function?, Biochim. Biophys. Acta - Biomembr. 1808 (2011) 1529–1537. doi:10.1016/j.bbamem.2010.10.015.

[44] C. Choe, J. Lademann, M.E. Darvin, A depth-dependent profile of the lipid conformation and lateral packing order of the stratum corneum in vivo measured using Raman microscopy, Analyst. 141 (2016) 1981–1987. doi:10.1039/c5an02373d.

[45] A. Tfayli, E. Guillard, M. Manfait, A. Baillet-Guffroy, Raman spectroscopy: Feasibility of in vivo survey of stratum corneum lipids, effect of natural aging, Eur. J. Dermatology. 22 (2012) 36–41. doi:10.1684/ejd.2011.1507.

[46] J. Caussin, G.S. Gooris, J.A. Bouwstra, FTIR studies show lipophilic moisturizers to interact with stratum corneum lipids, rendering the more densely packed, Biochim. Biophys. Acta - Biomembr. 1778 (2008) 1517–1524. doi:10.1016/j.bbamem.2008.03.006.

[47] S. Wartewig, R.H.H. Neubert, Properties of ceramides and their impact on the stratum corneum structure: A review: Part 1: Ceramides, Skin Pharmacol. Physiol. 20 (2007) 220–229. doi:10.1159/000104420.

[48] J. Ishikawa, H. Narita, N. Kondo, M. Hotta, Y. Takagi, Y. Masukawa, T. Kitahara, Y. Takema, S. Koyano, S. Yamazaki, A. Hatamochi, Changes in the ceramide profile of atopic dermatitis patients, J. Invest. Dermatol. 130 (2010) 2511–2514. doi:10.1038/jid.2010.161.

[49] C.H. Lee, Y. Kawasaki, H.I. Maibach, Effect of surfactant mixtures on irritant contact dermatitis potential in man: sodium lauroyl glutamate and sodium lauryl sulphate, Contact Dermatitis. 30 (1994) 205–209. doi:10.1111/j.1600-0536.1994.tb00644.x.

[50] D. Zhang, Q. Bian, J. Li, Q. Huang, J. Gao, Enhancing effect of fumaric acid on transdermal penetration of loxoprofen sodium, Int. J. Pharm. 588 (2020) 119722. doi:10.1016/j.ijpharm.2020.119722.

[51] L. Hollesen, D. Groen, J.A. Bouwstra, Permeability and lipid organization of a novel psoriasis stratum corneum substitute, Int. J. Pharm. 457 (2013) 275–282. doi:10.1016/j.ijpharm.2013.08.086.

[52] T. Berkers, D. Visscher, G.S. Gooris, J.A. Bouwstra, Degree of skin barrier disruption affects lipid organization in regenerated stratum corneum, Acta Derm. Venereol. 98 (2018) 421–427. doi:10.2340/00015555-2865.

[53] S. Tfaili, C. Gobinet, G. Josse, J.F. Angiboust, M. Manfait, O. Piot, Confocal Raman microspectroscopy for skin characterization: A comparative study between human skin and pig skin, Analyst. 137 (2012) 3673–3682. doi:10.1039/c2an16292j.

[54] M. Leroy, J.F. Labbé, M. Ouellet, J. Jean, T. Lefèvre, G. Laroche, M. Auger, R. Pouliot, A comparative study between human skin substitutes and normal human skin using Raman microspectroscopy, Acta Biomater. 10 (2014) 2703–2711. doi:10.1016/j.actbio.2014.02.007.

[55] D. Borchman, Lipid conformational order and the etiology of cataract and dry eye, J. Lipid Res. 62 (2021) 100039. doi:10.1194/JLR.TR120000874.

[56] C.S. Choe, J. Lademann, M.E. Darvin, Lipid organization and stratum corneum thickness determined in vivo in human skin analyzing lipid–keratin peak (2820–3030 cm -1) using confocal Raman microscopy, J. Raman Spectrosc. 47 (2016) 1327–1331. doi:10.1002/jrs.4975.

[57] C. Czekalla, K.H. Schönborn, J. Lademann, M.C. Meinke, Noninvasive Determination of Epidermal and Stratum Corneum Thickness in vivo Using Two-Photon Microscopy and Optical Coherence Tomography: Impact of Body Area, Age, and Gender, Skin Pharmacol. Physiol. 32 (2019) 142–150. doi:10.1159/000497475.

[58] H.J. Cha, C. He, H. Zhao, Y. Dong, I.S. An, S. An, Intercellular and intracellular functions of ceramides and their metabolites in skin (Review), Int. J. Mol. Med. 38 (2016) 16–22. doi:10.3892/ijmm.2016.2600.

[59] M.A. Bolzinger, S. Briançon, J. Pelletier, Y. Chevalier, Penetration of drugs through skin, a complex rate-controlling membrane, Curr. Opin. Colloid Interface Sci. 17 (2012) 156–165. doi:10.1016/j.cocis.2012.02.001.

[60] J. Schleusener, A. Salazar, J. von Hagen, J. Lademann, M.E. Darvin, Retaining Skin Barrier Function Properties of the Stratum Corneum with Components of the Natural Moisturizing Factor—A Randomized, Placebo-Controlled Double-Blind In Vivo Study, Molecules. 26 (2021) 1649. doi:10.3390/molecules26061649.

[61] B. Kim, H.-E. Cho, S.H. Moon, H.-J. Ahn, S. Bae, H.-D. Cho, S. An, Transdermal delivery systems in cosmetics, Biomed. Dermatology. 4 (2020) 1–12. doi:10.1186/s41702-020-0058-7.

[62] B.W. Barry, Novel mechanisms and devices to enable successful transdermal drug delivery, Eur. J. Pharm. Sci. 14 (2001) 101–114. doi:10.1016/S0928-0987(01)00167-1.

[63] S.A. Giannos, Identifying present challenges to reliable future transdermal drug delivery products, Ther. Deliv. 6 (2015) 1033–1041. doi:10.4155/tde.15.62.

[64] J. Lademann, M.C. Meinke, S. Schanzer, H. Richter, M.E. Darvin, S.F. Haag, J.W. Fluhr, H.J. Weigmann, W. Sterry, A. Patzelt, In vivo methods for the analysis of the penetration of topically applied substances in and through the skin barrier, Int. J. Cosmet. Sci. 34 (2012) 551–559. doi:10.1111/j.1468-2494.2012.00750.x.

[65] M.B. Delgado-Charro, R.H. Guy, Effective use of transdermal drug delivery in children, Adv. Drug Deliv. Rev. 73 (2014) 63–82. doi:10.1016/j.addr.2013.11.014.

[66] D. Ramadon, M.T.C. McCrudden, A.J. Courtenay, R.F. Donnelly, Enhancement strategies for transdermal drug delivery systems:

current trends and applications, Springer US, 2021. doi:10.1007/s13346-021-00909-6.

[67] E. Touitou, Drug delivery across the skin, Expert Opin. Biol. Ther. 2 (2002) 723–733. doi:10.1517/14712598.2.7.723.

[68] S. Andega, N. Kanikkannan, M. Singh, Comparison of the effect of fatty alcohols on the permeation of melatonin between porcine and human skin, J. Control. Release. 77 (2001) 17–25. doi:10.1016/S0168-3659(01)00439-4.

[69] C.F. Goh, J.G. Moffat, D.Q.M. Craig, J. Hadgraft, M.E. Lane, Nano-thermal imaging of the stratum corneum and its potential use for understanding of the mechanism of skin penetration enhancer, Thermochim. Acta. 655 (2017) 278–283. doi:10.1016/j.tca.2017.07.013.

[70] F. Strati, R.H.H. Neubert, L. Opálka, A. Kerth, G. Brezesinski, Non-ionic surfactants as innovative skin penetration enhancers: insight in the mechanism of interaction with simple 2D stratum corneum model system, Eur. J. Pharm. Sci. (2020). doi:10.1016/j.ejps.2020.105620.

[71] T. Marjukka Suhonen, J. A. Bouwstra, A. Urtti, Chemical enhancement of percutaneous absorption in relation to stratum corneum structural alterations, J. Control. Release. 59 (1999) 149–161. doi:10.1016/S0168-3659(98)00187-4.

[72] K.A. Walters, M. Walker, O. Olejnik, Non-ionic Surfactant Effects on Hairless Mouse Skin Permeability Characteristics, J. Pharm. Pharmacol. 40 (1988) 525–529. doi:10.1111/j.2042-7158.1988.tb05295.x.

[73] M.O. Danso, T. Berkers, A. Mieremet, F. Hausil, J.A. Bouwstra, An ex vivo human skin model for studying skin barrier repair, Exp. Dermatol. 24 (2015) 48–54. doi:10.1111/exd.12579.

[74] S.M. Ali, F. Bonnier, A. Tfayli, H. Lambkin, K. Flynn, V. McDonagh, C. Healy, T. Clive Lee, F.M. Lyng, H.J. Byrne, Raman spectroscopic analysis of human skin tissue sections ex-vivo : evaluation of the effects of tissue processing and dewaxing , J. Biomed. Opt. 18 (2012) 061202. doi:10.1117/1.jbo.18.6.061202.

[75] P. Sjövall, L. Skedung, S. Gregoire, O. Biganska, F. Clément, G.S. Luengo, Imaging the distribution of skin lipids and topically applied compounds in human skin using mass spectrometry, Sci. Rep. 8 (2018) 1–14. doi:10.1038/s41598-018-34286-x.

[76] G.K. German, E. Pashkovski, E.R. Dufresne, Surfactant treatments influence drying mechanics in human stratum corneum, J. Biomech. 46 (2013) 2145–2151. doi:10.1016/j.jbiomech.2013.07.003.

[77] T. Berkers, W.A. Boiten, S. Absalah, J. van Smeden, A.P.M. Lavrijsen, J.A. Bouwstra, Compromising human skin in vivo and ex vivo to study skin barrier repair, Biochim. Biophys. Acta - Mol. Cell Biol. Lipids. 1864 (2019) 1103–1108. doi:10.1016/j.bbalip.2019.04.005.

[78] J.H. Hwang, H. Jeong, N. Lee, S. Hur, N. Lee, J.J. Han, H.W. Jang, W.K. Choi, K.T. Nam, K.M. Lim, Ex vivo live full-thickness porcine skin model as a versatile in vitro testing method for skin barrier research, Int. J. Mol. Sci. 22 (2021) 1–16. doi:10.3390/ijms22020657.

[79] L.I.J.C. Bergers, C.M.A. Reijnders, L.J. van den Broek, S.W. Spiekstra, T.D. de Gruijl, E.M. Weijers, S. Gibbs, Immune-competent human skin disease models, Drug Discov. Today. 21 (2016) 1479–1488. doi:10.1016/j.drudis.2016.05.008.

[80] V. Planz, C.M. Lehr, M. Windbergs, In vitro models for evaluating safety and efficacy of novel technologies for skin drug delivery, J. Control. Release. 242 (2016) 89–104. doi:10.1016/j.jconrel.2016.09.002.

[81] U. Jacobi, M. Kaiser, R. Toll, S. Mangelsdorf, H. Audring, N. Otberg, W. Sterry, J. Lademann, Porcine ear skin: An in vitro model for human skin, Ski. Res. Technol. 13 (2007) 19–24. doi:10.1111/j.1600-0846.2006.00179.x.

[82] S. Albrecht, A. Elpelt, C. Kasim, C. Reble, L. Mundhenk, H. Pischon, S. Hedtrich, C. Witzel, J. Lademann, L. Zastrow, I. Beckers, M.C. Meinke, Quantification and characterization of radical production in human, animal and 3D skin models during sun irradiation measured by EPR spectroscopy, Free Radic. Biol. Med. 131 (2019) 299–308. doi:10.1016/j.freeradbiomed.2018.12.022.

[83] H. Niehues, J.A. Bouwstra, A. El Ghalbzouri, J.M. Brandner, P.L.J.M. Zeeuwen, E.H. van den Bogaard, 3D skin models for 3R research: The potential of 3D reconstructed skin models to study skin barrier function, Exp. Dermatol. 27 (2018) 501–511. doi:10.1111/exd.13531.

[84] M. Wolf, M. Halper, R. Pribyl, D. Baurecht, C. Valenta, Distribution of phospholipid based formulations in the skin investigated by combined ATR-FTIR and tape stripping experiments, Int. J. Pharm. 519 (2017) 198–205. doi:10.1016/j.ijpharm.2017.01.026.

[85] Y. Zhu, C.-S. Choe, S. Ahlberg, M.C. Meinke, U. Alexiev, J. Lademann, M.E. Darvin, Penetration of silver nanoparticles into

porcine skin ex vivo using fluorescence lifetime imaging microscopy, Raman microscopy, and surface-enhanced Raman scattering microscopy , J. Biomed. Opt. 20 (2014) 051006. doi:10.1117/1.jbo.20.5.051006.

[86] S. Mujica Ascencio, C.S. Choe, M.C. Meinke, R.H. Müller, G. V. Maksimov, W. Wigger-Alberti, J. Lademann, M.E. Darvin, Confocal Raman microscopy and multivariate statistical analysis for determination of different penetration abilities of caffeine and propylene glycol applied simultaneously in a mixture on porcine skin ex vivo, Eur. J. Pharm. Biopharm. 104 (2016) 51–58. doi:10.1016/j.ejpb.2016.04.018.

[87] N. Sekkat, Y.N. Kalia, R.H. Guy, Biophysical study of porcine ear skin in vitro and its comparison to human skin in vivo, J. Pharm. Sci. 91 (2002) 2376–2381. doi:10.1002/jps.10220.

[88] U. Jacobi, M. Kaiser, R. Toll, S. Mangelsdorf, H. Audring, N. Otberg, W. Sterry, J. Lademann, Porcine ear skin: An in vitro model for human skin, Ski. Res. Technol. 13 (2007) 19–24. doi:10.1111/j.1600-0846.2006.00179.x.

[89] M. Paz-Alvarez, P.D.A. Pudney, J. Hadgraft, M.E. Lane, Topical delivery of climbazole to mammalian skin, Int. J. Pharm. 549 (2018) 317–324. doi:10.1016/j.ijpharm.2018.07.058.

[90] C. Choe, J. Lademann, M.E. Darvin, Analysis of Human and Porcine Skin in vivo/ex vivo for Penetration of Selected Oils by Confocal Raman Microscopy, Skin Pharmacol. Physiol. 28 (2015) 318–330. doi:10.1159/000439407.

[91] V. Klang, J.C. Schwarz, B. Lenobel, M. Nadj, J. Auböck, M. Wolzt, C. Valenta, In vitro vs. in vivo tape stripping: Validation of the porcine ear model and penetration assessment of novel sucrose stearate emulsions, Eur. J. Pharm. Biopharm. 80 (2012) 604–614. doi:10.1016/j.ejpb.2011.11.009.

[92] C.S. Choe, J. Schleusener, J. Lademann, M.E. Darvin, Human skin in vivo has a higher skin barrier function than porcine skin ex vivo— comprehensive Raman microscopic study of the stratum corneum, J. Biophotonics. 11 (2018) 1–10. doi:10.1002/jbio.201700355.

[93] S. Ghanbarzadeh, A. Khorrami, S. Arami, Nonionic surfactant-based vesicular system for transdermal drug delivery, Drug Deliv. 22 (2015) 1071–1077. doi:10.3109/10717544.2013.873837.

[94] J.A. Bouwstra, D.A. Van Hal, H.E.J. Hofland, H.E. Junginger, Preparation and characterization of nonionic surfactant vesicles,

Colloids Surfaces A Physicochem. Eng. Asp. 123–124 (1997) 71–80. doi:10.1016/S0927-7757(96)03800-9.

[95] A. Berthod, S. Tomer, J.G. Dorsey, Polyoxyethylene alkyl ether nonionic surfactants: Physicochemical properties and use for cholesterol determination in food, Talanta. 55 (2001) 69–83. doi:10.1016/S0039-9140(01)00395-2.

[96] Z. Peng, Q. Wu, Y. Wang, S. Yang, Synthesis , Properties , and Application of Novel Silane-Modified Polyoxyethylene Ether Surfactants, J. Surfactants Deterg. 7 (2004) 277–283. doi:10.1007/s11743-004-0312-z.

[97] S. Yada, T. Suzuki, S. Hashimoto, T. Yoshimura, Adsorption and Aggregation Properties of Homogeneous Polyoxypropylene–Polyoxyethylene Alkyl Ether Type Nonionic Surfactants, Langmuir. 33 (2017) 3794–3801. doi:10.1021/acs.langmuir.7b00104.

[98] M.M. Fiume, B. Heldreth, W.F. Bergfeld, D. V. Belsito, R.A. Hill, C.D. Klaassen, D. Liebler, J.G. Marks, R.C. Shank, T.J. Slaga, P.W. Snyder, F.A. Andersen, Safety Assessment of Alkyl PEG Ethers as Used in Cosmetics, Int. J. Toxicol. 31 (2012) 169S-244S. doi:10.1177/1091581812444141.

[99] S. Matsuda, M. Hisama, H. Shibayama, N. Itou, M. Iwaki, In vitro eye irritancy test of lauryl derivatives and polyoxyethylene alkyl derivatives with the reconstructed rabbit corneal epithelium model, J. Oleo Sci. 58 (2009) 437–442. doi:10.5650/jos.58.437.

[100] S. Zhu, R. Huang, M. Hong, Y. Jiang, Z. Hu, C. Liu, Y. Pei, Effects of polyoxyethylene (40) stearate on the activity of P-glycoprotein and cytochrome P450, Eur. J. Pharm. Sci. 37 (2009) 573–580. doi:10.1016/j.ejps.2009.05.001.

[101] E. Lémery, S. Briançon, Y. Chevalier, C. Bordes, T. Oddos, A. Gohier, M.A. Bolzinger, Skin toxicity of surfactants: Structure/toxicity relationships, Colloids Surfaces A Physicochem. Eng. Asp. 469 (2015) 166–179. doi:10.1016/j.colsurfa.2015.01.019.

[102] C. Fruijtier-Pölloth, Safety assessment on polyethylene glycols (PEGs) and their derivatives as used in cosmetic products, Toxicology. 214 (2005) 1–38. doi:10.1016/j.tox.2005.06.001.

[103] C. Ban, M. Jo, Y.H. Park, J.H. Kim, J.Y. Han, K.W. Lee, D.H. Kweon, Y.J. Choi, Enhancing the oral bioavailability of curcumin using solid lipid nanoparticles, Food Chem. 302 (2020) 125328. doi:10.1016/j.foodchem.2019.125328.

[104] R.T. Abdel-Aziz, U.F. Aly, F.M. Mady, Enhanced skin delivery of propranolol HCl using nonionic surfactant-based vesicles for topical treatment of infantile hemangioma, J. Drug Deliv. Sci. Technol. 61 (2021) 102235. doi:10.1016/j.jddst.2020.102235.

[105] J. Jiao, Polyoxyethylated nonionic surfactants and their applications in topical ocular drug delivery, Adv. Drug Deliv. Rev. 60 (2008) 1663–1673. doi:10.1016/j.addr.2008.09.002.

[106] F. Otto, P. van Hoogevest, F. Syrowatka, V. Heinl, R.H.H. Neubert, Assessment of the applicability of HLB values for natural phospholipid emulsifiers for preparation of stable emulsions, Pharmazie. 75 (2020) 365–370. doi:10.1691/ph.2020.9174.

[107] S.C. Shin, C.W. Cho, K.H. Yang, Development of lidocaine gels for enhanced local anesthetic action, Int. J. Pharm. 287 (2004) 73–78. doi:10.1016/j.ijpharm.2004.08.012.

[108] D. Nandni, R.K. Mahajan, Micellar and interfacial behavior of cationic benzalkonium chloride and nonionic polyoxyethylene alkyl ether based mixed surfactant systems, J. Surfactants Deterg. 16 (2013) 587–599. doi:10.1007/s11743-012-1427-z.

[109] M. Rottke, D.J. Lunter, R. Daniels, In vitro studies on release and skin permeation of nonivamide from novel oil-in-oil-emulsions, Eur. J. Pharm. Biopharm. 86 (2014) 260–266. doi:10.1016/j.ejpb.2013.09.018.

[110] P.J. Holloway, W.W.-. Wong, H.J. Partridge, D. Seaman, R.B. Perry, Effects of some nonionic polyoxyethylene surfactants on uptake of ethirimol and diclobutrazol from suspension formulations applied to wheat leaves, Pestic. Sci. 34 (1992) 109–118. doi:10.1002/ps.2780340204.

[111] R.M. Barbosa, P. Severino, P.S.C. Preté, M.H.A. Santana, Influence of different surfactants on the physicochemical properties of elastic liposomes, Pharm. Dev. Technol. 22 (2017) 360–369. doi:10.3109/10837450.2016.1163387.

[112] S. Yada, K. Matsuoka, Y. Nagai Kanasaki, K. Gotoh, T. Yoshimura, Emulsification, solubilization, and detergency behaviors of homogeneous polyoxypropylene-polyoxyethylene alkyl ether type nonionic surfactants, Colloids Surfaces A Physicochem. Eng. Asp. 564 (2019) 51–58. doi:10.1016/j.colsurfa.2018.12.030.

[113] M. Manconi, C. Sinico, D. Valenti, G. Loy, A.M. Fadda, Niosomes as carriers for tretinoin. I. Preparation and properties, Int. J. Pharm. 234 (2002) 237–248. doi:10.1016/S0378-5173(01)00971-1.

[114] M.F. Saettone, P. Chetoni, R. Cerbai, G. Mazzanti, L. Braghiroli, Evaluation of ocular permeation enhancers: In vitro effects on corneal transport of four β-blockers, and in vitro/in vivo toxic activity, Int. J. Pharm. 142 (1996) 103–113. doi:10.1016/0378-5173(96)04663-7.

[115] R. Albash, C. Yousry, A.M. Al-Mahallawi, A.A. Alaa-Eldin, Utilization of PEGylated cerosomes for effective topical delivery of fenticonazole nitrate: in-vitro characterization, statistical optimization, and in-vivo assessment, Drug Deliv. 28 (2021) 1–9. doi:10.1080/10717544.2020.1859000.

[116] L. Chiappisi, Polyoxyethylene alkyl ether carboxylic acids: An overview of a neglected class of surfactants with multiresponsive properties, Adv. Colloid Interface Sci. 250 (2017) 79–94. doi:10.1016/j.cis.2017.10.001.

[117] A. Otto, J. Du Plessis, J.W. Wiechers, Formulation effects of topical emulsions on transdermal and dermal delivery, Int. J. Cosmet. Sci. 31 (2009) 1–19. doi:10.1111/j.1468-2494.2008.00467.x.

[118] S.C. Shin, C.W. Cho, I.J. Oh, Effects of non-ionic surfactants as permeation enhancers towards piroxicam from the poloxamer gel through rat skins, Int. J. Pharm. 222 (2001) 199–203. doi:10.1016/S0378-5173(01)00699-8.

[119] E.S. Park, S.Y. Chang, M. Hahn, S.C. Chi, Enhancing effect of polyoxyethylene alkyl ethers on the skin permeation of ibuprofen, Int. J. Pharm. 209 (2000) 109–119. doi:10.1016/S0378-5173(00)00559-7.

[120] A. Casiraghi, M. Di Grigoli, F. Cilurzo, C.G.M. Gennari, G. Rossoni, P. Minghetti, The influence of the polar head and the hydrophobic chain on the skin penetration enhancement effect of poly(ethylene glycol) derivatives, AAPS PharmSciTech. 13 (2012) 247–253. doi:10.1208/s12249-011-9745-4.

[121] E. Bárány, M. Lindberg, M. Lodén, Unexpected skin barrier influence from nonionic emulsifiers, Int. J. Pharm. 195 (2000) 189–195. doi:10.1016/S0378-5173(99)00388-9.

[122] H. Okuyama, Y. Ikeda, S. Kasai, K. Imamori, K. Takayama, T. Nagai, Influence of non-ionic surfactants, pH and propylene glycol on percutaneous absorption of piroxicam from cataplasm, Int. J. Pharm. 186 (1999) 141–148. doi:10.1016/S0378-5173(99)00154-4.

[123] A. Pandey, Role of Surfactants as Penetration Enhancer in Transdermal Drug Delivery System, J. Mol. Pharm. Org. Process Res. 02 (2014). doi:10.4172/2329-9053.1000113.

[124] S.A.V. Morris, K.P. Ananthapadmanabhan, G.B. Kasting, Anionic surfactant-induced changes in skin permeability, J. Pharm. Sci. (2019) 1–9. doi:10.1016/j.xphs.2019.06.030.

[125] R.M. Walters, G. Mao, E.T. Gunn, S. Hornby, Cleansing Formulations That Respect Skin Barrier Integrity, Dermatol. Res. Pract. 2012 (2012) 1–9. doi:10.1155/2012/495917.

[126] K.P. Ananthapadmanabhan, K.K. Yu, C.L. Meyers, M.P. Aronson, Binding of surfactants to stratum corneum, J. Cosmet. Sci. 47 (1996) 185–200.

[127] J.W. Fluhr, A. Akengin, A. Bornkessel, S. Fuchs, J. Praessler, J. Norgauer, R. Grieshaber, P. Kleesz, P. Elsner, Additive impairment of the barrier function by mechanical irritation, occlusion and sodium lauryl sulphate in vivo, Br. J. Dermatol. 153 (2005) 125–131. doi:10.1111/j.1365-2133.2005.06430.x.

[128] A.W. Fulmer, G.J. Kramer, Stratum Corneum Lipid Abnormalities in Surfactant-Induced Dry Scaly Skin, J. Invest. Dermatol. 86 (1986) 598–602. doi:10.1111/1523-1747.ep12355351.

[129] M. Denda, J. Koyama, R. Namba, I. Horii, Stratum corneum lipids morphology and transepidermal water loss in normal skin and surfactant induced scaly skin, Arch. Dermatol. Res. 286 (1994) 41–46.

[130] P. Saad, C.R. Flach, R.M. Walters, R. Mendelsohn, Infrared spectroscopic studies of sodium dodecyl sulphate permeation and interaction with stratum corneum lipids in skin, Int. J. Cosmet. Sci. 34 (2012) 36–43. doi:10.1111/j.1468-2494.2011.00678.x.

[131] A. Nokhodchi, J. Shokri, A. Dashbolaghi, D. Hassan-Zadeh, T. Ghafourian, M. Barzegar-Jalali, The enhancement effect of surfactants on the penetration of lorazepam through rat skin, Int. J. Pharm. 250 (2003) 359–369. doi:10.1016/S0378-5173(02)00554-9.

[132] Z. Zhang, D.J. Lunter, Confocal Raman microspectroscopy as an alternative to differential scanning calorimetry to detect the impact of emulsifiers and formulations on stratum corneum lipid conformation, Eur. J. Pharm. Sci. 121 (2018) 1–8. doi:10.1016/j.ejps.2018.05.013.

[133] D. Lunter, R. Daniels, Confocal Raman microscopic investigation of the effectiveness of penetration enhancers for procaine delivery to the skin, J. Biomed. Opt. 19 (2014) 126015. doi:10.1117/1.jbo.19.12.126015.

[134] L. Binder, C. Valenta, D. Lunter, Determination of skin penetration profiles by confocal Raman microspectroscopy: Evaluation of

interindividual variability and interlab comparability, J. Raman Spectrosc. (2020) 1–7. doi:10.1002/jrs.5871.

[135] Z. Zhang, D.J. Lunter, Confocal Raman microspectroscopy as an alternative method to investigate the extraction of lipids from stratum corneum by emulsifiers and formulations, Eur. J. Pharm. Biopharm. 127 (2018) 61–71. doi:10.1016/j.ejpb.2018.02.006.

[136] A. Lalloz, M.A. Bolzinger, S. Briançon, J. Faivre, J.M. Rabanel, A. Garcia Ac, P. Hildgen, X. Banquy, Subtle and unexpected role of PEG in tuning the penetration mechanisms of PLA-based nano-formulations into intact and impaired skin, Int. J. Pharm. 563 (2019) 79–90. doi:10.1016/j.ijpharm.2019.02.039.

[137] Z. Nizioł-łukaszewska, P. Osika, T. Wasilewski, T. Bujak, Hydrophilic dogwood extracts as materials for reducing the skin irritation potential of body wash cosmetics, Molecules. 22 (2017). doi:10.3390/molecules22020320.

[138] P.N. Moore, S. Puvvada, D. Blankschtein, Challenging the surfactant monomer skin penetration model: Penetration of sodium dodecyl sulfate micelles into the epidermis, J. Cosmet. Sci. 54 (2003) 29–46.

[139] S.A.V. Morris, R.T. Thompson, R.W. Glenn, K.P. Ananthapadmanabhan, G.B. Kasting, Mechanisms of anionic surfactant penetration into human skin: Investigating monomer, micelle and submicellar aggregate penetration theories, Int. J. Cosmet. Sci. 41 (2019) 55–66. doi:10.1111/ics.12511.

[140] M.A. James-Smith, B. Hellner, N. Annunziato, S. Mitragotri, Effect of surfactant mixtures on skin structure and barrier properties, Ann. Biomed. Eng. 39 (2011) 1215–1223. doi:10.1007/s10439-010-0190-4.

[141] Y. Chen, F. Qiao, Y. Fan, Y. Han, Y. Wang, Interactions of Cationic/Anionic Mixed Surfactant Aggregates with Phospholipid Vesicles and Their Skin Penetration Ability, Langmuir. 33 (2017) 2760–2769. doi:10.1021/acs.langmuir.6b04093.

[142] P.N. Moore, A. Shiloach, S. Puvvada, D. Blankschtein, Penetration of mixed micelles into the epidermis: Effect of mixing sodium dodecyl sulfate with dodecyl hexa(ethylene oxide), J. Cosmet. Sci. 54 (2003) 143–159.

[143] T.J. Hall-Manning, G.H. Holland, G. Rennie, P. Revell, J. Hines, M.D. Barratt, D.A. Basketter, Skin irritation potential of mixed surfactant systems, Food Chem. Toxicol. 36 (1998) 233–238. doi:10.1016/S0278-6915(97)00144-0.

[144] K. Miyazawa, M. Ogawa, T. Mitsui, The physico‑chemical properties and protein denaturation potential of surfactant mixtures, Int. J. Cosmet. Sci. 6 (1984) 33–46. doi:10.1111/j.1467-2494.1984.tb00356.x.

[145] H. Tadenuma, K. Yamada, T. Tamura, Analysis of Protein-Mixed Surfactant System Interactions ;, J. Japan Oil Chem. Soc. 48 (1999) 207-213,258. doi:10.5650/jos1996.48.207.

[146] L. Nasdala, O. Beyssac, J. William Schopf, B. Bleisteiner, Application of Raman-based images in the earth sciences, 2012. doi:10.1007/978-3-642-28252-2-5.

[147] S.N. White, Laser Raman spectroscopy as a technique for identification of seafloor hydrothermal and cold seep minerals, Chem. Geol. 259 (2009) 240–252. doi:10.1016/j.chemgeo.2008.11.008.

[148] E. Munnier, A. Tfayli, I. Chourpa, F. Bonnier, Depth profiling of cosmetic active molecules penetration in human skin using hyperspectral Raman imaging coupled with multivariate statistical analysis, IFSCC Congr. 2018. (2018).

[149] D.W. Shipp, F. Sinjab, I. Notingher, Raman spectroscopy: techniques and applications in the life sciences, Adv. Opt. Photonics. 9 (2017) 315. doi:10.1364/aop.9.000315.

[150] M. Ledinský, B. Paviet-Salomon, A. Vetushka, J. Geissbühler, A. Tomasi, M. Despeisse, S. De Wolf, C. Ballif, A. Fejfar, Profilometry of thin films on rough substrates by Raman spectroscopy, Sci. Rep. 6 (2016) 4–10. doi:10.1038/srep37859.

[151] J. Kim, J. Hwang, Y.A. Woo, H. Chung, Investigation on Raman spectral features of a coated tablet under variation of its orientation respective to laser illumination and measurement of nominal coating thickness of packed tablets, J. Pharm. Biomed. Anal. 131 (2016) 281–286. doi:10.1016/j.jpba.2016.08.038.

[152] A. Tfayli, O. Piot, F. Pitre, M. Manfait, Follow-up of drug permeation through excised human skin with confocal Raman microspectroscopy, Eur. Biophys. J. 36 (2007) 1049–1058. doi:10.1007/s00249-007-0191-x.

[153] L. Binder, J. Mazál, R. Petz, V. Klang, C. Valenta, The role of viscosity on skin penetration from cellulose ether-based hydrogels, Ski. Res. Technol. (2019) 1–10. doi:10.1111/srt.12709.

[154] L. Franzen, J. Anderski, V. Planz, K.H. Kostka, M. Windbergs, Combining confocal Raman microscopy and freeze-drying for

quantification of substance penetration into human skin, Exp. Dermatol. 23 (2014) 942–944. doi:10.1111/exd.12542.

[155] C. V. Raman, K.S. Krishnan, A new type of secondary radiation, Nature. 121 (1928) 501–502. doi:10.1038/121501c0.

[156] C. V. Raman, K.S. Krishnan, Polarisation of Scattered Light-quanta, Nature. 122 (1928) 169.

[157] K.J.I. Ember, M.A. Hoeve, S.L. McAughtrie, M.S. Bergholt, B.J. Dwyer, M.M. Stevens, K. Faulds, S.J. Forbes, C.J. Campbell, Raman spectroscopy and regenerative medicine: a review, Npj Regen. Med. 2 (2017) 1–9. doi:10.1038/s41536-017-0014-3.

[158] S.P.S. Porto, D.L. Wood, Ruby Optical Maser as a Raman Source, J. Opt. Soc. Am. 52 (1962) 251. doi:10.1364/JOSA.52.000251.

[159] D.L. Jeanmaire, R.P. Van Duyne, Surface raman spectroelectrochemistry: Part I. Heterocyclic, aromatic, and aliphatic amines adsorbed on the anodized silver electrode, J. Electroanal. Chem. Interfacial Electrochem. 84 (1977) 1–20. doi:10.1016/S0022-0728(77)80224-6.

[160] W.M. Tolles, J.W. Nibler, J.R. McDonald, A.B. Harvey, A Review of the Theory and Application of Coherent Anti-Stokes Raman Spectroscopy (CARS), Appl. Spectrosc. 31 (1977) 253–271. doi:10.1366/000370277774463625.

[161] M.G. Albrecht, J.A. Creighton, Anomalously Intense Raman Spectra of Pyridine at a Silver Electrode, J. Am. Chem. Soc. 99 (1977) 5215–5217. doi:10.1021/ja00457a071.

[162] N. Hayazawa, Y. Inouye, Z. Sekkat, S. Kawata, Metallized tip amplification of near-field Raman scattering, Opt. Commun. 183 (2000) 333–336. doi:10.1016/S0030-4018(00)00894-4.

[163] M. Artin, G. Shim, B.C. Wilson, E. Marple, M.W. Ach, Study of Fiber-Optic Probes for in Vivo Medical Raman Spectroscopy, 1999.

[164] M.G. Shim, B.C. Wilson, Development of an in vivo Raman spectroscopic system for diagnostic applications, J. Raman Spectrosc. 28 (1997) 131–142. doi:10.1002/(sici)1097-4555(199702)28:2/3<131::aid-jrs68>3.0.co;2-s.

[165] R. Hara, M. Ishigaki, Y. Kitahama, Y. Ozaki, T. Genkawa, Excitation wavelength selection for quantitative analysis of carotenoids in tomatoes using Raman spectroscopy, Food Chem. 258 (2018) 308–313. doi:10.1016/j.foodchem.2018.03.089.

[166] J. Zhao, H. Lui, D.I. Mclean, H. Zeng, Automated autofluorescence background subtraction algorithm for biomedical raman spectroscopy, Appl. Spectrosc. 61 (2007) 1225–1232. doi:10.1366/000370207782597003.

[167] A. Hédoux, Recent developments in the Raman and infrared investigations of amorphous pharmaceuticals and protein formulations: A review, Adv. Drug Deliv. Rev. 100 (2016) 133–146. doi:10.1016/j.addr.2015.11.021.

[168] P.J. Caspers, G.W. Lucassen, R. Wolthuis, H.A. Bruining, G.J. Puppels, In vitro and in vivo Raman spectroscopy of human skin., Biospectroscopy. 4 (1998) S31-9. doi:10.1002/(SICI)1520-6343(1998)4:5+<S31::AID-BSPY4>3.0.CO;2-M.

[169] P.J. Caspers, G.W. Lucassen, H.A. Bruining, G.J. Puppels, Automated depth-scanning confocal Raman microspectrometer for rapid in vivo determination of water concentration profiles in human skin, J. Raman Spectrosc. 31 (2000) 813–818. doi:10.1002/1097-4555(200008/09)31:8/9<813::AID-JRS573>3.0.CO;2-7.

[170] P.J. Caspers, G.W. Lucassen, E.A. Carter, H.A. Bruining, G.J. Puppels, G.W. Lucassen, E.A. Carter, In vivo confocal raman microspectroscopy of the skin: Noninvasive determination of molecular concentration profiles, J. Invest. Dermatol. 116 (2001) 434–442. doi:10.1046/j.1523-1747.2001.01258.x.

[171] D. Mohammed, P.J. Matts, J. Hadgraft, M.E. Lane, In vitro-in vivo correlation in skin permeation, Pharm. Res. 31 (2014) 394–400. doi:10.1007/s11095-013-1169-2.

[172] M. Gniadecka, O.F. Nielsen, D.H. Christensen, H.C. Wulf, Structure of water, proteins, and lipids in intact human skin, hair, and nail, J. Invest. Dermatol. 110 (1998) 393–398. doi:10.1046/j.1523-1747.1998.00146.x.

[173] A.K. Dąbrowska, C. Adlhart, F. Spano, G.-M. Rotaru, S. Derler, L. Zhai, N.D. Spencer, R.M. Rossi, In vivo confirmation of hydration-induced changes in human-skin thickness, roughness and interaction with the environment , Biointerphases. 11 (2016) 031015. doi:10.1116/1.4962547.

[174] P.J. Caspers, G.W. Lucassen, E.A. Carter, H.A. Bruining, G.J. Puppels, In vivo confocal raman microspectroscopy of the skin: Noninvasive determination of molecular concentration profiles, J. Invest. Dermatol. 116 (2001) 434–442. doi:10.1046/j.1523-1747.2001.01258.x.

[175] J.S. Ri, S.H. Choe, J. Schleusener, J. Lademann, C.S. Choe, M.E. Darvin, In vivo Tracking of DNA for Precise Determination of the Stratum Corneum Thickness and Superficial Microbiome Using Confocal Raman Microscopy, Skin Pharmacol. Physiol. 33 (2020) 30–37. doi:10.1159/000503262.

[176] A. Böhling, S. Bielfeldt, A. Himmelmann, M. Keskin, K.P. Wilhelm, Comparison of the stratum corneum thickness measured in vivo with confocal Raman spectroscopy and confocal reflectance microscopy, Ski. Res. Technol. 20 (2014) 50–57. doi:10.1111/srt.12082.

[177] R. Vyumvuhore, A. Tfayli, O. Piot, M. Le Guillou, N. Guichard, M. Manfait, A. Baillet-Guffroy, Raman spectroscopy: in vivo quick response code of skin physiological status , J. Biomed. Opt. 19 (2014) 111603. doi:10.1117/1.jbo.19.11.111603.

[178] L. Franzen, C. Mathes, S. Hansen, M. Windbergs, Advanced chemical imaging and comparison of human and porcine hair follicles for drug delivery by confocal Raman microscopy, J. Biomed. Opt. 18 (2012) 061210. doi:10.1117/1.jbo.18.6.061210.

[179] A. Tfayli, O. Piot, F. Draux, F. Pitre, M. Manfait, Molecular characterization of reconstructed skin model by Raman microspectroscopy: Comparison with excised human skin, Biopolymers. 87 (2007) 261–274. doi:10.1002/bip.20832.

[180] L. Miloudi, F. Bonnier, A. Tfayli, F. Yvergnaux, H.J. Byrne, I. Chourpa, E. Munnier, Confocal Raman spectroscopic imaging for in vitro monitoring of active ingredient penetration and distribution in reconstructed human epidermis model, J. Biophotonics. 11 (2018) 1–12. doi:10.1002/jbio.201700221.

[181] F.D. Fleischli, S. Mathes, C. Adlhart, Label free non-invasive imaging of topically applied actives in reconstructed human epidermis by confocal Raman spectroscopy, Vib. Spectrosc. 68 (2013) 29–33. doi:10.1016/j.vibspec.2013.05.003.

[182] E. Atef, N. Altuwaijri, Using Raman Spectroscopy in Studying the Effect of Propylene Glycol, Oleic Acid, and Their Combination on the Rat Skin, AAPS PharmSciTech. 19 (2018) 114–122. doi:10.1208/s12249-017-0800-7.

[183] A. Mieremet, W. Boiten, R. van Dijk, G. Gooris, H.S. Overkleeft, J.M.F.G. Aerts, J.A. Bouwstra, A. El Ghalbzouri, Unravelling effects of relative humidity on lipid barrier formation in human skin equivalents, Arch. Dermatol. Res. 311 (2019) 679–689. doi:10.1007/S00403-019-01948-3.

[184] C.W. Freudiger, R. Pfannl, D.A. Orringer, B.G. Saar, M. Ji, Q. Zeng, L. Ottoboni, W. Ying, C. Waeber, J.R. Sims, P.L. De Jager, O. Sagher, M.A. Philbert, X. Xu, S. Kesari, X.S. Xie, G.S. Young, Multicolored stain-free histopathology with coherent Raman imaging, Lab. Investig. 92 (2012) 1492–1502. doi:10.1038/labinvest.2012.109.

[185] C.J.H. Ho, Y.W. Yew, U.S. Dinish, A.H.Y. Kuan, M.K.W. Wong, R. Bi, K. Dev, X. Li, G. Singh, M. Moothanchery, J. Perumal, S.T.G. Thng, M. Olivo, Handheld confocal Raman spectroscopy (CRS) for objective assessment of skin barrier function and stratification of severity in atopic dermatitis (AD) patients, J. Dermatol. Sci. 98 (2020) 20–25. doi:10.1016/j.jdermsci.2020.02.001.

[186] P. Donfack, M. Rehders, K. Brix, P. Boukamp, A. Materny, Micro raman spectroscopy for monitoring alterations between human skin keratinocytes haCat and their tumorigenic derivatives a5RT3 - toward a raman characterization of a skin carcinoma model, J. Raman Spectrosc. 41 (2010) 16–26. doi:10.1002/jrs.2400.

[187] L. Franzen, M. Windbergs, Applications of Raman spectroscopy in skin research - From skin physiology and diagnosis up to risk assessment and dermal drug delivery, Adv. Drug Deliv. Rev. 89 (2015) 91–104. doi:10.1016/j.addr.2015.04.002.

[188] C.A. Lieber, S.K. Majumder, D. Billheimer, D.L. Ellis, A. Mahadevan-Jansen, Raman microspectroscopy for skin cancer detection in vitro, J. Biomed. Opt. 13 (2008) 024013. doi:10.1117/1.2899155.

[189] C.A. Lieber, S.K. Majumder, D.L. Ellis, D.D. Billheimer, A. Mahadevan-Jansen, In vivo nonmelanoma skin cancer diagnosis using Raman microspectroscopy, Lasers Surg. Med. 40 (2008) 461–467. doi:10.1002/lsm.20653.

[190] I.P. Santos, E.M. Barroso, T.C. Bakker Schut, P.J. Caspers, C.G.F. Van Lanschot, D.H. Choi, M.F. Van Der Kamp, R.W.H. Smits, R. Van Doorn, R.M. Verdijk, V. Noordhoek Hegt, J.H. Von Der Thüsen, C.H.M. Van Deurzen, L.B. Koppert, G.J.L.H. Van Leenders, P.C. Ewing-Graham, H.C. Van Doorn, C.M.F. Dirven, M.B. Busstra, J. Hardillo, A. Sewnaik, I. Ten Hove, H. Mast, D.A. Monserez, C. Meeuwis, T. Nijsten, E.B. Wolvius, R.J. Baatenburg De Jong, G.J. Puppels, S. Koljenović, Raman spectroscopy for cancer detection and cancer surgery guidance: Translation to the clinics, Analyst. 142 (2017) 3025–3047. doi:10.1039/c7an00957g.

[191] M. Janssens, J. van Smeden, G.J. Puppels, A.P.M. Lavrijsen, P.J. Caspers, J.A. Bouwstra, Lipid to protein ratio plays an important role

in the skin barrier function in patients with atopic eczema, Br. J. Dermatol. 170 (2014) 1248–1255. doi:10.1111/bjd.12908.

[192] R. Vyumvuhore, R. Michael-Jubeli, L. Verzeaux, D. Boudier, M. Le Guillou, S. Bordes, D. Libong, A. Tfayli, M. Manfait, B. Closs, Lipid organization in xerosis: the key of the problem?, Int. J. Cosmet. Sci. 40 (2018) 549–554. doi:10.1111/ics.12496.

[193] A. Quatela, L. Miloudi, A. Tfayli, A. Baillet-Guffroy, In vivo Raman microspectroscopy: Intra- and intersubject variability of stratum corneum spectral markers, Skin Pharmacol. Physiol. 29 (2016) 102–109. doi:10.1159/000445079.

[194] A. Quatela, A. Tfayli, A. Baillet-Guffroy, Examination of the effect of Stratum Corneum isolation process on the integrity of the barrier function: A confocal Raman spectroscopy study, Ski. Res. Technol. 22 (2016) 75–80. doi:10.1111/srt.12231.

[195] G. Mao, C.R. Flach, R. Mendelsohn, R.M. Walters, Imaging the distribution of sodium dodecyl sulfate in skin by confocal raman and infrared microspectroscopy, Pharm. Res. 29 (2012) 2189–2201. doi:10.1007/s11095-012-0748-y.

[196] M. Mélot, P.D.A. Pudney, A.M. Williamson, P.J. Caspers, A. Van Der Pol, G.J. Puppels, Studying the effectiveness of penetration enhancers to deliver retinol through the stratum cornum by in vivo confocal Raman spectroscopy, J. Control. Release. 138 (2009) 32–39. doi:10.1016/j.jconrel.2009.04.023.

[197] L. Franzen, J. Anderski, M. Windbergs, Quantitative detection of caffeine in human skin by confocal Raman spectroscopy - A systematic in vitro validation study, Eur. J. Pharm. Biopharm. 95 (2015) 110–116. doi:10.1016/j.ejpb.2015.03.026.

[198] M. Ashtikar, C. Matthäus, M. Schmitt, C. Krafft, A. Fahr, J. Popp, Non-invasive depth profile imaging of the stratum corneum using confocal Raman microscopy: First insights into the method, Eur. J. Pharm. Sci. 50 (2013) 601–608. doi:10.1016/j.ejps.2013.05.030.

[199] M. Essendoubi, C. Gobinet, R. Reynaud, J.F. Angiboust, M. Manfait, O. Piot, Human skin penetration of hyaluronic acid of different molecular weights as probed by Raman spectroscopy, Ski. Res. Technol. 22 (2016) 55–62. doi:10.1111/srt.12228.

[200] M. Bakonyi, A. Gácsi, A. Kovács, M.B. Szűcs, S. Berkó, E. Csányi, Following-up skin penetration of lidocaine from different vehicles by Raman spectroscopic mapping, J. Pharm. Biomed. Anal. 154 (2018) 1–6. doi:10.1016/j.jpba.2018.02.056.

[201] M. Bakonyi, A. Gácsi, A. Kovács, M.B. Szűcs, S. Berkó, E. Csányi, Following-up skin penetration of lidocaine from different vehicles by Raman spectroscopic mapping, J. Pharm. Biomed. Anal. 154 (2018) 1–6. doi:10.1016/j.jpba.2018.02.056.

[202] Y. Pyatski, Q. Zhang, R. Mendelsohn, C.R. Flach, Effects of permeation enhancers on flufenamic acid delivery in Ex vivo human skin by confocal Raman microscopy, Int. J. Pharm. 505 (2016) 319–328. doi:10.1016/j.ijpharm.2016.04.011.

[203] R. Krombholz, Y. Liu, D.J. Lunter, In-Line and Off-Line Monitoring of Skin Penetration Profiles Using Confocal Raman Spectroscopy, Pharmaceutics. 13 (2021) 67. doi:10.3390/pharmaceutics13010067.

[204] S. Tfaili, C. Gobinet, G. Josse, J.F. Angiboust, M. Manfait, O. Piot, Confocal Raman microspectroscopy for skin characterization: A comparative study between human skin and pig skin, Analyst. 137 (2012) 3673–3682. doi:10.1039/c2an16292j.

[205] R. Gautam, S. Vanga, F. Ariese, S. Umapathy, Review of multidimensional data processing approaches for Raman and infrared spectroscopy, EPJ Tech. Instrum. 2 (2015) 8. doi:10.1140/epjti/s40485-015-0018-6.

[206] S. Stöckel, J. Kirchhoff, U. Neugebauer, P. Rösch, J. Popp, The application of Raman spectroscopy for the detection and identification of microorganisms, J. Raman Spectrosc. 47 (2016) 89–109. doi:10.1002/jrs.4844.

[207] C.S. Choe, J. Lademann, M.E. Darvin, Lipid organization and stratum corneum thickness determined in vivo in human skin analyzing lipid–keratin peak (2820–3030 cm−1) using confocal Raman microscopy, J. Raman Spectrosc. 47 (2016) 1327–1331. doi:10.1002/jrs.4975.

[208] C. Choe, J. Schleusener, S. Choe, J. Ri, J. Lademann, M.E. Darvin, Stratum corneum occlusion induces water transformation towards lower bonding state: a molecular level in vivo study by confocal Raman microspectroscopy, Int. J. Cosmet. Sci. 42 (2020) 482–493. doi:10.1111/ics.12653.

[209] F. Bonnier, S.M. Ali, P. Knief, H. Lambkin, K. Flynn, V. McDonagh, C. Healy, T.C. Lee, F.M. Lyng, H.J. Byrne, Analysis of human skin tissue by Raman microspectroscopy: Dealing with the background, Vib. Spectrosc. 61 (2012) 124–132. doi:10.1016/j.vibspec.2012.03.009.

[210] L.T. Kerr, H.J. Byrne, B.M. Hennelly, Optimal choice of sample substrate and laser wavelength for Raman spectroscopic analysis of

biological specimen, Anal. Methods. 7 (2015) 5041–5052. doi:10.1039/c5ay00327j.

[211] M. Procházka, Biological and Medical Physics, Biomedical Engineering Surface-Enhanced Raman Spectroscopy Bioanalytical, Biomolecular and Medical Applications, n.d. http://www.springer.com/series/3740.

[212] S. Mujica Ascencio, C.S. Choe, M.C. Meinke, R.H. Müller, G. V. Maksimov, W. Wigger-Alberti, J. Lademann, M.E. Darvin, Confocal Raman microscopy and multivariate statistical analysis for determination of different penetration abilities of caffeine and propylene glycol applied simultaneously in a mixture on porcine skin ex vivo, Eur. J. Pharm. Biopharm. 104 (2016) 51–58. doi:10.1016/j.ejpb.2016.04.018.

[213] G. Yu, G. Zhang, C.R. Flach, R. Mendelsohn, Vibrational spectroscopy and microscopic imaging: novel approaches for comparing barrier physical properties in native and human skin equivalents, J. Biomed. Opt. 18 (2012) 061207. doi:10.1117/1.JBO.18.6.061207.

[214] D.J. Lunter, How confocal is confocal raman microspectroscopy on the skin? Impact of microscope configuration and sample preparation on penetration depth profiles, Skin Pharmacol. Physiol. 29 (2016) 92–101. doi:10.1159/000444806.

[215] M. Zou, B. Barton, G. Geertz, R. Brüll, Accurate determination of the layer thickness of a multilayer polymer film by non-invasive multivariate confocal Raman microscopy, Analyst. 144 (2019) 5600–5607. doi:10.1039/c9an00664h.

[216] N. Uzunbajakava, A. Lenferink, Y. Kraan, B. Willekens, G. Vrensen, J. Greve, C. Otto, Nonresonant Raman imaging of protein distribution in single human cells, Biopolym. - Biospectroscopy Sect. 72 (2003) 1–9. doi:10.1002/bip.10246.

[217] G. Pezzotti, Raman piezo-spectroscopic analysis of natural and synthetic biomaterials, (n.d.). doi:10.1007/s00216-004-2780-1.

[218] D. Tuschel, Selecting an excitation wavelength for raman spectroscopy, Spectroscopy. 31 (2016) 14–23.

[219] S. Tfaili, G. Josse, C. Gobinet, J.F. Angiboust, M. Manfait, O. Piot, Shedding light on the laser wavelength effect in Raman analysis of skin epidermises, Analyst. 137 (2012) 4241–4246. doi:10.1039/c2an16115j.

[220] B.W. Barry, H.G.M. Edwards, A.C. Williams, Fourier transform Raman and infrared vibrational study of human skin: Assignment of spectral bands, J. Raman Spectrosc. 23 (1992) 641–645. doi:10.1002/jrs.1250231113.

[221] V. Rouchon, H. Badet, O. Belhadj, O. Bonnerot, B. Lavódrine, J.G. Michard, S. Miska, Raman and FTIR spectroscopy applied to the conservation report of paleontological collections: Identification of Raman and FTIR signatures of several iron sulfate species such as ferrinatrite and sideronatrite, J. Raman Spectrosc. 43 (2012) 1265–1274. doi:10.1002/jrs.4041.

[222] L. Binder, E.M. Kulovits, R. Petz, J. Ruthofer, D. Baurecht, V. Klang, C. Valenta, Penetration monitoring of drugs and additives by ATR-FTIR spectroscopy/tape stripping and confocal Raman spectroscopy – A comparative study, Eur. J. Pharm. Biopharm. 130 (2018) 214–223. doi:10.1016/j.ejpb.2018.07.007.

[223] A.A. Makki, F. Bonnier, R. Respaud, F. Chtara, A. Tfayli, C. Tauber, D. Bertrand, H.J. Byrne, E. Mohammed, I. Chourpa, Qualitative and quantitative analysis of therapeutic solutions using Raman and infrared spectroscopy, Spectrochim. Acta Part A Mol. Biomol. Spectrosc. 218 (2019) 97–108. doi:10.1016/j.saa.2019.03.056.

[224] C.A. Téllez Soto, L.P. Medeiros-Neto, L. dos Santos, A.B.O. Santos, I. Ferreira, P. Singh, R.A. Canevari, A.A. Martin, Infrared and confocal Raman spectroscopy to differentiate changes in the protein secondary structure in normal and abnormal thyroid tissues, J. Raman Spectrosc. 49 (2018) 1165–1173. doi:10.1002/jrs.5370.

[225] D. F.H.Wallach, S. P.Verma, F. Jeffrey, Application of laser Raman and infrared spectroscopy to the analysis of membrane structure, Biochim. Biophys. Acta - Rev. Biomembr. 559 (1978) 153–208.

[226] A. Opitz, M. Wirtz, D. Melchior, A. Mehling, H.W. Kling, R.H.H. Neubert, Improved method for stratum corneum lipid analysis by automated multiple development HPTLC, Chromatographia. 73 (2011) 559–565. doi:10.1007/s10337-011-1913-x.

[227] E.N. Tessema, T. Gebre-Mariam, S. Lange, B. Dobner, R.H.H. Neubert, Potential application of oat-derived ceramides in improving skin barrier function: Part 1. Isolation and structural characterization, J. Chromatogr. B Anal. Technol. Biomed. Life Sci. 1065–1066 (2017) 87–95. doi:10.1016/j.jchromb.2017.09.029.

[228] R. Martins Cardoso, S. Absalah, M. Van Eck, J.A. Bouwstra, Barrier lipid composition and response to plasma lipids: A direct comparison

of mouse dorsal back and ear skin, Exp. Dermatol. 29 (2020) 548–555. doi:10.1111/exd.14106.

[229] M. Ochalek, S. Heissler, J. Wohlrab, R.H.H. Neubert, Characterization of lipid model membranes designed for studying impact of ceramide species on drug diffusion and penetration, Eur. J. Pharm. Biopharm. 81 (2012) 113–120. doi:10.1016/j.ejpb.2012.02.002.

[230] J. van Smeden, H. Al-Khakany, Y. Wang, D. Visscher, N. Stephens, S. Absalah, H.S. Overkleeft, J.M.F.G. Aerts, A. Hovnanian, J.A. Bouwstra, Skin barrier lipid enzyme activity in Netherton patients is associated with protease activity and ceramide abnormalities, J. Lipid Res. 61 (2020) 859–869. doi:10.1194/jlr.ra120000639.

[231] J. Van Smeden, M. Janssens, W.A. Boiten, V. Van Drongelen, L. Furio, R.J. Vreeken, A. Hovnanian, J.A. Bouwstra, Intercellular skin barrier lipid composition and organization in netherton syndrome patients, J. Invest. Dermatol. 134 (2014) 1238–1245. doi:10.1038/jid.2013.517.

[232] S. Chermprapai, F. Broere, G. Gooris, Y.M. Schlotter, V.P.M.G. Rutten, J.A. Bouwstra, Altered lipid properties of the stratum corneum in Canine Atopic Dermatitis, Biochim. Biophys. Acta - Biomembr. 1860 (2018) 526–533. doi:10.1016/j.bbamem.2017.11.013.

[233] L. Opálka, A. Kováčik, P. Pullmannová, J. Maixner, K. Vávrová, Effects of omega-O-acylceramide structures and concentrations in healthy and diseased skin barrier lipid membrane models, J. Lipid Res. 61 (2020) 219–228. doi:10.1194/jlr.RA119000420.

[234] Z. Luo, C. Liu, P. Quan, Y. Zhang, L. Fang, Effect of Chemical Penetration Enhancer-Adhesive Interaction on Drug Release from Transdermal Patch: Mechanism Study Based on FT-IR Spectroscopy, 13C NMR Spectroscopy, and Molecular Simulation, AAPS PharmSciTech. 22 (2021) 1–14. doi:10.1208/s12249-021-02055-1.

[235] T. Berkers, D. Visscher, G.S. Gooris, J.A. Bouwstra, Topically Applied Ceramides Interact with the Stratum Corneum Lipid Matrix in Compromised Ex Vivo Skin, Pharm. Res. 35 (2018) 1–13. doi:10.1007/s11095-017-2288-y.

[236] M. Gunnarsson, E.H. Mojumdar, D. Topgaard, E. Sparr, Extraction of natural moisturizing factor from the stratum corneum and its implication on skin molecular mobility, J. Colloid Interface Sci. 604 (2021) 480–491. doi:10.1016/j.jcis.2021.07.012.

2. Objectives

The primary goal of this research was to determine the effects of a series of PEGylated emulsifiers on skin barrier and dermal drug delivery properties. The SC and skin penetration properties were evaluated using the CRS analytical instrument. Simultaneously, it aimed to develop optimized procedures for future use in the skin field. Based on the overall concept of this thesis, the following aims were summarized:

- To collect and statistically compare available lipid-related Raman spectral signals using ex-vivo skin samples.
- To identify the most sensitive and effective Raman signals for determining the lipid content, lipid lateral packing order, lipid conformational order, and thickness of SCs.
- To investigate the influences of a series of PEGylated emulsifiers with varying hydrophilic chain, hydrophobic chain, and saturation degree on SC lipids.
- To select optimal CRS configurations, including objectives and pinhole sizes, for precisely determining SC thickness and SC lipid content.
- To find the influences of a group of PEG-stearyl ethers with extended hydrophilic chains on altering SC thickness.
- To investigate the effectiveness of selected PEGylated emulsifiers in enhancing the penetration of different model drugs.
- To compare the application of CRS and conventional tape stripping method in analyzing dermal drug delivery of actives.
- To evaluate the effects of a mixed PEGylated emulsifier system on SC's molecular and penetration properties.
- To determine the relationship between the CMC values of emulsifiers or emulsifier mixtures and skin interruptions.
- To assess the suitability and applicability of different CRS laser wavelengths in analyzing SC and skin samples.

3. Selective and sensitive spectral signals on confocal Raman spectroscopy for detection of ex vivo skin lipid properties

Yali Liu, Dominique Jasmin Lunter*

Department of Pharmaceutical Technology, Faculty of Science, Eberhard Karls Universität Tübingen, Auf der Morgenstelle 8, 72076 Tuebingen, Germany

Graphical Abstract
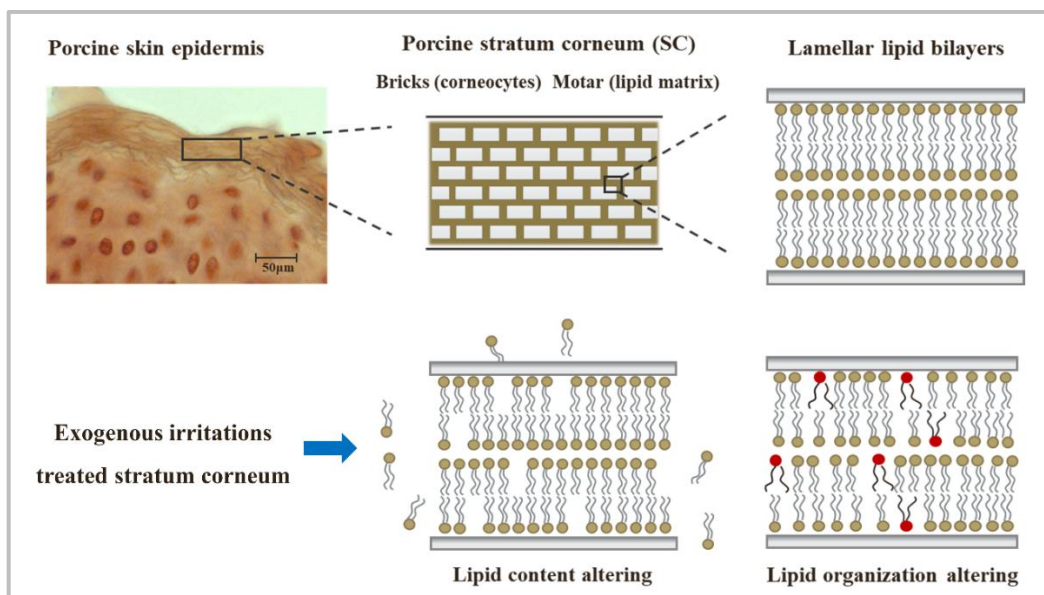
FULL ARTICLE

Selective and sensitive spectral signals on confocal Raman spectroscopy for detection of ex vivo skin lipid properties

Yali Liu [ID] | Dominique Jasmin Lunter

Department of Pharmaceutical Technology, Faculty of Science, Eberhard Karls Universität Tübingen, Tuebingen, Germany

Correspondence
Dominique Jasmin Lunter, Department of Pharmaceutical Technology, Faculty of Science, Eberhard Karls Universität Tübingen, Auf der Morgenstelle 8, 72076 Tuebingen, Germany.
Email: dominique.lunter@uni-tuebingen.de

Abstract

Spectral signals of stratum corneum (SC) acquired from confocal Raman spectroscopy (CRS) are employed to track lipid variations and the most sensitive and efficient signals are of high interest. Herein, 1% of sodium lauryl sulfate treated SC was compared to water-treated one to evaluate statistical difference of spectral signals concerning lipid content, SC thickness and lipid molecular structures. Results showed that peak ratio of 1425 to 1490 cm^{-1} and 1630 to 1710 cm^{-1} in fingerprint region and Gaussian-function deconvoluted lipid-keratin peak ratio in high wavenumber (HWN) region were both responsive for analyzing lipid content. SC thickness measurement using the full width of half-maximum (FWHM) of 2920 to 2960 cm^{-1} signal presented good sensitivity. Nevertheless, the shift of peak 2850 cm^{-1} indicated less sensitivity compared to trans-gauche peak signals and 1300 cm^{-1} peak position for lipid conformation analysis. Meanwhile, the ratio of peak 2880 and 2850 cm^{-1} indicating lipid lateral packing structure presented to be less responsive. More strikingly, FWHM of peak 2850 cm^{-1} appeared to be unable for lipid lateral packing order analysis in our study. In summary, this research can serve as a pilot study for further investigation of direct drug delivery and interaction between topical applied compounds and skin components.

KEYWORDS

confocal Raman spectroscopy, intercellular lipids, skin, spectral signals, stratum corneum
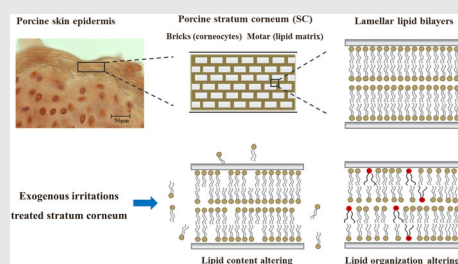
1 | INTRODUCTION

The skin forms an outermost interfacial film of the human body separating the external environment with various unique properties to protect the body against external irritations. It consists of different layers and the stratum corneum (SC) as the uppermost layer plays an important role to provide a solid basis [1–4]. Among the SC components, the highly organized multilamellar lipid matrix serves as the key for making the SC to be special to constitute the main barrier function, leading to the fact that the lipid-related information is of great interest to

reflect the state of the skin [5–7]. In previous studies, the changes in lipid content and structural properties have been extensively evidenced with the effects of dermal products, skin aging, solar UV radiation and a variety of skin diseases, for example, atopic dermatitis, psoriasis and lamellar ichthyosis [8–12]. The reduction of SC lipid content and disordering of the lipid lateral packing and trans-gauche conformation are usually the observed behaviors which thus, make them the targets to be analyzed to represent skin barrier function.

With the importance of aforementioned lipid properties, a variety of emerging techniques come into service, such as high-performance thin-layer chromatography (HPTLC), Fourier transform infrared spectroscopy (FTIR), small-angle X-ray scattering (SAXS), and so forth [13, 14]. Compared with HPTLC and SAXS, confocal Raman spectroscopy (CRS) as a powerful tool presents advantages to be noninvasive to monitor the molecular distributions/quantifications and structures of skin components simultaneously without complex sample preparations. Besides, it allows the dimensional series of spectral data acquisition and avoids the interference from solvents when compared to FTIR [15–17]. With those benefits, CRS has been widely employed in skin research and especially in lipid analysis. The pioneer work that referred to the spectral assignments of skin lipids was first carried out by Barry et al. who applied the Fourier transform Raman demonstrating the molecular conformational changes induced by chemical treatment of human skin [18]. Besides, Caspers et al also demonstrated that the lipid content can be obtained in straightforward by the means of CRS [19].

So far, plenty of lipid-related spectral features have been established for diverse parameters, like lipid content, lateral and conformational structural analysis [20, 21]. Ali et al have summarized the ceramides-related Raman descriptors with their thermotropic behaviors. The well-discussed spectral markers including C—C skeletal stretching (1060-1130 cm^{-1}) for trans-gauche conformation, the CH$_2$ twisting mode relevant to the intrachain conformational order and the CH$_2$ twisting peak linked to the lipid lateral packing crystalline state have been determined [22, 23]. More recently, Choe et al applied some extra spectral signals originated from the FTIR analysis of lipids for studying the lipid-related differences of aging, depth profiling and skin oil treatments [24–26]. It was proposed that the Gaussian-deconvoluted C—H stretching region (2800-3050 cm^{-1}) can be used to calculate the lipid content with the lipid-keratin peak ratio. The position and full width of half-maximum (FWHM) of peak 2850 cm^{-1} could be used to successfully determine the lipid trans-gauche conformation and lateral packing state simultaneously [27]. However, on the

second thought, some of those existing spectral signals can sometimes give us the same information about skin properties [28, 29]. At this point, what is the most appropriate and responsive spectral signal to use would be the primary concern. The employment of less sensitive spectral signals would, to some extent, underestimate or overestimate the actual value and condition of skin. We, therefore, in this study, focus on finding the capability of spectral signals for analyzing intercellular lipid properties since currently only limited information is available concerning this issue.

We aim to collect the available lipid-related spectral signals and statistically compare their application to ex vivo skin samples. Herein, the porcine skin is used as model for its morphological and structural similarities with human skin since it has been demonstrated to have less variability toward SC thickness, lipid compositions and drug penetration and permeation behaviors [30]. Subsequently, sodium lauryl sulfate (SLS) and water are employed on the skin samples by utilizing Franz diffusion cells, respectively, to assess their impact on SC lipid properties via CRS. Water was used as a negative control, whereas SLS was employed here as positive control due to its wide application and demonstration in many studies to exhibit harsh influence of topical applications and percutaneous absorption of exogenous substances. It has been proved to dramatically damage the skin barrier function, extract skin lipids and disrupt skin lipid organization [31–33]. Thus, the statistical difference of SLS-treated SC compared with water-treated SC would be an appropriate evaluation for filtrating selective and sensitive CRS spectral signals. By analyzing their significant differences, the most sensitive and selective lipid-related spectral signals could be determined and the present study could lay the foundation for further relevant lipid analysis by using Raman spectroscopy.

2 | MATERIALS AND METHODS

2.1 | Materials

SLS was achieved from Cognis GmbH & Co. KG (Düsseldorf, Germany). Trypsin type II- S and trypsin inhibitor were provided by Sigma-Aldrich Chemie GmbH (Steinheim, Germany). Parafilm was obtained from Bemis Company Inc (Oshkosh, Wisconsin). Sodium chloride, disodium hydrogen phosphate, potassium dihydrogen phosphate and potassium chloride were of European Pharmacopeia grade. All aqueous solutions were prepared with ultrapure water (Elga Maxima, High Wycombe, UK).

Porcine ears (German land race; age: 15-30 weeks; weight: 40-65 kg) were supplied by Department of Experimental Medicine at University of Tuebingen. The

department of Pharmaceutical Technology in University of Tuebingen has been registered for the use of animal products (registration number: DE 08 416 1052 21).

2.2 | Dermatomed porcine ear skin

Fresh porcine ears were cleaned with isotonic saline and removed from cartilage. After cleaned from blood, the full skin sheets were dried with soft tissue, wrapped with aluminum foil and stored in freezer at −30°C. On the day of experiment, skin sheet was thawed to room temperature, cut into strips of approximately 3 cm width and stretched onto a Styrofoam plate (wrapped with aluminum foil) with pins. Hairs were then shaved to 0.5 mm with electric hair clippers (QC5115/15, Philips, Netherlands). Subsequently, the skin was cut with dermatome to thickness of 0.8 mm (Dermatome GA 630, Aesculap AG & Co. KG, Tuttlingen, Germany) and punched out for circles to a diameter of 25 mm. The procedure has previously been described in ref. [34].

2.3 | Skin incubation and SC isolation

Dermatomed skin circle was held with clamp between donor and accepter chambers of Franz diffusion cells. The acceptor compartment was filled with 12 mL of degassed and prewarmed phosphate buffer saline (pH 7.4). The receptor fluid was stirred at speed of 500 rpm. A total volume of 1 mL of water and 1% SLS were topically applied on the excised skin individually in the donor compartment and capped with a piece of parafilm for preventing water evaporation. The equipped cells were kept at 32°C in water bath. After 4 hours incubation, the skin was gently washed with isotonic saline and cotton swabs for 30 times to clean the remaining samples on skin surface. The actual involved area (15 mm in diameter) of skin was punched out and patted dry with cotton swabs.

Subsequently, the obtained skin sheets were placed dermal side down on the filter paper soaked with 0.2% trypsin. After digestion for overnight, SC was peeled off and washed with 0.05% trypsin inhibitor for 1 minute. The isolated SC was cleaned with purified water for minimum of five times to remove underlayer tissues and dried in desiccator for minimum of 3 days. These methods have been detailly described by our group [35].

2.4 | Confocal Raman microspectroscopy

SC sheets were mounted on the scan table of alpha 500 R confocal Raman microscope (WITec GmbH, Ulm,

Germany) for collecting measurements. The instrument is equipped with UHTS 300 spectrometer, DV401-BV CCD camera and 532-nm laser source. Laser power was set at 10 mW with optimal power meter (PM100D, Thorlabs GmbH, Dachau, Germany) for protecting the SC sheets from thermal damage. Measurements in the spectral region between 400 and 3800 cm^{-1} were obtained with the backscattered light from skin dispersed by optical grating of 600 g/mm and analyzed on charge-coupled device (DV401-BV CCD detector, −60°C). A ×100 objective (numerical aperture 0.9, EC Epiplan-neofluor, Carl Zeiss, Germany) was used incoporated with 50 μm confocal size. The actual depth resolution in this study was around 1.25 μm. This CRS measurements were performed based on the method developed by Zhang et al [36, 37]. The example of the skin spectrum obtained is shown in Figure 1.

2.5 | Determination of skin surface and thickness

CRS spectra were recorded with the focus point starting from −50 μm beneath the skin up to 50 μm above the skin with 1 μm step size. The skin surface was determined based on the intensity profile of keratin signal ($\nu(CH_3)$, 2920-2960 cm^{-1}) which was plotted with the area under the curve (AUC) of keratin signal against scan depth. The point of half the value of maximum keratin intensity was identified as the boundary between skin surface and air or between glass slide and skin bottom. As Figure 2 shows, the point on profile consistent with the boundary between skin and air was set as skin surface. Accordingly, SC thickness was calculated based on detection of skin surface and bottom. Thus, the FWHM was set as SC thickness [37].

2.6 | Lipid content analysis

As presented in Table 1, peak 1425 to 1490 cm^{-1} is relevant to the $\delta(CH_2, CH_3)$-mode for proteins and most of the intercellular lipids. Peak 1630 to 1710 cm^{-1} corresponds to the $\nu(C=O)$-mode for amide-I, showing least variations for SC detection from different donors. Thereby, with extraction of lipids, the AUC of peak 1425 to 1490 cm^{-1} becomes lower and the relative AUC can be calculated by the normalization of amide I peak [38, 39]. According to the equation of normalized lipids = $AUC_{1425\ to\ 1490}/AUC_{1630\ to\ 1710}$, lipid content can be analyzed in fingerprint region.

In high wavenumber (HWN) region, since lipid and keratin related peaks overlapped to a broad peak, four
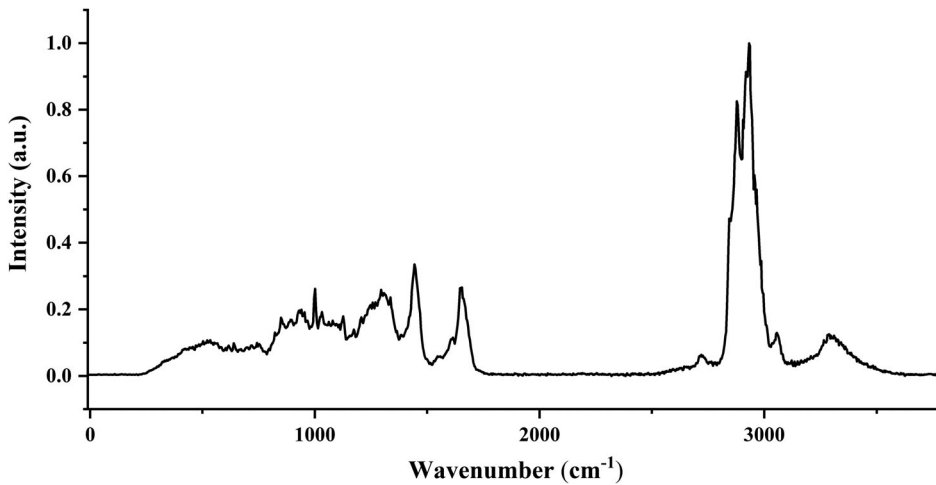
FIGURE 1 Example of stratum corneum (SC) spectrum achieved by the confocal Raman spectroscopy (CRS) instrument in this study
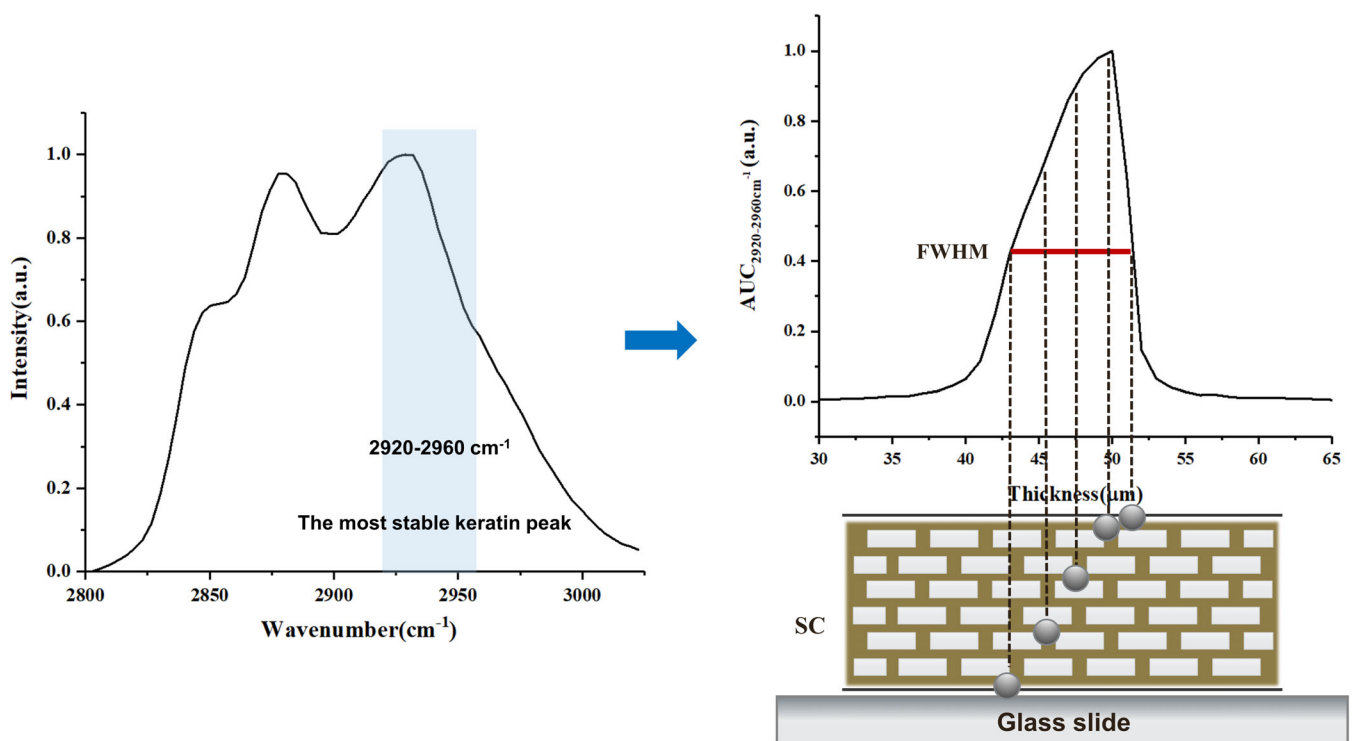
FIGURE 2 Schematic overview of thickness determination by plotting the area under the curve of keratin signal (2920-2960 cm^{-1}) against depth

Gaussian functions are applied for deconvolution process which is automatically performed by applying curve fitting toolbox on MATLAB software (MathWorks, version R2019a) [26]. The goodness of fitting results is generated with R^2 greater than .98. As shown in Figure 3, peaks around 2850 and 2880 cm^{-1} correspond to ν(C—H) symmetric and ν(C—H) asymmetric stretching mode of lipids. Peaks at 2930 and 2980 cm^{-1} are assigned to ν(CH$_3$) symmetric and ν(CH$_3$) asymmetric stretching mode of keratin [40]. Thus, lipid content is calculated as

the equation of Normalized$_{lipid}$ = (AUC$_{2880}$ + AUC$_{2850}$)/ (AUC$_{2930}$ + AUC$_{2980}$).

2.7 | Lipid conformational organization

In fingerprint region, peaks originated from C—C skeleton vibration mode are sensitive to lipid trans-gauche conformation. Peak 1080 cm^{-1} represents gauche-conformation (disordered state) while peaks at 1060 and

TABLE 1 Relevant peak assignments of spectral signals on Raman for analyzing lipid properties

Wavenumber (cm^{-1})	Major assignment	Origin of peak
1060	ν(C—C) skeleton, trans-conformation	Lipids
1080	ν(C—C) skeleton, gauche-conformation	Lipids
1130	ν(C—C) skeleton, trans-conformation	Lipids
1300	δ(CH$_2$) twisting	Lipids
1425-1490	δ(CH$_2$, CH$_3$) vibration	Lipids
1450	δ(CH$_2$) scissoring	Lipids
1630-1710	Amide-I, ν(C=O) vibration	Keratin
2850	ν(C—H) symmetric vibration	Lipids
2880	ν(C—H) asymmetric vibration	Lipids
2930	ν(CH$_3$) symmetric vibration	Keratin
2980	ν(CH$_3$) asymmetric vibration	Keratin

Note: ν denotes the stretching vibrations and δ represents the bending vibration modes.
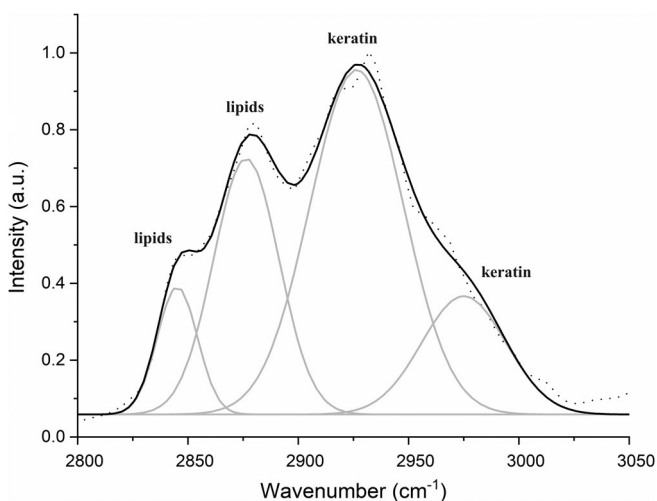
FIGURE 3 Deconvolution of lipid-keratin spectrum into four Gaussian components. Dotted line represents the smoothed line of raw spectral data; the solid lines are the fitted curves

FIGURE 4 Lipid signals at 1050 to 1150 cm^{-1} on Raman spectrum of porcine skin originated from C—C skeleton vibration. Principle component analysis (PCA) has been employed to reduce the noise of variations. Background subtraction based on the fitting of polynomial function has been applied and marked with red dotted line

1130 cm^{-1} correspond to all-trans conformation (ordered state) [41]. As presented in Figure 4, these peaks have lower intensity and narrow band shape. To decrease spectra noise and obtain precise calculation, principle component analysis (PCA) is applied here and the first three components are used for reconstruction. Detailed description has been introduced elsewhere [42]. With the equation of conformational order = AUC$_{1080}$/(AUC$_{1060}$ + AUC$_{1130}$), higher value indicates more disordered state of lipids. The spectral signal of CH$_2$ twisting mode at 1300 cm^{-1} in fingerprint region serves as another signal. It has been defined that this peak shifts to higher wavenumber represents lipid transformation to more conformational disordered state [22, 43].

In HWN region, peak 2850 cm^{-1} is assigned to ν(C—H) symmetric stretching mode and has been introduced by Berkers et al to examine the conformational ordered-disordered transitions of lipids. With this peak shifts to higher wavenumber area, lipid conformational state tends to be more gauche and disordered [44].

2.8 | Lipid lateral packing state

In fingerprint region, peak 1430 to 1470 cm^{-1} corresponding to the CH$_2$ scissoring vibration mode is relevant to the lateral packing state (orthorhombic order, hexagonal order, and liquid-like chain packing) of intercellular lipids. It was introduced to reflect the nature of lateral packing between ceramide molecules. The peak shifts to higher wavenumber area reflects the tendency to more hexagonal or liquid like lateral packing state [45].

In HWN region, the overlapping of peaks at 2850 and 2880 cm^{-1} is properly corrected due to deconvolution process. Hereby, Ratio$_{lat}$ = AUC$_{2880}$/AUC$_{2850}$ is calculated and determined as a criterion for evaluating lipid lateral packing state. A lower value indicates the presence of orthorhombic phase of SC lipids whereas higher value represents more hexagonal or liquid phase [42]. Furthermore, FWHM of peak 2850 cm^{-1} is achieved in
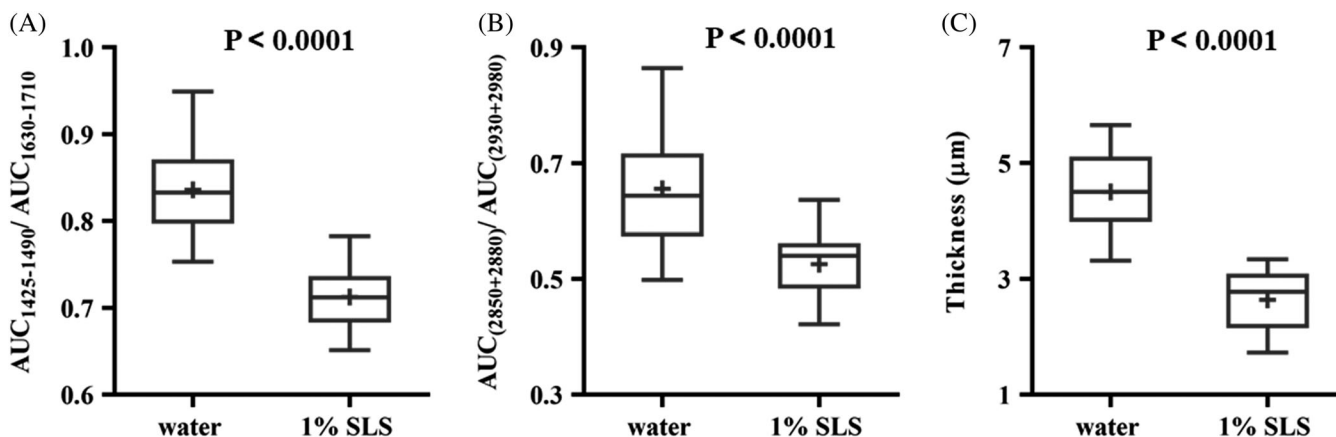
FIGURE 5 Box and whisker plots (min to max) comparing the significant difference between water and 1% sodium lauryl sulfate (SLS)-treated skin samples: A, normalized lipid content in fingerprint region; B, peak shift of CH_2 twisting mode; and C, thickness measurements. The line in the box represents the median and the plus sign represents the mean

the meantime and was introduced by Snyder et al to be relevant to lipid packing state. It has been reported that the broader the FWHM is, the more orthorhombic structures and densely packed states the SC lipid is [46].

2.9 | Data analysis

Data preprocessing steps of obtained CRS spectra were performed using the spectral cosmic ray removal, smoothing and background subtraction on WITec Project Software (WITec GmbH, Ulm, Germany). In smoothing process, Savitzky-Golay (SG) filter was applied with third polynomial order and nine smoothing point. For background subtraction, an automatic polynomial function was fitted to the spectrum and subtracted.

Statistical evaluation was performed using MATLAB software, WITec Project Software and GraphPad Prism 7.0 (GraphPad Software Inc., La Jolla, California). AUC extracted in this study is the integrated area under a specified peak of the spectrum and is calculated using trapezoidal method. Statistical differences were determined by applying unpaired student's t test. Significant differences were presented with different range of P-values. Spectra data obtained from this study were from repeated measurements ($n \geq 18$).

3 | RESULTS

3.1 | Spectral signals for analyzing lipid content and SC thickness

In fingerprint region, the ratio of $AUC_{1425 \text{ to } 1490}/AUC_{1630 \text{ to } 1710}$ was utilized for lipid content calculation. As shown

in Figure 5A, water-treated SCs have obviously higher lipid content compared to SLS-treated SCs, indicating that SLS treatment on skin leads to a huge amount of extraction of lipids from SC. The difference between these two groups is found to be strongly significant ($P < .0001$).

In HWN region, the ratio of $(AUC_{2880} + AUC_{2850})/(AUC_{2930} + AUC_{2980})$ was calculated. It is clearly visible from Figure 5B that the mean value of water-treated SCs is around 0.65, higher than that of SLS-treated SCs of about 0.52. Difference between these two groups is strongly significant ($P < .0001$), indicating that both spectral signals in fingerprint and HWN region could be effectively applied for detecting skin lipid content.

The thickness of isolated and dried SCs appeared to be thinner and to have lower values. As shown in Figure 5C, the average value of water-treated SC thickness is around 4.5 μm. With the treatment of SLS, the SC thickness extremely declined to the average value around 2.5 μm. With SLS treatment, SC thickness presented significant ($P < .0001$) thinner compared to water-treated SC.

3.2 | Spectral signals for analyzing lipid conformation

Figure 6A shows the result of trans-gauche conformational order calculated by spectral signal of C—C skeleton vibration mode. It is clear that water-treated SCs have lower values of ratio $AUC_{1080}/(AUC_{1060} + AUC_{1130})$ whereas SLS-treated SCs have higher values. Statistically differences between these two groups are found to be highly significant ($P < .0001$). Figure 6B shows the average position of the band around 1300 cm^{-1} obtained from

(A)

(B)

(C)
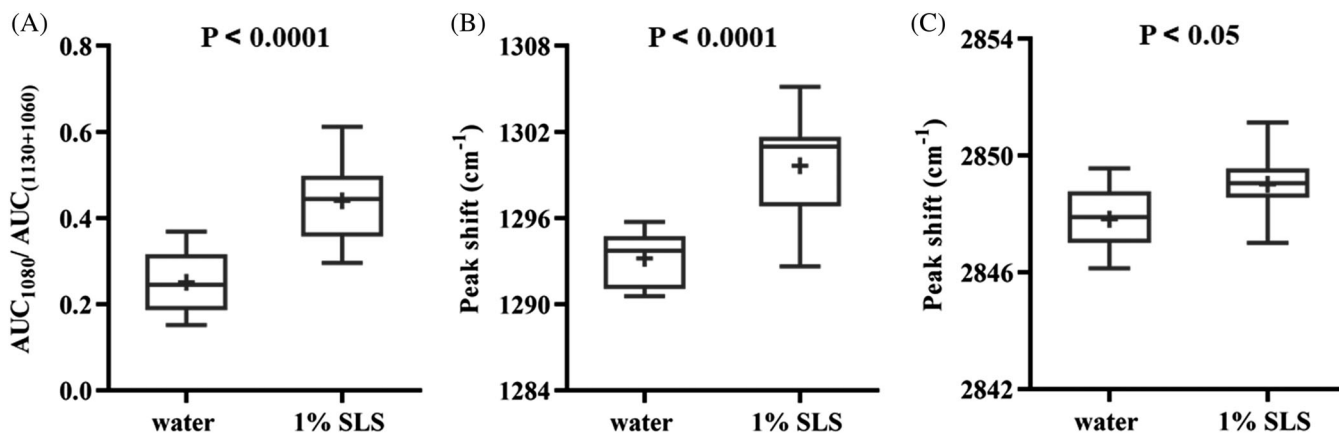
FIGURE 6 Box and whisker plots (min to max) comparing the significant difference between water and 1% sodium lauryl sulfate (SLS)-treated skin samples: A, lipid conformation analysis by C—C skeleton vibration; B, normalized lipid content in HWN region; and C, band shift of peak 2850 cm^{-1}. The line in the box represents the median and the plus sign represents the mean

(A)

(B)

(C)
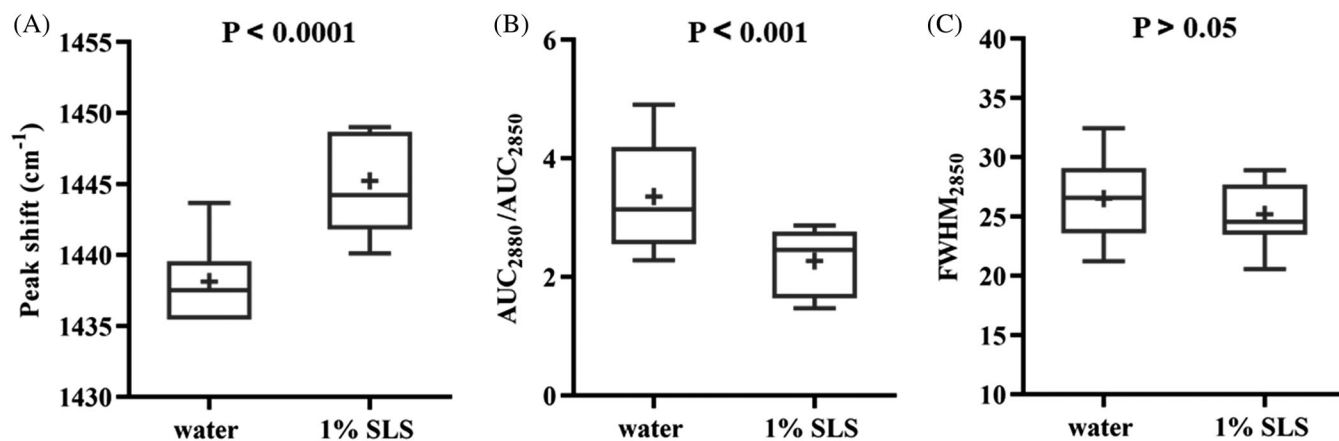
FIGURE 7 Box and whisker plots (min to max) comparing the significant difference between water and 1% sodium lauryl sulfate (SLS)-treated skin samples: A, peak shift of CH$_2$ scissoring mode; B, lateral packing order analyzed by AUC ratio of band 2850 and 2880 cm^{-1}; C, FWHM of peak 2850 cm^{-1}. The line in the box represents the median and the plus sign represents the mean

fingerprint region. It is visible that the mean value of peak position of water-treated group is largely lower than that of SLS treatment group. Comparing these two groups, statistical difference appears highly significant ($P < .0001$). Both results demonstrate that the treatment of SLS changes the intercellular lipid conformation to more gauche (less-ordered) state. They also suggest that both spectral signals are proper and sensitive for detecting the lipid conformational alteration.

The lipid conformational order of skin can be represented by using the shift of band at around 2850 cm^{-1} in HWN region. Figure 6C shows that the treatment of SLS on skin increased the wavenumber of band position, indicating the tendency of intercellular lipid conformational organization to gauche state. The differences are only statistically significant ($P < .05$), in comparison to the strong significance of the other two signals.

3.3 | Spectral signals for analyzing lipid lateral packing state

In fingerprint region, CH$_2$ scissoring vibration mode was monitored. As shown in Figure 7A, comparing the average peak position of water-treated SCs at around 1437 cm^{-1}, the one of SLS-treated SCs shifts to higher wavenumber area of around 1444 cm^{-1}. Statistical difference is highly significant ($P < .0001$) which means that the great effects of SLS in interrupting skin lipid structure and altering the lateral packing state to be more hexagonal or even liquid state can be detected reliably.

In HWN region, Figure 7B shows that the SLS-treated skin samples have obviously lower average value of Ratio$_{lat}$ than water-treated group which indicates less ordered lateral packing organization of skin lipids after SLS treatment. However, there is only modest difference appeared ($P < .001$),

indicating less prevalence can be detected with this spectral signal for analyzing lateral packing state. As presented in Figure 7C, although the mean value of $FWHM_{2850}$ of water-treated skin is higher than that of SLS-treated skin, no significant difference is found ($P > .05$). It means that this spectral signal may not be fully sensitive for analyzing the difference of lipid lateral packing organization.

4 | DISCUSSION

In the present study, spectral signals for detecting skin lipid properties were selected. The results of lipid content analysis in both fingerprint and HWN region were in good correlation and showed great sensitivity. It demonstrates that after curve fitting process, the lipid-keratin peak ratio in HWN region could be used as a proper and highly responsive lipid signal. Nevertheless, compared to the direct calculation of lipid content in fingerprint region, deconvolution process in HWN region is more time-consuming and less convenient. Furthermore, SC thickness was detected to be reduced after SLS treatment. This is in accordance to the previous results showing the decreased skin thickness after treatment of different emulsifiers [37]. The statistical difference was found to be strongly significant, demonstrating that the investigation of SC thickness is available to evaluate the extent of lipid reduction and further reflects the skin barrier condition.

C—C skeleton vibration mode and CH_2 twisting mode have been proved to be able to analyze the lipid conformational arrangement. However, C—C skeleton vibration bands are consisted of three small peaks. PCA analysis and polynomial background subtraction are needed to remove noise and obtain more precise results (Figure 4). Meanwhile, peak 1130 cm^{-1} contains part of the contribution of keratin at 1125 cm^{-1}. Thus, an adequate integration area should be selected to eliminate the influence of keratin peak [47]. Comparing a series complicated data processing steps, the prominent peak shift of CH_2 twisting mode would be a better choice and less time-consuming. Besides, the result of Figure 6C revealed that the detected difference was less pronounced using the spectral signal of peak shift of $\nu(C—H)$ symmetric stretching mode since only slight statistical difference was found. Water-SLS are the extremes effects in between can possibly not be detected reliably using this signal.

For lipid lateral packing order analysis, CH_2 scissoring mode revealed the most significant difference which was deemed to be the most outstanding signal. In HWN region, the signal of $Ratio_{lat}$ only appeared modest statistical difference which may not be fully detectable for the alteration of skin properties. The signal of $FWHM_{2850}$ was discovered to be unable to monitor the lipid lateral

packing as no significant difference was found which is contradictory to the findings of other groups, who claimed that the FWHM of band 2850 cm^{-1} is sensitive to the crystallographic properties of intercellular lipids [27, 46]. One explanation might be the errors and differences caused by the deconvolution process. Although the deconvolution process has eliminated the influence from the keratin signal, the differences between the results of SLS-treated SC and water-treated SC are not large enough to reach statistical significance. This finding illustrates that this signal is better not to be used for further analysis as it may underestimate the interaction of topical applied substances and SC lipids.

In summary, it seems that the spectral signals in fingerprint region have better sensitivity and feasibility than those in HWN region although the peak interference has been eliminated by deconvolution process. The application of less-sensitive spectral signals will affect the accuracy of evaluating skin lipid properties. The employment of the most appropriate signals will better monitor the penetration and irritation of applied products for cosmetic and pharmaceutical development.

5 | CONCLUSION

This study focuses on evaluating selective spectral signals on CRM for analyzing skin lipid properties. The prominent changes of skin lipid content and structures were caused by SLS treatment and different spectral signals were applied for assessing the extent of SLS influence. The results of quantification of lipid extraction including lipid content analysis and SC thickness detection were of great correlation and all signals showed relatively high sensitivity. On the other hand, spectral signals in fingerprint region were more responsive than those in HWN region for lipid conformation and later packing order analysis.

Overall, this work can serve as a pilot study for further estimation and evaluation for skin properties. The assessment of different lipid signals is meaningful to filtrate more sensitive spectral features for deeper differentiations. These findings should also be taken into consideration for future investigation with the application of different spectral signals.

CONFLICT OF INTEREST
Both the authors declare no potential conflicts of interest.

ETHICS STATEMENT

Porcine ears were achieved from Department of Experimental Medicine of University Hospital Tuebingen. Live animals used were kept at Department of Experimental Medicine and sacrificed in the course of their experiments, which are approved by the ethics committee of University Hospital Tuebingen. Those ears were received directly after the death of the animals. Prior to study, Department of Pharmaceutical Technology has registered for the use of animal products at the District Office of Tuebingen (registration number: DE 08 416 1052 21).

ORCID

Yali Liu https://orcid.org/0000-0002-3170-7178

REFERENCES

[1] L. Norlén, *J. Invest. Dermatol.* **2001**, *117*, 830.

[2] M. J. Cork, *J. Dermatolog. Treat.* **1997**, *8*(suppl 1), S7.

[3] J. A. Bouwstra, M. Ponec, *Biochim. Biophys. Acta Biomembr.* **2006**, *1758*, 2080.

[4] J. Bouwstra, G. Pilgram, G. Gooris, H. Koerten, M. Ponec, *Skin Pharmacol. Appl. Skin Physiol.* **2001**, *14*, 52.

[5] T. Schmitt, R. H. H. Neubert, *Chem. Phys. Lipids* **2018**, *216*, 91.

[6] R. R. Warner, K. J. Stone, Y. L. Boissy, *J. Invest. Dermatol.* **2003**, *120*, 275.

[7] J. A. Bouwstra, G. S. Gooris, J. A. van der Spek, W. Bras, *J. Invest. Dermatol.* **1991**, *97*, 1005.

[8] M. Lodén, A. C. Andersson, *Br. J. Dermatol.* **1996**, *134*, 215.

[9] A. Tfayli, E. Guillard, M. Manfait, A. Baillet-Guffroy, *Eur. J. Dermatol.* **2012**, *22*, 36.

[10] E. Boireau-Adamezyk, A. Baillet-Guffroy, G. N. Stamatas, *Ski. Res. Technol.* **2014**, *20*, 409.

[11] S. Chermprapai, F. Broere, G. Gooris, Y. M. Schlotter, V. P. M. G. Rutten, J. A. Bouwstra, *Biochim. Biophys. Acta Biomembr.* **2018**, *1860*, 526.

[12] K. Biniek, K. Levi, R. H. Dauskardt, *Proc. Natl. Acad. Sci. U. S. A.* **2012**, *109*, 17111.

[13] A. Hinder, C. E. H. Schmelzer, A. V. Rawlings, R. H. H. Neubert, *Skin Pharmacol. Physiol.* **2011**, *24*, 127.

[14] V. S. Thakoersing, J. van Smeden, W. A. Boiten, G. S. Gooris, A. A. Mulder, R. J. Vreeken, A. el Ghalbzouri, J. A. Bouwstra, *Exp. Dermatol.* **2015**, *24*, 669.

[15] D. W. Shipp, F. Sinjab, I. Notingher, *Adv. Opt. Photon.* **2017**, *9*, 315.

[16] G. P. S. Smith, C. M. McGoverin, S. J. Fraser, K. C. Gordon, *Adv. Drug Deliv. Rev.* **2015**, *89*, 21.

[17] Atta-ur-Rahman, (Ed.), *Studies in Natural Products Chemistry*, Elsevier, Amsterdam, Netherlands, Vol. 61, **2018**.

[18] B. W. Barry, H. G. M. Edwards, A. C. Williams, *J. Raman Spectrosc.* **1992**, *23*, 641.

[19] P. J. Caspers, G. W. Lucassen, R. Wolthuis, H. A. Bruining, G. J. Puppels, *Biospectroscopy* **1998**, *4S5*, S31.

[20] A. C. Williams, H. G. M. Edwards, B. W. Barry, *J. Raman Spectrosc.* **1994**, *25*, 95.

[21] S. Wartewig, R. Neubert, W. Rettig, K. Hesse, *Chem. Phys. Lipids* **1998**, *91*, 145.

[22] A. Tfayli, E. Guillard, M. Manfait, A. Baillet-Guffroy, *Anal. Bioanal. Chem.* **2010**, *397*, 1281.

[23] E. Guillard, A. Tfayli, M. Manfait, A. Baillet-Guffroy, *Anal. Bioanal. Chem.* **2011**, *399*, 1201.

[24] C. Choe, J. Schleusener, J. Lademann, M. E. Darvin, *J. Dermatol. Sci.* **2017**, *87*, 183.

[25] C. S. Choe, J. Schleusener, J. Lademann, M. E. Darvin, *Mech. Ageing Dev.* **2018**, *172*, 6.

[26] C.-S. Choe, J. Lademann, M. E. Darvin, *Laser Phys.* **2014**, *24*, 105601.

[27] C. S. Choe, J. Lademann, M. E. Darvin, *J. Raman Spectrosc.* **2016**, *47*, 1327.

[28] K. Biniek, A. Tfayli, R. Vyumvuhore, A. Quatela, M. F. Galliano, A. Delalleau, A. Baillet-Guffroy, R. H. Dauskardt, H. Duplan, *Exp. Dermatol.* **2018**, *27*, 901.

[29] S. M. Ali, F. Bonnier, A. Tfayli, H. Lambkin, K. Flynn, V. McDonagh, C. Healy, T. Clive Lee, F. M. Lyng, H. J. Byrne, *J. Biomed. Opt.* **2012**, *18*, 061202.

[30] U. Jacobi, M. Kaiser, R. Toll, S. Mangelsdorf, H. Audring, N. Otberg, W. Sterry, J. Lademann, *Ski. Res. Technol.* **2007**, *13*, 19.

[31] P. Saad, C. R. Flach, R. M. Walters, R. Mendelsohn, *Int. J. Cosmet. Sci.* **2012**, *34*, 36.

[32] K. P. Wilhelm, C. Surber, H. I. Maibach, *Arch. Dermatol. Res.* **1989**, *281*, 293.

[33] A. di Nardo, K. Sugino, P. Wertz, J. Ademola, H. I. Maibach, *Contact Dermatitis* **1996**, *35*, 86.

[34] D. J. Lunter, *J. Raman Spectrosc.* **2017**, *48*, 152.

[35] D. Lunter, R. Daniels, *J. Biomed. Opt.* **2014**, *19*, 126015.

[36] Z. Zhang, D. J. Lunter, *Eur. J. Pharm. Sci.* **2018**, *121*, 1.

[37] Z. Zhang, D. J. Lunter, *Eur. J. Pharm. Biopharm.* **2018**, *127*, 61.

[38] M. E. Darvin, C.-S. Choe, J. Schleusener, J. Lademann, *Biomed. Opt. Express* **2019**, *10*, 3092.

[39] G. N. Stamatas, J. de Sterke, M. Hauser, O. von Stetten, A. van der Pol, *J. Dermatol. Sci.* **2008**, *50*, 135.

[40] C. S. Choe, J. Schleusener, J. Lademann, M. E. Darvin, *J. Biophoton.* **2018**, *11*, 1.

[41] P. J. Caspers, G. W. Lucassen, R. Wolthuis, H. A. Bruining, G. J. Puppels, *Biospectroscopy* **1998**, *4*, S31.

[42] C. Choe, J. Lademann, M. E. Darvin, *Analyst* **2016**, *141*, 1981.

[43] M. Gniadecka, O. F. Nielsen, D. H. Christensen, H. C. Wulf, *J. Invest. Dermatol.* **1998**, *110*, 393.

[44] T. Berkers, D. Visscher, G. S. Gooris, J. A. Bouwstra, *Pharm. Res.* **2018**, *35*, 1.

[45] J. C. Schwarz, V. Klang, M. Hoppel, D. Mahrhauser, C. Valenta, *Eur. J. Pharm. Biopharm.* **2012**, *81*, 557.

[46] R. G. Snyder, S. L. Hsu, S. Krimm, *Spectrochim. Acta Part A: Mol. Spectrosc.* **1978**, *34*, 395.

[47] H. G. M. Edwards, D. E. Hunt, M. G. Sibley, *Spectrochim. Acta Part A: Mol. Biomol. Spectrosc.* **1998**, *54*, 745.

4. Systematic investigation of the effect of non-ionic emulsifiers on skin by confocal Raman spectroscopy—a comprehensive lipid analysis
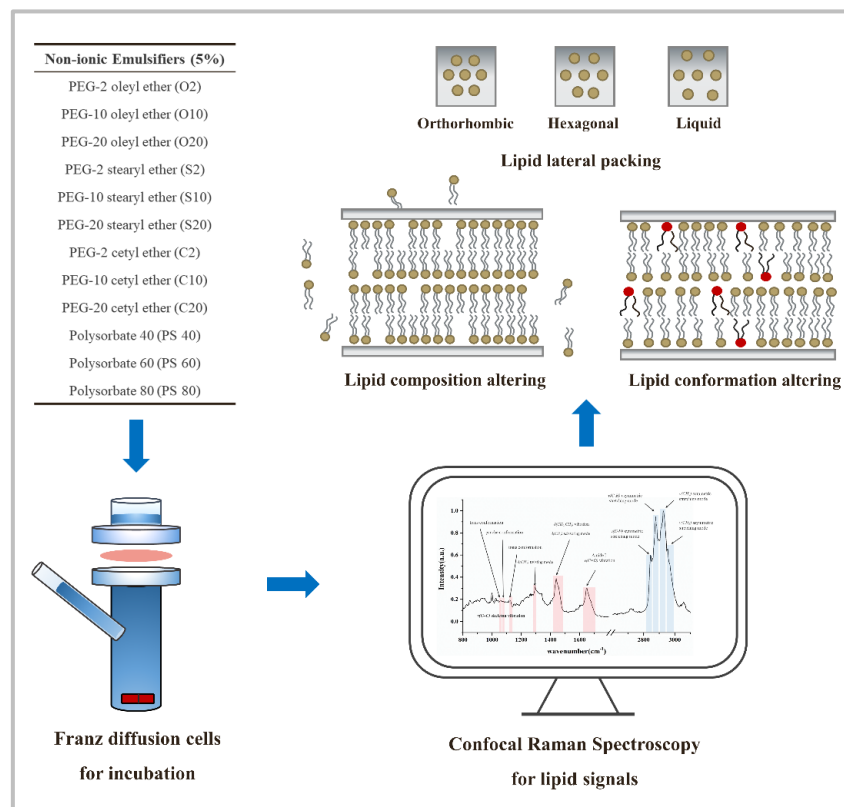
Yali Liu, Dominique Jasmin Lunter*

Department of Pharmaceutical Technology, Faculty of Science, Eberhard Karls Universität Tübingen, Auf der Morgenstelle 8, 72076 Tuebingen, Germany

Graphical Abstract

Article

Systematic Investigation of the Effect of Non-Ionic Emulsifiers on Skin by Confocal Raman Spectroscopy—A Comprehensive Lipid Analysis

Yali Liu and Dominique Jasmin Lunter *

Department of Pharmaceutical Technology, Eberhard Karls University, Auf der Morgenstelle 8,
72076 Tuebingen, Germany; cpuyali@gmail.com
* Correspondence: dominique.lunter@uni-tuebingen.de; Tel.: +49-7071-297-4558; Fax: +49-7071-295-531

Abstract: Non-ionic emulsifiers are commonly found in existing pharmaceutical and cosmetic formulations and have been widely employed to enhance the penetration and permeation of active ingredients into the skin. With the potential of disrupting skin barrier function and increasing fluidity of stratum corneum (SC) lipids, we herein examined the effects of two kinds of non-ionic emulsifiers on intercellular lipids of skin, using confocal Raman spectroscopy (CRS) with lipid signals on skin CRS spectrum. Non-ionic emulsifiers of polyethylene glycol alkyl ethers and sorbitan fatty acid esters were studied to obtain a deep understanding of the mechanism between non-ionic emulsifiers and SC lipids. Emulsifier solutions and dispersions were prepared and applied onto excised porcine skin. Water and sodium laureth sulfate solution (SLS) served as controls. SC lipid signals were analysed by CRS regarding lipid content, conformation and lateral packing order. Polyethylene glycol (PEG) sorbitan esters revealed no alteration of intercellular lipid properties while PEG-20 ethers appeared to have the most significant effects on reducing lipid content and interrupting lipid organization. In general, the polyoxyethylene chain and alkyl chain of PEG derivative emulsifiers might indicate their ability of interaction with SC components. HLB values remained critical for complete explanation of emulsifier effects on skin lipids. With this study, it is possible to characterize the molecular effects of non-ionic emulsifiers on skin lipids and further deepen the understanding of enhancing substance penetration with reduced skin barrier properties and increased lipid fluidity.

Keywords: non-ionic emulsifiers; intercellular lipids; confocal Raman spectroscopy (CRS); polyethylene glycol alkyl ethers; polyethylene glycol sorbitan fatty acid esters

1. Introduction

Skin represents the largest organ of the human organism and forms the outermost barrier film that protects the human body from external environment impacts and exogenous irritations and corrosions. Stratum corneum (SC) is the uppermost layer of the skin, composed of a highly ordered, multilamellar lipid matrix with embedded flattened, keratin-filled corneocytes [1,2]. The particular intercellular lipids in SC consist of ceramides, free fatty acids and cholesterol in an approximately equimolar ratio [3,4]. It has been well accepted that intercellular lipids in SC play an important role in maintaining skin barrier function and keeping the skin in a proper hydration state [5]. The removal and organizational alteration of intercellular lipids would disrupt the barrier function from multiple aspects and deteriorate into some chronic skin diseases [6,7]. With the importance of assuring the solid structures and ordered properties of skin lipids, it is essential to monitor the molecular lipid interactions with exposed substances and maintain the protective barrier state for further optimization of dermatological treatments.

In everyday life, the skin is exposed to different environments and mostly exposed to various sanitary and cosmetic products and cleansers. Among the main components of them, non-ionic emulsifiers have been widely used and become the potential class to be exposed on the skin and may simultaneously interact with molecular skin components [8,9]. Although non-ionic emulsifiers are usually considered to be relatively safe and better tolerated in comparison to cationic and anionic emulsifiers, they have been proved having the potential to interact with biological membranes, especially skin, with their increasing applications [10–12]. In particular, recent studies from our group found that polyethylene glycol (PEG)-20 glycerol monostearate displayed negative effects on skin lipid extraction and structural disruption while polysorbate 80 reflected no such effects [13,14]. For this reason, the selection and usage of non-ionic emulsifiers in pharmaceutical and cosmetic formulations are currently of high interest. In order to gain mechanistic insights into their skin effects, PEG alkyl ethers and sorbitan fatty acid esters (e.g., polysorbate or Tween) were taken into consideration which are both non-ionic PEG derivatives. They are composed of a hydrophilic polyoxyethylene head group and a lipophilic alkyl chain. Keeping constant either of these two parts, the other part of size and chain length etc. would be potential parameters to monitor the governing rules [15]. Furthermore, these two groups of emulsifiers are widely applied in cosmetic and dermal products due to their solubility and viscosity properties with low toxicity according to the existing safety assessments identified in previous studies [16,17]. We therefore chose to further investigate these two groups of emulsifiers in a systematic approach and evaluate their possibilities for prospective development of skin products with relatively mild effects on skin lipids [18].

Up to now, considerable number of studies have made efforts on obtaining more information about the quantitative and structural properties of skin lipids [19–21]. The means of small- and wide-angle X-ray scattering, neutron scattering, and liquid chromatography coupled with mass spectrometry have been intensively applied. However, those methodologies have potential risks of sample contamination, being time-consuming and sample destruction [22,23]. In this area confocal Raman spectroscopy (CRS) has emerged as a promising non-invasive tool in skin research and caught increasing attention for skin characterizations such as skin penetration and permeation of topically applied materials [24,25]. CRS is also an efficient and label-free method and has been increasingly used to study the macroscopic alterations of skin properties with humidity changes, age difference and hair removal comparisons [26–28]. Detailed information about biochemical molecules can be obtained from CRS, including the chemical structure, phase and molecular interactions. Recent findings from our group have demonstrated that CRS could be used as an alternative method to analyze lipid extraction and conformation in SC [13,14]. Based on this proof and listed advantages, CRS was used in this study as a useful and convenient approach for lipid analysis.

For studying the physiological parameters of SC lipids, many researchers have focused on finding spectral signals in CRS for skin research [29,30]. Those spectral signals in this study are the identified Raman bands associated with molecular vibrations of lipids inside the skin. They are originated from the methylene ($-CH_2-$) and methyl ($-CH_3$) groups in lipid molecular structures. Using them a comprehensive study measuring lipid content, conformational order, lateral packing order and SC thickness could be conducted at the same time. However, the skin CRS spectrum is extremely complex and the lipid-derived Raman bands usually overlap with bands originating from molecular vibrations of proteins [19,31]. In order to track the individual lipid-related spectral signals, a Gaussian-function based mathematical procedure could be applied on account of a previous report from Choe et al. [32].

As we know, many hypotheses regarding the interactions between emulsifiers and skin are still not well grounded [33], making it essential to perform a systematic investigation of non-ionic emulsifiers. Therefore, the aim of this study is to use different lipid-related spectral signals to analyse the interactions between non-ionic emulsifiers and intercellular lipids. PEG alkyl ethers and sorbitan fatty acid esters were selected. To the best of our knowledge, this is the first systematic report considering PEG derivatives with different number of oxyethylene groups and different hydrophobic alkyl chain lengths using CRS to better understand their mechanism of influence on skin components.

Results should be helpful to find a rule for further selections of non-ionic emulsifiers which is beneficial to the development of skin products.

2. Materials and Methods

2.1. Materials

PEG alkyl ethers including PEG-2 oleyl ether (O2), PEG-10 oleyl ether (O10), PEG-20 oleyl ether (O20), PEG-2 stearyl ether (S2), PEG-10 stearyl ether (S10), PEG-20 stearyl ether (S20), PEG-2 cetyl ether (C2), PEG-10 cetyl ether (C10), PEG-20 cetyl ether (C20) were purchased from Croda GmbH, (Nettetal, Germany). PEG sorbitan fatty acid esters containing PEG-20 sorbitan monopalmitate (Polysorbate 40, PS40), PEG-20 sorbitan monostearate (Polysorbate 60, PS60), PEG-20 sorbitan monooleate (Polysorbate 80, PS80) were obtained from Caesar & Loretz GmbH (Hilden, Germany). Sodium lauryl sulfate (SLS) was obtained from Cognis GmbH & Co. KG (Düsseldorf, Germany). Trypsin type II- S (lyophilized powder) and trypsin inhibitor (lyophilized powder) were obtained from Sigma-Aldrich Chemie GmbH (Steinheim, Germany). Parafilm® was from Bemis Company Inc., (Oshkosh, WI, USA). Sodium chloride, disodium hydrogen phosphate, potassium dihydrogen phosphate, and potassium chloride were of European Pharmacopoeia grade. All aqueous solutions were prepared with ultra-pure water (Elga Maxima, High Wycombe, UK). Porcine ear skins (German land race; age: 15 to 30 weeks; weight: 40 to 65 kg) were provided by Department of Experimental Medicine at the University of Tuebingen. The Department of Pharmaceutical Technology at the University of Tuebingen has been registered for the use of animal products [13].

2.2. Preparation of Dermatomed Porcine Ear Skin

Porcine ear skin was selected as substitute for human skin in this study due to their histologically and morphologically similarity with human skin [34,35]. Porcine ears used in this study were achieved from the Department of Experimental Medicine of the University Hospital Tuebingen. The live animals used were kept at the Department of Experimental Medicine and sacrificed in the course of their experiments, which are approved by the ethics committee of the University Hospital Tuebingen. Those ears were received directly after the death of the animals. Prior to study start, the Department of Pharmaceutical Technology has registered for the use of animal products at the District Office of Tuebingen (registration number: DE 08 416 1052 21). Fresh porcine ears were cleaned with isotonic saline. Full-thickness skin was removed from cartilage and gently cleaned from blood with cotton swabs and isotonic saline. The obtained postauricular skin sheets were then dried with soft tissue, wrapped with aluminium foil and stored in freezer at −30 °C. On the day of experiment, skin sheet was thawed to room temperature, cut into strips of approximately 3 cm width and stretched onto a Styrofoam plate (wrapped with aluminium foil) with pins to minimize the effect of furrows. Skin hairs were trimmed to approximately 0.5 mm with electric hair clippers (QC5115/15, Philips, Netherlands). Subsequently, the skin was dermatomed to a thickness of 0.8 mm (Dermatom GA 630, Aesculap AG & Co. KG, Tuttlingen, Germany) and punched out for circles to a diameter of 25 mm.

2.3. Incubation of Porcine Ear Skin in Franz Diffusion Cells

Franz diffusion cells have been commonly used as a specific analytical setup for ex vivo determination of skin absorption. Here, degassed, prewarmed (32 °C) phosphate buffered saline (PBS) was used as receptor fluid and filled in the Franz diffusion cells of 12 mL. The stirring speed of the receptor fluid was 500 rpm. The dermatomed skin circles were mounted onto the cells with donor compartment on above. The equipped Franz diffusion cells were put into water bath with temperature of 32 °C. After a short equilibrium of 30 min, 1 mL of each emulsifier solution/dispersion was applied to each skin sample (all non-ionic emulsifiers used in this study are listed in Table 1 with detailed information). Then, a piece of parafilm was capped onto each donor compartment to prevent evaporation. After 4 h incubation, skin samples were removed from cells and each skin surface was gently washed and cleaned with isotonic saline and cotton swabs for 30 times in order to remove the

remaining samples and avoid erroneous measuring result. Finally, the actual application area (15 mm in diameter) was punched out and patted dry with cotton swabs. This part of the method has been detailly described by our group [13].

Table 1. Characteristics of non-ionic emulsifiers including polyethylene glycol (PEG) alkyl ethers and PEG sorbitan esters used in this study.

Non-Ionic Emulsifiers	Alkyl Chain	Alkyl Chain LENGTH and Saturation	Number of Oxyethylene Group	Abbreviations	HLB Value
PEG-2 oleyl ether	Oleyl alcohol	C18, C9–C10 unsaturated	2	O2	5.0
PEG-10 oleyl ether	Oleyl alcohol	C18, C9–C10 unsaturated	10	O10	12.4
PEG-20 oleyl ether	Oleyl alcohol	C18, C9–C10 unsaturated	20	O20	15.3
PEG-2 stearyl ether	Stearyl alcohol	C18	2	S2	4.9
PEG-10 stearyl ether	Stearyl alcohol	C18	10	S10	12.4
PEG-20 stearyl ether	Stearyl alcohol	C18	20	S20	15.3
PEG-2 cetyl ether	Cetyl alcohol	C16	2	C2	5.3
PEG-10 cetyl ether	Cetyl alcohol	C16	10	C10	12.9
PEG-20 cetyl ether	Cetyl alcohol	C16	20	C20	15.7
PEG-20 sorbitan monopalmitate	Palmitic acid	C16	20	PS40	15.6
PEG-20 sorbitan monostearate	Stearic acid	C18	20	PS60	14.9
PEG-20 sorbitan monooleate	Oleic acid	C18, C9–C10 unsaturated	20	PS80	15

2.4. Isolation of Stratum Corneum

The stratum corneum was isolated following the trypsin digestion process as described by Kligman et al. and Zhang [14,36]. This isolation procedure has been proved to have no influence on the lamellar lipid organization [37]. The obtained skin circles (with diameter of 15 mm) from last step were placed dermal side down on filter paper soaked with a 0.2% trypsin and PBS solution. After the incubation of skin sample for overnight at room temperature, digested SC was peeled off gently and immersed into 0.05% trypsin inhibitor solution for 1 min. Afterwards, the isolated SC was washed with fresh purified water for min. five times to remove the underlayer tissues. The final obtained SC sheet was then placed onto glass slide and stored in desiccator to dry for min. three days.

2.5. Confocal Raman Spectroscopy (CRS)

In order to investigate the effects of different non-ionic emulsifiers on SC, CRS served as the primary instrument to detect their differences. After drying, the SC sheets were taken out of the desiccator and fitted onto the scan table of alpha 500 R confocal Raman microscope (WITec GmbH, Ulm, Germany). This CRS device was equipped with a 532-nm excitation laser, UHTS 300 spectrometer and DV401-BV CCD camera. To avoid the damage of skin sample due to higher laser intensity, the laser power used was 10 mW, which could be adjusted using the optimal power meter (PM100D, Thorlabs GmbH, Dachau, Germany). A 100× objective with numerical aperture of 0.9 (EC

Epiplan-neofluor, Carl Zeiss, Jena, Germany) was used to focus the light on skin surface. The backscattered light from the skin was then dispersed by an optical grating (600 g/mm) to achieve the spectral range from 400–3800 cm^{-1}. Collected scattered light was analysed on a charge-coupled device (DV401-BV CCD detector) which had been cooled down to −60 °C in advance. The CRS measurements were performed based on a method developed by Zhang et al. [13,14].

2.6. Determination of Skin Surface and Thickness

In order to achieve spectral signals of lipids from skin surface and measure SC thickness at the same time, the spectra were detected with the focus point moving from −50 μm beneath the skin to 50 μm above the skin. The spectra were recorded with the step size of 1 μm. The skin surface was determined using the intensity difference of keratin signal (ν (CH$_3$), 2920–2960 cm^{-1}). The area under the curve (AUC) of the keratin peak was calculated and plotted against depth. While the intensity of the keratin signal reaches the half maximum, the laser spot would be located at the boundary between glass slide and skin bottom or the boundary between skin surface and air [13,38]. So that the spectrum extracted from the boundary between skin surface and air was regarded as skin surface and used for lipid signal analysis. Moreover, with the description above, the full width of half maximum (FWHM) could serve as the thickness of skin sample.

2.7. Lipid Signals in Fingerprint Region

2.7.1. C–C Skeleton Vibration Mode

The first three small peaks in Figure 1 highlighted in red are assigned to the vibration of C–C skeleton. They are sensitive to the trans–gauche conformational order of long chain hydrocarbons which exist mostly in intercellular lipids [39,40]. The peaks located at 1060 cm^{-1} and 1130 cm^{-1} arise from all-trans conformation which stand for a more ordered state of lipids. The peak at 1080 cm^{-1} corresponds to the gauche conformation which represents a more disordered state of lipids [41,42]. In this case, PCA analysis and polynomial background subtraction are needed to remove the noise and obtain a more precise result. On the other hand, the band at 1130 cm^{-1} contains part of the contribution of keratin at 1125 cm^{-1}. As a result, an adequate integration area is selected to eliminate the influence of keratin peak. Then, the conformational order could be calculated with the ratio of AUC of those three peaks: conformational order = AUC$_{1080}$ / (AUC$_{1060}$ + AUC$_{1130}$) as originally described by Snyder, et al. [43]. Thus, a higher value of conformational order represents an indication to the gauche conformation and disordered state of lipids.

2.7.2. CH$_2$ Twisting and Scissoring Mode

The peak located at about 1300 cm^{-1} in Figure 1 is assigned to the CH$_2$ twisting mode. The shift of this peak could also indicate the order or disorder of lipid conformations because of the sensitivity of this peak to hydrocarbon chains [44]. The broadening and shift to a higher wavenumber of this peak indicates a tendency of intercellular lipids turning into a more disordered and gauche conformation state.

Apart from the detection of conformational order on Raman spectra, vibrational characteristics are also convenient to determine the lateral packing state (orthorhombic order, hexagonal order, and liquid-like chain packing) influenced by the intramolecular interactions [44]. The CH$_2$ scissoring band at 1430–1470 cm^{-1} reflects the nature of lateral packing between ceramide molecules. The shift of this peak to a higher wavenumber in the Raman spectrum stands for a more hexagonal or even liquid like packing state.

2.7.3. CH$_2$ and CH$_3$ Stretching and C=O Vibration Mode

The last two bands marked in fingerprint region of Figure 1 are assigned to δ (CH$_2$, CH$_3$)– mode at 1425–1490 cm^{-1} and ν (C=O)– mode at 1630–1710 cm^{-1} respectively. The band at 1630–1710 cm^{-1} arises from the Amide I mode which showed the least variation within one donor or among different

donors. Thus, this band has been often used in the normalization of other Raman peaks derived from SC [30,42]. The band at 1425–1490 cm^{-1} originates from both keratins and lipids. In this study, this band was regarded as "lipids-peak" for calculation of lipid content.

Based on the equation of Normalized lipids = AUC$_{1425–1490}$/AUC$_{1630–1710}$, the lipid-keratin peak was normalized by the amide I peak. The final calculated result would indicate the content variation of lipids. Therefore, the lipid content in fingerprint region in this study was calculated as equation above.

2.8. Lipid Signals in High Wavenumber Region

In order to achieve further information about lipid content and lateral packing order state for a more precise and forceful result, the lipid-keratin peak (2800–3030 cm^{-1}) in the HWN region was taken into consideration. This band is also derived from the CH_2 and CH_3 vibrations.

2.8.1. Gaussian Deconvolution Process

As depicted in Figure 1, it is obvious that the peaks originated from lipids and keratins overlapped and formed a peak with higher intensity and broad width. In order to track the information of each peak individually, a mathematical process based on Gaussian functions was employed. As described by Choe, the Gaussian function type exhibited the least fitting error and demonstrated to be the best fitting function for Raman spectra of the skin [32].
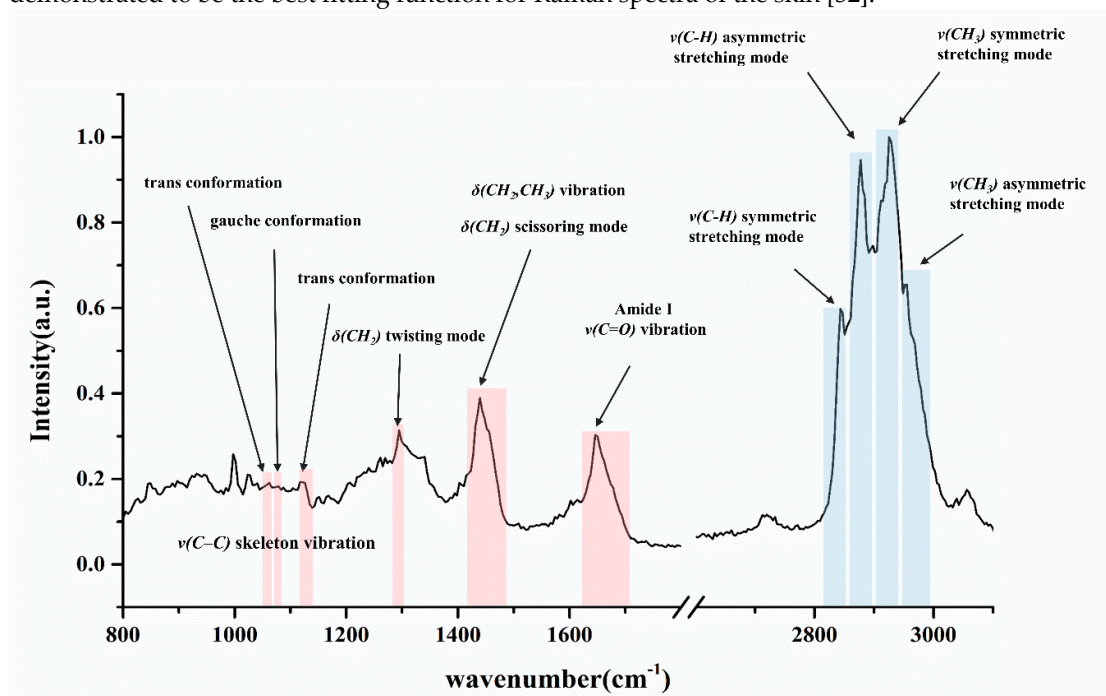
Figure 1. Major band assignments of CRS spectrum obtained from skin sample. The red/blue areas represent the specific peak referring to different molecular vibrations. The break on the axis of wavenumber separates the fingerprint region (left side) and high wavenumber region (right side). The peaks assigned to trans and gauche conformations are both originated from C–C skeleton vibration.

In this study, the obtained spectrum of SC was deconvoluted into four Gaussian peaks automatically with the application of curve fitting toolbox on Matlab software (version R2019a, MathWorks GmbH, Natick, MA, USA). The summation of four Gaussian functions was used as the fitting formula. In order to achieve reproducible result and reduce the fitting error, the Gaussian peak maximum positions and FWHMs were allowed to vary in defined intervals only. Afterwards, a non-linear iteration process was applied. It can be seen from Figure 2 that each fitted peak was labelled in

different colour. The goodness of fitting results could also be generated automatically with all R^2 above than 0.98.
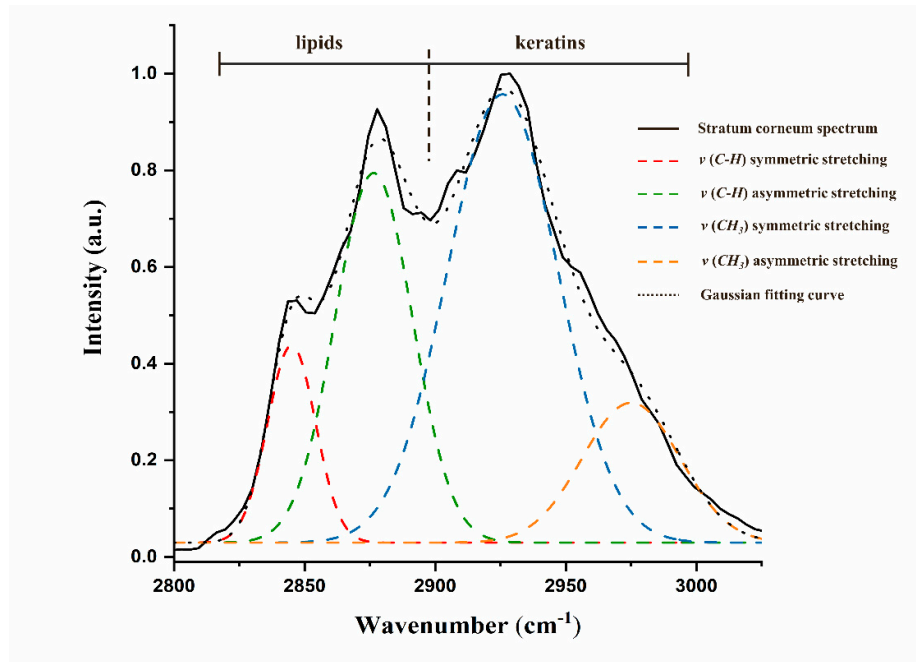
Figure 2. Deconvolution of lipid-keratin peak from skin spectrum by using four Gaussian peaks in high wavenumber region. The assignments were labelled with different colours.

2.8.2. ν (C–H) Symmetric and Asymmetric Stretching

As illustrated in Figure 2, peaks located at 2850 cm^{-1} and 2880 cm^{-1} stand for the ν (C–H) symmetric and ν (C–H) asymmetric stretching mode respectively which are both derived from the vibration of lipids. These two peaks are sensitive to the packing order of alkyl chains of lipids. Based on some research, the ratio of the intensities of these two peaks could be used as a sign of crystalline phase of intercellular lipids [39,45]. In this study, peak areas after deconvolution were applied for the calculation of lateral packings $Ratio_{lat} = AUC_{2880}/AUC_{2850}$ according to ref. [46]. This procedure has effectively eliminated the influence of multi-peak overlap phenomenon. Hereby, the higher $Ratio_{lat}$ represents a prevalence towards highly crystalline and orthorhombic phase. The lower $Ratio_{lat}$ reveals a tendency towards disordered and liquid-like phase.

2.8.3. ν (CH₃) Symmetric and Asymmetric Stretching

As is shown in Figure 2, the blue and orange peaks at 2930 cm^{-1} and 2980 cm^{-1} arise from the contribution of keratins and originated from the ν (CH₃) symmetric and ν (CH₃) asymmetric stretching separately. Previous studies often use the area of these two keratin related peaks to normalize lipid related peaks in order to determine the lipid content [47,48]. As described in this study, the AUC extracted directly in high wavenumber would contain the contribution of adjacent peaks. The deconvolution process would exclude the influence of peak superposition. As a result, the Gaussian areas after deconvolution were employed for calculation of lipid content: Normalized lipid = $(AUC_{2880} + AUC_{2850})/(AUC_{2930} + AUC_{2980})$.

2.9. Data Analysis

2.9.1. Raman Spectra Pre-Processing

The initial processing step of Raman spectra usually included the spectral cosmic ray removal, smoothing as well as background subtraction which were all performed by the WITec Project

Software (WITec GmbH). Referring to the smoothing process, Savitzky-Golay (SG) filter was applied with third polynomial order and nine smoothing point. For the type of background subtraction, an automatic polynomial function was fitted to the spectrum and subtracted. Furthermore, the AUC extracted in this study is the integrated area under a specified peak of the spectrum and could be calculated using trapezoidal method on WITec Project Software or MatLab software.

2.9.2. Principle Component Analysis

Multivariate data analysis was also performed on the WITec Project Software. For the study, Principle component analysis (PCA) was employed to further analysis the grouped spectra and reduce minor variations. PCA is the underlying method for many multivariate methods and could effectively obtain a reduced data set from multiple dimensions. Among the grouped Raman spectra, the first three principle components (PCs) are selected for reconstruction since they have contained most of essential information. In this study, PCA was applied for lipid conformation analysis.

2.9.3. Statistical Analysis

Spectra data were obtained from repeated measurements ($n \geq 18$). The graphs were shown with mean values ± standard deviations (mean ± SD). Statistical differences were determined using one-way or two-way analysis of variance (ANOVA) followed by Student-Newman-Keuls (SNK) which were employed by GraphPad Prism 7.0 (GraphPad Software Inc., La Jolla, CA, USA). Diagrams and statistical differences were ultimately generated. Significant differences were marked with different number of asterisks: * $p < 0.05$, ** $p < 0.01$, *** $p < 0.001$.

3. Results

3.1. Lipid Content Analysis with Normalized Lipid Signal

Lipid content in SC was analysed in the fingerprint and HWN regions by using lipid signals normalized by keratin signals. With the aim of detecting their impacts on lipids, different non-ionic emulsifiers were used to treat the SC, respectively. The alterations of lipid content are shown in Figure 3a,b. As can be seen, the red bars indicate the relative lipid content in fingerprint region while the blue bars represent the content in HWN region. It is evident that most of the PEG ethers cause a reduction of lipid content (Figure 3a) while all the polysorbate emulsifiers show no effects on SC lipid content (Figure 3b). Specifically speaking, the group of PEG ethers treated SC shows different extent of lipid reduction. Among them, only O2 and S2 treated SCs indicate no effects on SC lipid content. Focusing on the rest of the emulsifiers, all the PEG-20 alkyl ethers display to dramatically reduce lipid content. Regarding the PEG-10 alkyl ethers, O10 shows a relatively smaller difference compared to S10 and C10 which both indicate a greater reduction of skin lipid content. Interestingly, only C2 in PEG-2 alkyl ethers shows a slight impact on reducing lipid content. In contrast, polysorbate emulsifiers reflect completely no extraction of lipids. It turns out a part of this outcome is correlated with a previous result in our group that showed 5% of polysorbate 60 had no effects on lipids [13]. In general, the result of lipid content analysis in fingerprint region is complementary to that in HWN region and exhibited the same tendency of emulsifier effects.
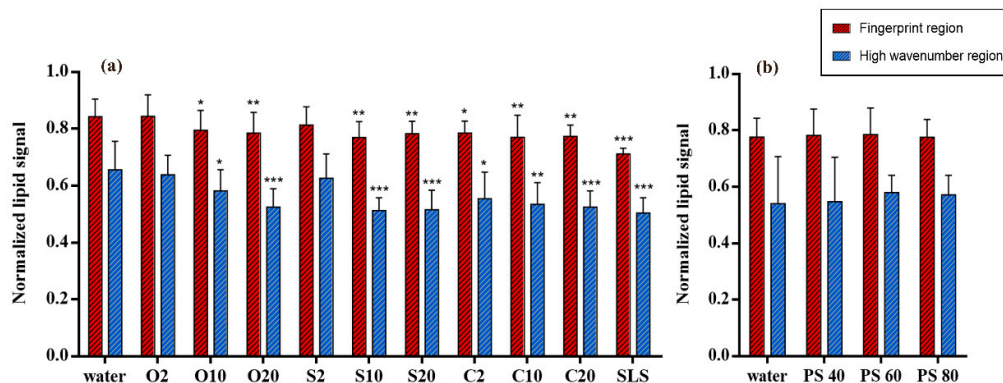
Figure 3. Normalized lipid signals in fingerprint and HWN region for lipid composition analysis of (**a**) PEG alkyl ethers treated SC and (**b**) PEG sorbitan esters treated SC. Mean ± SD, *n* = 18. * $p < 0.05$; ** $p < 0.01$; *** $p < 0.001$.

3.2. CH₂ Twisting and Scissoring Mode Analysis

CH_2 twisting mode in fingerprint region was selected in this study. It is also feasible to analyse the lipid conformational order. The band derived from CH_2 twisting mode is located at about 1300 cm⁻¹. The band shift is sensible to the conformation of hydrocarbon chains of lipids, so that it could be used as another conformational signal. Figure 4 shows the comparison of twisting mode between emulsifier treated and water treated skin samples. The peak location is in between 1285–1303 cm⁻¹. It can be clearly seen that SLS has the most significant effect on SC lipid as the band shifts from about 1293 cm⁻¹ to about 1299 cm⁻¹. Among PEG ethers, relatively higher effects on lipids are caused by the PEG ether emulsifiers with the average number of oxyethylene groups of 20 as well as O10 and S10. Interestingly, C10 only shows small effects on lipid conformation. Nevertheless, in lipid content and C–C skeleton conformation analysis presented above, C10 has been determined to strikingly extract lipids and change conformational order. Apart from this slight discordance, the result is still a confirmation of emulsifier effects on lipid signals. Further, no significant effects are noted in polysorbate emulsifier treated SCs.
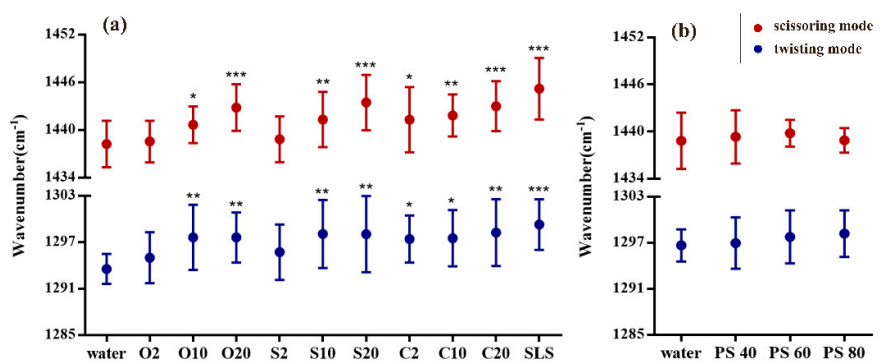
Figure 4. Lipid signals of CH_2 twisting and scissoring mode for analyzing (**a**) PEG alkyl ethers treated SC and (**b**) PEG sorbitan esters treated SC. Mean ± SD, *n* = 18. * $p < 0.05$; ** $p < 0.01$; *** $p < 0.001$.

Except for the detailed information of hydrocarbon chains of lipids, CRS is also available to determine the lateral packing of lipids with CH_2 scissoring mode in fingerprint region. Using the peak at 1434–1452 cm⁻¹, Figure 4 shows the differences of scissoring mode when comparing emulsifier treated and water treated skin samples. It can be observed that some bands strikingly shift to higher

wavenumbers after treatment with emulsifiers such as PEG-20 alkyl ethers and SLS. It means that the lateral packing tends to be transformed from orthorhombic phase to hexagonal or liquid-like phase. C10 and S10 shows to moderately lower the lateral packing density. However, the influence of O10 on SC is slightly lower than what we expected but similar to the impact of C10 on SC. In line with results from C–C skeleton vibration mode analysis, the results from scissoring mode analysis show no significant difference for polysorbate emulsifiers treated SCs.

3.3. C–C Skeleton Conformation Analysis

C–C skeleton vibrations in fingerprint region contain the all-*trans* signal (1060 cm^{-1} and 1130 cm^{-1}) and *gauche* signal (1080 cm^{-1}) of SC lipids. With the application of non-ionic emulsifiers, lipid conformation in SC was influenced to different degree. As displayed in Figure 5a, most of the PEG ethers show significant effects on lipid conformation when compared with water treated SC. Especially S10 and S20 as well as C10 and C20 present huge effects on SC lipid conformation, indicating the intercellular lipids have more gauche conformation (more disorder state). Surprisingly, O10 and O20 only show small influence on altering lipid conformation which is even less than the impact of C2. Whereas O2 and S2 show no effects on turning lipids into a more *gauche* conformation. Focusing on the investigation of the polysorbate group, it can be seen from Figure 5b that no significant difference has been found in polysorbate emulsifiers-treated SCs. It turns out that, with the application of polysorbate emulsifiers, lipid conformation remains in a more *trans* and ordered state.
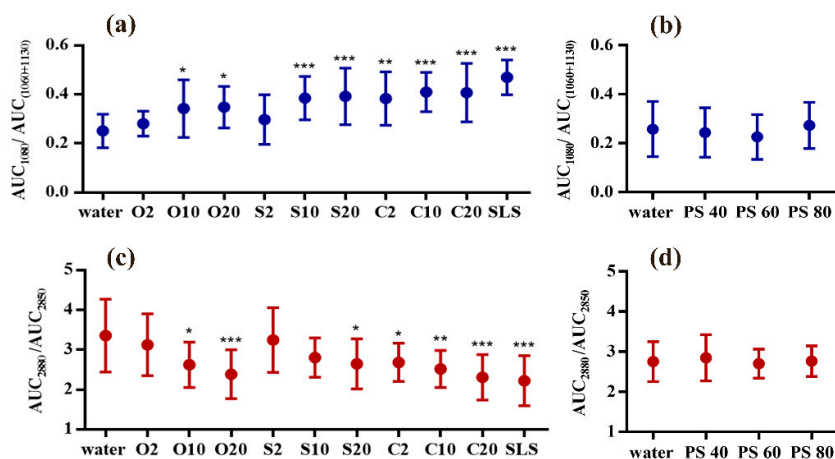
Figure 5. C–C skeleton vibration mode for lipid conformation analysis of (**a**) PEG alkyl ethers treated SC and (**b**) PEG sorbitan esters treated SC; lateral packing order analysis by AUC ratio of band 2850 cm^{-1} and 2880 cm^{-1}: (**c**) PEG alkyl ethers treated SC and (**d**) PEG sorbitan esters treated SC. Mean ± SD, *n* = 18. * $p < 0.05$; ** $p < 0.01$; *** $p < 0.001$.

3.4. Lateral Packing Analysis in HWN Region

Commonly, the broad shaped lipid-keratin peak originated from C–H vibration in HWN region is used to calculate lipid content and lipid lateral packing. The ratio of AUCs of 2880/2850 cm^{-1} has been defined to evaluate the lateral packing density of intercellular lipids. In this spectral region, peaks reflecting vibrations of SC lipids overlap with peaks derived from keratin. After the deconvolution process of lipids-keratin signals, the calculation of lateral packing in HWN is more precise owing to the exclusion of keratin peak influences.

As the results shown in Figure 5c, O20 and C20 have the highest effects on decreasing the lateral packing density which are nearly the same as the effect of SLS. C10 tends to transform the lipid structure to hexagonal phase (more disordered structure). In addition, O10, S20 as well as C2 treated SC only indicate relatively lower effects. Whereas S10 treated SC unexpectedly presents no statistical

difference which is unlike the lateral packing result shown in the scissoring mode analysis. The results depicted in Figure 5d reconfirmed that polysorbate emulsifiers appeared to exert no significant effects on SC lipids and maintained the orthorhombic structure of intercellular lipids.

3.5. Skin Thickness Measurement

The thickness of skin samples was measured after the treatment with different emulsifiers. It has to be noted that SC thickness was measured on dried SC sheets and will thus give lower values as in (hydrated) full thickness skins. With the comparison to references, the results are shown in Figure 6. It is apparent from Figure 6a that the water treated SC was measured to be the thickest with the average thickness of 4.50 ± 0.64 μm. In contrast, SLS treated SC exhibited the thinnest skin samples (2.55 ± 0.54 μm), followed by the C20 and C10 treated SC with thickness of 2.84 ± 0.69 μm and 3.27 ± 1.20 μm respectively. O10 and O20 treated SC showed a tendency towards a reduced thickness as well. Unexpectedly, no indication was found of reduction of SC thickness after treatment with S10. In another experiment depicted in Figure 6b, the water treated SC was measured to have the thickness of 4.04 ± 1.16 μm, while the polysorbate emulsifiers treated SCs showed no significant difference when compared with water treated SC.
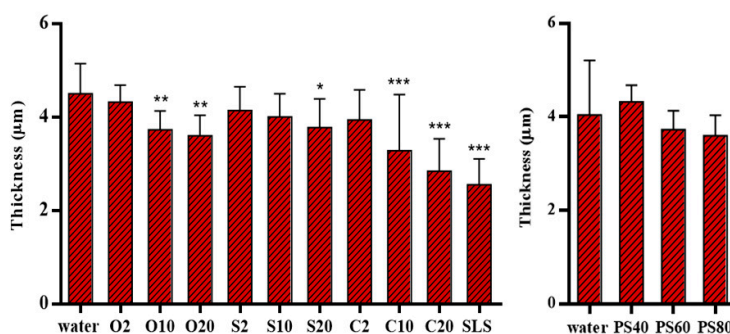
Figure 6. Thickness of SC after treatment with (**a**) PEG alkyl ethers treated SC and (**b**) PEG sorbitan esters treated SC. Mean ± SD, *n* = 18. * *p* < 0.05; ** *p* < 0.01; *** *p* < 0.001.

4. Discussion

Throughout this study, different spectral signals were utilized to analyse the effects of non-ionic emulsifiers on SC lipids. The result of lipid content analysis was achieved with the combination of lipid spectral signals from fingerprint region and HWN region. We could clearly see that PEG ethers were more capable to extract the lipids from SC than polysorbate emulsifiers. Meanwhile, both results of lipid content analysis were in good correlation with each other. It proved that after curve fitting process, the lipid-keratin peak ratio could serve as a sensitive lipid signal to calculate the lipid content. As an alternative, the lipid-keratin peak ratio in fingerprint region may be used and gives similar results.

The conformational analysis was evaluated in this study with the band shift of the twisting mode and calculated by the ratio of three small peaks related to *gauche/trans* conformation which originated from the C–C skeleton vibration bands. In view of the same tendency of detected emulsifier effects, both of the lipid spectral signals are capable to analyse lipid conformation accurately. However, comparing a series of complicated data processing steps in C–C skeleton vibration features, the prominent peak shift related to CH$_2$ twisting mode at about 1300 cm^{-1} would be a better choice and less time-consuming.

There was a slightly difference in lipid analysis of lateral packing density. The ratio calculated by 2880/2850 cm^{-1} revealed that S10 had no significant effect. Whereas the results of scissoring mode indicated significant difference ($p <$ 0.01). Although the deconvolution process has eliminated the influence of the keratin signal in the HWN region, the differences between results from S10 treated SC and water treated SC are not large enough to reach statistical significance. With the consideration

of minor errors may result from the curve fitting process, the signal of scissoring mode might provide a more sensitive and efficient detection in our further study.
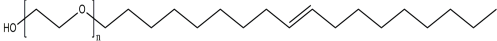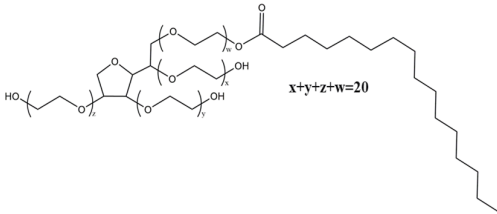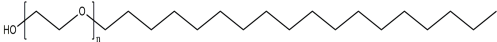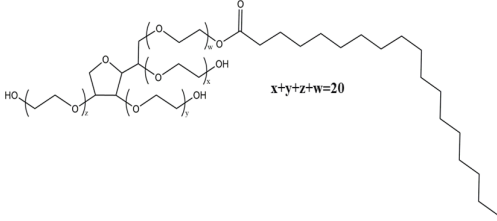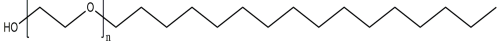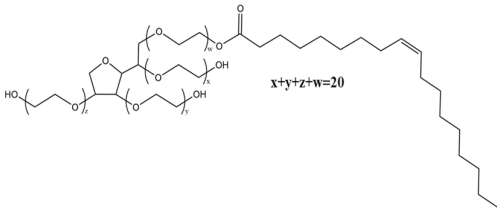
As the preliminary study of our group presented, the thinning of SC was assumptively caused by the extraction of lipids, subsequently leading to a loosened cohesion of SC and thereby fascinating keratinocytes removal [13]. In the skin thickness analysis of present work, most results complied with expectations and previous findings although the results of S10 and C2 reflected inconsistent with former lipid signals which may be triggered by the influence of different donors. The thinner the SC thickness originally, the less accurate the measuring result. Besides, the isolation of SC may also induce measurement errors.

Since this systematic study has proved that non-ionic emulsifiers have the potential to interact with SC lipids, we may find some rules or mechanisms to explain the ability of them to extract lipid components and decrease lipid order of SC. First, their capability to affect SC lipids might be governed by their structural properties as they contain both polar head region of hydrophilic chain and nonpolar tail region of hydrophobic chain. The characteristics of non-ionic emulsifiers used in this study has been listed in Table 1. As the influence of PEG ethers on SC shown, we may suggest that the higher the average number of oxyethylene groups, the stronger the interaction between PEG ethers and SC lipids. Meanwhile, the alkyl chain was highlighted in the potency of emulsifier interaction with SC lipid as well. With the results shown in this study, C2 appeared to be the only emulsifier to reduce lipid content and increase lipid disorder compared to other PEG-2 ethers. As they own the same number of oxyethylene groups, we may speculate that PEG derivatives with less carbon numbers of alkyl chain present higher ability to disturb SC lipid properties. Furthermore, keeping constant the number of carbon atoms in hydrophobic chain, similar effects of PEG oleyl ethers (unsaturated alkyl chain, C18) and PEG stearyl ethers (saturated alkyl chain, C18) on SC lipids were observed. We might then assume that with the same length of alkyl chain, the double bound only show little impact on SC lipids.

In the present study of polysorbate emulsifiers, they have been confirmed to have no influence on SC lipids, although they have longer polyoxyethylene chain ($n = 20$) and different length of alkyl chain. In this case, the molecular weight and structures could also serve as underlying factors for explaining the effects of polysorbate emulsifiers. The molecular structures of PEG ethers and esters used in this study are given in Table 2. It is apparent that polysorbate emulsifiers have larger molecular structure sizes which are expected to make it difficult for them to penetrate the skin and interact with SC lipids. Furthermore, although a recent finding from another group revealed a slight toxicity of polysorbate emulsifiers towards skin cells, it is not contradictory to our results that presented more friendly effects of them on skin lipids [49]. Our investigation suggests that polysorbates do not penetrate the skin and thus do not reach the deeper levels of the skin where living cells are located. Thus, it can be concluded that they may be regarded as safe excipients as long as they are not taken up into viable cell layers. Meanwhile, the emulsifier incorporated in various formulations may also display different influence on skin properties [13,49].

Last, according to the HLB values listed in Table1, we first expect that the HLB values of non-ionic emulsifiers correlate to their effects on SC lipids. We could suggest from the result of PEG ethers that the higher the HLB value, the more intensive effects of emulsifiers on SC lipids. However, C2 with HLB value of 5.3 sometimes revealed relatively similar influence with O10 and S10 (HLB value 12.4). More strikingly is that all polysorbate emulsifiers present no effects on SC lipids with HLB values all around 15. Therefore, we may conclude that HLB value alone is not a reliable predictor of interactions between non-ionic emulsifiers and SC lipids. On the other hand, the molecular weight and structures may be the main factor of polysorbate emulsifiers to interact with skin lipids. Concerning these debatable factors, further research needs to be done for deeper understandings of possible mechanisms to describe how non-ionic emulsifiers penetrate the skin and interact with skin components.

Table 2. Chemical structures of PEG alkyl ethers and PEG sorbitan fatty acid esters.

PEG Alkyl Ethers	Chemical Structures	PEG Sorbitan Fatty Acid Esters	Chemical Structures
PEG-n oleyl ether		PEG-20 sorbitan monopalmitate (Polysorbate 40)	
PEG-n stearyl ether		PEG-20 sorbitan monostearate (Polysorbate 60)	
PEG-n cetyl ether		PEG-20 sorbitan monooleate (Polysorbate 80)	

5. Conclusions

This study systematically examined the effects of non-ionic emulsifiers, including PEG alkyl ethers and PEG sorbitan fatty acid esters, on SC lipids. CRS was employed in this study as a non-invasive, efficient and versatile instrument. Different spectral signals of CRS in both fingerprint and HWN regions were applied to assess the alteration of lipid content, conformation, lateral packing order and SC thickness which caused by the interaction of non-ionic emulsifiers with SC. To sum up, it has been demonstrated that the results of conformation and lateral packing order analysis were basically correlated with the results of content analysis, indicating that the extraction of lipids from SC may disturb the lipid structures in SC, and to some extent weaken the skin structural integrity. Furthermore, our results so far implied that non-ionic emulsifiers of polysorbates as well as PEG ethers with a smaller number of oxyethylene groups would be better choices to incorporate into topical formulations due to their lower effects regarding extraction of lipids, interruption of lipid organizations and further damage of skin barrier functions.

Overall, based on these findings, the assessment of different lipid signals played a meaningful role to filtrate more effective spectral features for deeper differentiations. This research on non-ionic emulsifiers could also serve as a basis and be helpful to screen suitable emulsifiers for further formulation development.

Author Contributions: Conceptualization, Y.L. and D.J.L.; Data curation, Y.L.; Funding acquisition, Y.L. and D.J.L.; Investigation, Y.L.; Methodology, Y.L. and D.J.L.; Project administration, D.J.L.; Supervision D.J.L.; Writing—original draft, Y.L.; Writing—review & editing, D.J.L. Both authors have read and agreed to the published version of the manuscript.

References

1. Bouwstra, J.A.; Gooris, G.S. The Lipid Organisation in Human Stratum Corneum and Model Systems. *Open Derm. . J.* **2014**, *4*, 10–13.
2. Bouwstra, J.A. The skin barrier in healthy and diseased state. *Biochim. Biophys. Acta - Biomembr.* **2006**, *1758*, 2080–2095.
3. Weerheim, A.; Ponec, M. Determination of stratum corneum lipid profile by tape stripping in combination with high-performance thin-layer chromatography. *Arch. Derm. . Res.* **2001**, *293*, 191–199.
4. Caussin, J.; Gooris, G.S.; Janssens, M.; Bouwstra, J.A. Lipid organization in human and porcine stratum corneum differs widely, while lipid mixtures with porcine ceramides model human stratum corneum lipid organization very closely. *Biochim. Biophys. Acta - Biomembr.* **2008**, *1778*, 1472–1482.
5. Warner, R.R.; Boissy, Y.L.; Lilly, N.A.; Spears, M.J.; McKillop, K.; Marshall, J.L.; Stone, K.J. Water disrupts stratum corneum lipid lamellae: Damage is similar to surfactants. *J. Invest. Derm. .* **1999**, *113*, 960–966.
6. Smeden, J. Van; Janssens, M.; Boiten, W.A.; Drongelen, V. Van; Furio, L.; Vreeken, R.J.; Hovnanian, A.; Bouwstra, J.A. Intercellular Skin Barrier Lipid Composition and Organization in Netherton Syndrome Patients. *J. Invest. Derm. .* **2014**, *134*, 1238–1245.
7. Broere, F.; Gooris, G.; Schlotter, Y.M.; Rutten, V.P.M.G.; Bouwstra, J.A. Altered lipid properties of the stratum corneum in Canine Atopic Dermatitis. *Bba - Biomembr.* **2018**, *1860*, 526–533.
8. Kumar, G.P.; Rajeshwarrao, P. Nonionic surfactant vesicular systems for effective drug delivery—An overview. *Acta Pharm. Sin. B* **2011**, *1*, 208–219.
9. Ghanbarzadeh, S.; Khorrami, A.; Arami, S. Nonionic surfactant-based vesicular system for transdermal drug delivery. *Drug Deliv.* **2015**, *22*, 1071–1077.
10. Park, E.S.; Chang, S.Y.; Hahn, M.; Chi, S.C. Enhancing effect of polyoxyethylene alkyl ethers on the skin permeation of ibuprofen. *Int. J. Pharm.* **2000**, *209*, 109–119.

11. Bárány, E.; Lindberg, M.; Lodén, M. Unexpected skin barrier influence from nonionic emulsifiers. *Int. J. Pharm.* **2000**, *195*, 189–195.

12. Silva, S.M.C.; Hu, L.; Sousa, J.J.S.; Pais, A.A.C.C.; Michniak-Kohn, B.B. A combination of nonionic surfactants and iontophoresis to enhance the transdermal drug delivery of ondansetron HCl and diltiazem HCl. *Eur. J. Pharm. Biopharm.* **2012**, *80*, 663–673.

13. Zhang, Z.; Lunter, D.J. Confocal Raman microspectroscopy as an alternative method to investigate the extraction of lipids from stratum corneum by emulsifiers and formulations. *Eur. J. Pharm. Biopharm.* **2018**, *127*, 61–71.

14. Zhang, Z.; Lunter, D.J. Confocal Raman microspectroscopy as an alternative to differential scanning calorimetry to detect the impact of emulsifiers and formulations on stratum corneum lipid conformation. *Eur. J. Pharm. Sci.* **2018**, *121*, 1–8.

15. Walters, K.A.; Walker, M.; Olejnik, O. Non-ionic Surfactant Effects on Hairless Mouse Skin Permeability Characteristics. *J. Pharm. Pharm. .* **1988**, *40*, 525–529.

16. Fiume, M.M.; Heldreth, B.; Bergfeld, W.F.; Belsito, D.V.; Hill, R.A.; Klaassen, C.D.; Liebler, D.; Marks, J.G.; Shank, R.C.; Slaga, T.J.; et al. Safety Assessment of Alkyl PEG Ethers as Used in Cosmetics. *Int. J. Toxicol.* **2012**, *31*, 169S–244S.

17. Fruijtier-Pölloth, C. Safety assessment on polyethylene glycols (PEGs) and their derivatives as used in cosmetic products. *Toxicology* **2005**, *214*, 1–38.

18. Chiappisi, L. Polyoxyethylene alkyl ether carboxylic acids: An overview of a neglected class of surfactants with multiresponsive properties. *Adv. Colloid Interface Sci.* **2017**, *250*, 79–94.

19. Czamara, K.; Majzner, K.; Pacia, M.Z.; Kochan, K.; Kaczor, A.; Baranska, M. Raman spectroscopy of lipids: A review. *J. Raman Spectrosc.* **2015**, *46*, 4–20.

20. Ali, S.M.; Bonnier, F.; Ptasinski, K.; Lambkin, H.; Flynn, K.; Lyng, F.M.; Byrne, H.J. Raman spectroscopic mapping for the analysis of solar radiation induced skin damage. *Analyst* **2013**, *138*, 3946–3956.

21. Stamatas, G.N.; de Sterke, J.; Hauser, M.; von Stetten, O.; van der Pol, A. Lipid uptake and skin occlusion following topical application of oils on adult and infant skin. *J. Derm. . Sci.* **2008**, *50*, 135–142.

22. van Smeden, J.; Janssens, M.; Kaye, E.C.J.; Caspers, P.J.; Lavrijsen, A.P.; Vreeken, R.J.; Bouwstra, J.A. The importance of free fatty acid chain length for the skin barrier function in atopic eczema patients. *Exp. Derm. .* **2014**, *23*, 45–52.

23. Ibrahim, S.A.; Li, S.K. Chemical enhancer solubility in human stratum corneum lipids and enhancer mechanism of action on stratum corneum lipid domain. *Int. J. Pharm.* **2010**, *383*, 89–98.

24. Lunter, D.; Daniels, R. Confocal Raman microscopic investigation of the effectiveness of penetration enhancers for procaine delivery to the skin. *J. Biomed. Opt.* **2014**, *19*, 126015.

25. Lunter, D.; Daniels, R. Measuring skin penetration by confocal Raman microscopy (CRM): Correlation to results from conventional experiments. In Proceedings of the Medical Imaging 2016: Biomedical Applications in Molecular, Structural, and Functional Imaging, San Diego, CA, USA, 1–3 March 2016; Volume 9788, p. 978829.

26. Choe, C.S.; Schleusener, J.; Lademann, J.; Darvin, M.E. Age related depth profiles of human Stratum Corneum barrier-related molecular parameters by confocal Raman microscopy in vivo. *Mech. Ageing Dev.* **2018**, *172*, 6–12.

27. Pany, A.; Klang, V.; Peinhopf, C.; Zecevic, A.; Ruthofer, J.; Valenta, C. Hair removal and bioavailability of chemicals: Effect of physicochemical properties of drugs and surfactants on skin permeation ex vivo. *Int. J. Pharm.* **2019**, *567*, 118477.

28. Vyumvuhore, R.; Tfayli, A.; Duplan, H.; Delalleau, A.; Manfait, M.; Baiilet-Guffroy, A. Effects of atmospheric relative humidity on Stratum Corneum structure at the molecular level: Ex vivo Raman spectroscopy analysis. *Analyst* **2013**, *138*, 4103–4111.

29. Vyumvuhore, R.; Tfayli, A.; Duplan, H.; Delalleau, A.; Manfait, M.; Baillet-Guffroy, A. Raman spectroscopy: A tool for biomechanical characterization of Stratum Corneum. *J. Raman Spectrosc.* **2013**, *44*, 1077–1083.

30. Tfayli, A.; Guillard, E.; Manfait, M.; Baillet-Guffroy, A. Raman spectroscopy: Feasibility of in vivo survey of stratum corneum lipids, effect of natural aging. *Eur. J. Derm. .* **2012**, *22*, 36–41.

31. Rygula, A.; Majzner, K.; Marzec, K.M.; Kaczor, A.; Pilarczyk, M.; Baranska, M. Raman spectroscopy of proteins: A review. *J. Raman Spectrosc.* **2013**, *44*, 1061–1076.

32. Choe, C.S.; Lademann, J.; Darvin, M.E. Gaussian-function-based deconvolution method to determine the penetration ability of petrolatum oil into in vivo human skin using confocal Raman microscopy. *Laser Phys.* **2014**, *24*, 105601.

33. Savić, S.; Weber, C.; Savić, M.M.; Müller-Goymann, C. Natural surfactant-based topical vehicles for two model drugs: Influence of different lipophilic excipients on in vitro/in vivo skin performance. *Int. J. Pharm.* **2009**, *381*, 220–230.

34. Jacobi, U.; Kaiser, M.; Toll, R.; Mangelsdorf, S.; Audring, H.; Otberg, N.; Sterry, W.; Lademann, J. Porcine ear skin: An in vitro model for human skin. *Ski. Res. Technol.* **2007**, *13*, 19–24.

35. Tfaili, S.; Gobinet, C.; Josse, G.; Angiboust, J.F.; Manfait, M.; Piot, O. Confocal Raman microspectroscopy for skin characterization: A comparative study between human skin and pig skin. *Analyst* **2012**, *137*, 3673–3682.

36. Kligman, A.M. Preparation of Isolated Sheets of Human Stratum Corneum. *Arch. Derm. .* **2011**, *88*, 702.

37. Van Smeden, J.; Janssens, M.; Gooris, G.S.; Bouwstra, J.A. The important role of stratum corneum lipids for the cutaneous barrier function. *Biochim. Biophys. Acta-Mol. Cell Biol. Lipids* **2014**, *1841*, 295–313.

38. Bridges, T.E.; Houlne, M.P.; Harris, J.M. Spatially Resolved Analysis of Small Particles by Confocal Raman Microscopy: Depth Profiling and Optical Trapping. *Anal. Chem.* **2004**, *76*, 576–584.

39. Hathout, R.M.; Mansour, S.; Mortada, N.D.; Geneidi, A.S.; Guy, R.H. Uptake of microemulsion components into the stratum corneum and their molecular effects on skin barrier function. *Mol. Pharm.* **2010**, *7*, 1266–1273.

40. Hoppel, M.; Baurecht, D.; Holper, E.; Mahrhauser, D.; Valenta, C. Validation of the combined ATR-FTIR/tape stripping technique for monitoring the distribution of surfactants in the stratum corneum. *Int. J. Pharm.* **2014**, *472*, 88–93.

41. Choe, C.; Lademann, J.; Darvin, M.E. A depth-dependent profile of the lipid conformation and lateral packing order of the stratum corneum in vivo measured using Raman microscopy. *Analyst* **2016**, *141*, 1981–1987.

42. Williams, A.C.; Edwards, H.G.M.; Barry, B.W. Raman spectra of human keratotic biopolymers: Skin, callus, hair and nail. *J. Raman Spectrosc.* **1994**, *25*, 95–98.

43. Snyder, R.G.; Hsu, S.L.; Krimm, S. Vibrational spectra in the CH stretching region and the structure of the polymethylene chain. *Spectrochim. Acta Part A Mol. Spectrosc.* **1978**, *34*, 395–406.

44. Tfayli, A.; Guillard, E.; Manfait, M.; Baillet-Guffroy, A. Thermal dependence of Raman descriptors of ceramides. Part I: Effect of double bonds in hydrocarbon chains. *Anal. Bioanal. Chem.* **2010**, *397*, 1281–1296.

45. Schwarz, J.C.; Klang, V.; Hoppel, M.; Mahrhauser, D.; Valenta, C. Natural microemulsions: Formulation design and skin interaction. *Eur. J. Pharm. Biopharm.* **2012**, *81*, 557–562.

46. F.H.Wallach, D.; P.Verma, S.; Jeffrey, F. Application of laser Raman and infrared spectroscopy to the analysis of membrane structure. *Biochim. Biophys. Acta-Rev. Biomembr.* **1978**, *559*, 153–208.

47. Choe, C.; Lademann, J.; Darvin, M.E. Analysis of Human and Porcine Skin in vivo/ex vivo for Penetration of Selected Oils by Confocal Raman Microscopy. *Ski. Pharm. . Physiol.* **2015**, *28*, 318–330.

48. Choe, C.; Lademann, J.; Darvin, M.E. Confocal Raman microscopy for investigating the penetration of various oils into the human skin in vivo. *J. Derm. . Sci.* **2015**, *79*, 176–178.

49. Vater, C.; Adamovic, A.; Ruttensteiner, L.; Steiner, K.; Tajpara, P.; Klang, V.; Elbe-Bürger, A.; Wirth, M.; Valenta, C. Cytotoxicity of lecithin-based nanoemulsions on human skin cells and ex vivo skin permeation: Comparison to conventional surfactant types. *Int. J. Pharm.* **2019**, *566*, 383–390.

5. Tracking heavy-water-incorporated confocal Raman spectroscopy for evaluating the effects of PEGylated emulsifiers on skin barrier
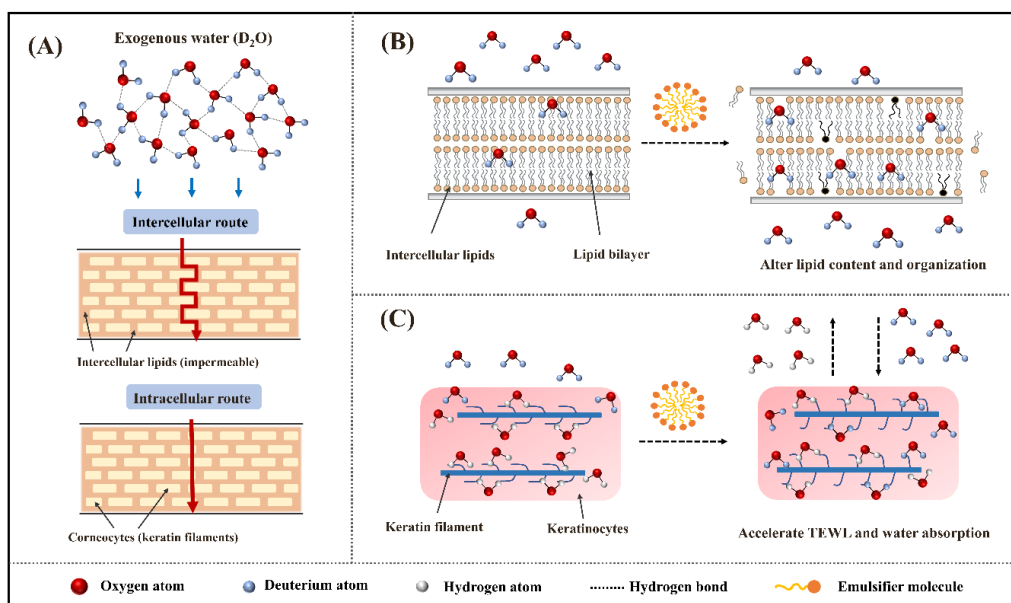
Yali Liu, Dominique Jasmin Lunter*

Department of Pharmaceutical Technology, Faculty of Science, Eberhard Karls Universität Tübingen, Auf der Morgenstelle 8, 72076 Tuebingen, Germany

Graphical Abstract

JOURNAL OF
BIOPHOTONICS

Tracking heavy-water-incorporated confocal Raman spectroscopy for evaluating the effects of PEGylated emulsifiers on skin barrier

Yali Liu [ORCID] | Dominique Jasmin Lunter*

Department of Pharmaceutical Technology, Faculty of Science, Eberhard Karls Universität Tübingen, Tuebingen, Germany

*Correspondence
Dominique Jasmin Lunter, Department of Pharmaceutical Technology, Faculty of Science, Eberhard Karls Universität Tübingen, Auf der Morgenstelle 8, Tuebingen 72076, Germany.
Email: dominique.lunter@uni-tuebingen.de

Abstract

The class of PEGylated emulsifiers finds broad application in the pharmaceutical and cosmetic industry. We target on one of the categories of polyethylene glycol (PEG) alkyl ethers with different lipophilic and hydrophilic chain length and aim to examine their effects on the skin comprehensively. In this study, we employed confocal Raman spectroscopy for skin depth profiling and imaging. A unique probe of heavy water (D_2O) was incorporated, which can be tracked percutaneously and simultaneously monitor the effects caused by emulsifiers. According to the results, most of the PEGylated emulsifiers caused changes in skin lipid content/organization and induced the alteration in relative water content/hydrogen bonding structure. The results obtained from the depth profiling analysis provided the possibility to estimate the least penetration depth of emulsifiers. Among them, PEG-20 ethers displayed the most penetration ability. Meanwhile, it is interesting to find that the treatment of emulsifiers also affected the spatial distribution of D_2O whose differences were in line with the molecular skin variations. In particular, the isotopic H/D substitution in the skin was highlighted in detail. This result supports the possibility to use D_2O as an excellent and cost-effective probe to evaluate the skin barrier function.
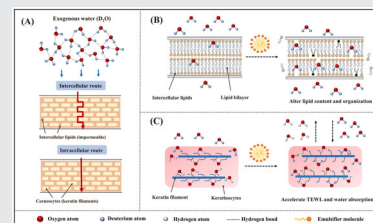
KEYWORDS

confocal Raman spectroscopy, heavy water, PEGylated emulsifiers, skin barrier function, skin molecular properties

1 | INTRODUCTION

In everyday life, our skin is facing contact with sanitary, cosmetic, or pharmaceutical products, gaining the potential of external irritations [1–3]. Establishing a significant barrier against environmental influences, stratum corneum (SC) makes up the outermost layer of the skin, providing mechanical protection with commonly described

"bricks and mortar" model [4, 5]. Primary protection of SC is provided by the intercellular lipids (the mortar) [6, 7]. At ambient conditions, skin lipids are highly structured and mainly assembled in densely packed orthorhombic lamellar phases. Nevertheless, with the skin exposed to foreign substances, physical and chemical interactions may happen to each other, changing the molecular properties of skin components. When the skin

is highly irritated, the lipid structures will tend to be a more fluid state [8–10]. Except for the lipids, the skin water-related property is also considered as an attractive property due to the common observation of transepidermal water loss in skin research [11]. In particular, in recent, the tight relationship of skin water regulation with intercellular lipids was introduced. Although the role of the skin lipids and water-related properties has been highlighted in some studies, the deepened understanding of their molecular variation is still limited [12–14].

There is extensive literature describing the irritation triggered by topically applied compounds in which emulsifiers are the main considering targets, owing to their intrinsic surface activity and intensive applications [15, 16]. However, conflicting data are emerging about their adverse effects on the skin [17, 18]. Walters et al stated that PEG alkyl ethers based on a C_{12} alkyl chain were effective in disrupting the lipid monolayer [19]. Our previous study also found reduced skin lipid content and altered lipid structures after applying the PEG-20 glycerol monostearate [20, 21]. Recently, we evidenced the different influence of a series of PEG alkyl ethers and PEG sorbitan esters on skin lipids [22]. Compared with the previous study, our current research focuses more on the depth-dependent comparison of molecular skin properties due to different penetration depth of emulsifiers. Furthermore, the relative water content and hydrogen bonding state are taken into consideration to gain insight view of interactions with lipid properties.

The insights into the mechanisms of molecular skin alterations gain complete attention in skin research. Considerable studies have been evaluating the skin barrier function based on the electrical, microscopic, and scattering approaches, which provide limited information on the insights of molecular skin interactions [23–25]. The fluidity and mobility of skin components regarding their structural changes were recently announced by using nuclear magnetic resonance, which is more precise but challenging to elucidate the skin depth variations [26, 27]. For a more comprehensive look, confocal Raman spectroscopy (CRS) is introduced. It is sensitive to identify minor changes in molecular skin components and available to detect skin from different depth [28].

Skin lipid analysis has been well grounded using CRS. Lipid content and lateral packing structure analysis have been comprehensively discussed by selecting useful Raman signals [29, 30]. However, skin water regulation and the associated hydrogen bonding state still need to be well elucidated. Recently, the hydrogen bond water molecular types were suggested by Choe et al using CRS to analyze the skin water-related properties of intact skin. Although it is an effective way, the shortage was uncovered when treating the skin with moisturizing solutions or formulations. In this case, extra water will penetrate the skin and subsequently induce a variation of OH bond signal on CRS spectra [31, 32]. To minimize the effects of external water penetration, we introduced a probe of heavy water (D_2O) to dissolve the model substances applied to the skin. With this probe, the effects of external penetrated water can be eliminated due to different Raman spectral features of OD bond and inherent skin OH bond [33]. Thus, skin water-related properties can be effectively detected. Meanwhile, as the CRS spectra recorded, D_2O distribution can be monitored and visualized across skin depth. As is known that water penetration dynamics can be regulated by the skin barrier integrity [34, 35], the D_2O penetration depth can be expected to differ following the effects of emulsifiers. Therefore, we assume the application of D_2O as a promising approach for evaluating the skin barrier state. The isotopic substitution and water diffusion behavior are also taken into adequate account.

2 | MATERIALS AND METHODS

2.1 | Materials and animal

Deuterium oxide (D_2O, 99.9 atom % D) is obtained from Sigma Aldrich (St. Louis, Missouri). PEG alkyl ethers including PEG-2 oleyl ether (O2), PEG-10 oleyl ether (O10), PEG-20 oleyl ether (O20), PEG-2 stearyl ether (S2), PEG-10 stearyl ether (S10), PEG-20 stearyl ether (S20), PEG-2 cetyl ether (C2), PEG-10 cetyl ether (C10) and PEG-20 cetyl ether (C20) were purchased from Croda
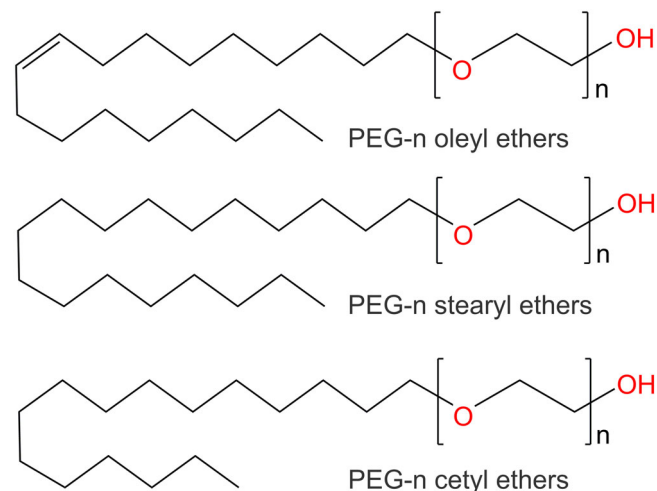
FIGURE 1   Chemical structures of PEGylated emulsifiers investigated in this study

Gmbh (Nettetal, Germany) (Figure 1 shows their chemical structures with different oxyethylene groups; Figure S1 represents the CRS spectrum of pure substances). Sodium lauryl sulfate (SLS) was achieved from Cognis GmbH & Co. KG (Düsseldorf, Germany). Sodium chloride, disodium hydrogen phosphate, potassium dihydrogen phosphate and potassium chloride were of European Pharmacopeia grade. Porcine ear skins (German landrace; age: 15 to 30 weeks; weight: 40 to 65 kg) were provided by the Department of Experimental Medicine at the University of Tuebingen and local butcher.

2.2 | Dermatomed porcine skin

Porcine ears were achieved on the day of slaughter and cleaned with isotonic saline. The skin was removed from cartilage, cleaned from blood, and cut into strips of approximately 3 cm width. The strips were stretched onto a Styrofoam plate with pins. Skin hairs were trimmed to around 0.5 mm with electric hair clippers. Thereafter, the skin was dermatomed to a thickness of 1 mm (Dermatom GA 630, Aesculap AG & Co. KG, D-Melsungen), punched out for circles to a diameter of 25 mm, wrapped with aluminum foil and stored into the refrigerator at −30°C. Upon use, the circular skin samples were thawed to room temperature and washed clean with phosphate-buffered saline (PBS). This procedure has been previously described in ref. [36]. Besides, two donors were used for the depth profiling analysis of PEGylated emulsifiers, which were slaughtered from the same slaughterhouse on the same day. The first donor was used for the studies of PEG-2 ethers and PEG-10 ethers. The second donor was used for investigations of PEG-20 ethers and SLS. D_2O only treatment was performed in both donors and used as a reference to normalize the slight data differences and make the emulsifier-treated samples comparable, which meant to decrease the inter-experiment variations.

2.3 | Franz diffusion cells

D_2O dissolved PEGylated emulsifiers were applied on porcine skin using Franz diffusion cells. Degassed and prewarmed (32°C) PBS was used as receptor fluid. A circular skin sheet was placed on the cell with SC facing up. The donor compartment was put on top of the skin and clamped tightly. The equipped cell was put into a water bath with a temperature of 32°C and stirring speed of 500 rpm. After 30-min equilibrium, 1 mL of each sample was applied to the skin (D_2O or D_2O dissolved). PEGylated emulsifiers used in this study are shown in Table S1. A piece of parafilm was then capped onto each donor compartment to prevent evaporation. After 2 hour incubation, the skin samples were removed from cells and cleaned with isotonic saline and cotton swabs for 30 times. The actual involved skin area was punched out and mounted onto the device for CRS measurement. The cross-sectional view of the device is depicted in Figure 2. A full description was provided in supporting information (Figure S2) and has been reported in the previous publication of our group [37].

2.4 | Confocal Raman spectroscopy

2.4.1 | CRS setting

Skin spectra were acquired with an alpha 500R confocal Raman microscope (WITec GmbH, Ulm, Germany) which was equipped with a 532 nm excitation laser, UHTS 300 spectrometer and DV401-BV CCD camera. The optical grating was 600 g/mm for recording the spectra in the range
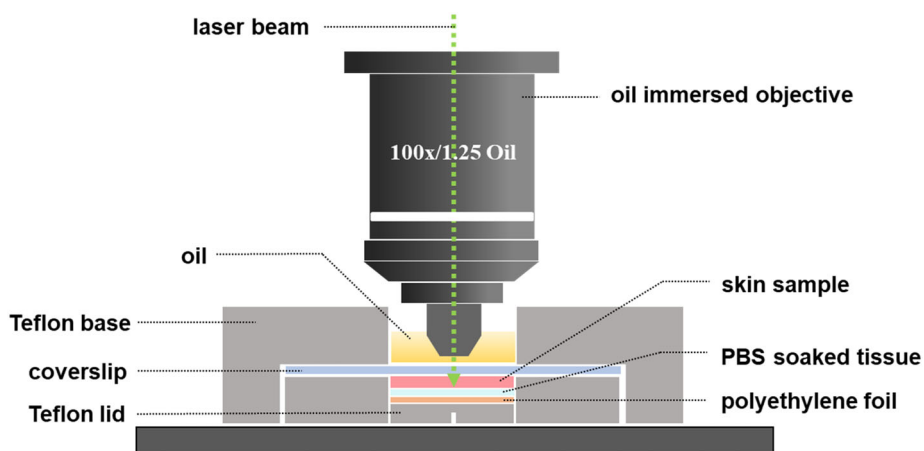
FIGURE 2 The schematic profile of the device for confocal Raman measurement

of 0 to 3800 cm^{-1}. Herein, 100×/1.25 NA (numerical aperture) oil immersion objective (E Plan, Nikon, Tokyo, Japan) in combination with a 50 μm pinhole was utilized [38]. Laser power was adjusted to 5 mW by the optimal power meter (PM100D, Thorlabs GmbH, Dachau, Germany) to avoid skin sample damage. For non-biological samples (eg, H_2O, D_2O and their mixtures), 40×/0.6 NA objective was used (EC Epiplan-neofluor, Carl Zeiss, Germany).

2.4.2 | CRS depth profiling

Line scans were conducted to collect skin spectra in-depth with the laser spot recording from 10 μm above the skin down to 50 μm inside the skin. The step size was 1 μm and the exposure time was 2 seconds for one measurement followed by 2 accumulations for each spectrum. The complete acquisition time was around 4 min for each depth analysis. The obtained spectra were preprocessed by the WITec Project Software (WITec GmbH, Ulm, Germany) including the smoothing process (Savitzky-Golay filter with third polynomial order and nine smoothing points) and background subtraction (automatic polynomial function was fitted to the spectrum and subtracted). Principal component (PC) analysis was then employed to reduce the noise of spectra. The first three PCs are selected for gaining the reconstructed spectra, as they can mostly describe the dataset and obtain the critical characteristic information of skin and D_2O. The skin surface was determined based on the detection of the boundary between SC and coverslip. The area under the curve (AUC) of keratin peak (ν(CH$_3$), 2920-2960 cm^{-1}) was plotted against scan depth. The left point of the full-width of half-maximum of this plotted profile was identified as the boundary between the skin surface and coverslip. The AUC was calculated using the trapezoidal method. Data were acquired from three replicates repeated for over three times (total n = 9). Diagrams show arithmetic mean ± SD.

2.4.3 | CRS spectral image

The third donor was used for CRS image scanning. Two-dimensional CRS maps were obtained by using image scans. A scanning area of 25 × 50 μm^2 (25 × 50 pixels) in x-z direction was mapped with 1 μm step size in both directions and 0.05 s integration time per spectrum. The scan was started from above the skin surface to obtain a complete skin cross-sectional image. After a series of preprocedures including cosmic ray removal, smoothing and background subtraction, a color-coded image was generated. In these images, each pixel corresponds to one CRS spectrum. In order to visualize the skin layer and track the spatial distribution of D_2O, the pure, untreated skin spectrum and D_2O spectrum were assigned, respectively, to different colors to indicate their location within the examined area.

2.5 | Evaluation of skin properties

### 2.5.1 | Gaussian-function based decomposition

The decomposition process in high wavenumber (HWN) region has been mainly introduced by Choe et al in skin research [31, 32]. In brief, in our work, the band of 2800 to 3800 cm^{-1} was decomposed into 10 subbands using Gaussian functions (see Figure 3). This process was automatically performed by applying curve-fitting toolbox on Matlab software (Math work, version R2019a). The goodness of fitting results was generated with R^2 over 0.98. As shown in Figure 3A, the four subbands centered at around 2800 to 3000 cm^{-1} are assigned to lipids and keratin. Peaks at 2850 and 2880 cm^{-1} correspond to ν(C-H) symmetric and ν(C-H) asymmetric stretching mode of lipids. Peaks at 2930 and 2980 cm^{-1} are assigned to ν(CH$_3$) symmetric and ν(CH$_3$) asymmetric stretching mode of keratin. The other six subbands in the spectral range of 3000 to 3800 cm^{-1} represent the various hydrogen bonding types of the water molecule and the small contribution of keratin. Among them, the peaks centered at 3070 and 3325 cm^{-1} are assigned to the unsaturated methylene stretching vibration of keratin and the N-H vibration of keratin separately. The four peaks corresponding to the hydrogen bond of water molecules were located at around 3010, 3280, 3460 and 3600 cm^{-1}, associated to tightly bound DAA-OH (single donor-double acceptor), strongly bound DDAA-OH (double donor-double acceptor), weakly bound DA-OH (single donor-single acceptor) and free water (superposition of very weakly DDA-OH bond, double donor-single acceptor and unbound OH). The hydrogen bonding configurations are represented in Figure 3B, which have been introduced in detail by Sun [39].

2.5.2 | Intercellular lipid properties

Lipid content could be analyzed in the fingerprint region. The peak at 1425 to 1490 cm^{-1} is composed of mostly the intercellular lipids. The peak at 1630 to 1710 cm^{-1} is corresponding to the ν(C=O)-mode for amide-I, representing the least variations from different donors. Thus, relative lipid content can be calculated according to the equation of normalized lipid = AUC$_{1425-1490}$/AUC$_{1630-1710}$.

FIGURE 3 Raman band decomposition procedure in high wavenumber region based on ten Gaussian peaks, A, and the schematic drawing of the hydrogen bonded water molecules corresponding to the types of OH bond assignments in skin spectra, B
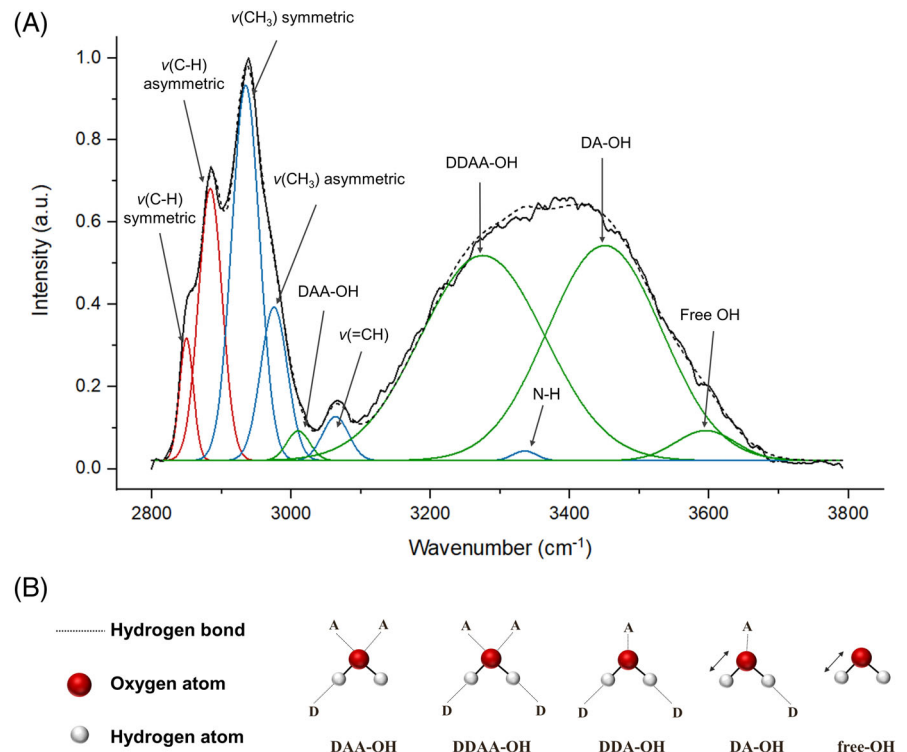
The detailed explanation has been described previously by our group [21].

The decomposed lipid and keratin related peaks in the HWN region have been demonstrated to be able to calculate the lipid content following the function of $Normalized_{lipid} = (AUC_{2880} + AUC_{2850})/(AUC_{2930} + AUC_{2980})$ [40]. In this study, skin lipid content analysis in fingerprint and HWN region can be mutually verified and provide a better comparison of these two signals in-depth profiling analysis.

For indicating the transition of skin lateral packing state from orthorhombic to hexagonal (more disorder state) phase, decomposed peaks at 2850 and 2880 cm^{-1} were utilized for calculation of $Ratio_{lat} = AUC_{2880}/AUC_{2850}$ based on the findings from previous research [41]. The higher value of $Ratio_{lat}$ represents a prevalence of highly crystalline and orthorhombic phases.

2.5.3 | Skin water-related properties

In this study, different hydrogen bound water types were used to calculate the relative water content. With the sum of AUCs of all OH-related bands normalized by keratin band ($\nu(CH_3)$, 2920-2960 cm^{-1}), the total water content can be calculated in different skin depths. Furthermore, the DDAA-OH and DA-OH bounds are mainly focused, as they account for over 90% of water molecular type in the skin. The hydrogen bonding state of water molecules can be represented by the ratio of

AUCs of DA-OH- and DDAA-OH-related bands, which was firstly proposed by Choe et al [42].

2.5.4 | Heavy water as a probe in skin

By extracting the spectrum from each pixel in-depth, the relative O-D content was calculated by applying the spectral feature of the O-D stretching band (2250-2750 cm^{-1}) normalized by keratin band ($\nu(CH_3)$, 2920-2960 cm^{-1}). This ratio represents the relative intensity of the O-D bond and the D_2O distribution quantitatively.

3 | RESULTS

3.1 | Intercellular skin lipid content and lateral packing state

The findings of lipid-related differences were shown in Figure 4 and Figure 5. Lipid content variations against depth were plotted in both fingerprint and HWN regions based on the calculations mentioned above (Figure 4A-C and Figure 4D-F). It is visible from the both regions that skin lipid distribution is inhomogeneous and intercellular lipid content keeps decreasing from the skin surface. Comparing the variations of calculated content values, the analysis in the fingerprint region showed better selectivity and sensitivity, as shown in previous study [30]. It is apparent that the variations of the normalized ratio
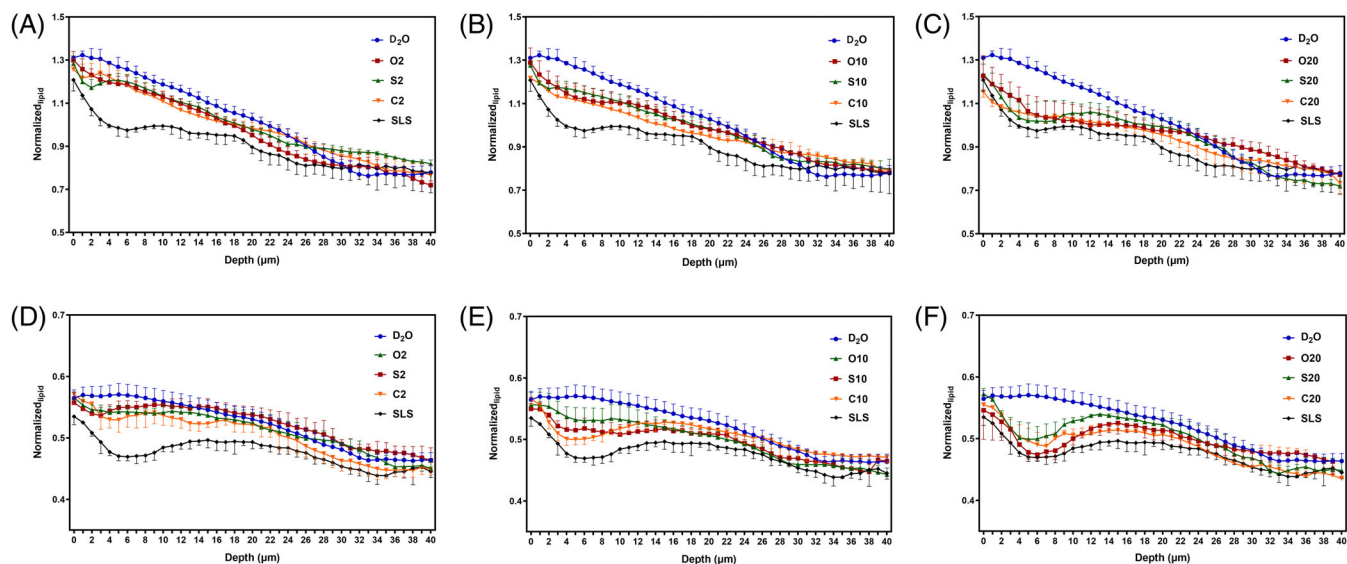
FIGURE 4 Depth-dependent profiles of skin lipid content of D_2O and emulsifiers treated skin, calculated by using the lipid signals in fingerprint region, A-C, and lipid signals in high wavenumber region based on the decomposition process, D-F, mean $\pm$ SD, n = 9
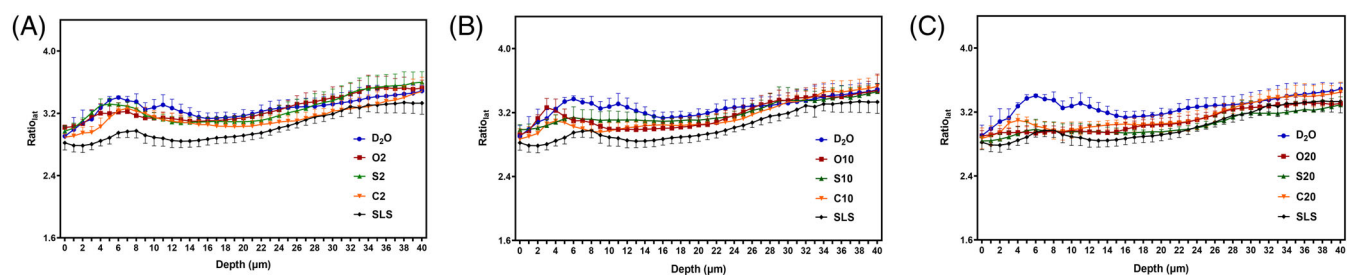
FIGURE 5 Depth-dependent profiles of calculated $Ratio_{lat}$ of D_2O and emulsifier-treated skin representing the order of lipid lateral packing structure, mean $\pm$ SD, n = 9

(from about 0.8 to 1.3) are intensively larger than in the HWN region (from about 0.46 to 0.57). It indicates that the lipid signal in the fingerprint region can provide more information on smaller differences of lipid molecular changes, which could be a better choice for future studies. However, the lipid signal HWN region can also be a second verification in our study to investigate the effects of PEGylated effects.

The depth profiling results among the investigated emulsifiers revealed the different extent of lipid extraction in both regions. SLS, as the positive control, showed the most reduction of lipids, especially at the upper layer of the skin, which is line with previous reports [1, 43]. PEGylated emulsifiers presented different effects on extracting lipids from the skin. As both figures showed, O2, S2 and C2 treated skin only showed a slight reduction from the surface of the skin comparing with the result from reference (heavy water only treated skin). O10, S10 and C10 have similar effects on the levels of detected lipid contents, mainly located at the upper layer of

approximately 8 μm. The trend is more evident in O20, S20 and C20 treated skin. Their ability to extract skin lipids increased remarkably from the depth analysis. Comparing the different extent of lipid reduction, the number of hydrophilic groups of PEGylated emulsifiers highlights their crucial role in lowering skin lipid content.

The variation of lipid lateral packing order state could be identified from the viewpoint of calculated $Ratio_{lat}$ vs skin depth. As shown in Figure 5A-C, the lateral packing states of lipids in the skin are inhomogeneous. The highest ordered lateral packing state of lipid structure is located in the intermediate part of the SC (approximately 4-10 μm), whereas less ordered lipid packing state was found on the skin surface. We could clearly see from Figure 5 that the SLS treated skin exhibits the most vital ability in decreasing the ordering state of lamellar lipids, and this influence spreads deep into the viable epidermis. Whereas for PEGylated emulsifiers treated skin, O2, S2 and C2 only show small variation by depth on their lipid packing state. Significant differences are hard to notice in

this category of emulsifiers, indicating more friendly effects of them on skin. O10, S10 and C10 lead to a modest decrease of Ratio$_{lat}$ compared with the reference, which can be observed at the upper part of the SC, indicating a slight increase of disordered lateral packing state. In comparison, the lateral packing orders are more disordered after the treatment of O20, S20 and C20. Clear decrease of Ratio$_{lat}$ can be observed in the intermediate layers (approximately 12 μm) of skin. The comparison among all the emulsifier effects on the lipid lateral packing order suggests nearly consistent results with the reductions of lipid contents.

3.2 | Skin water-related properties

Figure 6A-C shows the relative skin water content by depth. It can be seen that the application of SLS on skin significantly reduced skin water content. The treatments of PEGylated emulsifiers reveal different extent on affecting the water content. O2 and S2 only slightly decrease the water content from the upper layer of SC, whereas C2 causes slightly more reduced compared with O2 and S2. O10, S10 and C10 have a similar tendency to cause relative more reduction in water content. The most substantial effect can be observed with the applications of O20, S20 and C20 on skin from skin surface to around 15 μm depth. By comparing the water content profiles with the effects of emulsifiers, it is not difficult to find that the trend of water content variation is generally consistent

with the extraction of lipids and the disordering of lipid lateral packing order. Besides, the relationship between their distribution statuses is also noticeable that the skin layer with the most ordered state of lipids presents the highest water content. Meantime, the skin layer with the lowest water content on the uppermost layer and the substrate of the SC shows the more disordered state of lipid packing state.

Figure 6D-F presents the profiles of hydrogen bonding skin water molecular types calculated by the ratio of AUCs of DA-OH- and DDAA-OH-related bands. It can be seen that the water molecules on the skin surface have a higher content of weakly bound water, corresponding to the less ordered lamellar lipids on the skin surface, which may easily cause breaks of OH bonds and loss of water. With the treatment of emulsifiers, the transition state to a
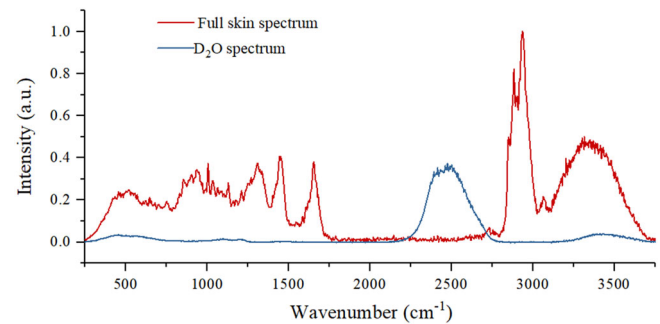

**FIGURE 7** Raman spectra of full-thickness skin and heavy water
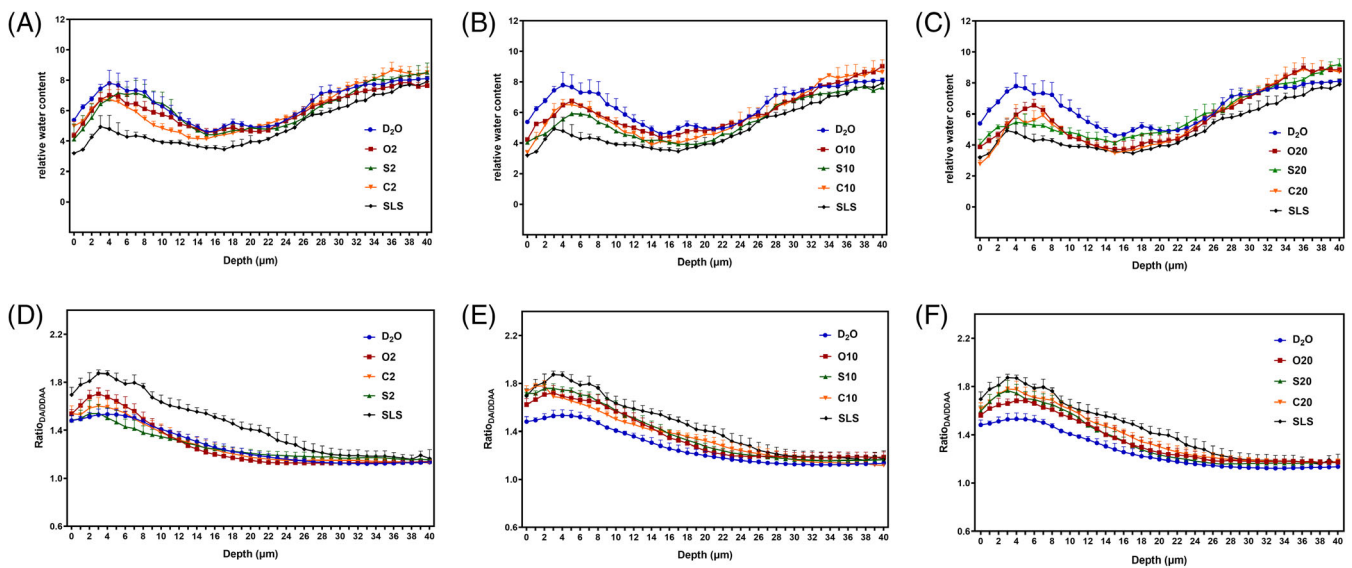
FIGURE 6 Depth-dependent profiles of the water content of D$_2$O and emulsifier-treated skin calculated by integrating the signal intensities of O-H stretching vibrations normalized by keratin band after decomposition process, A-C, and the hydrogen bonding state of skin water molecules obtained from the ratio of weakly bound (DA)/strongly bound (DDAA) water molecule types, D-F, mean ± SD, n = 9

weaker bound water type can be observed at different levels. The differences are not significant after applying O2 and S2 on the skin. Only slight differences can be observed on the skin surface layer when treating skin with C2 on the skin. The emulsifiers of PEG-10 ethers and PEG-20 ethers exhibit similar differences in DA/DDAA values. The influences are generally following the lipid-related properties, although the PEG-20 ethers revealed more potent effects on skin lipid properties. Based on these results, we may assume that when the skin lipid phases convert into a more disordered lipid packing state, the bonding state of skin water molecules might be more weakly bound. This correlation between skin water-related properties and lipid variations also complies with
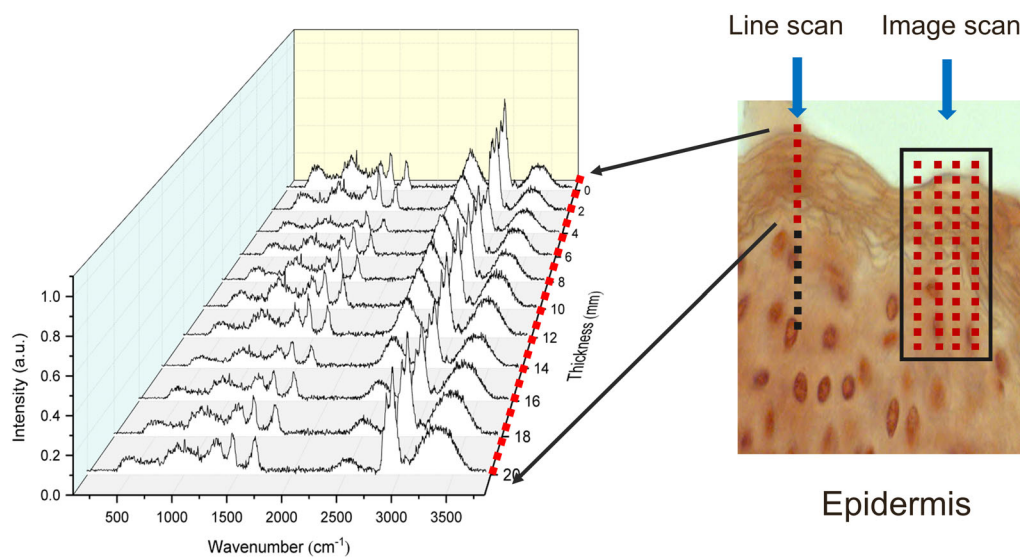
FIGURE 8 CRS analysis of the skin. Recorded CRS spectra associated with the red points representing each depth of the skin after incorporation of heavy water showing the basic principle for obtaining the skin depth profile by using spectral line scan and skin map of cross section by using spectral image scan
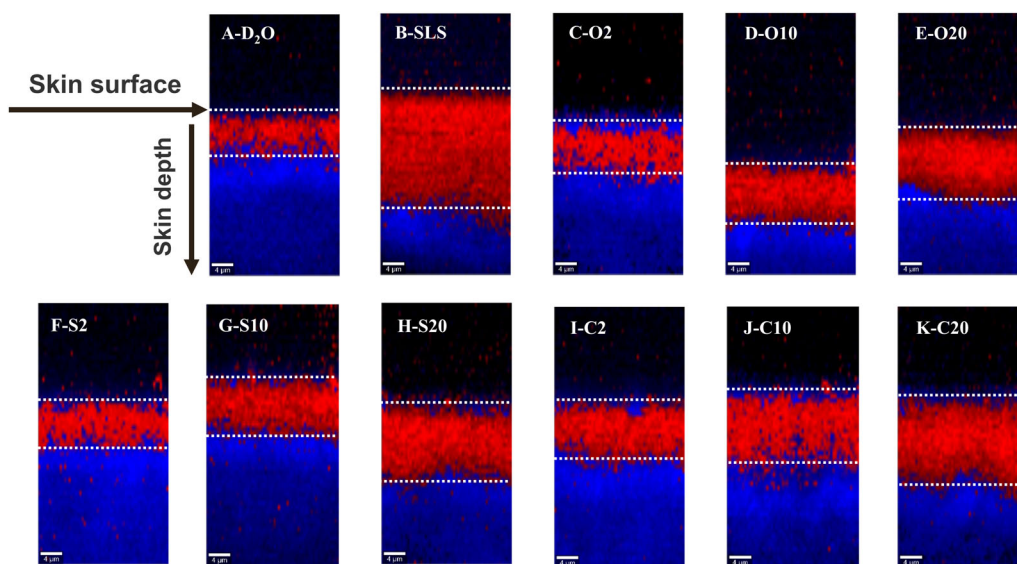
FIGURE 9 Color-coded Raman images representing the x-z direction distribution of heavy water in skin samples with the treatment of D_2O and different emulsifiers. The spectral characteristics of D_2O was shown in red, while the blue region presented the spectral features of skin components

other studies when analyzing the distribution of human/ porcine skin or age-related profiles, etc. [32, 44].

3.3 | CRS for monitoring heavy water within the skin

Deuterium is a heavier isotope compared with hydrogen, which shifts the OH stretching vibration into a lower wavenumber area in Raman spectra. As shown in Figure 7, the O-D stretching band is located at 2250 to 2750 cm^{-1}, which completely stands out from the skin spectrum without any overlapping area. It indicates that the exogenous penetrated water (D_2O) can be easily identified and distinguished from the endogenous skin hydrogen bonds (O-H). The approach for CRS measurement has been shown in Figure 8.

Figure 9 depicts the images of D_2O distributions from x, z-directions. The D_2O alone treated skin shows the minimal distribution of D_2O, which is mostly located in the upper layer of the skin with relatively lower content. With the SLS treatment, D_2O shown in red penetrates the deepest inside the skin. It shows densely packed red color overlaid, indicating more presence of OD bond in each pixel. Among the PEGylated emulsifiers, O2 and S2 treated skin represent similar behavior of D_2O distribution with D_2O alone treated skin. O10, S10 and C2 slightly accelerated the penetration of D_2O in the skin with the observation of O-D signals in a relatively deeper layer. C10 seems to promote the penetration more compared with O10 and S10 even with some slight inhomogeneous spread in skin. The deeper penetration of D_2O followed to be affected by O20 and S20, which displayed similar depth location of D_2O. The strongest impact came from C20, which revealed the deepest distribution of D_2O compared to other PEGylated emulsifiers. In summary, the D_2O penetration depth is clearly influenced by selected PEGylated emulsifiers. The impact behaviors were mostly in accordance with the variation of lipid and water-related properties, which reflected the potential of tracking heavy water diffusion in skin to evaluate the influences of compounds on skin.

3.4 | H/D substitution in D_2O-incorporated skin

The application of D_2O on skin was mentioned in a few studies. However, the behavior of isotopic substitution that happened in skin was only briefly discussed [45, 46]. To better understand the distribution process of D_2O in skin, isotopic substitution cannot be simply ignored. First of all, the C-H/C-D substitution was taken into account. In order to have a clear view of C-H/C-D substitution,
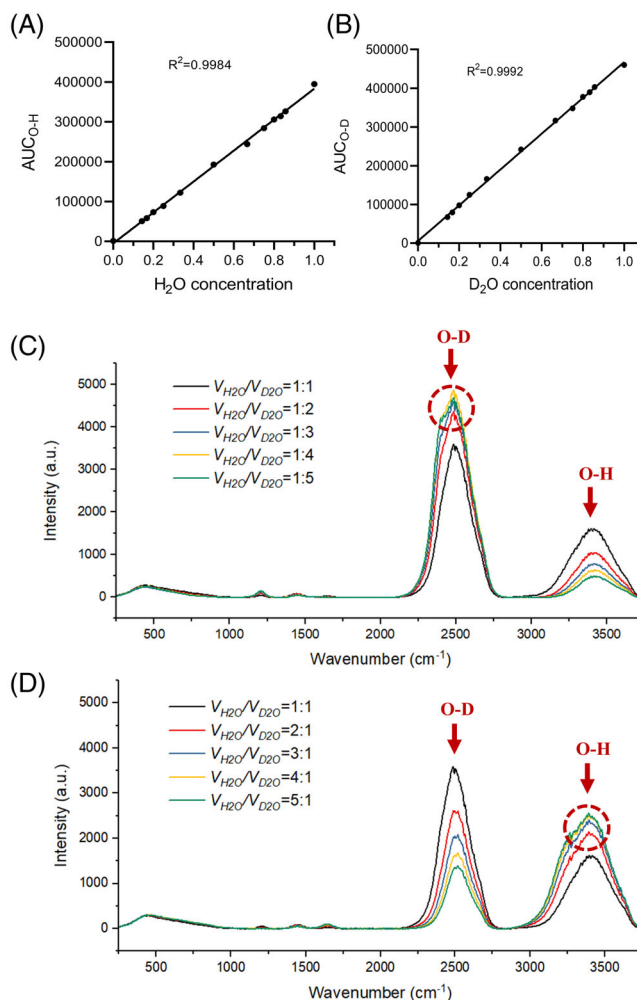
FIGURE 10 Simulation of isotopic substitution collecting the spectra of different volume ratio of H_2O and D_2O. A, The linearity curve between the H_2O concentration and the integrated intensity of OH stretch band. B, The linearity curve between the D_2O concentration and the integrated intensity of OD stretch band. C, The OD/OH stretch bands for isotopic substitution with the V_{H2O}/V_{D2O} of 1:1, 1:2, 1:3, 1:4, 1:5. D, The OD/OH stretch bands for isotopic substitution with the V_{H2O}/V_{D2O} of 1:1, 2:1, 3:1, 4:1, 5:1

the mixture of methanol and deuterated methanol was detected to simulate the substitution process (full description can be found in supplementary information). As shown in Figure S3, the C-D stretching mode is located at 2000 to 2300 cm^{-1}. However, there is no prominent peak appeared on the skin spectra in this region (Figure 8), indicating that the C-H/C-D substitution in the skin is not detectable.

O-H/O-D substitution is commonly highlighted in deuterated water applications [47, 48]. To elucidate the action between skin H_2O with penetrated D_2O, the mixtures of different volume ratios of H_2O and D_2O were used as models. As shown in Figure 9A-B, the intensity of the OH/OD bond increases linearly with the H_2O/D_2O

content, demonstrating a convincible spectra display. It is clear from Figure 10C-D that the signal intensity increases with the increased volume proportion and corresponding molecular vibration. However, the O-D bond has a greatly higher intensity than the O-H bond. When the H_2O molecule dominates the significant proportion, the O-H bond appears relatively similar intensity with O-D bond. In this case, the increase of H_2O volume (see V_{H_2O}/V_{D_2O} of 2:1, 3:1, 4:1) only show a slight increase of O-H bond intensity. If we compare the dynamic spectra of D_2O in the skin (Figure S1), it is easy to find that the penetrated D_2O amount is less than the skin H_2O amount. It indicates that the proportion of D_2O molecule in the skin is less than the H_2O molecule. Thus, the actual O-H bond intensity will only be slightly underestimated due to the O-H/O-D substitution.

4 | DISCUSSION

The alterations of skin lipid properties are associated with the impairment of skin barrier function [14, 49]. According to the effects of PEGylated emulsifiers, the decrease of skin water content and the prevalence of weakly bound hydration state of skin water are parallel to the adverse effects on lipid properties. The mechanism can be speculated that the disorder of lipid packing and subsequently caused impairment of skin barrier function lowered skin water content and further reflected the decrease of water holding capacity. In specific, our results supported the finding that the disorders skin lipids will loosen some tight hydrogen bonds surrounded and reduce the ratio value of DA/DDAA [42].

By tracking the distribution of D_2O, emulsifiers appeared different effects on its penetration depth. It turns out that the extent of their effects on molecular skin segments correlates to the permeability of simultaneously applied D_2O. The potential mechanism might be triggered by the increase of SC lipids mobility and fluidity, which facilitated the interactions of water molecules with lipid polar head groups and making the D_2O easily to be penetrated. With these correlated results, it demonstrates that the application of D_2O on the skin enables the assessment of skin barrier function. Meanwhile, the research by Wang et al also provided support to our study which found out that the treatment of glycerin on skin promoted the penetration of D_2O [46]. Besides, the advantage of using D_2O is clearly highlighted in our study to enable the detection of skin water-related properties. Even with the effects of isotopic substitution, the variation of skin water content and hydrogen bonding state of skin water can also be identified.

Overall, the tendency for skin interactions mainly follows the sequence: PEG-20 alkyl ethers > PEG-10 alkyl ethers ≥PEG-2 alkyl ethers. The hydrophilic chain length seems to be the primary determinant in the activity of skin interactions. Many reports also underlined the importance of alkyl chain length in the potency of skin interactions [18, 50]. However, it is still debatable in our study, as its influence is not clearly highlighted when comparing the results of PEG oleyl ethers, PEG stearyl ethers and PEG cetyl ethers. In addition, little differences were found when comparing to the PEG oleyl ethers (C_{18}, unsaturated), and PEG stearyl ethers (C_{18}, saturated). It indicates that the effects of PEGylated emulsifiers with unsaturated hydrocarbon chains are similar to those with saturated chains. The more information provided in this work referred to the penetration depth of them. The spectral signal of lipid content in the fingerprint region appeared to be the most sensitive one. With this result, we could have a clue about the least penetration depth of each emulsifier due to their effects on different depths of the skin.

5 | CONCLUSION

In this work, we investigated the effects of a class of PEGylated emulsifiers using CRS to monitor their effects on molecular skin properties. D_2O was simultaneously incorporated to visualize its distribution in the skin. The comprehensive depth-dependent profiling results illustrated the changes in the skin lipid and skin water-related properties. They clearly showed the prevalence of disordering skin molecular properties by the treatment of PEGylated emulsifiers with longer hydrophilic chain length. Besides, the least penetration depth of emulsifiers in the skin can be estimated based on their depth of influences. The application of D_2O allows the differentiation of endogenous and exogenous hydrogen bonds, which enables the detection of skin water-related properties. The overall results stressed the correlation data of different D_2O penetration depth with different extent of molecular skin effects, supporting the idea of using D_2O as a convenient and inexpensive target in the skin for multiple roles. The H/D substitution as a frequently missing part has been considered to compensate for the incomplete description of their occurrence and behavior in the skin. Finally, this study performed a multifactorial analysis of emulsifiers on skin and enhanced our understanding in skin molecular variability with topically applied compounds. It would be of interest in the future for us to deepen the understanding of mechanisms of emulsifiers used as penetration enhancers for evaluating drug penetration and permeation behaviors.

ACKNOWLEDGMENTS

CONFLICT OF INTEREST

The authors declare no conflict of interest.

DATA AVAILABILITY STATEMENT

Research data are not shared.

ETHICS STATEMENT

Porcine ears were achieved from Department of Experimental Medicine of University Hospital Tuebingen. Live animals used were kept at Department of Experimental Medicine and sacrificed in the course of their experiments, which are approved by the Ethics Committee of University Hospital Tuebingen. Those ears were received directly after the death of the animals. Prior to study, Department of Pharmaceutical Technology has registered for the use of animal products at the District Office of Tuebingen (registration number: DE 084161052 21).

ORCID

Yali Liu https://orcid.org/0000-0002-3170-7178

REFERENCES

[1] M. Lodén, A. C. Andersson, *Br. J. Dermatol.* **1996**, *134*, 215.
[2] A. W. Fulmer, G. J. Kramer, *J. Invest. Dermatol.* **1986**, *86*, 598.
[3] P. G. M. Van der Valk, J. P. Nater, E. Bleumink, *J. Invest. Dermatol.* **1984**, *82*, 291.
[4] J. C. Mackenzie, *Nature* **1969**, *222*, 881.
[5] T. Marjukka Suhonen, J. A. Bouwstra, A. Urtti, *J. Control. Release* **1999**, *59*, 149.
[6] J. Ishikawa, H. Narita, N. Kondo, M. Hotta, Y. Takagi, Y. Masukawa, T. Kitahara, Y. Takema, S. Koyano, S. Yamazaki, A. Hatamochi, *J. Invest. Dermatol.* **2010**, *130*, 2511.
[7] J. A. Bouwstra, *Biophys. Acta Biomembr.* **2006**, *1758*, 2080.
[8] J. M. Jungersted, J. K. Høgh, L. I. Hellgren, G. B. E. Jemec, T. Agner, *Contact Dermatitis* **2010**, *63*, 313.
[9] S. Hatziantoniou, I. P. Nezis, L. H. Margaritis, C. Demetzos, *Micron* **2007**, *38*, 777.
[10] F. Damien, M. Boncheva, *J. Invest. Dermatol.* **2010**, *130*, 611.
[11] M. Loden, H. Olsson, T. Axell, Y. W. Linde, *Br. J. Dermatol.* **1992**, *126*, 137.
[12] E. H. Mojumdar, Q. D. Pham, D. Topgaard, E. Sparr, *Sci. Rep.* **2017**, *7*, 1.
[13] R. Notman, J. Anwar, *Adv. Drug Deliv. Rev.* **2013**, *65*, 237.
[14] L. Zhang, T. Cambron, Y. Niu, Z. Xu, N. Su, H. Zheng, K. Wei, P. Ray, *Anal. Chem.* **2019**, *91*, 2784.
[15] C. L. Froebe, F. A. Simion, L. D. Rhein, R. H. Cagan, A. Kligman, *Dermatology* **1990**, *181*, 277.
[16] M. Mélot, P. D. A. Pudney, A. M. Williamson, P. J. Caspers, A. Van Der Pol, G. J. Puppels, *J. Control. Release* **2009**, *138*, 32.
[17] S. C. Shin, C. W. Cho, I. J. Oh, *Int. J. Pharm.* **2001**, *222*, 199.
[18] E. Bárány, M. Lindberg, M. Lodén, *Int. J. Pharm.* **2000**, *195*, 189.
[19] K. A. Walters, A. T. Florence, P. H. Dugard, *J. Colloid Interface Sci.* **1982**, *89*, 584.
[20] Z. Zhang, D. J. Lunter, *Eur. J. Pharm. Sci.* **2018**, *121*, 1.
[21] Z. Zhang, D. J. Lunter, *Eur. J. Pharm. Biopharm.* **2018**, *127*, 61.
[22] Y. Liu, D. J. Lunter, *Pharmaceutics* **2020**, *12*, 223.
[23] T. Schmitt, R. Gupta, S. Lange, S. Sonnenberger, B. Dobner, T. Hauß, B. Rai, R. H. H. Neubert, *Chem. Phys. Lipids* **2018**, *214*, 58.
[24] J. M. Andersson, C. Grey, M. Larsson, T. M. Ferreira, E. Sparr, *Proc. Natl. Acad. Sci. U. S. A.* **2017**, *114*, E3592.
[25] A. Pany, V. Klang, M. Brunner, J. Ruthofer, E. Schwarz, C. Valenta, *Skin Pharmacol. Physiol.* **2018**, *32*, 8.
[26] Q. D. Pham, E. H. Mojumdar, G. S. Gooris, J. A. Bouwstra, E. Sparr, D. Topgaard, *Q. Rev. Biophys.* **2018**, *51*, 1926. https://doi.org/10.1017/S0033583518000069
[27] Q. D. Pham, D. Topgaard, E. Sparr, *Proc. Natl. Acad. Sci. U. S. A.* **2017**, *114*, E112.
[28] N. Jung, M. Windbergs, *Phys. Sci. Rev.* **2018**, *3*, 1.
[29] A. Tfayli, E. Guillard, M. Manfait, A. Baillet-Guffroy, J. Eur, *Dermatology* **2012**, *22*, 36.
[30] Y. Liu, D. J. Lunter, *Transl. Biophotonics* **2020**, *2*, 1.
[31] A. Y. Sdobnov, M. E. Darvin, J. Schleusener, J. Lademann, V. V. Tuchin, *J. Biophotonics* **2019**, *12*, 1.
[32] C. S. Choe, J. Schleusener, J. Lademann, M. E. Darvin, *J. Biophotonics* **2018**, *11*, 1.
[33] S. R. Pattenaude, L. M. Streacker, D. Ben-Amotz, *J. Raman Spectrosc.* **2018**, *49*, 1860.
[34] C. M. Blattner, G. Coman, N. R. Blickenstaff, H. I. Maibach, *Rev. Environ. Health* **2014**, *29*, 175.
[35] C. Barba, M. Martí, A. Semenzato, G. Baratto, A. M. Manich, L. Coderch, *J. Therm. Anal. Calorim.* **2015**, *120*, 297.
[36] D. Lunter, R. Daniels, *J. Biomed. Opt.* **2014**, *19*, 126015.
[37] D. J. Lunter, *J. Raman Spectrosc.* **2017**, *48*, 152.
[38] D. J. Lunter, *Skin Pharmacol. Physiol.* **2016**, *29*, 92.
[39] Q. Sun, *Vib. Spectrosc.* **2009**, *51*, 213.
[40] C.-S. Choe, J. Lademann, M. E. Darvin, *Laser Phys.* **2014**, *24*, 105601.
[41] A. Tfayli, E. Guillard, M. Manfait, A. Baillet-Guffroy, *Anal. Bioanal. Chem.* **2010**, *397*, 1281.
[42] C. Choe, J. Lademann, M. E. Darvin, *Analyst* **2016**, *141*, 6329.
[43] A. Di Nardo, K. Sugino, P. Wertz, J. Ademola, H. I. Maibach, *Contact Dermatitis* **1996**, *35*, 86.
[44] C. S. Choe, J. Schleusener, J. Lademann, M. E. Darvin, *Mech. Ageing Dev.* **2018**, *172*, 6.
[45] M. Ashtikar, C. Matthäus, M. Schmitt, C. Krafft, A. Fahr, J. Popp, *Eur. J. Pharm. Sci.* **2013**, *50*, 601.
[46] H. Wang, Q. Zhang, G. Mao, O. Conroy, Y. Pyatski, M. J. Fevola, G. O. Cula, P. Maitra, R. Mendelsohn, C. R. Flach, *Skin Res. Technol.* **2019**, *25*, 653.
[47] C. Eklouh-Molinier, T. Happillon, N. Bouland, C. Fichel, M. D. Diébold, J. F. Angiboust, M. Manfait, S. Brassart-Pasco, O. Piot, *Analyst* **2015**, *140*, 6260.
[48] Q. Zhang, K. L. Andrew Chan, G. Zhang, T. Gillece, L. Senak, D. J. Moore, R. Mendelsohn, C. R. Flach, *Biopolymers* **2011**, *95*, 607.

[49] A. M. Champagne, H. C. Allen, R. C. Bautista-Jimenez, J. B. Williams, *Chem. Phys. Lipids* **2016**, *195*, 47.

[50] M. Förster, M. A. Bolzinger, D. Ach, G. Montagnac, S. Briançon, *Pharm. Res.* **2011**, *28*, 858.

SUPPORTING INFORMATION

Additional supporting information may be found online in the Supporting Information section at the end of this article.

Supporting Information

Tracking heavy-water-incorporated confocal Raman spectroscopy for evaluating the effects of PEGylated emulsifiers on skin barrier

Yali Liu[1], Dominique Jasmin Lunter[1]*

[1] Department of Pharmaceutical Technology, Faculty of Science, Eberhard Karls Universität Tübingen, Auf der Morgenstelle 8, 72076 Tuebingen, Germany

***Correspondence**: Dominique Jasmin Lunter, Department of Pharmaceutical Technology, Faculty of Science, Eberhard Karls Universität Tübingen, Auf der Morgenstelle 8, 72076 Tuebingen, Germany

E-mail: dominique.lunter@uni-tuebingen.de,

Tel: +49-7071-297-4558

TABLE S1 Characteristics of PEGylated emulsifiers used in this study

PEGylated emulsifiers	Alkyl chain	Alkyl chain length and saturation	Number of oxyethylene group	Abbreviations	HLB value
PEG-2 oleyl ether	Oleyl alcohol	C18, C7-C8 unsaturated	2	O2	5.0
PEG-10 oleyl ether	Oleyl alcohol	C18, C7-C8 unsaturated	10	O10	12.4
PEG-20 oleyl ether	Oleyl alcohol	C18, C7-C8 unsaturated	20	O20	15.3
PEG-2 stearyl ether	Stearyl alcohol	C18	2	S2	4.9
PEG-10 stearyl ether	Stearyl alcohol	C18	10	S10	12.4
PEG-20 stearyl ether	Stearyl alcohol	C18	20	S20	15.3
PEG-2 cetyl ether	Cetyl alcohol	C16	2	C2	5.3
PEG-10 cetyl ether	Cetyl alcohol	C16	10	C10	12.9
PEG-20 cetyl ether	Cetyl alcohol	C16	20	C20	15.7

Figure S1 Single spectra of pure PEGylated emulsifiers compared with the skin spectrum

1. Detailed description of Raman measuring device

The device used for Raman measurements was custom built and modified according to the device used by Bonnist et al. [1] and has been reported in our previous work [2,3]. As shown in Figure S2, it is made of Teflon and consists of three parts that tightly fix the skin sample between a coverslip and the lid of the device. The whole setup prevents the full-thickness skin sample from drying during the Raman measurement.

The upper and middle parts of the device both contain a hole that allows the laser beam to go through the skin sample for collecting Raman spectra. To build the setup, a coverslip is fixed in between the two parts to completely cover the hole. Subsequently, the skin is put onto the coverslip with the skin surface (stratum corneum) down to the coverslip. Afterward, a piece of tissue soaked with PBS is put onto the dermis side and a circular polyethylene foil is placed on top of it. Finally, the lid of the device is screwed tight, making the skin pressed gently against the coverslip.

FIGURE S2 The whole setup used for confocal Raman measurements in this study. (A) unassembled three parts of the device, (B) assembled device.

2. Simulated C-D/C-H substitution

We model the Raman spectra using all-H forms methanol (CH_3OH: H_2O, 1:1) and all-D forms of deuterated methanol (CD_3OD: D_2O, 1:1) for identifying the induced isotopic substitution behaviors (Figure S3). It is easy to recognize the Raman shift of C-H stretch bands from the region 2750-3100 cm^{-1} to 2000-2300 cm^{-1}(C-D stretch bands) and O-H stretch mode from 3100-3750 cm^{-1} to 2300-2750 cm^{-1} (O-D stretch mode). Furthermore, it is interesting to find that the intensity of all-D forms spectra appeared nearly twice the intensity of all-H forms spectra.

Some literature stated that the D atom can be incorporated into lipids via the fatty acid biosynthesis pathways or proteins via the amino acid and carbohydrate biosynthesis [4–6]. While turning to the spectra of D_2O incorporated skin in our study, it is simple to notice from Figure S1 that there is no C-D band appeared, indicating no C-H/C-D substitution occurred. It assures the complete access of spectra we obtained to the molecular information of lipids and proteins. Further, the excised porcine skin detected in this study is not metabolically active which provides the

basis of this result, since it is in line with the finding from Berry et al, that the abiotic H/D exchange does not occur at levels measurable by Raman microspectroscopy [7]. Therefore, the C-H/C-D substitution in the skin is not detectable.
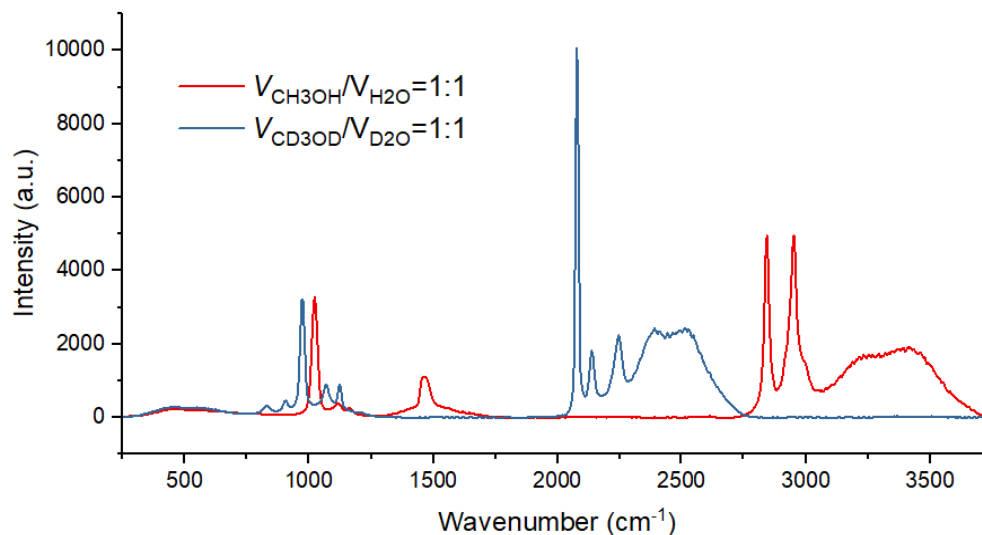
FIGURE S3 Raman spectra of all-H forms methanol/water (CH$_3$OH: H2O, 1:1) and all-D forms deuterated methanol/heavy water (CD$_3$OD: D2O, 1:1).

References

[1] E. Y. M. Bonnist, J. P. Gorce, C. MacKay, R. U. Pendlington, P. D. A. Pudney, *Skin Pharmacol. Physiol.* **2011**, *24*, 274.

[2] D. J. Lunter, *Skin Pharmacol. Physiol.* **2016**, *29*, 92.

[3] D. J. Lunter, *J. Raman Spectrosc.* **2017**, *48*, 152.

[4] X. Zhang, A. L. Gillespie, A. L. Sessions, *Proc. Natl. Acad. Sci. U. S. A.* **2009**, *106*, 12580.

[5] B. J. Campbell, C. Li, A. L. Sessions, D. L. Valentine, *Geochim. Cosmochim. Acta* **2009**, *73*, 2744.

[6] C. R. Fischer, B. P. Bowen, C. Pan, T. R. Northen, J. F. Banfield, *ACS Chem. Biol.* **2013**, *8*, 1755.

[7] D. Berry, E. Mader, T. K. Lee, D. Woebken, Y. Wang, D. Zhu, M. Palatinszky, A. Schintlmeister, M. C. Schmid, B. T. Hanson, N. Shterzer, I. Mizrahi, I. Rauch, T. Decker, T. Bocklitz, J. Popp, C. M. Gibson, P. W. Fowler, W. E. Huang, M. Wagner, D. E. Canfield, *Proc. Natl. Acad. Sci. U. S. A.* **2015**, *112*, E194.

6. Optimal configuration of confocal Raman spectroscopy for precisely determining stratum corneum thickness: evaluation of the effects of polyoxyethylene stearyl ethers on skin
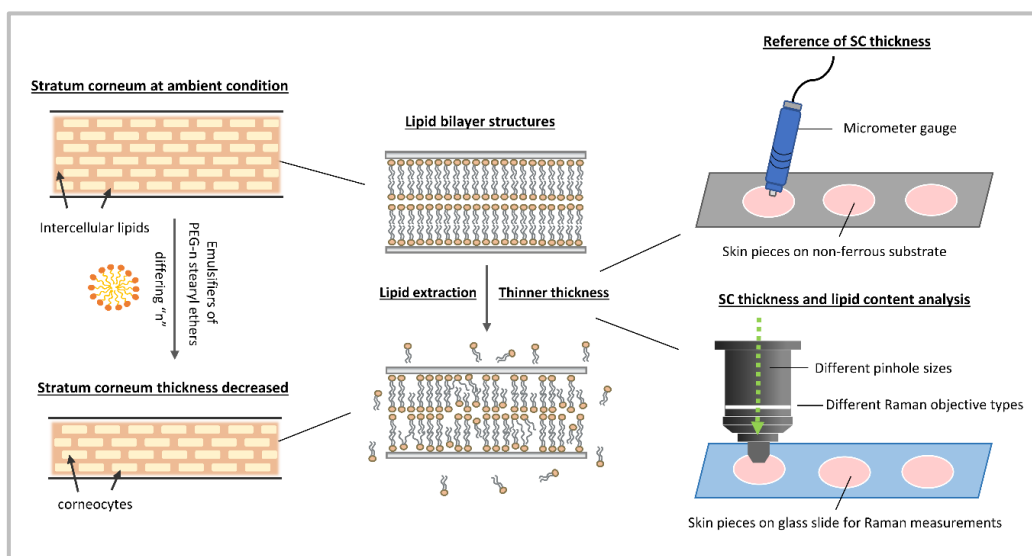
Yali Liu, Dominique Jasmin Lunter*

Department of Pharmaceutical Technology, Faculty of Science, Eberhard Karls Universität Tübingen, Auf der Morgenstelle 8, 72076 Tuebingen, Germany

Graphical Abstract

Optimal configuration of confocal Raman spectroscopy for precisely determining stratum corneum thickness: Evaluation of the effects of polyoxyethylene stearyl ethers on skin

Yali Liu, Dominique Jasmin Lunter [*]

Department of Pharmaceutical Technology, Faculty of Science, Eberhard Karls Universität Tübingen, Auf der Morgenstelle 8, 72076 Tuebingen, Germany

ABSTRACT

Properties regarding stratum corneum (SC), the outermost membrane of the skin, remain an active area in dermatologic and cosmetic research. The reduced thickness of SC is associated with varied adverse statuses such as skin lipid deficiency, skin barrier dysfunctions and skin deceases, etc. Emulsifiers with existing irritative effects on skin components also face the risk of decreasing SC thickness. We have been focusing on the effects of PEGylated emulsifiers on the skin and have an interest in finding the role of their polyethylene glycol (PEG)-chain length in tuning skin irritations. With this aim, PEG-stearyl ethers with different numbers of hydrophilic chains were applied on the skin, and their influence on skin thickness was discovered to determine their skin barrier effect. Confocal Raman spectroscopy (CRS) with extensive application in skin research was used here. To obtain the precise determination of skin thickness, our secondary aim was to find the optimal CRS configuration referring to varied objectives and pinhole sizes where further study is still in demand. Therefore, SC thickness measured via eddy current approach served as reference. The applied PEG-stearyl ethers formed the system to achieve varied thicknesses. Results confirmed that the skin interactions rose with increasing PEG-chain length, however only up to a certain limit, with decreasing effects recorded from PEG-40 stearyl ether and no effects observed from PEG-100 stearyl ether. Simultaneously, CRS combined with water immersion objective and 50 μm pinhole presented the most consistent values to the references and exhibited better spectral intensity and signal-to-noise ratio. Correlation plots involving different cases of configurations were calculated for error corrections. Taken together, this work helps to identify the potential mechanisms governing the interactions between PEG-stearyl ethers and skin and offers powerful evidence of using CRS as a reliable alternative to obtain accurate thickness values.

1. Introduction

In recent years, stratum corneum (SC) has caught extensive attention in skin research as the outermost and multifunctional layer of skin (Ashtikar et al., 2013; Biniek et al., 2015; Ghadially et al., 1996). As an effective barrier preventing the entry of foreign substances, the morphology and composition of it have always been the study focuses (Pham et al., 2016; Schmitt and Neubert, 2018; Vyumvuhore et al., 2015). Since the skin is exposed to everyday life, facing potential irritative factors, the interactions between SC and exogenous substances are of high interest to be discovered. Non-ionic emulsifiers have a wide range of applications in pharmaceutical and dermatological fields, offering many opportunities to be in contact with skin (Ghanbarzadeh et al., 2015; Kumar and Rajeshwarrao, 2011). However, some of them have been reported to have negative impacts on skin epidermal layers. Their ability to cause skin abnormalities have been revealed from plenty of aspects, e.g. skin pH, skin hydration, *trans*-epidermal water loss (TEWL), skin mechanical stress, etc. (Bárány et al., 2000; Sahle et al., 2012; Walters et al., 1982).

As one of the main types, PEGylated emulsifiers also gained great attention in skin analysis. Due to their similar chemical formula containing the hydrophilic PEG-chain and corresponding hydrophobic tail of ethers or fatty acid esters, there may be a pattern hidden to govern their interactions with skin components. In preliminary studies, their potential law in tuning the influence of drug enhancing effects have been widely investigated. The crucial roles of alkyl chain and PEG-chain have

---

* Corresponding author.
E-mail address: dominique.lunter@uni-tuebingen.de (D.J. Lunter).

been discussed (Park et al., 2000; Shin et al., 2001). The chain length of polar head groups and the different fatty acids, alkyl chain lengths and degrees of saturation have all reflected varying importance. However, our previous study evidenced that their structure–activity was exposed prominently from hydrophilic PEG-chain length regarding their influence on skin barrier functions. It was found that the increasing length of PEG-chain can lead to stronger effects on skin lipid extractions and structural disorders. Following this interesting finding, one can be aware that this potential law was only examined within limited PEG numbers. To better understand their structural mechanism in interacting with the skin, extended PEG-chain length of PEGylated emulsifiers is highly expected to be investigated.

Except for the viewpoint of structural rules, the molecular weight is also an important factor. Bárány et al. investigated the TEWL after treating the skin with a series of PEG fatty acid esters (Bárány et al., 2000). The results suggested that PEG derivatives with lower molecular weight had higher potency to increase the TEWL and damage the skin. In the meantime, our group also found that the PEG derivatives of polysorbate emulsifiers with higher molecular weight did not show the property of extracting skin lipids (Liu and Lunter, 2020a; Zhang and Lunter, 2018a). According to these, one can assume that the PEG alkyl ethers with more PEG units possessing higher molecular weight may also be struggling to interfere with the skin barrier. Therefore, to find the approximate boundary of PEG number limiting the access of PEGylated emulsifiers into the skin, our work first aimed to investigate PEG-stearyl ethers' interaction potential with increasing PEG-chain length.

To assess the skin barrier properties with the percutaneous application of emulsifiers, SC thickness, as associated with the reduction of SC components and change of morphology, has become an attractive reflection (Choe et al., 2016; Dąbrowska et al., 2016). Preliminary works, dealing with the alteration of SC thickness, can be traced from varying aspects. Zhang et al. found that the removal of SC lipids by emulsifiers were in line with the trend of decreasing SC thickness, which evidenced the link of skin irritation and skin thickness (Zhang and Lunter, 2018a). Application of skin thickness as a diagnostic criterion has also been discussed. In this regard, Sedky et al. found that skin thickening can be considered a characteristic manifestation of systemic sclerosis (Sedky et al., 2013). Additionally, comparable thickness values served as a measure for the SC integrity in plenty of studies (Berthaud and Boncheva, 2011; Pany et al., 2018). Based on these findings, SC thickness is of high interest to be analyzed and of great importance to be correctly and accurately determined.

Currently, varying attempts to develop excellent approaches for measuring SC thickness have been implemented. Comparing these techniques, CRS as a non-destructive method shows the benefit of controlling the measurement depth and, in the meantime, saves time and effort. The application of CRS in evaluating layer thickness has been considerably discussed, especially in the field of physical and material science (Belu et al., 2008; Ledinský et al., 2016). In skin research, our group applied the keratin signal to evaluate the SC thickness of isolated SC (Zhang and Lunter, 2018a). Caspers et al. reported measuring the in vivo SC thickness according to the water mass percentage profile against depth (Caspers et al., 2000). Ri et al. developed a new method based on determining the DNA concentration profile (Ri et al., 2020). As described above, there have been continuous efforts to find dermal spectral features to identify the epidermal layers, while the correct instrument configurations inducing accurate skin thickness estimations have not yet been fully studied. However, literature underlining the selections of objectives, including the types of dry objectives (metallurgic air objectives) and immersion objectives (normally immersion medium: water or oil) have already been investigated. Everall (Everall, 2010; 2000a) discussed the refraction-induced distortion in exquisite detail while using dry objectives, and introduced a mathematical model to correct such errors. Lunter also showed the penetration profiles are affected by different objectives and pinhole sizes (Lunter, 2017). Although much has been learned, there is still little known about the

optimal configuration for precise thickness value determination.

Thus, we also aimed at optimizing the CRS configuration including the varying types of objectives and differing sizes of the pinhole (Everall et al., 2007) which have both been reported to influence the detected thickness values in different studying areas. With this goal, this practical experimental design, particularly for skin samples, can provide the most authentic data and reference for further skin studies. Mathematical correction of measured thickness with non-optimal microscopic setup is also provided. The establishment of correlation within varying combinations can also be used for simple data corrections and reliable interlaboratory comparison. The comparable thickness values can help identify novel insight to assess the PEG-stearyl ethers' influence on skin.

2. Materials and methods

2.1. Material

PEG alkyl ethers (Chemical structure was shown in Fig. 1) including PEG-10 stearyl ether (S10), PEG-20 stearyl ether (S20), PEG-40 stearyl ether (S40) and PEG-100 stearyl ether (S100) were purchased from Croda GmbH, (Nettetal, Germany). Sodium lauryl sulfate (SLS) was obtained from Cognis GmbH & Co. KG (Düsseldorf, Germany). Trypsin type II-S (lyophilized powder) and trypsin inhibitor (lyophilized powder) were obtained from Sigma-Aldrich Chemie GmbH (Steinheim, Germany). Parafilm® was from Bemis Company Inc., (Oshkosh, WI, USA). Sodium chloride, disodium hydrogen phosphate, potassium dihydrogen phosphate, and potassium chloride were of European Pharmacopoeia grade. All aqueous solutions were prepared with ultrapure water (Elga Maxima, High Wycombe, UK).

Porcine ear skins (German landrace; age: 15–30 weeks; weight: 40–65 kg) were provided by Department of Experimental Medicine at the University of Tuebingen. The Department of Pharmaceutical Technology at the University of Tuebingen has been registered to use animal products (registration number: DE 08 416 1052 21).

2.2. Dermatomed porcine ear skin

Fresh porcine ears were cleaned with isotonic saline. Full-thickness skin was removed from cartilage and gently cleaned from blood with cotton swabs and isotonic saline. The obtained postauricular skin sheets were then dried with soft tissue, cut into strips of approximately 3 cm width and stretched onto a Styrofoam plate (wrapped with aluminium foil) with pins to minimize the effect of furrows. Skin hairs were trimmed to approximately 0.5 mm with electric hair clippers (QC5115/15, Philips, Netherlands). Subsequently, the skin was dermatomed to a thickness of 0.8 mm (Dermatom GA 630, Aesculap AG & Co. KG, Tuttlingen, Germany) and punched out for circle diameter 25 mm. Afterwards, the skin circles were wrapped with aluminium foil and stored in a freezer at − 30 °C. On the day of the experiment, the skin sample was thawed to room temperature and ready for next the procedures. This dermatome procedure has been previously described by our group (Liu and Lunter, 2020b).
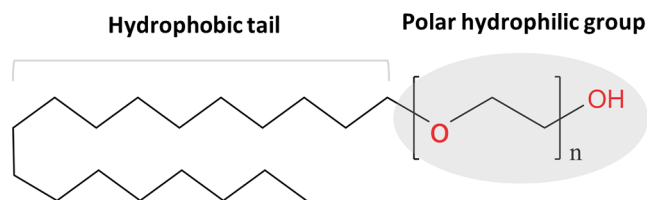

Fig. 1. Chemical structure of PEG-n stearyl ether which is composed of polar hydrophilic group and hydrophobic tail and where "n" represents the average number of oxyethylene groups.

2.3. Franz cells incubation of skin samples

Franz diffusion cells have been commonly used as a specific analytical setup for ex vivo determination of skin absorption. Here, degassed, prewarmed (32 °C) phosphate-buffered saline (PBS) was used as receptor fluid and filled in the Franz diffusion cells (Gauer Glas, Püttlingen, Germany) of 12 mL. The stirring speed of the receptor fluid was 500 rpm. The dermatomed skin circles were mounted onto the cells with donor compartment on above. The equipped Franz diffusion cells were put into a water bath with a temperature of 32 °C. After a short equilibration time of 30 min, 1 mL of each emulsifier solution was applied to each skin sample. Then, a piece of parafilm was capped onto each donor compartment to prevent evaporation. After 4 h incubation, skin samples were removed from the cells, and each skin surface was gently washed and cleaned with isotonic saline and cotton swabs for 30 times to remove the remaining sample and avoid erroneous measuring results. Finally, the actual application area (15 mm in diameter) was punched out and patted dry with cotton swabs. Herein, each sample was applied to the skin in triplicate. A detailed description of this method is available in a previous publication from our group (Zhang and Lunter, 2018b).

2.4. Stratum corneum isolation and drying

The stratum corneum was isolated following the trypsin digestion process described by Kligman et al. (Kligman, 1963; Zhang and Lunter, 2018a). This isolation procedure has been proven not to influence the lamellar lipid organization. The obtained skin circles (with a diameter of 15 mm) were placed dermal side down on filter paper soaked with a 0.2% trypsin and PBS solution. After the incubation of skin samples overnight at room temperature, digested SC was peeled off gently and immersed into 0.05% trypsin inhibitor solution for 1 min. Afterwards, the isolated SC was washed with fresh purified water for min. five times. In order to control variables and reduce errors when comparing thickness measuring approaches. The final obtained SC sheet was split into two parts. Half of it was placed onto a glass slide for CRS measurements. Another half was put onto a non-ferrous substrate for measurements with the micrometer gauge. Before the measurements, samples were stored in a desiccator to dry for min. three days.

2.5. Characterization of SC thickness measurements

2.5.1. Authentic SC thickness value measured by micrometer gauge

After treatment with different emulsifiers, the SC thicknesses were measured with eddy current method, using a Fischer ISOSCOPE® FMP10 portable instrument equipped with FTA3.3H probe (Helmut Fisher, Sindelfingen, Germany). To reduce the effects of skin hair which can accidentally cause errors when measuring the distance between SC surface to sample substrate, hair was very gently removed when washing the isolated SC in water. SC samples were then put on non-ferrous substrates. Each skin sample was measured for over 18 times at different places. The averages and standard deviations were then calculated for comparisons.

2.5.2. Instrumentation details of confocal Raman spectroscopy (CRS)

CRS configurations were taken into account to find the optimal settings for precise measurement of SC thickness. After drying, the SC sheets were taken out of the desiccator and fit onto the scan table of alpha 500 R confocal Raman microscope (WITec GmbH, Ulm, Germany). This CRS device was equipped with a 532 nm excitation laser, UHTS 300 spectrometer and DV401-BV CCD camera. To avoid skin samples' damage due to higher laser intensity, the laser power was set to 10 mW, which could be adjusted using the optimal power meter (PM100D, Thorlabs GmbH, Dachau, Germany).

Objectives and pinhole sizes were the main factors that were meant to be investigated to discover the optimal configuration for accurate SC thickness measurements. The objectives investigated in this study include the 40x 0.6NA (S Plan Fluor ELWD, Nikon, Tokyo, Japan), 100 × 0.9NA (EC Epiplan-neofluor, Carl Zeiss, Jena, Germany) dry objectives as well as the 63x 1.0NA water immersion objective (W Plan-Apochromat, Carl Zeiss, Jena, Germany) and 100x 1.25NA oil immersion objective (E Plan, Nikon, Tokyo, Japan)). Different pinhole sizes of 25 μm and 50 μm were combined separately. In specific, the samples measured with immersion objectives were mounted with a coverslip to avoid sample contaminations.

During the measurement, the light was focused through the objectives onto the skin surface. The backscattered light from the skin was then dispersed by an optical grating (600 g/mm) to achieve the spectral range from 0 to 4000 cm^{-1}. The scattered light was collected and analyzed on a charge-coupled device (DV401-BV CCD detector) which had been cooled down to − 60 °C in advance. The CRS measurements were performed based on a method developed by Zhang et al. (Zhang and Lunter, 2018b).

To measure SC thickness, the spectra were detected with the focus point moving from − 50 μm beneath the skin to 50 μm above the skin with the step size of 1 μm. The spectra were then collected for each spot with an integration time of 1 s and 4 accumulations. The skin surface was determined using the keratin signal intensity (ν (CH$_3$), 2920–2960 cm^{-1}). The area under the curve (AUC) of the keratin peak was calculated and plotted against depth. While the keratin signal intensity reaches the half maximum, the laser spot would be located at the boundary between the glass slide and the skin bottom or the boundary between the skin surface and the air. The spectrum extracted from the boundary between the skin surface and the air was regarded as skin surface and used for lipid signal analysis. The full width of half maximum (FWHM) could serve as skin sample thickness with the description above.

2.6. Skin lipid content analysis via CRS spectral markers

It has been well demonstrated that the skin lipid extraction and reduced lipid content were in line with skin thickness reduction (Zhang and Lunter, 2018a). Thus, SC lipid contents were supposed to be analyzed to evidence the alteration of SC thickness after treating the skin with PEG-n stearyl ethers.

Based on previous research, the spectral signal in the fingerprint region is more sensitive to analyze the skin lipid content used in this study (Liu and Lunter, 2020c). In detail, the δ (CH$_2$, CH$_3$)-mode at 1425–1490 cm^{-1} is relevant to the lipid signal. The ν (C═O)-mode at 1630–1710 cm^{-1} is derived from the amide I mode. In general, the spectral intensity varies to some extent between different skin samples and different donors. The amide-I mode displays the least variation within one donor or among different donors. To account for the described variation of spectral intensity, the lipid-related signal can be normalized by the amide-I signal for calculating the relevant lipid content.

2.7. Spectral and statistical data analysis

The initial processing step of Raman spectra usually included the spectral cosmic ray removal, smoothing as well as background subtraction which was performed by the WITec Project Software (WITec GmbH). The smoothing process, Savitzky-Golay (SG) filter was applied with third polynomial order and nine smoothing points. For the type of background subtraction, an automatic polynomial function was fit to the spectrum and subtracted. Furthermore, the AUC extracted in this study is the integrated area under a specified peak of the spectrum and could be calculated using the trapezoidal method on WITec Project Software.

Data were acquired from three replicates repeated for over 6 times, generating repeated measurements of over 18 times (n ≥ 18). The graphs are shown with mean values ± standard deviations (mean ± SD). Statistical differences were determined using one-way or two-way analysis of variance (ANOVA) followed by Student-Newman-Keuls (SNK) which were employed by GraphPad Prism 7.0 (GraphPad

Software Inc., La Jolla, CA, USA). Diagrams and statistical differences were ultimately generated. Significant differences are marked with different number of asterisks: * p < 0.05, ** p < 0.01, *** p < 0.001.

3. Results

Skin samples treated with PEG-n stearyl ethers were investigated for SC thicknesses. According to previous results, different PEG numbers of PEGylated emulsifiers will show different effects on the skin barrier. In this work, results from micrometer gauge were used to optimize the different configurations of CRS detected thicknesses. Insights concerning the effects caused by PEGylated emulsifiers can then be obtained. Simultaneously, water was used here as a negative control for skin treatment, and SLS was used as a positive control due to its extensively documented skin irritative effects. Besides, after treating the skin with different emulsifiers, the skin lipid content should also follow the SC thickness changes. Therefore, the lipid contents were subsequently calculated for verification of thickness results and emulsifier effects.

3.1. Authentic SC thicknesses after skin treatments of emulsifiers

Accurate detection of SC thickness should be first established to be used as a reference for verifying and correcting the CRS results. Subsequently, the thickness differences among varying PEG-stearyl ethers treated skins can thus also be determined precisely. Here, a micrometer gauge with the principle of magnetic induction and eddy current approach was applied since it has been widely accepted to gain accurate results and is often regarded as the reference for studying advanced alternatives. Then the thicknesses of obtained SCs after the treatment with PEG-stearyl ethers were detected. Fig. 2 shows the comparison of their different thickness values. The SC thickness of the reference (water treated skin) exhibits an average thickness of 13.69 ± 2.45 μm. The decrease of SC thickness compared with water treated skin can reflect the irritative effects on the skin barrier. The most prominent reduction of SC thickness was observed after the cutaneous application of SLS, which can be easily expected to damage the skin barrier to a great extent. Furthermore, PEG-stearyl ethers were focused and indicated different impacts on the skin. It can be seen that S10 and S20 both showed significant effects on decreasing the SC thickness with the detected values of 10.93 ± 1.98 μm and 8.76 ± 1.45 μm respectively, suggesting their capability of extracting skin components or producing loosely-packed skin barrier structures. Interestingly, an only moderate effect was observed when applying S40, indicating smaller skin irritation. More surprisingly, S100 was observed to have no significant effect on reducing the SC thickness, which shows the average thickness of 13.86 ± 1.87 μm. The results of S40 and S100 were not expected since our previous study found increasing irritating effects with the increase PEG chain length.
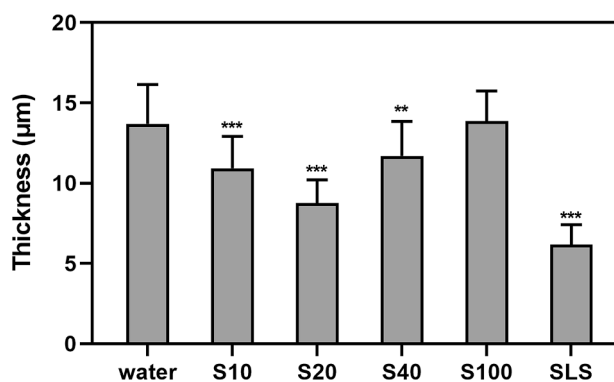

Fig. 2. Thickness of SC measured with micrometer gauge after treatment of PEG-stearyl ethers. Each individual skin sample was split in two halves for analysis with micrometer gauge and CRS separately. Mean $\pm$ SD, n ≥ 18. * p < 0.05, ** p < 0.01, *** p < 0.001.

On the other hand, they were in line with the previous results of polysorbate emulsifiers which showed mild effects on the skin (Liu and Lunter, 2020a; Zhang and Lunter, 2018a).

3.2. SC thickness measured by CRS with different configurations

The same SC pieces were analyzed on the CRS instrument. Two dry objectives and two immersion objectives were combined separately with two different pinhole sizes (25 μm and 50 μm). It is easy to observe from Fig. 3a and b that the SC thicknesses measured by dry objectives are significantly lower than those measured by the micrometer gauge. To be specific, the SC thicknesses evaluated by the dry 40 × 0.6NA objective varied in the range of 4.5–7.6 μm whereas assessed by the dry 100 × 0.9NA objective the thickness differed between 2.0 and 4.5 μm. Thus, both objectives underestimated SC thicknesses. Meanwhile, the emulsifiers' effects cannot be well discriminated. Using the dry 100 × 0.9NA objective, only S20 and SLS were determined to reduce the SC thickness. Via the dry 40 × 0.6NA objective, only slight differences can be identified for S10 and S40. In the meantime, although pinhole size seems to be an inconsequential factor here, slight differences can still be noticed from Fig. 3a. Only 40 × objective combined with 50 μm pinhole captured the decrease of thickness caused by S40. Thus, the dry objectives were found to be less sensitive to evaluate the sample differences here.

As shown in Fig. 3c and d, immersion objectives seem to give a closer estimation of SC thicknesses. Both objectives gave results from which statistical differences could be found between skin samples. The combinations of water objective or oil objective with 50 μm pinhole displayed identical results compared with the micrometer gauge. Instead, immersion objectives combined with 25 μm pinhole size appeared relatively less sensitive to differentiate between samples. It can be observed from Fig. 3c that S10 and S40 only showed moderate and slight differences between each other when evaluated by the water objective in combination with the 25 μm pinhole. Similar results were also found when using the oil objective mounted with 25 μm pinhole. Thus, when analyzing the statistical differences, larger pinhole size is better suited to compare emulsifiers' impact in SC thickness. Even so, the role of immersion objectives can still be highlighted. They have more advantages than dry objectives. The obtained values were much closer to the real thickness values. The factor of pinhole size did not show a great impact on the examined values. However, slight impacts can still be identified with a smaller pinhole size.

3.3. Effects of CRS configuration on spectral signals

The signal to noise ratio (SNR) and signal intensity of spectra are two important issues affecting the discrimination of spectral signals. Fig. 4a presents the SC spectra using oil or water objectives equipped with 25 μm or 50 μm pinholes. These spectra were extracted from the depth point of highest intensity, i.e., just below the SC surface. It can be noticed that the oil objective setups generate lower SNR. In particular, the spectrum obtained from the oil objective combined with 25 μm pinhole represents the lowest SNR. In contrast, the SNR of spectra obtained from the water objectives was drastically improved. However, obvious differences in spectra cannot be clearly found by using different pinhole sizes. As is generally known, good SNR is essential to display more biochemical information about biological samples. Thus, water objectives obviously have a greater advantage than oil objectives in skin analysis.

Fig. 4b shows the AUC profiles of the keratin peak signal against skin depth. Obviously, spectra collected by the water objective equipped with 50 μm pinhole exhibit the highest intensity. The intensity curves generated by water objective/25 μm pinhole and oil objective/50 μm pinhole are similar to each other, while their intensities in deeper layers are relatively lower. The lowest intensity profile was obtained from the configuration of oil objective and 25 μm pinhole. According to these
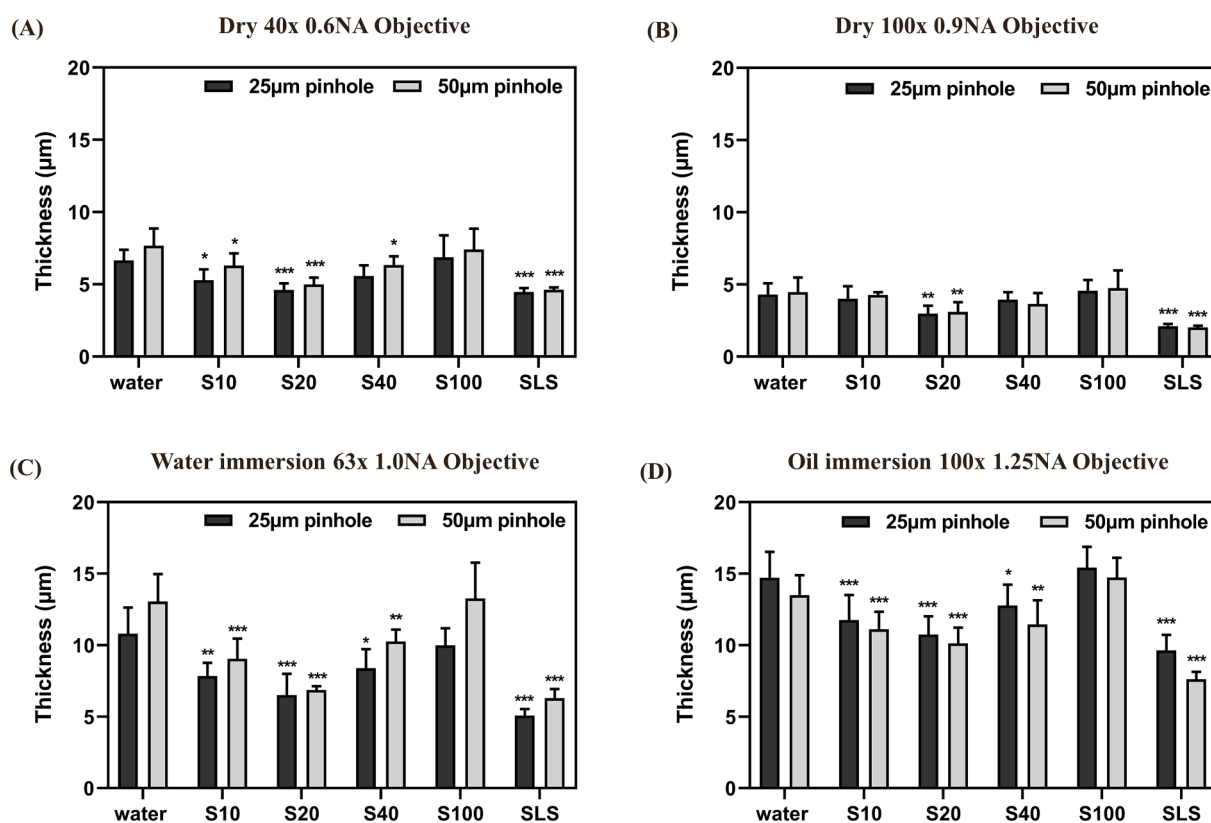
Fig. 3. Thickness of SC measured with different configurations of CRS device after treatment of emulsifiers, (A) dry 40 × 0.6NA objective, (B) dry 100 × 0.9NA objective, (C) water immersion 63 × 1.0NA objective, (D) oil immersion 100 × 1.25NA objective. Each individual skin sample was split in two halves for analysis with micrometer gauge and CRS separately. Mean ± SD, n ≥ 18. * $p < 0.05$, ** $p < 0.01$, *** $p < 0.001$.
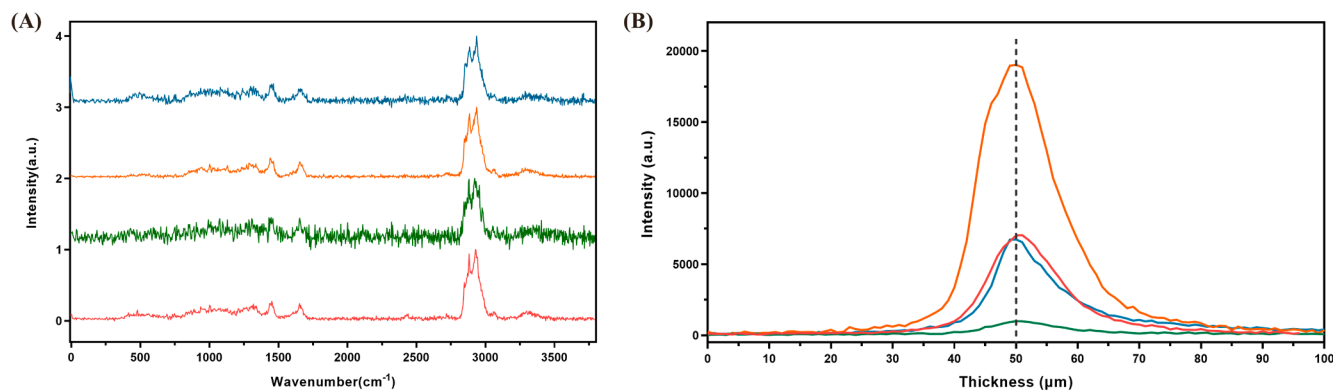

Fig. 4. (A) Signal to noise ratio and (B) intensity of skin spectra obtained from different configurations of CRS including the water/oil immersion objectives incoporated with 25 μm/50 μm pinholes (blue: pinhole-50 μm/oil immersion 100 × 1.25NA; green: pinhole-25 μm/oil immersion 100 × 1.25NA; organge: pinhole-25 μm/water immersion 63 × 1.0NA; red: pinhole-50 μm/water immersion 63 × 1.0NA).

comparisons, the use of smaller pinhole diameter decreased the signal intensity. For the practical experiment, the spectral signal should be as high as possible when ensuring the appropriate resolution. Thus, 50 μm pinhole combined with water objective represents a greater advantage in our study.

3.4. Correlations and corrections of SC thickness measured via CRS

Fig. 5 and 6 show the correlations of dry objectives and immersion objectives, respectively. The p-values represented indicate all comparisons of significant correlations. Strong positive correlations are observed from both figures as the correlation coefficients (R^2) are close to 1. It can be deduced that the thicknesses detected by CRS show the same trend as

the reference values. These good correlations give us a hint that the use of varying CRS configurations only causes the decrease or increase of values as a whole. The comparison between one and other can still be rightly performed.

Simultaneously, linear regressions were calculated, which produced equations enabling the verification of the most accurate skin thickness determinations. As can be seen from Fig. 5 and 6, the slope of the regression of the water objective/50 μm pinhole is the closest to 1 ($r^2 = 0.962$), allowing the most precise determination. Concerning the oil objective, although the slope is also close to 1, the intercept added will cause overestimation of thickness. However, it can be found that the equations generated can also be used to correct the thickness values determined using sub-optimal CRS configurations. This can provide
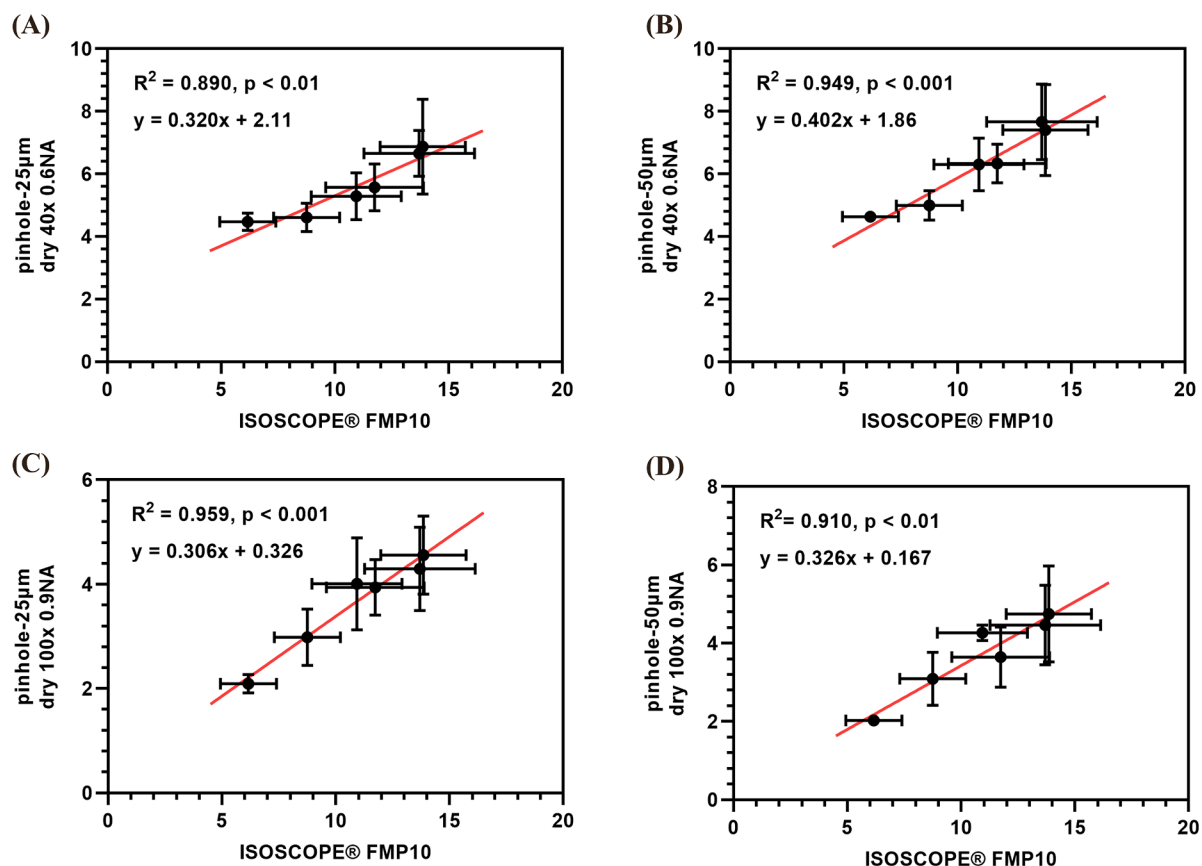
Fig. 5. Correlation plot and linear regression of SC thickness measured by different configurations of CRS and micrometer gauge after treatment of emulsifiers, (A) dry 40 × 0.6NA objective and 25 μm pinhole, (B) dry 40 × 0.6NA objective and 50 μm pinhole, (C) dry 100 × 0.6NA objective and 25 μm pinhole, (B) dry 100 × 0.6NA objective and 50 μm pinhole.

practical support for other laboratories to correct the depth analysis values obtained using the same configurations.

3.5. Lipid content analysis utilizing CRS

Lipid content was analyzed to verify the influences caused by emulsifiers since the findings from our group have demonstrated that the extraction or reduction of skin lipid components will simultaneously decrease the skin thickness by using varying emulsifiers or formulations treated skin samples (Liu and Lunter, 2020a; Zhang and Lunter, 2018a). Thus, in this study, we calculated the SC lipid content after normalizing the CRS spectra (as shown in Fig. 7). The water treated SC presented the normalized value of around 1.14, which was used as a reference here. A lower normalized value than that of the reference indicates a higher tendency of emulsifiers to extract the lipid components and disrupt the barrier function. The most significant decrease can be seen from SLS, and S20 treated SCs, which reduced the lipid content by approximately 19.7% and 14.9%. Subsequently, S10 also showed the ability to impair the SC lipid content. Moderate significance was observed with the decrease of the lipid content by nearly 8.93%. In the meantime, no prominent effect was observed with the skin treatment of S100, indicating lower extraction of lipids and thus fewer irritant effects. Those above-mentioned significant differences were in line with the differences observed in comparing the differences in SC thicknesses obtained after incubation with the emulsifiers except for S40 treated skin. Interestingly, no lipid extraction caused by S40 was detected although its negative effects on SC thickness have been identified. We speculate that the spectral signal might not be sensitive enough to differentiate the small differences of lipid contents since the other variations of lipid contents are broadly consistent with the changes of SC thicknesses. In

summary, we believe this analysis provided a better chance to verify emulsifiers' influences on the skin barrier.

4. Discussion

One of our study's main purposes was to examine the varying effects of PEG-n stearyl ethers on skin. According to the results, the most prominent influence was interestingly found after the treatment with S20. To some extent, this finding was unexpected as it has been inferred previously that the increasing PEG number will encourage irritating effects on the skin (Liu and Lunter, 2020a). However, S100 surprisingly indicated no influence on the skin, and the results found for S40 suggested weaker effects. These discoveries can clearly offer an interesting mechanism in explaining their skin barrier irritation. Presumably, their performance could be explained by the influence theory of molecular structure sizes, which can be described such that the large molecule structures limit their penetration into the skin. Some evidence can be traced from the study of Casiraghi et al. who investigated the skin permeation of ketoprofen and found that PEG-40 stearate induced no significant increase of permeation whereas PEG-8 stearate and PEG-12 stearate did show significant increases (Casiraghi et al., 2012). Although the systematic study of the other PEG-n stearates is lacking, it could still be suggested that the number of oxyethylene groups governing the entry of PEGylated emulsifiers inside skin might be around 40. This promising finding give us the hint that different key factors can dominate the irritative effects induced by PEGylated emulsifiers. Their ability to damage the skin barrier can be estimated by the oxyethylene group numbers and simultaneously considering their structure sizes. Therefore, it can also be advantageous to select potential candidates for drug delivery systems that generate milder skin effects. Except for the
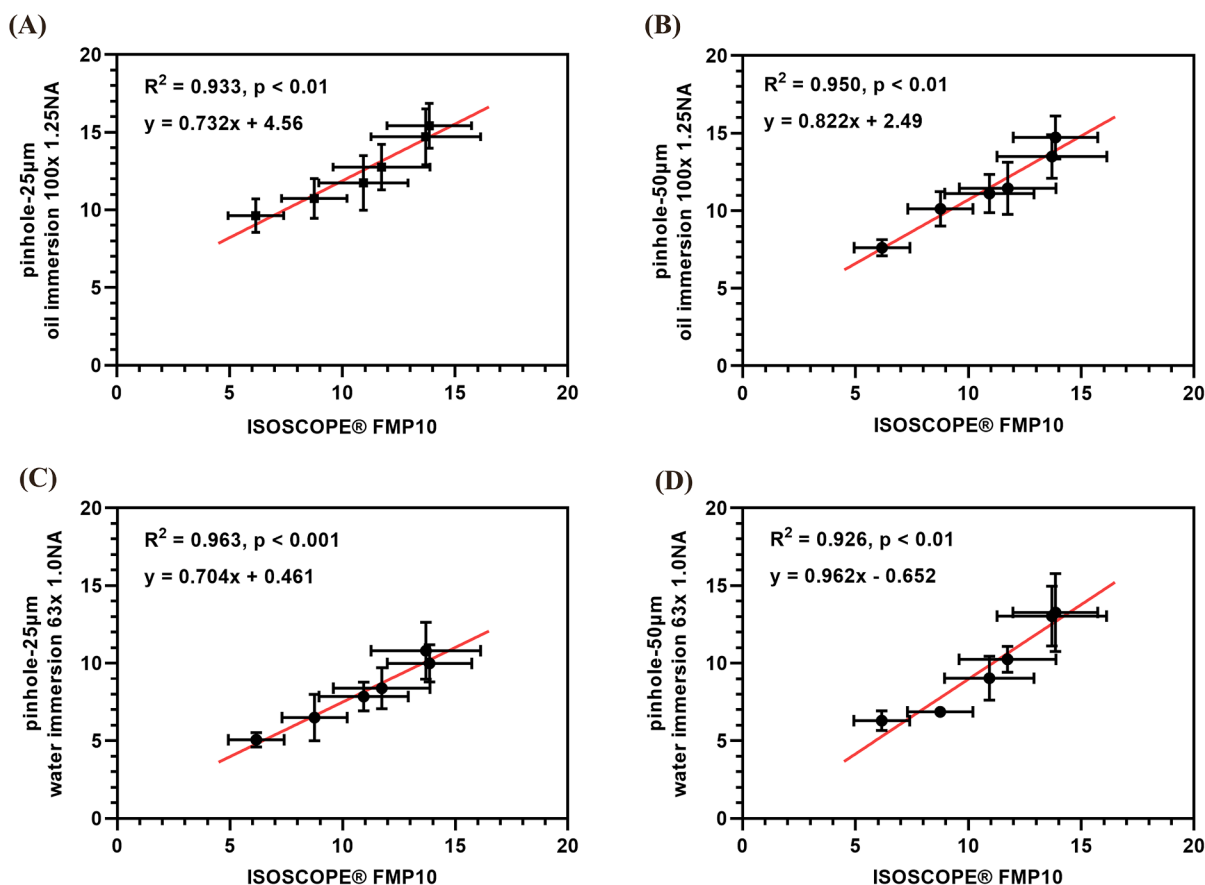
Fig. 6. Correlation plot and linear regression of SC thickness measured by different configurations of CRS and micrometer gauge after treatment of emulsifiers, (A) oil immersion 100×1.25NA objective and 25 µm pinhole, (B) oil immersion 100×1.25NA objective and 50 µm pinhole, (C) water immersion 63×1.0NA objective and 25 µm pinhole, (B) water immersion 63×1.0NA objective and 50 µm pinhole.
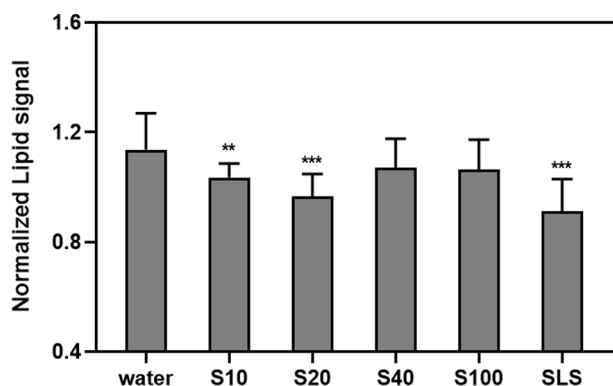

Fig. 7. Skin lipid content analysis by CRS after treatment of emulsifiers, mean $\pm$ SD, n = 18. * $p < 0.05$, ** $p < 0.01$, *** $p < 0.001$.

direct summary of PEGylated emulsifiers, non-irritative influences of polysorbate emulsifiers found in our previous studies (Liu and Lunter, 2020a; Zhang and Lunter, 2018a) can also be explained. It can be suggested that the polysorbate emulsifiers with relatively larger molecular sizes or polar head groups will be more friendly to the skin.

We also aimed to optimize CRS configuration to find its capability to determine the SC thickness accurately. Based on the results, one can be clearly aware that the immersion objectives improved the accuracy of the SC thickness measurements considerably. From a theoretical view, the refractive indices between SC (1.41) and air (1.00) differ widely, resulting in optical distortion whereas the refractive indices of water (1.33) and oil (1.51) are closer to that of the SC which can help to

improve the correctness. In this respect, our findings of better-suited immersion objectives agree with the inner principles of reducing the refractive distortions (Everall, 2010; 2000b). On a more refined level, water immersion objective outperformed the oil objective in our study with slightly better accuracy regarding thickness estimation and greatly improved SNR. Except that, oil is also not an elegant choice in experimental practice. It exhibits higher viscosity than water which is thus difficult to wipe off and in turn, easily causes measuring errors as it sticks to the cover glass. In contrast, water as an alternative has no risk of contaminating the samples. Still, there is no need for special cleanup methods, and the cost is negligible. On the other hand, the importance of pinhole size cannot be neglected. Our findings confirm that smaller pinhole size will prominently cause a decrease in the intensity of the signal reaching the detector. Although the larger pinhole will theoretically reduce depth resolution, good compensation can still be observed using the 50 µm pinhole in conjunction with immersion objectives to achieve precise results.

5. Conclusion

We found varying effects of a series of PEG-stearyl ethers on skin. The presented data broke the supposition that the number of oxyethylene groups primarily governs PEGylated emulsifiers' irritation of the skin. New guidance concerning their molecular structure sizes was suggested. The number of 40 oxyethylene groups may be considered the boundary to determine PEG-stearyl ether's ability to irritate the skin. Further experiments should be done about their penetration and permeation ability which will be of high interest to find the optimal candidate with penetration or permeation enhancement abilities and less-irritative and skin-friendly properties.

CRS showed the possibility to be used as a strong alternative for precisely determining SC thickness. The CRS configuration was optimized to be the combination of water immersion objective and 50 μm pinhole. In conclusion, metallurgic air objectives significantly underestimated the thickness values, whereas the immersion objectives gave more precise results. Improved SNR and signal intensity were the benefits of this configuration compared with oil immersion objectives and smaller pinhole size. Furthermore, the established correlations can be an excellent example of authentic skin thickness studies and can correct errors to some extent.

6. Statement of ethics

Porcine ears were acquired from the Department of Experimental Medicine of University Hospital Tuebingen. Live animals used were kept at the Department of Experimental Medicine and sacrificed in their experiments approved by the ethics committee of University Hospital Tuebingen. Those ears were received directly after the death of the animals. Before the study, Department of Pharmaceutical Technology has registered for the use of animal products at the District Office of Tuebingen (registration number: DE 08 416 1052 21).

CRediT authorship contribution statement

Yali Liu: Conceptualization, Data curation, Funding acquisition, Investigation, Methodology, Writing - original draft. **Dominique Jasmin Lunter:** Conceptualization, Funding acquisition, Methodology, Project administration, Supervision, Writing - review & editing.

Declaration of Competing Interest

The authors declare that they have no known competing financial interests or personal relationships that could have appeared to influence the work reported in this paper.

Acknowledgments

References

Ashtikar, M., Matthäus, C., Schmitt, M., Krafft, C., Fahr, A., Popp, J., 2013. Non-invasive depth profile imaging of the stratum corneum using confocal Raman microscopy: First insights into the method. Eur. J. Pharm. Sci. 50 (5), 601–608. https://doi.org/10.1016/j.ejps.2013.05.030.

Bárány, E., Lindberg, M., Lodén, M., 2000. Unexpected skin barrier influence from nonionic emulsifiers. Int. J. Pharm. 195 (1-2), 189–195. https://doi.org/10.1016/S0378-5173(99)00388-9.

Belu, A., Mahoney, C., Wormuth, K., 2008. Chemical imaging of drug eluting coatings: Combining surface analysis and confocal Raman microscopy. J. Control. Release 126 (2), 111–121. https://doi.org/10.1016/j.jconrel.2007.11.015.

Berthaud, F., Boncheva, M., 2011. Correlation between the properties of the lipid matrix and the degrees of integrity and cohesion in healthy human Stratum corneum. Exp. Dermatol. 20, 255–262. https://doi.org/10.1111/j.1600-0625.2010.01164.x.

Biniek, K., Kaczvinsky, J., Matts, P., Dauskardt, R.H., 2015. Understanding age-induced alterations to the biomechanical barrier function of human stratum corneum. J. Dermatol. Sci. 80 (2), 94–101. https://doi.org/10.1016/j.jdermsci.2015.07.016.

Casiraghi, A., Di Grigoli, M., Cilurzo, F., Gennari, C.G.M., Rossoni, G., Minghetti, P., 2012. The influence of the polar head and the hydrophobic chain on the skin penetration enhancement effect of poly(ethylene glycol) derivatives. AAPS PharmSciTech 13 (1), 247–253. https://doi.org/10.1208/s12249-011-9745-4.

Caspers, P.J., Lucassen, G.W., Bruining, H.A., Puppels, G.J., 2000. Automated depth-scanning confocal Raman microspectrometer for rapid in vivo determination of water concentration profiles in human skin. J. Raman Spectrosc. 31, 813–818. https://doi.org/10.1002/1097-4555(200008/09)31:8/9<813::AID-JRS573>3.0.CO;2-7.

Choe, C.S., Lademann, J., Darvin, M.E., 2016. Lipid organization and stratum corneum thickness determined in vivo in human skin analyzing lipid–keratin peak

(2820–3030 cm−1) using confocal Raman microscopy. J. Raman Spectrosc. 47, 1327–1331. https://doi.org/10.1002/jrs.4975.

Dąbrowska, A.K., Adlhart, C., Spano, F., Rotaru, G.-M., Derler, S., Zhai, L., Spencer, N.D., Rossi, R.M., 2016. In vivo confirmation of hydration-induced changes in human-skin thickness, roughness and interaction with the environment. Biointerphases 11 (3), 031015. https://doi.org/10.1116/1.4962547.

Everall, N., Lapham, J., Adar, F., Whitley, A., Lee, E., Mamedov, S., 2007. Optimizing depth resolution in confocal Raman microscopy: A comparison of metallurgical, dry corrected, and oil immersion objectives. Appl. Spectrosc. 61 (3), 251–259. https://doi.org/10.1366/000370207780220859.

Everall, N.J., 2010. Confocal Raman microscopy: Common errors and artefacts. Analyst 135, 2512–2522. https://doi.org/10.1039/c0an00371a.

Everall, N.J., 2000a. Modeling and measuring the effect of refraction on the depth resolution of confocal Raman microscopy. Appl. Spectrosc. 54 (6), 773–782. https://doi.org/10.1366/0003702001950382.

Everall, N.J., 2000b. Confocal Raman microscopy: Why the depth resolution and spatial accuracy can be much worse than you think. Appl. Spectrosc. 54 (10), 1515–1520. https://doi.org/10.1366/0003702001948439.

Ghadially, R., Reed, J.T., Elias, P.M., 1996. Stratum Corneum structure and function correlates with phenotype in psoriasis. J. Invest. Dermatol. 107 (4), 558–564. https://doi.org/10.1111/1523-1747.ep12582813.

Ghanbarzadeh, S., Khorrami, A., Arami, S., 2015. Nonionic surfactant-based vesicular system for transdermal drug delivery. Drug Deliv. 22 (8), 1071–1077. https://doi.org/10.3109/10717544.2013.873837.

Kligman, A.M., 1963. Preparation of Isolated Sheets of Human Stratum Corneum. Arch. Dermatol. 88, 702. https://doi.org/10.1001/archderm.1963.01590240026005.

Kumar, G.P., Rajeshwarrao, P., 2011. Nonionic surfactant vesicular systems for effective drug delivery—an overview. Acta Pharm. Sin. B 1 (4), 208–219. https://doi.org/10.1016/j.apsb.2011.09.002.

Ledinský, M., Paviet-Salomon, B., Vetushka, A., Geissbühler, J., Tomasi, A., Despeisse, M., De Wolf, S., Ballif, C., Fejfar, A., 2016. Profilometry of thin films on rough substrates by Raman spectroscopy. Sci. Rep. 6, 4–10. https://doi.org/10.1038/srep37859.

Liu, Y., Lunter, D.J., 2020a. Systematic investigation of the effect of non-ionic emulsifiers on skin by confocal Raman spectroscopy—a comprehensive lipid analysis. Pharmaceutics 12, 223. https://doi.org/10.3390/pharmaceutics12030223.

Liu, Y., Lunter, D.J., 2020b. Tracking heavy water incorporated confocal Raman spectroscopy for evaluating the effects of PEGylated emulsifiers on skin barrier. J. Biophotonics 1–12. https://doi.org/10.1002/jbio.202000286.

Liu, Y., Lunter, D.J., 2020c. Selective and sensitive spectral signals on confocal Raman spectroscopy for detection of ex vivo skin lipid properties. Transl. Biophotonics 2 (3). https://doi.org/10.1002/tbio.v2.310.1002/tbio.202000003.

Lunter, D.J., 2017. Determination of skin penetration profiles by confocal Raman microspectroscopy: statistical evaluation of optimal microscope configuration. J. Raman Spectrosc. 48 (2), 152–160. https://doi.org/10.1002/jrs.v48.210.1002/jrs.5001.

Pany, A., Klang, V., Brunner, M., Ruthofer, J., Schwarz, E., Valenta, C., 2018. Effect of physical and chemical hair removal methods on skin barrier function in vitro: Consequences for a hydrophilic model permeant. Skin Pharmacol. Physiol. 32 (1), 8–21. https://doi.org/10.1159/000493168.

Park, E.S., Chang, S.Y., Hahn, M., Chi, S.C., 2000. Enhancing effect of polyoxyethylene alkyl ethers on the skin permeation of ibuprofen. Int. J. Pharm. 209, 109–119. https://doi.org/10.1016/S0378-5173(00)00559-7.

Pham, Q.D., Björklund, S., Engblom, J., Topgaard, D., Sparr, E., 2016. Chemical penetration enhancers in stratum corneum - Relation between molecular effects and barrier function. J. Control. Release 232, 175–187. https://doi.org/10.1016/j.jconrel.2016.04.030.

Ri, J., Choe, S., Schleusener, J., Lademann, J., Choe, C., Darvin, M., 2020. In vivo tracking of DNA for precise determination of the stratum corneum thickness and superficial microbiome using confocal Raman microscopy. Skin Pharmacol. Physiol. 33 (1), 30–37. https://doi.org/10.1159/000503262.

Sahle, F.F., Metz, H., Wohlrab, J., Neubert, R.H.H., 2012. Polyglycerol fatty acid ester surfactant-based microemulsions for targeted delivery of ceramide AP into the stratum corneum: Formulation, characterisation, in vitro release and penetration investigation. Eur. J. Pharm. Biopharm. 82 (1), 139–150. https://doi.org/10.1016/j.ejpb.2012.05.017.

Schmitt, T., Neubert, R.H.H., 2018. State of the art in Stratum Corneum research: The biophysical properties of ceramides. Chem. Phys. Lipids 216, 91–103. https://doi.org/10.1016/j.chemphyslip.2018.09.017.

Sedky, M.M., Fawzy, S.M., Baki, N.A.E., Eishi, N.H.E., Bohy, A.E.M.M.E., 2013. Systemic sclerosis: An ultrasonographic study of skin and subcutaneous tissue in relation to clinical findings. Ski. Res. Technol. 19 (1), e78–e84. https://doi.org/10.1111/j.1600-0846.2012.00612.x.

Shin, S.-C., Cho, C.-W., Oh, I.-J., 2001. Effects of non-ionic surfactants as permeation enhancers towards piroxicam from the poloxamer gel through rat skins. Int. J. Pharm. 222 (2), 199–203. https://doi.org/10.1016/S0378-5173(01)00699-8.

Vyumvuhore, R., Tfayli, A., Biniek, K., Duplan, H., Delalleau, A., Manfait, M., Dauskardt, R., Baillet-Guffroy, A., 2015. The relationship between water loss, mechanical stress, and molecular structure of human stratum corneum ex vivo. J. Biophoton. 8 (3), 217–225. https://doi.org/10.1002/jbio.201300169.

Walters, K.A., Florence, A.T., Dugard, P.H., 1982. Interaction of polyoxyethylene alkyl ethers with cholesterol monolayers. J. Colloid Interface Sci. 89 (2), 584–587. https://doi.org/10.1016/0021-9797(82)90214-4.

Zhang, Z., Lunter, D.J., 2018a. Confocal Raman microspectroscopy as an alternative method to investigate the extraction of lipids from stratum corneum by emulsifiers and formulations. Eur. J. Pharm. Biopharm. 127, 61–71. https://doi.org/10.1016/j.ejpb.2018.02.006.

Zhang, Z., Lunter, D.J., 2018b. Confocal Raman microspectroscopy as an alternative to differential scanning calorimetry to detect the impact of emulsifiers and formulations on stratum corneum lipid conformation. Eur. J. Pharm. Sci. 121, 1–8. https://doi.org/10.1016/j.ejps.2018.05.013.

7. Profiling skin penetration using PEGylated emulsifiers as penetration enhancers via confocal Raman spectroscopy and fluorescence spectroscopy
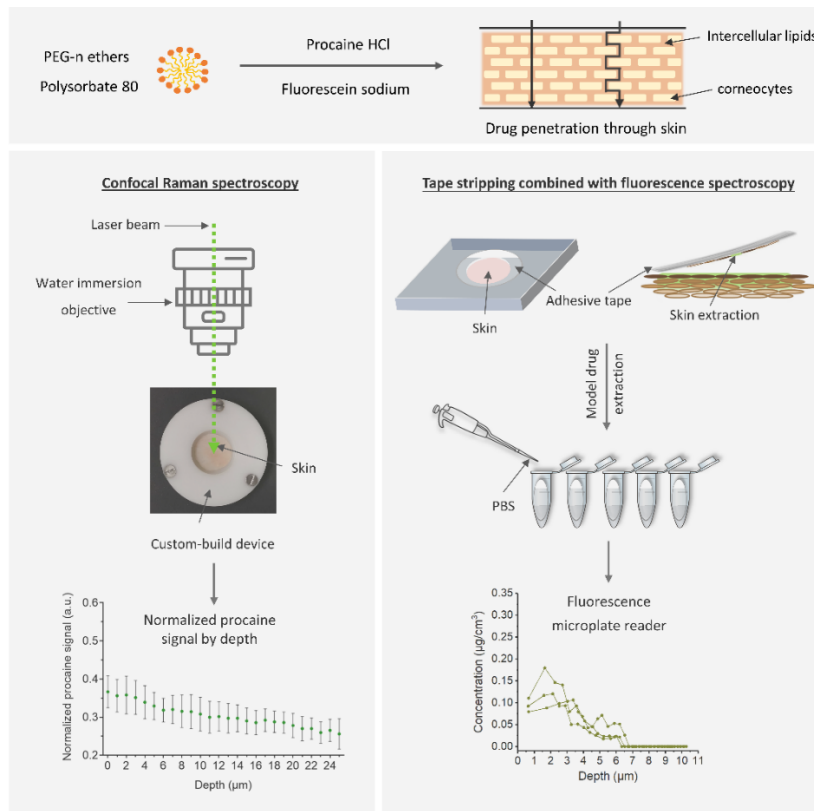
Yali Liu, Dominique Jasmin Lunter*

Department of Pharmaceutical Technology, Faculty of Science, Eberhard Karls Universität Tübingen, Auf der Morgenstelle 8, 72076 Tuebingen, Germany

Graphical Abstract

Profiling skin penetration using PEGylated emulsifiers as penetration enhancers via confocal Raman spectroscopy and fluorescence spectroscopy

Yali Liu, Dominique Jasmin Lunter [*]

Department of Pharmaceutical Technology, Faculty of Science, Eberhard Karls Universität Tübingen, Auf der Morgenstelle 8, 72076 Tuebingen, Germany

A R T I C L E   I N F O

A B S T R A C T

Non-ionic emulsifiers have been continuous research focus in skin analysis. With the aim of finding their role as penetration enhancers in dermal drug delivery systems, PEGylated emulsifiers of polyethylene glycol (PEG) ethers were targeted to be investigated ex-vivo. The effectiveness of them in the enhancement of skin penetration was examined by conventional tape stripping method and confocal Raman spectroscopy (CRS). Fluorescein sodium salt (Fluo-Na) and procaine HCl were respectively used as model drugs. The drug delivery performances were compared in the aspects of penetration amount and depth. Based on the results from both analyses, all investigated emulsifiers have the ability to enhance the amount of drug penetration. PEG-20 ethers showed higher ability than PEG-2 oleyl ether (O2) in promoting drug distribution by depth, especially PEG-20 cetyl ether (C20) showed a distinct effect. According to this study, their penetration enhancing performances seem to be linked to their interruption of intercellular lipids, which can be considered as the underlying mechanism for governing the ability of PEGylated emulsifiers as penetration enhancers. Further instrumental comparison highlighted the benefits of using CRS as an alternative in skin penetration analysis.

1. Introduction

The main challenge of dermal drug delivery comes from the skin barrier of stratum corneum (SC) [1]. As the protective layer of the human body, SC restricts the passage of desirable drugs as well [2]. To effectively deliver actives into the skin, plenty of means have been developed. Among them, using additives to assist drug penetration has been extensively accepted [3,4]. As the simplest way in drug delivery systems, the effectiveness of additives for percutaneous penetration and permeation is of great importance to be confirmed.

Emulsifiers as the common excipients have wide applications in dermatological and pharmaceutical developments [5,6]. As an important category, non-ionic emulsifiers attract attention with potential use as penetration enhancers. Increased rate of transport, including both permeation and penetration, were observable in previous studies [7,8]. The targeted PEGylated emulsifiers were from a category of non-ionic emulsifiers. In our study, three PEG-ethers with 20 oxyethylene groups were selected. Our preliminary study found that they were able to decrease the skin lipid content and disorder the skin lipid packing and conformation [9,10]. With those effects, our current perspectives aim at their corresponding effectiveness as penetration enhancers. To gain more insights on this kind of emulsifiers, PEG-2 oleyl ether was also considered, since no such influences have been found [10]. However, enhanced drug permeation performances were observed in some studies [11–13]. It is, thus, of interest to verify its function in penetration study as well.

Monitoring drug penetration has been serviced by varying techniques [14,15]. Promising choices have been emerging with different requirements. The conventional tape stripping method has been a common demand in clinical studies, which can be employed in in-vivo measurements [16,17]. With a simple procedure to apply the tape on skin and remove the skin layer, this method is still popular today in the skin research area for various purposes [18,19]. Most importantly, it allows the quantification of topically delivered drugs, enabling the determination of drug penetration profiles. Thus, in our study, tape stripping technique is one of the choices to monitor drug distribution. The hydrophilic substance of fluorescein sodium salt (Fluo-Na) was used as a model drug. However, to obtain accurate interpretations using this technique, plenty of small challenges can be encountered. Based on preliminary research, a standardized procedure is necessary to be established in performing tape stripping steps [20]. Critical parameters should also be properly considered, such as tape application method,

---

skin rinsing process and analytical approach [21,22].

Apart from the direct measurements of extracted skin components, non-invasive methods have been increasingly investigated in current trends [23,24]. Spectroscopic techniques have been well-developed to make this goal come true. In practical experiments, confocal Raman spectroscopy (CRS) and infrared spectroscopy (IR) are mostly utilized [25,26]. However, in comparison, CRS has more advantages over the latter. It allows the vertical detection through different skin depth instead of the spectroscopic signal collection from the surface only, which is an inevitable drawback for IR study. Thus, in IR analysis, other skin invasive procedures are combined, such as tape stripping or cryosectioning steps [27,28]. In contrast, CRS can give sufficient information without further steps. Therefore, CRS was applied as another choice to fulfil the plan of monitoring drug penetration. As a well-studied active for skin delivery in previous literature, procaine HCl was used as a model drug for CRS analysis [29,30]. It owns the characteristic signal which can be differentiated from skin spectra. By normalizing the peak area of the obtained signal, relative procaine concentration can be obtained for comparison.

Summarizing the main content, we chose to apply both tape stripping and Raman spectroscopic methodologies to monitor the drug distribution inside the skin with additives of PEGylated emulsifiers in this study. We aim at finding the ability of emulsifiers acting as penetration enhancers on two model drugs and simultaneously comparing the performances of the two techniques. Herein, benefits and drawbacks of techniques will be discussed. The critical role of using CRS as an alternative in skin analysis will be highlighted. Behind the intuitive observations of penetration profiles, deeper meaning and underlying mechanisms will be appropriately clarified.

2. Materials and method

2.1. Materials

The materials used were procaine HCl (Ceasar & Loretz GmbH, D-Hilden), fluorescein sodium salt (Fluo-Na, Sigma-Aldrich St. Louis, MO, USA), PEG-20 oleyl ether, PEG-20 stearyl ether, PEG-20 cetyl ether and PEG-2 oleyl ether (O20, S20, C20, O2; Croda GmbH, Nettetal, Germany), parafilm® (Bemis Company Inc., Oshkosh, WI, USA), and adhesive D-Squame® tapes (CuDerm Corporation, Dallas TX, USA). Sodium chloride, disodium hydrogen phosphate, potassium dihydrogen phosphate, and potassium chloride were of European Pharmacopoeia grade. All aqueous solutions were prepared with ultra-pure water (Elga Maxima, High Wycombe, UK).

Porcine ear skins (German landrace; age: 15 to 30 weeks; weight: 40 to 65 kg) were provided by Department of Experimental Medicine at the University of Tuebingen. The Department of Pharmaceutical Technology at the University of Tuebingen has been registered to use animal products (registration number: DE 08 416 1052 21).

2.2. Skin preparation

Porcine ears were obtained on the day of sacrifice and directly cleaned with isotonic saline. The skin was removed from cartilage, cleaned from blood, and cut into strips of approximately 3 cm width. The strips were stretched onto a Styrofoam plate with pins. Skin hairs were trimmed to around 0.5 mm with electric hair clipper (QC5115/15, Philips, Netherlands). Thereafter, the skin was dermatomed to a thickness of 1 mm (Dermatom GA 630, Aesculap AG & Co. KG, D- Melsungen), punched out for circles to a diameter of 25 mm, wrapped with aluminum foil and stored in a freezer at −28℃. This procedure has been previously described in ref. [31].

2.3. Sample application

Two different donors were separately used for procaine HCl and

Fluo-Na penetration analysis. Both experiments were performed by incubating the skin in Franz diffusion cells, which are currently the most common and acceptable technique for ex-vivo skin evaluations. In this respect, 12 mL of degassed and prewarmed (32℃) phosphate-buffered saline (PBS, pH 7.4) was used as the receptor fluid. Circular skin samples were thawed to room temperature, washed clean with PBS and placed between the cells and donor compartments. The assembled cells were clamped tight and transferred into a water bath with 500 rpm stirring speed inside cells. After the equilibration time of 30 min, prepared samples were respectively applied. With a certain application time, the actual applied area of skin sample was punched out for a diameter of 15 mm which was then used for further studies. This procedure has been carefully described in previous publications [32].

In the experiments of analyzing Fluo-Na penetrations, 5 mg/mL Fluo-Na was prepared and applied on the skin for 1 h, which was considered as reference. In comparison, different PEGylated emulsifiers were used as penetration enhancers. 5% of the respective emulsifier was incorporated into the solution and applied to the skin for 1 h.

Concerning the analysis of procaine penetration, 1% of procaine HCl was used as a reference. Likewise, 5% of PEGylated emulsifier was combined and applied to the skin for comparison.

2.4. Tape stripping method

Fluo-Na penetration was evaluated with tape stripping method followed by the quantification with fluorescence spectroscopy. After incubation in Franz diffusion cells, the applied solution was directly removed. 1 mL of water was pipetted into the donor compartment to rinse the skin surface clean. After repeating the rinsing procedure for 4 times, the skin was patted dry, punched out for the applied skin area and placed onto a piece of filter paper to dry for 30 min.

Subsequently, 30 tapes were weighed in advance and pressed onto the skin with a thumb rolling movement for 3 times, applying a relatively constant weight of 905 g/cm^2 (1.6 kg). When removing the skin from the tape, clamping to the skin from tweezer should be avoided, which can induce a depressed area to the skin surface and affect the homogeneity of skin extraction.

After 30 min of drying, tapes were weighed again to obtain the extracted skin mass. Skin thickness was calculated by dividing the skin mass by stratum corneum density (~1 g/cm^3) and skin area (diameter of 15 mm) [33]. The penetration depth of Fluo-Na was established by plotting the model drug concentration against cumulative skin depth.

2.5. Quantification of Fluo-Na

After gaining the extracted skin mass, tapes were transferred into brown Eppendorf tubes filled with 1.5 mL of PBS (pH 7.4). Fluo-Na was subsequently extracted from tapes by shaking for 10 min, putting into an ultrasonic bath for 15 min and centrifuging for 6 min. Samples containing a higher concentration of Fluo-Na were diluted.

To measure the fluorescence intensity of Fluo-Na from each tape, fluorescence microplate reader (Varioskan LUX, Thermo Fischer Scientific, USA) was employed with an excitation wavelength of 490 nm and an emission wavelength of 540 nm. The calibration curve of Fluo-Na dissolved in PBS (pH 7.4) was constructed by pipetting 100 μL of each sample in triplicate into 96-well plate within the concentration range from 0.004 to 0.7 μg/mL. The corresponding correlation coefficients between 0.9999 and 1 were obtained by conducting the Pearson correlation analysis. Equation obtained from the calibration curve was used for quantification. One empty tape with the addition of PBS following the same procedures was used as control.

2.6. Modified profile of Fluo-Na penetration

In the course of generating penetration profiles, Fluo-Na concentration was plotted against cumulative skin depth. According to previous

studies, the model drug concentration was usually calculated with the drug amount normalized to the stripped skin area [16,34]. However, the skin thickness value can be obtained from each tape. It means that the extracted skin on tape is columniform which has a certain area and height. Therefore, it is more plausible to calculate the drug concentration by dividing the drug amount by skin volume (skin area times skin thickness), giving a concentration value with the unit of $\mu g/cm^3$. Fig. 1A depicts a simple and intuitive view to easily understand the way of calculating the drug concentration.

Apart from the modified approach for calculating drug concentration, the cumulative skin depth for plotting the penetration profile should also be adjusted. Conventionally, the skin thickness obtained from each number of tapes is directly used as the point in profile corresponding to the drug concentration (Fig. 1B, blue line). However, the calculated drug concentration actually corresponds to the average concentration of the stripped skin column. Therefore, the points on profile should be adjusted to half the value of skin thickness (i.e., the class center), subsequently drawing the cumulative skin depth (Fig. 1B, orange line). Fig. 1 presents an example of analyzing the Fluo-Na penetration profile in this study.

2.7. Confocal Raman spectroscopy

CRS was used for profiling the procaine penetration. To this end, an alpha 500 confocal Raman spectroscopy (WiTec GmbH, Ulm, Germany) equipped with a 532 nm excitation laser, UHTS 300 spectrometer and DV401-BV CCD camera was applied. After performing the same rinsing procedures as in tape stripping method, the skin surface was blotted dry, a custom-built skin-placed device was used for embedding the full-thickness skin inside, allowing better spectral analysis (Description of the custom-built device in detail can be found in ref. [35]). The laser power was adjusted to 25 mW using the optical power meter (PM100D, Thorlabs GmbH, Dachau, Germany).

The CRS measurements were carried out by recording the skin spectra from 10 μm above the skin surface to −40 μm inside the skin with a step size of 1 μm using the 63x/1.0NA water immersion objective (W Plan-Apochromat, Carl Zeiss, Jena, Germany). The optical grating used was 1800 g/mm with the spectral center of 1300 cm^{-1} for recording the spectra in the range of 700 to 1800 cm^{-1}. In spectral line scanning analysis, the integration time was 2 s with two times accumulations. Data were acquired from three replicates repeated for over three times, generating repeated measurements of over nine times. All skin samples used for comparison were from the same donor.

2.8. Spectral analysis of procaine penetration

The collected spectra were preprocessed with cosmic ray removal,

smoothing and background subtraction using WITec Project Software (WITec GmbH). Thereinto, Savitzky-Golay (SG) filter was applied with third polynomial order and nine smoothing points. The background was subtracted by the shape method with a size of 400. For reducing noise, principal component analysis (PCA) was performed using the Project Plus 5 software (WITec GmbH). The first three principal components were selected for reconstructing the spectrum [36]. By calculating the area under the curve (AUC), the integrated area under a specified peak of the spectrum could be obtained using the trapezoidal method on WITec Project Software.

For profiling the drug penetration by depth, peak area of procaine signal (1612 cm^{-1}; ν (NH) δ(C-C) vibration) was normalized by the peak area of amide-I signal (1670 cm^{-1}; ν (C=O)-mode), as previous studies found that the amide-I peak was relatively stable within one donor and would be able to be used for spectral signal normalization [37]. With the achievement of different profiles, the skin surface was determined by the intersection of the amide-I signal and the glass signal [25]. The signal attributions are shown in Fig. 2 where the typical procaine signal from different skin depth is also depicted.

2.9. Statistics

In the analysis of Fluo-Na penetration in skin, penetration profiles were achieved from three different measurements with tape stripping method for calculating the skin depth. The cumulative drug concentration and depth can be directly obtained from the profiling data.

In CRS spectral analysis, the relative concentration was obtained by normalizing the procaine signal to the main amide-I peak. Due to the slight overlapping of amide-I peak and procaine peak, as shown in Fig. 2, the calculated ratio would not reach zero when the procaine was not detectable because of the residual intensities. Thus, the baseline should be determined by visualizing the disappearance of characteristic procaine signal and obtaining the stable value of the calculated ratio. In our study, the AUC of the penetration profiles were calculated and compared by setting the baseline at 0.27 (a.u.) where no procaine signal can be found from the spectra, and the normalized ratio was relatively stable.

All emulsifier treated skin samples were compared with the reference (non-emulsifier treated skins) for both model drugs. The graphs are shown with mean values ± standard deviations (mean ± SD). Statistical differences can be generated with the analysis of one-way analysis of variance (ANOVA) followed by Student-Newman-Keuls (SNK) which were employed by GraphPad Prism 8.0 (GraphPad Software Inc., La Jolla, CA, USA). Significant differences were marked with different number of asterisks: * $p < 0.05$, ** $p < 0.01$, *** $p < 0.001$.
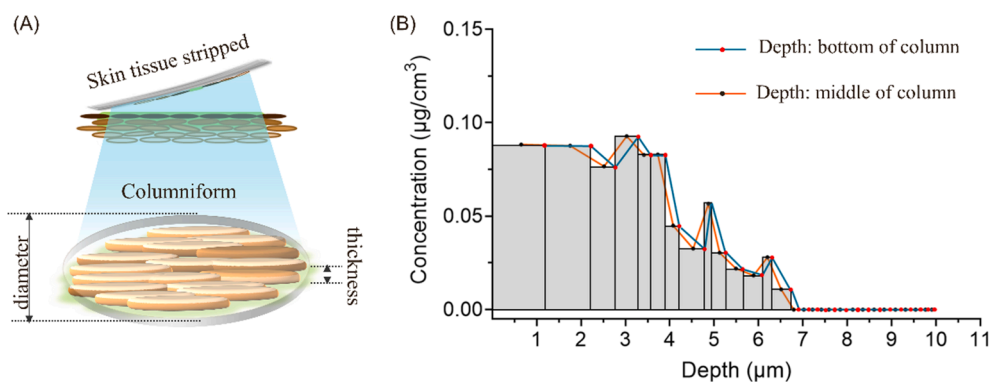

Fig. 1. (A) A simple view of regarding the skin from stripped tapes as a columniform for easier understanding the way of calculating drug concentration; (B) different ways of plotting the penetration profiles: directly using the skin depth for calculating cumulative depth (blue line/ red dots); using the average of skin depth from each tape for calculating cumulative depth (orange line/ black dots).
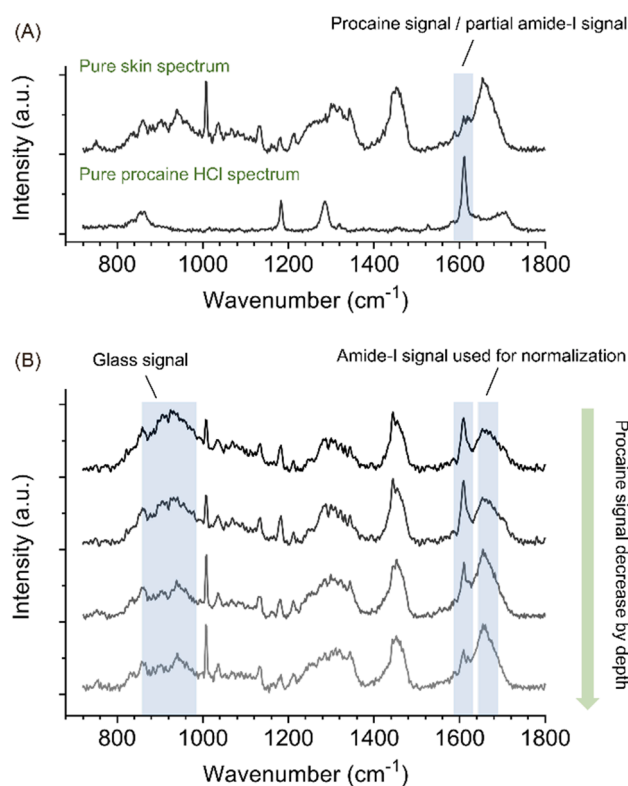
Fig. 2. Display of pure skin spectrum and pure procaine HCl spectrum (A); Typical spectra of skin incubated with procaine with crucial spectral features highlighted in colors (B).

3. Results

Recently, the impacts of PEGylated emulsifiers on skin have been investigated by CRS. Varying effects on skin components were

discovered, which proved CRS to be an effective and non-invasive approach [10]. Thus, it is of interest to examine the effectiveness of PEGylated emulsifiers as penetration enhancers by using CRS technique to evaluate the percutaneous drug delivery. The penetration properties of two model drugs were respectively obtained using conventional tape stripping approach and CRS. Afterwards, the techniques and penetration enhancing effects of emulsifiers on different model drugs were compared.

3.1. Fluo-Na penetration measurement by tape stripping method

The penetration behavior of Fluo-Na with and without emulsifier was aimed to be compared. Via the tape stripping technique and fluorescent spectroscopy measurements, the penetration profile of Fluo-Na can be achieved. Following the aforementioned modified evaluations, profiles were produced and summarized in Fig. 3.

The green dot-lines in Fig. 3A represent the Fluo-Na penetration without any additives. It can be seen that the penetration depth was nearly 6–7 μm with a decrease of the drug concentration by skin depth. Fig. 3B depicted the profiles with the addition of O2. A slightly higher amount of drug can be observed from the skin surface (within around 4 μm), indicating a slight effect of it in enhancing drug penetration.

The drug penetration behaviors with the treatment of PEG-20 ethers are shown in Fig. 3C-E. Steady decrease of drug concentration against depth was observed with the addition of C20. It can be seen that the drug concentration was improved compared with reference; meanwhile, the highest penetration depth of over 11 μm was achieved. Similar manners of S20 and O20 acting on the Fluo-Na penetration are displayed in Fig. 3D-E. Improved drug concentration and depth (8–9 μm and around 8 μm for S20 and O20 respectively) were visualized.

For better visualizing the results, cumulative drug concentration and depth were summarized and statistically compared, as shown in Fig. 4. In this manner, the penetration behaviors can be clear, legible and easy to declare. Based on the results, a quantitative comparison between investigated emulsifiers and reference showed all significant differences. The highest quantitative enhancement was reflected from C20.
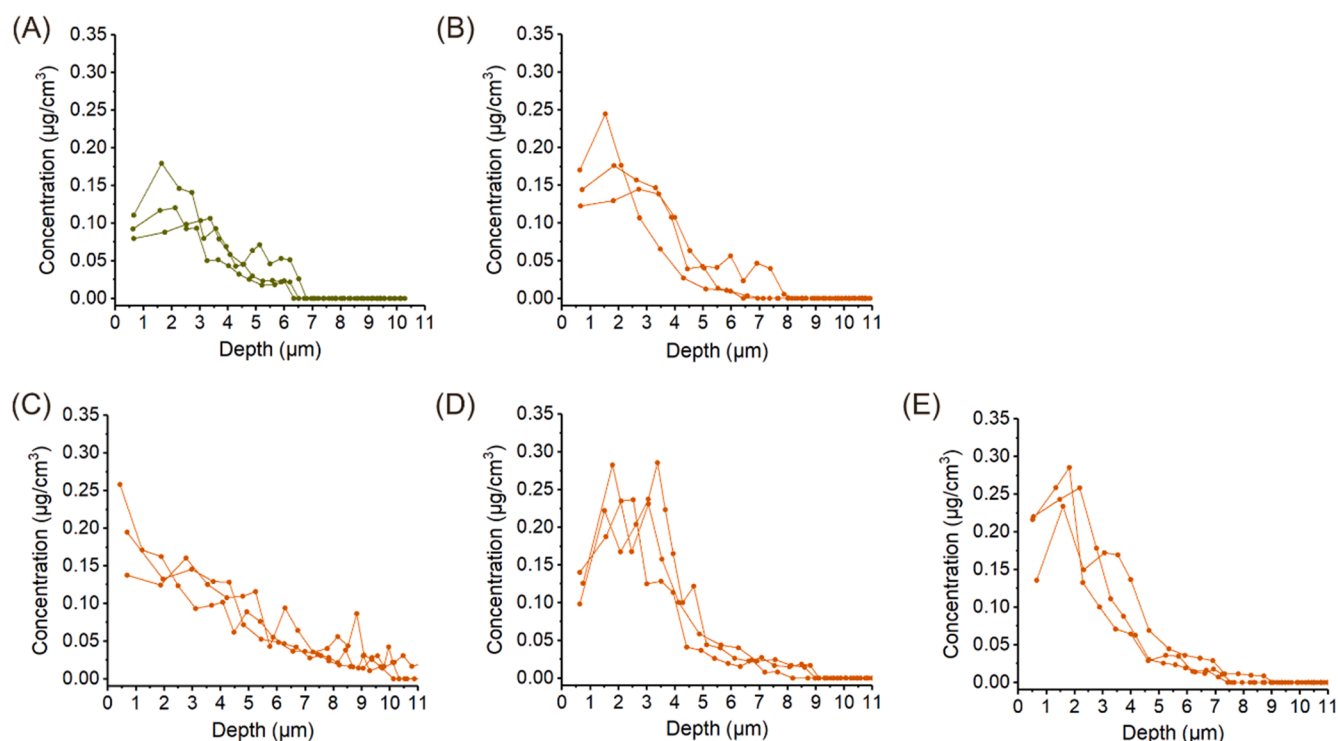

Fig. 3. Penetration profiles of Fluo-Na by plotting the drug concentration from each tape against depth: (A) Reference; (B) O2; (C) C20; (D) S20; (E) O20.
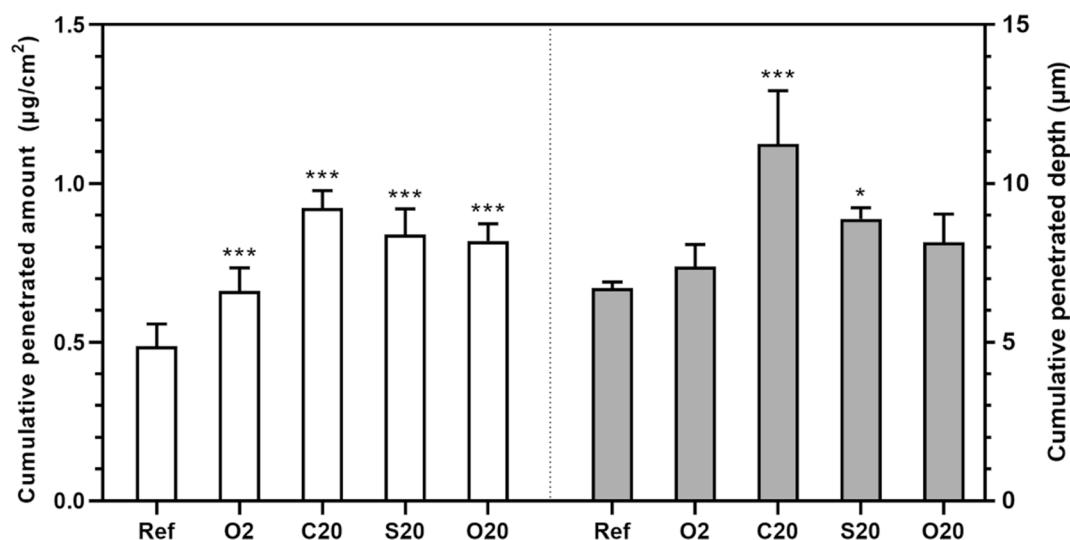
Fig. 4. Cumulative penetrated amount and depth of Fluo-Na penetration profiles. Skin samples with the addition of investigated emulsifiers were compared with reference to determine the significant differences for evaluating penetration enhancement effects. Mean $\pm$ SD, n = 3. * $p < 0.05$, ** $p < 0.01$, *** $p < 0.001$.

Relatively lower improvement was found from the addition of O2, although significantly different data were still achieved. Simultaneously, drug penetration depths were also compared. The penetration depth was determined as the depth at which the detection limit was reached. As expected, the highest penetration depth was achieved from C20, which led to the highest significance. Whereafter, slight significance was obtained from S20. In the case of O20, slight improvement was also visible; however, this difference did not reach statistical significance. Altogether, PEG-20 ethers seem to penetrate the skin deeper and act on the deeper distribution of the active.

3.2. Impact of emulsifiers on total removed SC amount

Another parameter of interest was found in our tape stripping studies. As shown in Fig. 5, the cumulative skin depth obtained from the total of 30 tapes was recorded. Each emulsifier treated skin sample was compared with reference. By evaluating the statistical significance, skin samples applied with PEG-20 ethers were evidenced to induce greater corneocytes removal with the same number of tape strips (30 times). Significant differences ($p < 0.01$) of C20 and S20, and slight significance of O20 ($p < 0.05$) were observed. It might be explained that these three emulsifiers have a higher potential to interrupt the skin barrier, hence, loosen the packing of the lipid matrix. This is in accordance with our
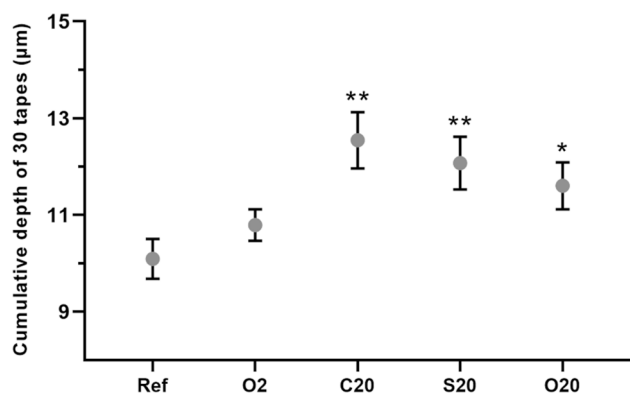
previous findings that PEG-20 ethers can generate the reduction of skin lipid contents and ordered structures, whereas O2 did not show the same trend [10,32].

3.3. Procaine penetration measurement by CRS

Parallel to the Fluo-Na measurements, procaine HCl was employed as another model drug analyzed by CRS. Full-thickness skin was directly measured by CRS after the application time of 12 h and 24 h. The penetration profile was generated according to the spectral analysis mentioned in Section 2.8. Experiments regarding the application time of 12 h and 24 h were all conducted from the single donor.

Fig. 6 shows the comparison of penetration profiles with the incubation time of 12 h. The green dots represent the result of reference. It can be noticed that the procaine penetrated approximately 13 µm into the skin. With the addition of O2 (Fig. 6A), the penetrated amount of active was slightly increased at the skin surface. However, the penetration depth was found unchanged compared with reference. Similar trends were visualized for the other emulsifiers including S20 (Fig. 6B) and O20 (Fig. 6C) in terms of the enhanced penetration amount and remained penetration depth. Surprisingly, a considerably higher drug amount was detected from C20 treated skin (Fig. 6D). The procaine signal can be found until around 20 µm, indicating significantly increased penetration depth.

After Franz cell incubation for 24 h, procaine penetration performances are respectively shown in Fig. 7. With prolonged application time, slightly increased penetrated amount and depth (nearly 15 µm) can be found for reference (green dots). The penetration enhancement effects due to the actions of emulsifiers (red triangles) were easier to be differentiated. Summarizing the results, the improved penetration amount can be found in all emulsifier treated samples. Among them, the effect of O2 in case of procaine delivery was more subtle, which can be specially visualized from its smallest effect. The rest of the emulsifiers revealed the ability of enhanced penetration depth ranked as C20 (over 30 µm) > S20 (around 25 µm) > O20 (around 17 µm). Apart from these observations, a more pronounced effect induced by C20 is worth to be mentioned. It can be clearly visible that the relative drug amount is several times higher than the reference. A large gap between the profiles indicates the outstanding potential of C20 in enhancing procaine penetration.

To enable a better comparison of the procaine penetration behaviors, the area under the curve (AUC) of the penetration profile was calculated, thereby the penetration enhancing effect can be more readable and
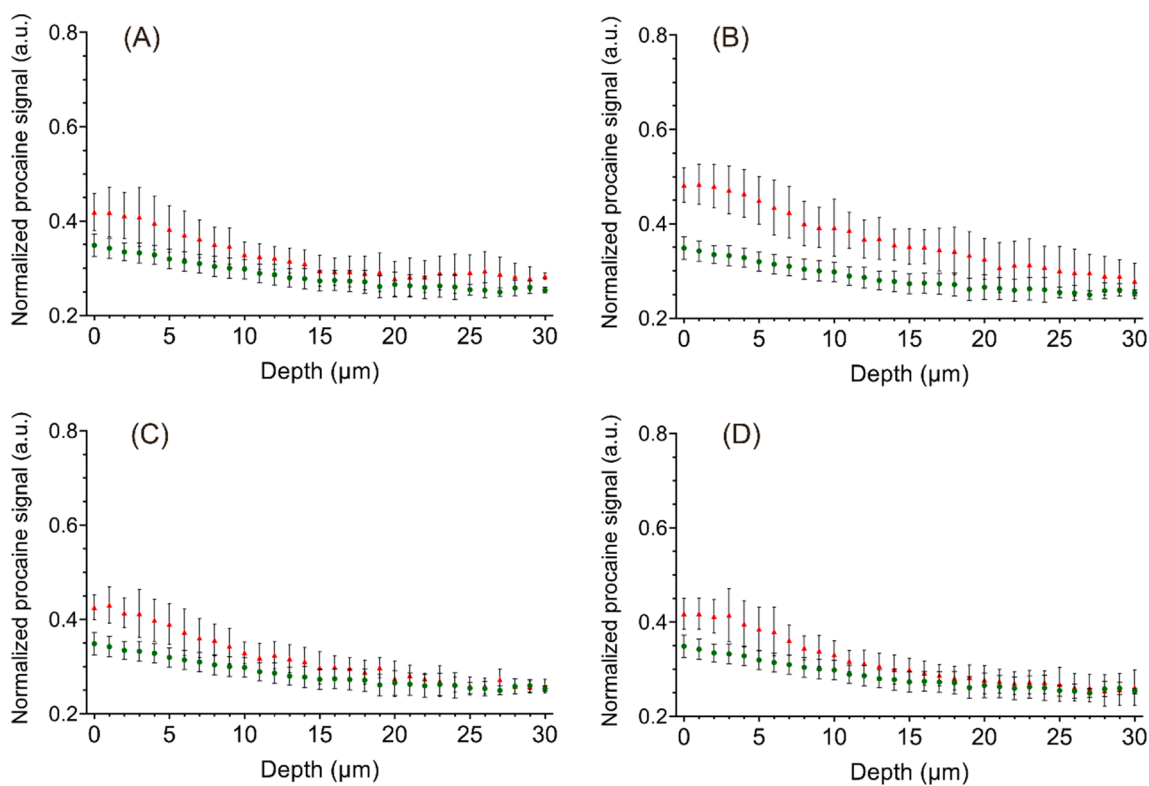

Fig. 5. Comparison of cumulative skin depth removed by a total of 30 tapes. Skin samples with the addition of investigated emulsifiers were compared with reference to determine the significant differences. Mean $\pm$ SD, n = 3. * $p < 0.05$, ** $p < 0.01$, *** $p < 0.001$.
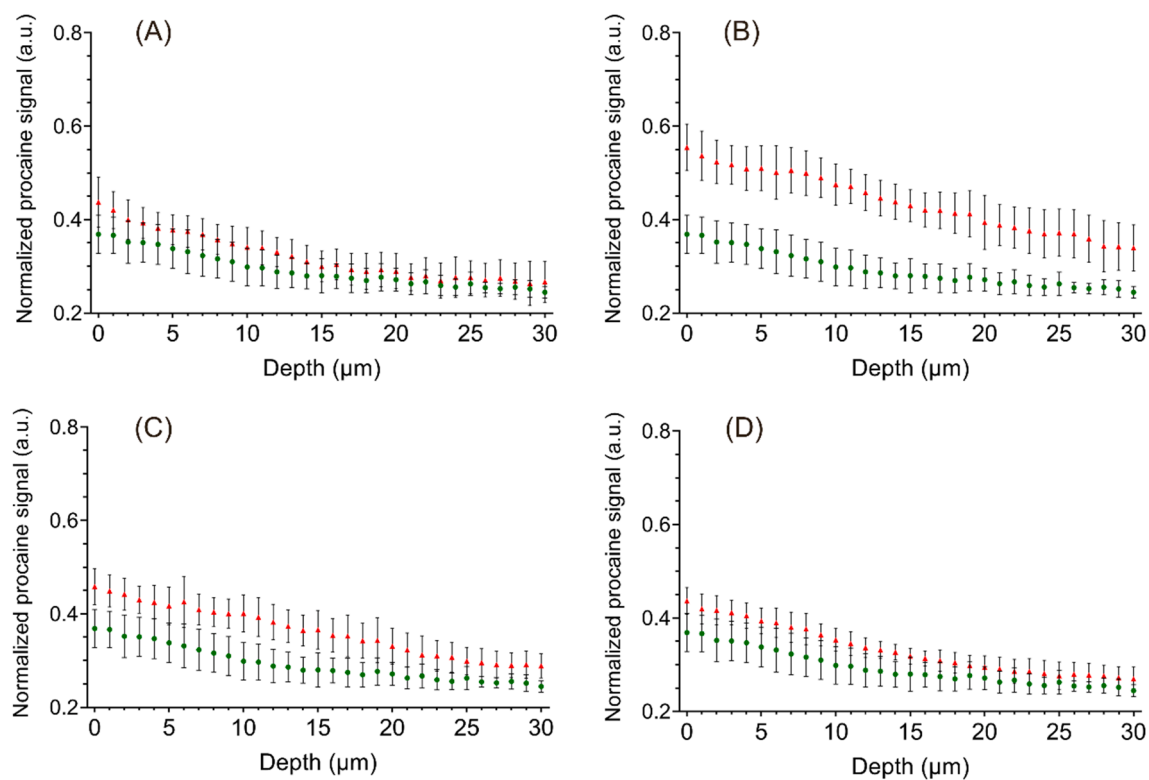
Fig. 6. Penetration profiles after 12 h application time by calculating the normalized procaine signal and comparing the procaine penetration with (red triangles) and without (green circles) the interaction of PEGylated emulsifier: (A) O2; (B) C20; (C) S20; (D) O20. Mean ± SD, n ≥ 9.

Fig. 7. Penetration profiles after 24 h application time by calculating the normalized procaine signal and comparing the procaine penetration with (red triangles) and without (green circles) the interaction of PEGylated emulsifier: (A) O2; (B) C20; (C) S20; (D) O20. Mean ± SD, n ≥ 9.
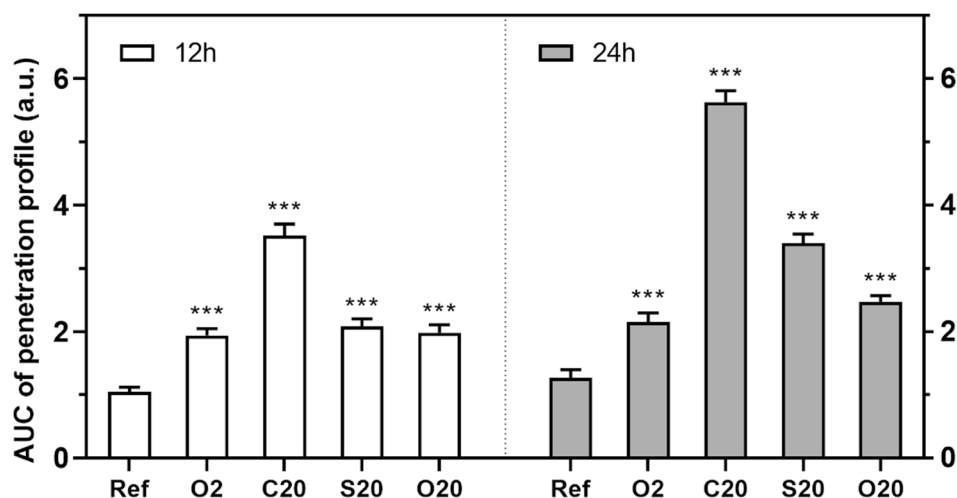
Fig. 8. Area under the curve (AUC) comparison after skin incubation time for 12 h and 24 h. Skin samples with the addition of investigated emulsifiers were compared with reference to determine the significant differences for evaluating penetration enhancement effects. Mean ± SD, n ≥ 9. * p < 0.05, ** p < 0.01, *** p < 0.001.

clarified with statistical analysis. In this process, the baseline was set at 0.27 (a.u.) to ensure better discrimination between sample groups. In Fig. 8, the statistical significance was marked by comparing emulsifier-incorporated samples with reference. The data regarding the application time of 12 h and 24 h were combined and individually assessed. According to the results, the actions of investigated emulsifiers facilitating drug penetration were statistically confirmed, which all showed high significance, regardless of the incubation time. However, comparing their effectiveness as penetration enhancers, variances between groups can still be identified. After 12 h skin treatment, C20 performed most distinctly, followed by similar trends of the other candidates. While extending the time enhanced action of emulsifiers to the skin, the enhancement ability was ranked as C20 > S20 > O20 > O2. This ability was, in fact, the promotion of penetrated drug amount, which was also in line with the above-mentioned ability in deepening drug distribution by depth.

3.4. Comparison of penetration results

Mainly two studies were performed for analyzing the penetration enhancing effects of PEGylated emulsifiers. Two model drugs were selected following two techniques for measurements. In comparison of both studies, similar tendencies towards their enhancements on drug penetration were confirmed. All applied emulsifiers investigated were capable of improving dermal drug delivery. The emulsifier of C20 led to the highest drug penetration amount and deepest penetration depth for both Fluo-Na and procaine. Small differences can also be found; C20 showed the improved penetration amount tightly followed by S20 and O20 in Fluo-Na penetration whereas much greater penetration improvements than other emulsifiers in procaine penetration. It can be explained that two different actives may not be affected similarly by the same penetration enhancers. But overall, their penetration enhancing trends were in line with their actions on skin lipids. To this point, PEG-20 ethers have been demonstrated to be able to impair the skin lipid domains [10]. It means that the impairment may increase the fluidity of lipid structures and enable drugs to easier pass through. However, enhanced penetration amount was also found by the addition of O2, which actually showed no negative effects on skin lipids. It can be speculated that O2 has relatively small influence on skin which was not detectable in previous study, while it can slightly promote drug penetration. This finding is also consistent with other studies showing the increased absorption of actives when using O2 as penetration enhancer [12,38]. Again, it needs to be kept in mind that the penetration

enhancing effect may be of different extent for different actives.

Another minor difference is regarding to the penetration depth; only C20 and S20 showed improved data in tape stripping method, while the CRS measurements confirmed the enhanced penetration depth by C20, S20, O20 after 24 h treatments. Herein, the tape stripping method has the limit of detection by depth, due to the number of tapes and mostly extraction of stratum corneum. In this case, it will be tough to reach significance when comparing penetration depths. Instead, CRS enables the signal collection in deeper skin zones based on the encounter of intolerable signal attenuations. Owing to the measurements of dozens of micrometers, CRS apparently outperformed tape stripping approach in skin depth evaluations.

4. Discussion

Penetration studies were performed in parallel with two techniques, presenting valuable information in evaluating the penetration abilities of tested excipients. As described above, the results regarding the penetration profiles were thoroughly compared. Except for the direct observation of drug penetration, underlying benefits and lacks of both techniques through experiments are also noticeable. In tape stripping experiment, standardized procedures are needed to ensure reproducible results. A lot of small aspects should be taken care of. For example, skin rinsing procedure is one of the critical points. It is easy to understand that drugs trapped inside the skin furrows can cause the erroneous calculation of the first several tapes. To avoid this, Alsheddi et al. have evidenced that the rinsing procedure can effectively remove maintaining residual of applied samples and reduce the erroneous interpretation [21]. In our practical experiments, we found that this step can also prevent the removal of corneocytes by wiping the skin surface, which is another key to quantify the depth of skin layer. Another point worth mentioning is the finger pressure applied on skin tape. Studies demonstrated that the finger pressure could remove higher skin amount than a constant weight and a roller [20,22,39]. Thus, a thumb was applied and rolled on the tape. Thereby, the same operator should be retained to avoid artifacts. Following these considerations, more steps of procedures come with a higher potential for error. Additionally, the individual tape stripping and drying process require a huge amount of time, which only allows one single measurement within 4 h. While in CRS analysis, a piece of skin sample can be multiply measured in a short time, as each line scan takes only 4 min based on our descriptions. More data can be obtained with the same number of samples. Besides, fewer procedures are needed for sample preparation. The full-thickness skin can be

directly used on the Raman microscope for measurements. This retains the skin properties without invasive operations. The problem of skin furrows can also be avoided by visualizing the detected skin area through Raman microscopes' video camera. Thus, as described, the tape stripping technique is more laborious, time-consuming and error-prone, whereas CRS exhibits more benefits of time-saving, easier-to-access, non-invasive properties in skin analysis.

However, inevitably, there are some inherent challenges for CRS techniques. One concern is the signal attenuation effect by probing the skin from the deeper layer, limiting the depth detections. Furthermore, CRS configuration was also one critical point for skin depth profiling. Previous studies have demonstrated that an inappropriate combination of pinhole sizes and objectives can lead to erroneous results [40,41]. The refractive indices are the main reason involved, which can underestimate the detected skin depth. In our study, the use of immersion objective can reduce this kind of effect, which should be paid attention to from different laboratory setups [35,42]. Another inherent challenge refers to the suitability of substances for CRS detection. The analysis of them can only be employed with characteristic signals different from CRS skin spectra. Otherwise, the deuterated form is needed for convenient use. With those challenges, sufficient knowledge and optimization of the instrument in use for skin analysis should be possessed.

Further discussion about the enhancing mechanisms of PEGylated emulsifiers was again noted. In our study, it can be intuitively known that skin lipid interactions govern drug penetration. In comparison, less effects of PEG-ethers on lipids can subsequently induce less capability of penetration enhancement, as can be deduced from the lack of penetration enhancement by O2.

5. Conclusion

Overall, tape stripping and CRS techniques were both successfully applied to examine the cutaneous drug penetration with the addition of PEGylated emulsifiers. The general enhancing ability of them has been presented to be correlated. Small variances concerning the penetration depths and amount between two techniques may be explained and clarified from the aspects of varying actives and inherent limitations of tape stripping method. Benefits and pitfalls of the two techniques were concluded in the study. CRS obviously offered more advantages from plenty of aspects than the tape stripping method in skin analysis, although some inherent challenges cannot be avoided. Several factors like objective numerical aperture, pinhole diameter or laser wavelengths have already been addressed by our group and others. Still, more research needs to be done to establish a correlation between conventional methods and CRS. In general, this study adds to the knowledge base of using CRS for skin penetration analysis and can also be seen as a highlight of using CRS as a powerful alternative to tape stripping method. Certainly, the tape stripping method can also be a valid prediction technique for novel drug delivery systems, if the lack of characteristic spectral features from target does not allow analysis by CRS. An additional finding is interesting as well that the tape stripped amount of skin components can be used as a sign for impaired barrier function.

6. Statement of ethics

Porcine ears were acquired from the Department of Experimental Medicine of University Hospital Tuebingen. Live animals used were kept at the Department of Experimental Medicine and sacrificed in their experiments approved by the ethics committee of University Hospital Tuebingen. Those ears were received directly after the death of the animals. Before the study, Department of Pharmaceutical Technology has registered for the use of animal products at the District Office of Tuebingen (registration number: DE 08 416 1052 21).

References

[1] P.V. Raykar, M.C. Fung, B.D. Anderson, The Role of Protein and Lipid Domains in the Uptake of Solutes by Human Stratum Corneum, Pharm. Res. An Off. J. Am. Assoc. Pharm. Sci. 5 (1988) 140–150, https://doi.org/10.1023/A:1015956705293.

[2] C.L. Froebe, F.A. Simion, L.D. Rhein, R.H. Cagan, A. Kligman, Stratum corneum lipid removal by surfactants: Relation to in vivo irritation, Dermatology. 181 (1990) 277–283, https://doi.org/10.1159/000247822.

[3] J. Shokri, A. Nokhodchi, A. Dashbolaghi, D. Hassan-Zadeh, T. Ghafourian, M. Barzegar Jalali, Barzegar Jalali, The effect of surfactants on the skin penetration of diazepam, Int. J. Pharm. 228 (1-2) (2001) 99–107, https://doi.org/10.1016/S0378-5173(01)00805-5.

[4] T.N. Engelbrecht, A. Schroeter, T. Hauß, R.H.H. Neubert, Lipophilic penetration enhancers and their impact to the bilayer structure of stratum corneum lipid model membranes: Neutron diffraction studies based on the example Oleic Acid, Biochim. Biophys. Acta - Biomembr. 1808 (12) (2011) 2798–2806, https://doi.org/10.1016/j.bbamem.2011.08.012.

[5] D.J. McClements, C.E. Gumus, Natural emulsifiers — Biosurfactants, phospholipids, biopolymers, and colloidal particles: Molecular and physicochemical basis of functional performance, Adv. Colloid Interface Sci. 234 (2016) 3–26, https://doi.org/10.1016/j.cis.2016.03.002.

[6] S. Petersen, J. Ulrich, Role of emulsifiers in emulsion technology and emulsion crystallization, Chem. Eng. Technol. 36 (3) (2013) 398–402, https://doi.org/10.1002/ceat.v36.310.1002/ceat.201200648.

[7] C. Marianecci, D. Paolino, C. Celia, M. Fresta, M. Carafa, F. Alhaique, Non-ionic surfactant vesicles in pulmonary glucocorticoid delivery: Characterization and interaction with human lung fibroblasts, J. Control. Release. 147 (1) (2010) 127–135, https://doi.org/10.1016/j.jconrel.2010.06.022.

[8] K.A. Walters, M. Walker, O. Olejnik, Non-ionic Surfactant Effects on Hairless Mouse Skin Permeability Characteristics, J. Pharm. Pharmacol. 40 (1988) 525–529, https://doi.org/10.1111/j.2042-7158.1988.tb05295.x.

[9] Y. Liu, D.J. Lunter, Tracking heavy water incorporated confocal Raman spectroscopy for evaluating the effects of PEGylated emulsifiers on skin barrier, J. Biophotonics. (2020) 1–12, https://doi.org/10.1002/jbio.202000286.

[10] Y. Liu, D.J. Lunter, Systematic investigation of the effect of non-ionic emulsifiers on skin by confocal raman spectroscopy—a comprehensive lipid analysis, Pharmaceutics. 12 (2020) 223, https://doi.org/10.3390/pharmaceutics12030223.

[11] W.-W. Shen, A.G. Danti, F.N. Bruscato, Effect of nonionic surfactants on percutaneous absorption of salicylic acid and sodium salicylate in the presence of dimethyl sulfoxide, J. Pharm. Sci. 65 (12) (1976) 1780–1783, https://doi.org/10.1002/jps.2600651222.

[12] C.-C. Hwang, A.G. Danti, Percutaneous absorption of flufenamic acid in rabbits: Effect of dimethyl sulfoxide and various nonionic surface-active agents, J. Pharm. Sci. 72 (8) (1983) 857–860, https://doi.org/10.1002/jps.2600720805.

[13] S.-C. Shin, C.-W. Cho, I.-J. Oh, Effects of non-ionic surfactants as permeation enhancers towards piroxicam from the poloxamer gel through rat skins, Int. J. Pharm. 222 (2) (2001) 199–203, https://doi.org/10.1016/S0378-5173(01)00699-8.

[14] K. Yamamoto, R. Flesch, T. Ohigashi, S. Hedtrich, A. Klossek, P. Patoka, G. Ulrich, S. Ahlberg, F. Rancan, A. Vogt, U. Blume-Peytavi, P. Schrade, S. Bachmann, M. Schäfer-Korting, N. Kosugi, E. Rühl, Selective probing of the penetration of dexamethasone into human skin by soft X-ray spectromicroscopy, Anal. Chem. 87 (12) (2015) 6173–6179, https://doi.org/10.1021/acs.analchem.5b00800.

[15] C.F. Goh, J.G. Moffat, D.Q.M. Craig, J. Hadgraft, M.E. Lane, Monitoring drug crystallization in percutaneous penetration using localized nanothermal analysis and photothermal microspectroscopy, Mol. Pharm. 16 (1) (2019) 359–370, https://doi.org/10.1021/acs.molpharmaceut.8b01027.

[16] V. Klang, J.C. Schwarz, B. Lenobel, M. Nadj, J. Auböck, M. Wolzt, C. Valenta, In vitro vs. in vivo tape stripping: Validation of the porcine ear model and penetration assessment of novel sucrose stearate emulsions, Eur. J. Pharm. Biopharm. 80 (3) (2012) 604–614, https://doi.org/10.1016/j.ejpb.2011.11.009.

[17] J.J. Escobar-Chávez, V. Merino-Sanjuán, M. López-Cervantes, Z. Urban-Morlan, E. Piñón-Segundo, D. Quintanar-Guerrero, A. Ganem-Quintanar, The tape-stripping technique as a method for drug quantification in skin, J. Pharm. Pharm. Sci. 11 (2008) 104–130, https://doi.org/10.18433/J3201Z.

[18] U. Lindemann, K. Wilken, H.-J. Weigmann, H. Schaefer, W. Sterry, J. Lademann, Quantification of the horny layer using tape stripping and microscopic techniques, J. Biomed. Opt. 8 (4) (2003) 601, https://doi.org/10.1117/1.1609200.

[19] R. Voegeli, J. Heiland, S. Doppler, A.V. Rawlings, T. Schreier, Efficient and simple quantification of stratum corneum proteins on tape strippings by infrared

densitometry, Ski. Res. Technol. 13 (3) (2007) 242–251, https://doi.org/10.1111/srt.2007.13.issue-310.1111/j.1600-0846.2007.00214.x.

[20] C. Nagelreiter, D. Mahrhauser, K. Wiatschka, S. Skipiol, C. Valenta, Importance of a suitable working protocol for tape stripping experiments on porcine ear skin: Influence of lipophilic formulations and strip adhesion impairment, Int. J. Pharm. 491 (1-2) (2015) 162–169, https://doi.org/10.1016/j.ijpharm.2015.06.031.

[21] L. Alsheddi, K. Ananthapadmanabhan, S.K. Li, Influence of skin furrows on tape stripping in characterizing the depth of skin penetration, Int. J. Pharm. 576 (2020) 118903, https://doi.org/10.1016/j.ijpharm.2019.118903.

[22] M. Breternitz, M. Flach, J. Präßler, P. Elsner, J.W. Fluhr, Acute barrier disruption by adhesive tapes is influenced by pressure, time and anatomical location: Integrity and cohesion assessed by sequential tape stripping; A randomized, controlled study, Br. J. Dermatol. 156 (2) (2007) 231–240, https://doi.org/10.1111/bjd.2007.156.issue-210.1111/j.1365-2133.2006.07632.x.

[23] A.C. Anselmo, Y. Gokarn, S. Mitragotri, Non-invasive delivery strategies for biologics, Nat. Publ. Gr. 18 (1) (2019) 19–40, https://doi.org/10.1038/nrd.2018.183.

[24] R. Darlenski, S. Sassning, N. Tsankov, J.W. Fluhr, Non-invasive in vivo methods for investigation of the skin barrier physical properties, Eur. J. Pharm. Biopharm. 72 (2) (2009) 295–303, https://doi.org/10.1016/j.ejpb.2008.11.013.

[25] R. Krombholz, Y. Liu, D.J. Lunter, In-Line and Off-Line Monitoring of Skin Penetration Profiles Using Confocal Raman Spectroscopy, Pharmaceutics. 13 (2021) 67, https://doi.org/10.3390/pharmaceutics13010067.

[26] G. Mao, C.R. Flach, R. Mendelsohn, R.M. Walters, Imaging the distribution of sodium dodecyl sulfate in skin by confocal raman and infrared microspectroscopy, Pharm. Res. 29 (8) (2012) 2189–2201, https://doi.org/10.1007/s11095-012-0748-y.

[27] L. Binder, E.M. Kulovits, R. Petz, J. Ruthofer, D. Baurecht, V. Klang, C. Valenta, Penetration monitoring of drugs and additives by ATR-FTIR spectroscopy/tape stripping and confocal Raman spectroscopy – A comparative study, Eur. J. Pharm. Biopharm. 130 (2018) 214–223, https://doi.org/10.1016/j.ejpb.2018.07.007.

[28] A. Hédoux, Recent developments in the Raman and infrared investigations of amorphous pharmaceuticals and protein formulations: A review, Adv. Drug Deliv. Rev. 100 (2016) 133–146, https://doi.org/10.1016/j.addr.2015.11.021.

[29] L. Binder, C. Valenta, D. Lunter, Determination of skin penetration profiles by confocal Raman microspectroscopy: Evaluation of interindividual variability and interlab comparability, J. Raman Spectrosc. 51 (7) (2020) 1037–1043, https://doi.org/10.1002/jrs.v51.710.1002/jrs.5871.

[30] D. Lunter, R. Daniels, Confocal Raman microscopic investigation of the effectiveness of penetration enhancers for procaine delivery to the skin, J. Biomed. Opt. 19 (12) (2014) 126015, https://doi.org/10.1117/1.JBO.19.12.126015.

[31] Y. Liu, D.J. Lunter, Selective and sensitive spectral signals on confocal Raman spectroscopy for detection of ex vivo skin lipid properties, Transl. Biophotonics. (2020) 1–9, https://doi.org/10.1002/tbio.202000003.

[32] Z. Zhang, D.J. Lunter, Confocal Raman microspectroscopy as an alternative to differential scanning calorimetry to detect the impact of emulsifiers and formulations on stratum corneum lipid conformation, Eur. J. Pharm. Sci. 121 (2018) 1–8, https://doi.org/10.1016/j.ejps.2018.05.013.

[33] R.L. Anderson, J.M. Cassidy, Variations in physical dimensions and chemical composition of human stratum corneum, J. Invest. Dermatol. 61 (1) (1973) 30–32, https://doi.org/10.1111/1523-1747.ep12674117.

[34] T. Haque, J.M. Crowther, M.E. Lane, D.J. Moore, Chemical ultraviolet absorbers topically applied in a skin barrier mimetic formulation remain in the outer stratum corneum of porcine skin, Int. J. Pharm. 510 (1) (2016) 250–254, https://doi.org/10.1016/j.ijpharm.2016.06.041.

[35] D.J. Lunter, How confocal is confocal raman microspectroscopy on the skin? Impact of microscope configuration and sample preparation on penetration depth profiles, Skin Pharmacol. Physiol. 29 (2016) 92–101, https://doi.org/10.1159/000444806.

[36] ChunSik Choe, J. Lademann, M.E. Darvin, A depth-dependent profile of the lipid conformation and lateral packing order of the stratum corneum in vivo measured using Raman microscopy, Analyst. 141 (6) (2016) 1981–1987, https://doi.org/10.1039/C5AN02373D.

[37] Z. Zhang, D.J. Lunter, Confocal Raman microspectroscopy as an alternative method to investigate the extraction of lipids from stratum corneum by emulsifiers and formulations, Eur. J. Pharm. Biopharm. 127 (2018) 61–71, https://doi.org/10.1016/j.ejpb.2018.02.006.

[38] C.-W. Cho, S.-C. Shin, Enhanced transdermal delivery of atenolol from the ethylene-vinyl acetate matrix, Int. J. Pharm. 287 (1-2) (2004) 67–71, https://doi.org/10.1016/j.ijpharm.2004.08.013.

[39] C. Nagelreiter, S. Raffeiner, C. Geyerhofer, V. Klang, C. Valenta, Influence of drug content, type of semi-solid vehicle and rheological properties on the skin penetration of the model drug fludrocortisone acetate, Int. J. Pharm. 448 (1) (2013) 305–312, https://doi.org/10.1016/j.ijpharm.2013.03.042.

[40] N.J. Everall, Modeling and measuring the effect of refraction on the depth resolution of confocal Raman microscopy, Appl. Spectrosc. 54 (6) (2000) 773–782, https://doi.org/10.1366/0003702001950382.

[41] N.J. Everall, Confocal Raman microscopy: Why the depth resolution and spatial accuracy can be much worse than you think, Appl. Spectrosc. 54 (10) (2000) 1515–1520, https://doi.org/10.1366/0003702001948439.

[42] D.J. Lunter, Determination of skin penetration profiles by confocal Raman microspectroscopy: statistical evaluation of optimal microscope configuration, J. Raman Spectrosc. 48 (2) (2017) 152–160, https://doi.org/10.1002/jrs.v48.210.1002/jrs.5001.

8. Confocal Raman spectroscopy at different laser wavelengths in analyzing stratum corneum and skin penetration properties of mixed PEGylated emulsifier systems
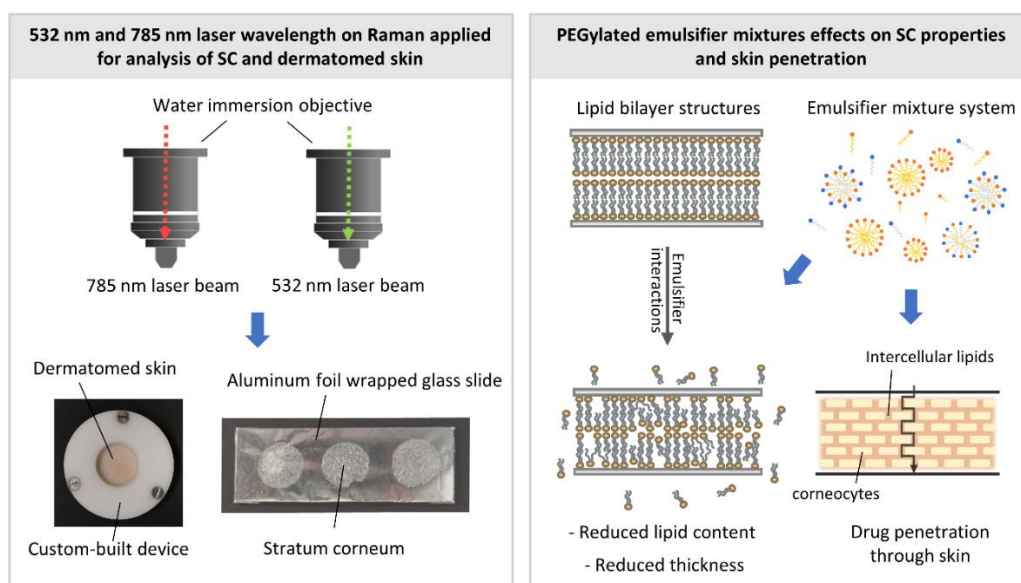
Yali Liu, Dominique Jasmin Lunter*

Department of Pharmaceutical Technology, Faculty of Science, Eberhard Karls Universität Tübingen, Auf der Morgenstelle 8, 72076 Tuebingen, Germany

Graphical Abstract

Confocal Raman spectroscopy at different laser wavelengths in analyzing stratum corneum and skin penetration properties of mixed PEGylated emulsifier systems

Yali Liu, Dominique Jasmin Lunter [*]

Department of Pharmaceutical Technology, Faculty of Science, Eberhard Karls Universität Tübingen, Auf der Morgenstelle 8, 72076 Tuebingen, Germany

ABSTRACT

Emulsifier mixtures are widely used in cosmetics and pharmaceutics and thus, brought extensive studies for their performances on skin applications. PEG-20 cetyl ether (C20) is recently proposed to induce skin irritation and is of interest to study its skin interactions when mixed with other emulsifiers. PEG-2 oleyl ether (O2) and PEG-20 stearyl ether (S20) are selected and in specific, 50 mM of C20, O2, S20 as well as Mix1 (50 mM C20 mixed with 50 mM O2) and Mix2 (50 mM C20 mixed with 50 mM S20) solutions were applied on skin samples. Confocal Raman spectroscopy (CRS) analyses of stratum corneum (SC) thickness and SC lipid content were performed after 4 h skin treatments. In parallel, skin penetration properties were also evaluated via CRS by applying procaine solutions with/without emulsifiers on skin samples for 24 h. In terms of the CRS measurements, two excitation wavelengths of 532 nm and 785 nm are both utilized in this study and we secondly aimed to compare their results and suitability in SC and skin analyses. Based on the experimental observations, comparable results are obtained by using both excitation wavelengths of 532 nm and 785 nm demonstrating their suitability in analyzing SC and skin samples. Thereinto, 785 nm laser wavelength shows the advantage of deeper skin penetration and allows the measurements of fluorescent skin samples; 532 nm laser wavelength enables simple measurement performance without substrate and coverslip interference. With regards to the results of emulsifier mixtures, the addition of S20 and O2 reduced the skin interactions and penetration enhancing ability of C20, giving us the hint to build milder systems with emulsifier mixtures. Besides, the CRS results of stronger skin interruption were also correlated with the higher critical micelle concentration (CMC) values of emulsifiers and their mixtures, which may provide evidence in explaining the interactions between emulsifiers and skin.

1. Introduction

Polyoxyethylated (PEGylated) nonionic emulsifiers have found increasing applications in plenty of pharmaceutical and cosmetic products (Ban et al., 2020; Chiappisi, 2017; Jiao, 2008; Park et al., 2000; Zhang et al., 2018). We studied a group of PEGylated emulsifiers with different lengths of PEG-chain and different types of fatty alcohols as the hydrophobic tail (Liu and Lunter, 2021a; Liu and Lunter, 2020a). Potential patterns that can explain their interactions with *ex-vivo* skin have also been addressed. According to previous studies, C20 showed the most significant influences on interrupting the skin barrier such as SC lipid extractions and disordered lipid structures (Liu and Lunter, 2020a, 2020b). The most penetration enhancing ability has also been proven with different actives (Liu and Lunter, 2021b).

To address the issue of lowering the impairment of the skin barrier function, techniques are required to decrease the interactions of C20 with the skin barrier. The most direct and simple consideration comes to the emulsifier mixtures which have been effective applications for various commercial products. For the same purpose, plenty of studies regarding different kinds of emulsifier mixtures have already been performed (Arora et al., 2010; Azum et al., 2014; Shiloach and Blankschtein, 1998). A representative study conducted by M. James-Smith showed that the addition of dodecyl trimethylammonium bromide lowered the skin irritative ability of sodium dodecyl sulfate (SDS) (James-Smith et al., 2011). T. Hall-Manning also proposed that the mixture of SDS and Dimethyl dodecyl amido betaine significantly reduced the irritation potential (Hall-Manning et al., 1998). Similar findings have been evidenced in studying different combinations of

---

emulsifiers (Blagojević et al., 2016; Chen et al., 2017). Despite such observations, little is known about the exact attempts of PEGylated emulsifier mixtures in influencing the skin. Thus, it is of interest to give extra information on whether the mixture system of PEGylated emulsifiers has milder interaction with the skin.

We selected PEGylated emulsifiers of S20 and O2 to be mixed with C20. Their interactions with the skin barrier and performances in affecting drug penetration have been previously studied, which enables the comparisons of their mixtures and single treatment in our study (Liu and Lunter, 2020a; Liu and Lunter, 2021b). Among them, S20 has strong interruptions with the skin barrier, which is potentially related to its highly similar molecular structures with C20, whereas O2 has shown lower effects on the skin which we speculate is the reason for fewer PEG numbers compared with C20. We expect these two mixtures with similar and different hydrophilic chain lengths to be a predict for similar combinations when discussing the skin interactions since it still remains unknown for PEGylated emulsifiers (Seweryn, 2018). On the other hand, the relationship between the CMC values of emulsifiers or emulsifier mixture systems and their extent to perturb the skin barrier has been proposed in some studies (Hall-Manning et al., 1998; Lee et al., 1994). It has been introduced that the higher the CMC value, the stronger the potential of emulsifiers to impair the skin barrier. It supports the statement that monomers with smaller size are easier to penetrate the skin and perturb the skin components and structures, which means the greater number of monomers, the stronger the disruption to the skin. This interesting correlation for PEGylated emulsifier systems remains still incomplete (de la Maza and Parra, 1994). Therefore, our study may offer extra details in this aspect.

Characterization of skin properties requires a proper approach to gain insights into the effects of emulsifiers or their mixtures on the skin barrier. Detailed SC lipid and thickness analysis, as well as the skin penetration properties, can be achieved by using CRS (Ali et al., 2012; Belsey et al., 2014; Binder et al., 2019; Mahrhauser et al., 2015; Mélot et al., 2009). It has been widely demonstrated to be a promising technique in skin analysis owing to its convenience, high efficiency, and non-invasiveness (Franzen and Windbergs, 2015; Pudlas et al., 2011; Vyumvuhore et al., 2014). According to our previous study, the methods of using 532 nm laser wavelength in analyzing the SC and skin properties have been established (Liu and Lunter, 2021b; Liu and Lunter, 2020). However, ongoing questions were still raised about the suitability of it compared with 785 nm laser wavelength, which was pointed out in some studies to be more acceptable and suitable for skin measurements (Darvin et al., 2009; dos Santos et al., 2019). With the concern that the systematic investigation regarding the use of different excitation wavelengths in analyzing various skin samples is still a lack, our study for both SC and skin can be an excellent opportunity to explore their comparisons in various aspects. Similar studies of using different excitation wavelengths have been conducted in particular areas and samples (Ghita et al., 2016; Hara et al., 2018; Harris et al., 2015; Trebolazabala et al., 2013). L. Kerr has reported Raman signals from healthy human cheek cells using different source laser wavelengths and different sample substrates for the analysis of biological specimens (Kerr et al., 2015). Additionally, the sample fluorescence and burning effects have also been considered to determine the availability of laser wavelengths in the analysis of nail polish (López-López et al., 2015). Although Tfaili has compared the spectra collected from different depths of the skin surface by using different excitation wavelengths, a thorough investigation of systematic SC and skin penetration properties in the respect of data comparison is still lacking (Tfaili et al., 2012). Besides, we also seek to investigate the benefits and pitfalls of different excitation wavelengths used at different types of skin samples

Therefore, SC and skin samples with the treatment of emulsifiers and their mixtures were evaluated with 532 nm and 785 nm excitation wavelengths in this work. Comparisons of obtained results can evidence their suitability and applicability in systematic SC and skin analysis. Their application on fluorescent skin samples and the challenge of

photoluminescence effects during measurements were also considered in the present study.

2. Materials and method

2.1. Materials

Procaine HCl was purchased from Ceasar & Loretz GmbH (D-Hilden, Germany). Emulsifiers of PEG alkyl ethers including PEG-20 cetyl ether (ceteth-20, C20), PEG-20 stearyl ether (steareth-20, S20), and PEG-2 oleyl ether (oleth-2, O2) were obtained from Croda GmbH (Nettetal, Germany). parafilm® was from Bemis Company Inc., (Oshkosh, WI, USA). Trypsin type II-S (lyophilized powder), trypsin inhibitor (lyophilized powder), and 1,6-diphenyl-hexatriene (DPH) were provided by Sigma-Aldrich Chemie GmbH (Steinheim, Germany). Sodium chloride, disodium hydrogen phosphate, potassium dihydrogen phosphate, and potassium chloride were of European Pharmacopoeia grade. All aqueous solutions were prepared with ultra-pure water (Elga Maxima, High Wycombe, UK).

Porcine ear skins (German landrace; age: 15–30 weeks; weight: 40–65 kg) were provided by the Department of Experimental Medicine at the University of Tuebingen. The Department of Pharmaceutical Technology at the University of Tuebingen has been registered to use animal products (registration number: DE 08 416 1052 21).

2.2. Preparation of porcine skin

Porcine ears were obtained on the day of sacrifice and directly cleaned with isotonic saline. The skin was removed from cartilage, cleaned from blood, and cut into strips of approximately 3 cm width. The strips were stretched onto a Styrofoam plate with pins. Then, skin hairs were trimmed to around 0.5 mm with an electric hair clipper (QC5115/15, Philips, Netherlands). Thereafter, the skin was dermatomed to a thickness of 1 mm (Dermatom GA 630, Aesculap AG & Co. KG, D-Melsungen), punched out for circles to a diameter of 25 mm, wrapped with aluminum foil (FORA Suisse GmbH, Kreuzlingen, Germany), and stored in a freezer at −28 ℃. This procedure has been previously described by our group (Lunter, 2016).

2.3. Skin incubation in Franz diffusion cells

Dermatomed skin samples were thawed to room temperature and incubated in Franz diffusion cells (Gauer Glas, Püttlingen, Germany) for application of emulsifier solutions and emulsifier-drug solutions. In detail, 12 mL of degassed and prewarmed (32℃) phosphate-buffered saline (PBS, pH 7.4) was used as the receptor fluid. Circular skin samples were thawed to room temperature, washed clean with PBS, and placed between the cells and donor compartments. The assembled cells were clamped tight and transferred into a water bath with a stirring speed of 500 rpm. After the equilibration time of 30 min, 1 mL of emulsifier solutions including C20, S20, O2, Mix1, and Mix2 were applied for 4 h. skin samples were gently cleaned with isotonic saline and cotton swabs. The real applied area was punched out for circle (diameter of 15 mm) and placed on 0.2 % trypsin solution overnight for digestion. Subsequently, the SC was peeled off gently, immersed into 0.05 % trypsin inhibitor solution for 1 min, washed in water for min. 5 times, and placed onto aluminum foil wrapped glass slides (VWR International bvba, Leuven, Belgium) to dry for min. 3 days (Zhang and Lunter, 2018). CRS was then used to study the obtained SC thickness and lipid properties. Another study refers to the skin measurements by CRS when using emulsifiers or their mixtures as penetration enhancers. For this purpose, 1 mL of emulsifier solution with 1 % procaine was applied onto the skin for 24 h after the preparation of Franz diffusion cells. For profiling the drug penetration, the incubated skin sample was washed with 1 mL water for 4 times and removed from the donor compartment for direct CRS measurements.

2.4. Confocal Raman spectroscopy

We focus on finding the differences of different excitation wavelengths of CRS in analyzing skin samples. A comprehensive evaluation was completed by evaluating the SC and skin samples. To this end, an alpha 500 confocal Raman spectroscopy (WiTec GmbH, Ulm, Germany) equipped with a DV401-BV CCD camera was utilized. The 532 nm laser wavelength combined with UHTS 300 spectrometer as well as 785 nm excitation wavelength combined with UHTS 400 spectrometer were both used for measurements. The laser power was adjusted to 25 mW (532 nm) and 50 mW (785 nm) separately using the optical power meter (PM100D, Thorlabs GmbH, Dachau, Germany). The optical gratings were 1800 g/mm with the spectral center of 1300 cm^{-1} (532 nm) and 300 g/mm with the spectral center of 900 cm^{-1} (785 nm). The grating of 600 g/mm with the spectral center of 2074 cm^{-1} in use of 532 nm laser wavelength was also applied to compare the skin spectra when investigating the SC properties. However, in this regard, the grating of 900 g/mm for 785 nm laser wavelength was not considered here due to the limited range of wavenumber for spectral signal identifications. The CRS measurements were carried out using a $63\times/1.0\text{NA}$ water immersion objective (W Plan-Apochromat, Carl Zeiss, Jena, Germany) which was found to be the most suitable for accurate skin depth or skin depth profiling analyses (Liu and Lunter, 2021a).

2.5. Stratum corneum properties

SC properties including the normalized lipid content and SC thickness were analyzed with CRS to represent the variation of skin barrier function. For this purpose, the isolated SC was placed onto a substrate, covered with a coverslip, and put under the Raman microscope for further evaluation. The substrates investigated in this study include a glass substrate, quartz substrate (Neubert Glas, Geschwenda, Germany) and aluminum foil wrapped glass slide. It has been studied that the use of the 785 nm laser can induce a huge effect of photoluminescence hiding the spectral information of the sample (Tuschel, 2016). Thus, different types of substrates were considered to compare the suitability of different excitation wavelengths in SC analysis. Likewise, the application of a coverslip has also the potential in generating a slight photoluminescence effect, covering part of the surface skin spectrum. For this reason, glass coverslip and quartz coverslip were compared towards their performances in skin spectra collections.

To investigate SC properties, skin depth scanning was conducted to acquire the spectral signals. The scan area of 5×80 μm containing 2×80 pixels (x-z directions) was recorded with a step size of 1 μm. The integration time was 1 s per each spectral point. After the data acquisition, the area under the curve (AUC) of the keratin signal (amide-I, ν (C=O)-mode, $1630–1710 \text{ cm}^{-1}$) intensity was plotted against scan depth. According to previous explanations, SC thickness can be determined using the full width of half maximum (FWHM) of this curve plot with the CRS focusing point moving from above the SC surface to below the SC bottom layer. On the other hand, the relative SC lipid content can also be calculated by determining the peak originating from δ (CH_2, CH_3)-mode as the 'lipid signal' which has been proven to contain most of the lipid-related signals. Meanwhile, the keratin signal derived from the ν (C=O)-mode (amide-I) remains stable within one donor and thus, is used to normalize the 'lipid signal' for calculating the relative lipid content (Zhang and Lunter, 2018).

2.6. Skin penetration properties

Characterization of drug penetration in dermatomed skin was conducted by placing the skin in a custom-built device. A coverslip with the size of 25×25 mm was put onto the skin surface. The depth profiles were obtained by scanning the area of 5×120 μm containing 2×24 pixels (x-z directions) with the step size of 5 μm. The integration time was 1 s per point. After the data acquisition of the scan-image, the spectral lines were vertically extracted and the depth profiles of procaine penetration were plotted. In detail, the most prominent characteristic procaine signal has been found to be located at 1612 cm^{-1} (ν (NH) δ (C-C) mode). The AUC of this peak area was in the same way as lipid content analysis normalized by the AUC of the keratin signal. The skin surface was determined with the half intensity of keratin profile, meaning the laser focus was half inside the skin and half inside the coverslip. Starting from this point, the depth profiles of procaine penetration were achieved.

When calculating the normalized procaine signals, a slight overlapping of keratin peak and procaine peak can be noticed. The calculated ratio would not reach zero when the procaine was undetectable due to the residual keratin signal intensities. Thus, the baseline was determined by visualizing the disappearance of the procaine signal and obtaining the stable value of the calculated ratio. In this study, the AUC of the penetration profiles was calculated and compared by setting the baseline at 0.23 (a.u.) for further comparisons.

2.7. CMC determination

CMC was determined using a hydrophobic fluorescent dye of DPH. Plenty of experiments has demonstrated the increase of fluorescent intensity when micelles are formed and the DPH is entrapped the hydrophobic micelle core (Bae et al., 2015; Wasan et al., 2004). In specific, DPH dispersion of 2 mM in water was prepared after sonication. The supernatant was used to dilute the emulsifier samples in various concentrations inside brown EP tubes. Prepared samples were put into a dark chamber overnight at 32℃ for equilibration. Each sample of 200 μL was then pipetted into 96-well dark plate and measured with a fluorescence plate reader with an incubation temperature of 32℃. The wavelength of excitation and emission was 355 nm and 430 nm. The obtained fluorescent intensities were then plotted against emulsifier concentrations (log $_{conc.}$). The CMC of each emulsifier was then estimated from the point at which the fluorescent intensity rapidly increased. The point of intersection between two regression curves was interpreted as the CMC. For each type of emulsifier, more than three replicates were evaluated.

2.8. Statistics

Data were acquired from three replicates repeated for min. three times, generating repeated measurements of min. nine times. All skin samples used for comparison were from the same donor. In CRS analysis, all collected spectra were preprocessed with cosmic ray removal, smoothing, and background subtraction using WITec Project Software (WITec GmbH). Herein, Savitzky-Golay (SG) filter was applied with third polynomial order and nine smoothing points. The background was subtracted by the shape method with a size of 400. For reducing noise, principal component analysis (PCA) was performed using the Project Plus 5 software (WITec GmbH). The first three principal components were selected for reconstructing the spectrum. By calculating the area under the curve (AUC), the integrated area under a specified peak of the spectrum could be obtained using the trapezoidal method on WITec Project Software.

The graphs are shown with mean values $\pm$ standard deviations (mean $\pm$ SD). Significant differences were analyzed with one-way analysis of variance (ANOVA) followed by the Student-Newman-Keuls (SNK) test, which was employed by GraphPad Prism 8.0 (GraphPad Software Inc., La Jolla, CA, USA). Significance was marked with different number of asterisks: * $p < 0.05$, ** $p < 0.01$, *** $p < 0.001$.

3. Results and discussion

The results of CRS analyses consist of the SC lipid and thickness properties and the skin penetration performances which were meant to investigate different effects of PEGylated emulsifiers and their mixtures.

For this purpose, different CRS excitation wavelengths of 532 nm and 785 nm were utilized to perform the measurements. The obtained comparable results can be an excellent sign of their suitability in SC and skin analysis. Detailed observations including the appearance of the spectrum, the applicability in analyzing fluorescent skin samples, and the challenge of photoluminescence effects were also intended to be elucidated.

3.1. SC lipid properties

The SC lipid properties were separately measured with 532 nm and 785 nm excitation wavelengths to present the effects of different emulsifiers and mixtures on extracting skin lipids. Normalized lipid content was calculated by normalizing the 'lipid peak' with the keratin signal as above mentioned. The larger the obtained lipid content value is relevant to the lower degree of lipid extraction when exposed to emulsifier samples. Significant differences were achieved by comparing each emulsifier applied skin with water treated samples, which allows easy and intuitive comparison between the results acquired with two excitation wavelengths. Based on the results shown in Fig. 1, a significant decrease of C20 and S20, and relatively insignificant changes of O2 were in good agreement with our previous finding (Liu and Lunter, 2020a). The weak interaction of O2 and skin can be also verified with a lower number of PEG units (Lim et al., 2009). The primary focus was on the assessment of emulsifier mixtures. We observed significantly decreased lipid content from the results measured by different laser wavelengths, indicating impairments of the skin barrier remain. However, rather than worsening the influence of C20 on skin lipids, the addition of another type of emulsifier regardless of S20 or O2 tends to have fewer skin interactions. Despite insignificant differences comparing the mixtures with C20 alone treated skin samples, the tendency towards reduced lipid extraction was still clear especially from the results obtained by 785 nm excitation wavelength. Therefore, we conclude that the influence of emulsifier mixtures on the skin is not a simple summation of their individual influence. Summarizing the results achieved from different lasers, their comparisons were broadly in line with each other. Small differences noticed are concerning the data collection at randomly chosen sample sites which can cause small differences that may lead to one data set just reaching significance while another one just misses significance. Thus, the results validate the suitability of 532 nm and 785 nm laser wavelengths in SC lipid analysis.

3.2. SC thickness properties

SC thickness is another attractive reflection of skin barrier function. The reduction of SC thickness is associated with the extraction of skin components and the loosened packing of SC lipid structures according to previous studies. The obtained SC samples after exposure to emulsifiers and mixtures were simultaneously measured by CRS at different excitation wavelengths.

According to the result (Fig. 2), we saw a significant decrease in SC thickness in presence of C20, S20, and two mixtures, indicating their impairment on the skin barrier. Our primary focus was on the influences induced by the mixtures and C20, which were statistically compared in this study. Upon the results, we observed a significantly lower SC thickness reduction when exposing the skin to emulsifier mixtures compared with skin treated with C20. It tells us extra information that not only will the addition of S20 or O2 to C20 solution not increase the impairment of SC, but it will to some extent decrease the negative effects. This evaluation, on the one hand, validates the result we achieved from SC lipid analysis (Zhang and Lunter, 2018) and on the other hand, reminds us of using a mixed emulsifier system to prevent the skin from irritating emulsifiers. Gathering two groups of analyses through 532 nm and 785 nm laser wavelength, identical assessments were achieved from their statistical comparisons, demonstrating the suitability of their application in SC thickness analysis.

3.3. Skin penetration profiles

In addition to the assessment on SC samples, drug penetration through the skin was also evaluated with the emulsifiers or mixtures used as penetration enhancers to gain further insight into their effects on skin penetration performances. To this end, CRS was again applied to record the spectral information and plot the relative procaine signal profiles by depth. The capability of using CRS in evaluating the procaine penetration has been validated with the conventional high pressure liquid chromatography-ultraviolet spectroscopy (HPLC-UV) method (Lunter and Daniels, 2014). For better comparison, the profile obtained from skin exposed to procaine solution without emulsifiers was seen as a reference to evaluate the penetration enhancement effects. We first observed a significant increase of procaine penetration with the addition of C20 (Figs. 3 and 4). Following, the influences of S20 and O2 act on the procaine penetration relatively decreased compared with C20. The main concern goes to the changes of emulsifier mixtures on the penetration performances. Mix1 was observed to have a relatively lower effect on
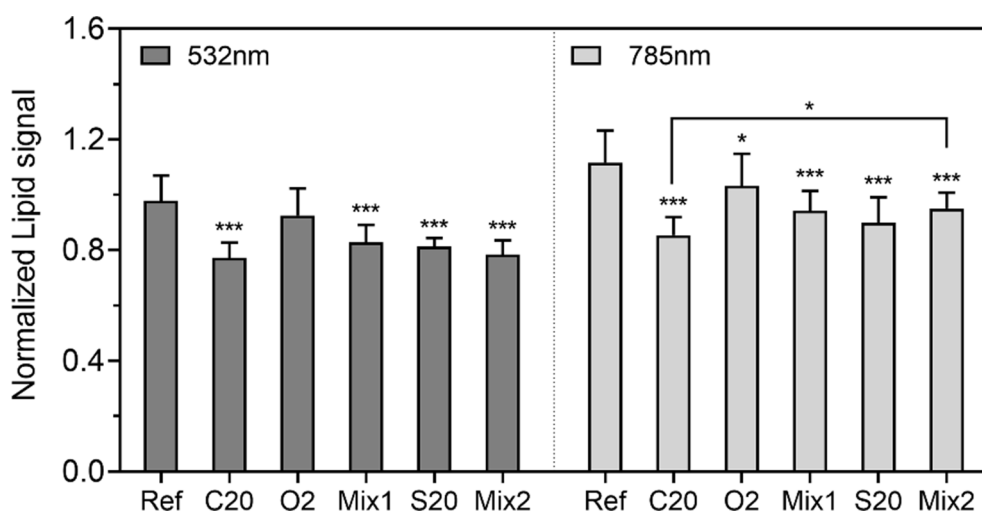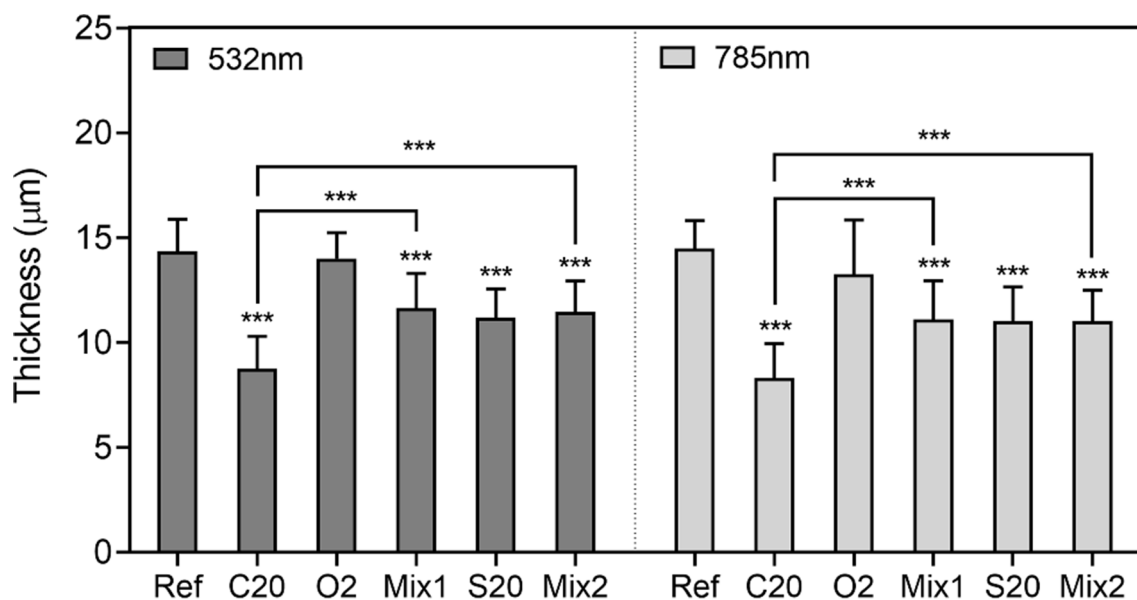

Fig. 1. Normalized lipid content of isolated SC measured with excitation wavelengths of 532 nm and 785 nm after the treatment of emulsifiers (C20, O2, and S20) and emulsifier mixtures (Mix1: C20 and O2; Mix2: C20 and S20); the result of each emulsifier treated skin sample was compared with reference for analyzing the significant differences; other statistic differences are also marked with asterisks. Mean ± SD, n ≥ 18, * p < 0.05, ** p < 0.01, *** p < 0.001.

Fig. 2. Thickness of isolated SC measured with excitation wavelengths of 532 nm and 785 nm after the treatment of emulsifiers (C20, O2, and S20) and emulsifier mixtures (Mix1: C20 and O2; Mix2: C20 and S20); the result of each emulsifier treated skin sample was compared with reference for analyzing the significant differences; other statistic differences are also marked with asterisks. Mean ± SD, n ≥ 18, * $p < 0.05$, ** $p < 0.01$, *** $p < 0.001$.
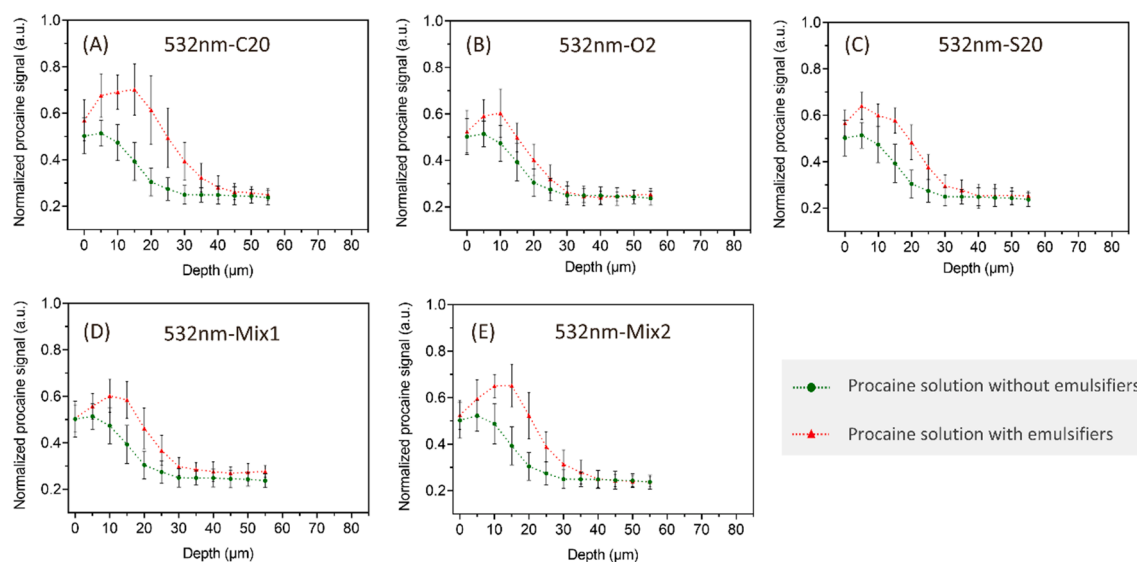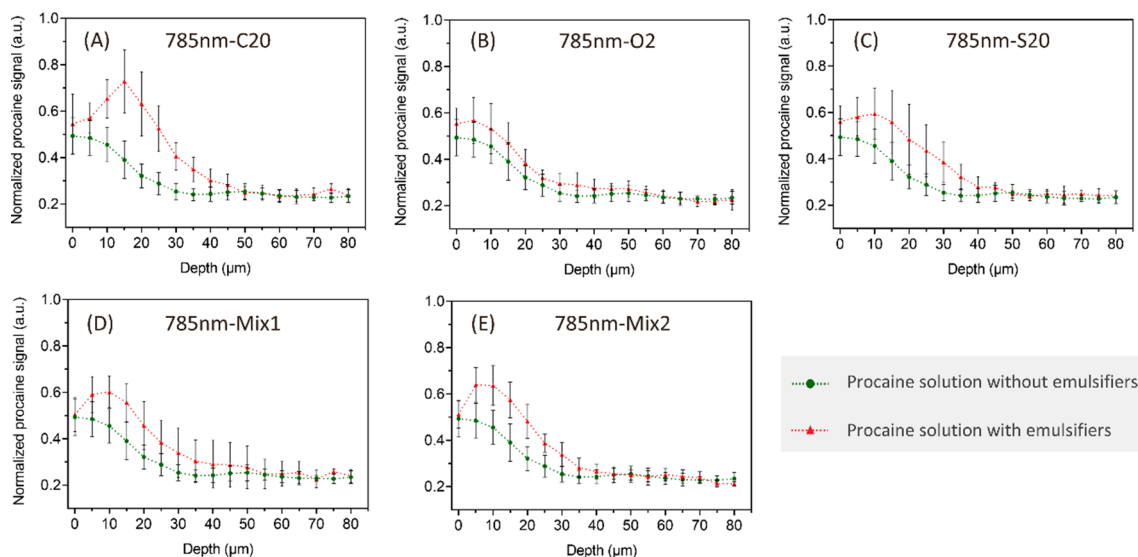

Fig. 3. Penetration profiles of procaine HCl in dermatomed porcine skin measured at 532 nm with the application of different emulsifier solutions including C20 (A), O2 (B), and S20 (C), and emulsifier mixtures of C20 with O2 (Mix1, D) and C20 with S20 (Mix2, E) in equimolar ratio. Penetration patterns were compared with (green circles) and without (red triangles) the addition of emulsifiers. Mean ± SD, n ≥ 9.

increasing the procaine penetration. Mix2 appeared to enhance the penetration to a greater extent. Nevertheless, their increases in penetration are still less than the enhanced penetration brought by C20. As the results mentioned above confirmed the reduced negative effects of emulsifier mixtures, we assume their decreased penetration enhancing ability is due to fewer interactions with skin components. Thus, we conclude that the addition of another type of emulsifier to C20 would not sum up their enhancement effects, but instead, decrease the penetration enhancing ability to some extent, which is in line with the reduced lipid extraction and SC thinning effects of the emulsifier mixtures compared to C20 solution. Similar correlations of using penetration enhancers for improved skin penetration with stronger lipid extractions can be another support for our finding here (Kumar et al., 2015).

Penetration profiles were achieved with both 532 nm and 785 nm

laser wavelengths (Figs. 3 and 4). We would like to highlight that profiles attributed from CRS configured with 785 nm laser wavelength were plotted against deeper skin depth up to 80 μm. Yet the profiles achieved at 532 nm laser wavelength showed a depth of only 55 μm. This difference is due to the stronger signal attenuation when using 532 nm laser wavelength which is unable to ensure the accuracy of collected information at skin depths deeper than 55 μm. The longer wavelength of 785 nm is capable of penetrating deeper into the skin samples, yet the characteristic peaks are not possible to be identified and also not reliable for data collection when the scan focus goes below around 80 μm. Detailed elucidation can be found in Section 3.7. Besides, we also observed the penetration properties achieved at 532 nm are in general accordance with the results obtained using 785 nm excitation wavelength. Small differences may be noticed due to the randomly selected detection on spots. Overall, the applicability and suitability of these two

Fig. 4. Penetration profiles of procaine HCl in dermatomed porcine skin measured at 785 nm with the application of different emulsifier solutions including C20 (A), O2 (B), and S20 (C), and emulsifier mixtures of C20 with O2 (Mix1, D) and C20 with S20 (Mix2, E) in equimolar ratio. Penetration patterns were compared with (green circles) and without (red triangles) the addition of emulsifiers. Mean ± SD, n ≥ 9.

excitation wavelengths applied on skin penetration analysis are confirmed.

### 3.4. Comparison of penetration performances

To gain further insight into the function of using emulsifiers and mixtures as penetration enhancers, an evaluation was made in terms of the statistical comparison of cumulative drug penetration, in which the penetration enhancing ability can be more easily addressed. We calculated the AUC of each penetration profile and made statistical comparisons (Fig. 5).

Significantly improved penetration was observed for all skin samples treated with emulsifier and emulsifier mixture solutions. The trend concerning their effectiveness used as penetration enhancers was in line with their effects on extracting SC lipids and reducing SC thickness.

Clear significant decreases were noted when comparing the effect of C20 with two mixtures on the content of procaine penetration. Identical results were achieved by CRS configured with both excitation wavelengths, indicating both potent configurations for analyzing skin penetration properties.

3.5. CMC of applied emulsifier samples

In existing studies, the interactions between emulsifiers in their mixtures were highly focused. Plenty of researchers set their sights on the reduced CMC values of emulsifier mixtures which were found to be well correlated with reduced irritant effects. (Hall-Manning et al., 1998; Zhou et al., 2016). Since we also stated above that mixtures of emulsifiers were capable of lowering their negative effects on SC properties, the CMC values of all investigated emulsifier samples were measured
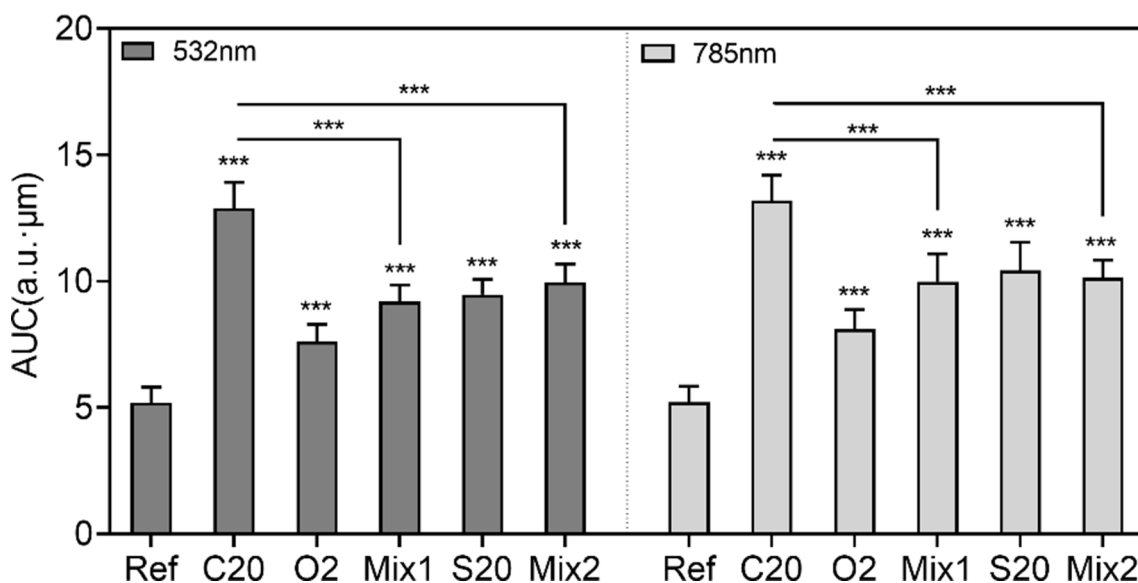
Fig. 5. Comparison of area under the curve (AUC) of different drug penetration profiles acquired at excitation wavelengths of 532 nm and 785 nm. The result of each emulsifier or emulsifier mixture treated skin sample was compared with reference to determine the significant differences for evaluating their penetration enhancement effects. Mixed emulsifier samples include mixtures of C20 with O2 (Mix1) and C20 with S20 (Mix2) in equimolar ratio. Mean ± SD, n ≥ 18, *** p < 0.001.

with fluorescence spectroscopy to figure out their roles in our study.

We see from Fig. 6 that C20 has the highest CMC value, while the CMC values of the two mixtures are in between the CMC values of single emulsifiers. Moreover, the decreasing order of the CMC values of the emulsifier samples was noticed to be consistent with the decreasing order of their impairment on skin. On the one hand, it indicates that the emulsifier with a lower CMC value (O2) may have fewer interactions with skin components. In this case, the monomers may play the main role in developing the skin barrier interruptions. The representative study by Morris found a correlation of greater skin penetration with higher monomer concentration when employing anionic emulsifiers with short exposure time (Morris et al., 2019). Some authors also claimed that the monomers can penetrate the skin barrier and interact with the skin components (Ananthapadmanabhan et al., 1996; Lu and Moore, 2012). Thus, the reduced CMC values of the emulsifier mixtures can decrease the concentration of emulsifier monomers, and then decrease the negative effects on SC. On the other hand, decreased CMC values of mixtures also mean decreased number of C20 monomers in mixtures, which decreases their intense interactions with SC lipids. Upon this finding, although the mechanisms behind their interactions with skin cannot be fully elucidated, this correlation can still give us ideas to use an emulsifier in a mixed state to reduce the impairment of the skin barrier.

3.6. Spectral comparison of SC samples

With the application of two excitation wavelengths in measuring SC samples, varying responses of Raman spectra are of importance to be compared. We plotted the AUC profiles of the keratin signal against SC depth as shown in Fig. 7. The orange and green lines represent curves acquired with 532 nm and 785 nm excitation wavelengths. The spot where laser focus placed at half the maximum of keratin profile was labeled as zero, representing the skin surface. The spectra extracted from the spot with the highest keratin signal intensity were also displayed. We noticed that the CRS spectra obtained at 532 nm excitation wavelength have a higher intensity than at 785 nm excitation wavelength. Normally, the higher the signal intensity the better the signal differentiation. It indicates that the 532 nm source laser records SC spectra with clearer signal information which is advantageous to differentiate signal variations. Besides, spectra obtained at 532 nm and 785 nm excitation wavelength showed different relative intensities of keratin signal which is due to the background removal of photoluminescence effect existed in measurements with 785 nm excitation wavelength. This signal decrease leads to slightly higher values of calculated relative lipid content, as can
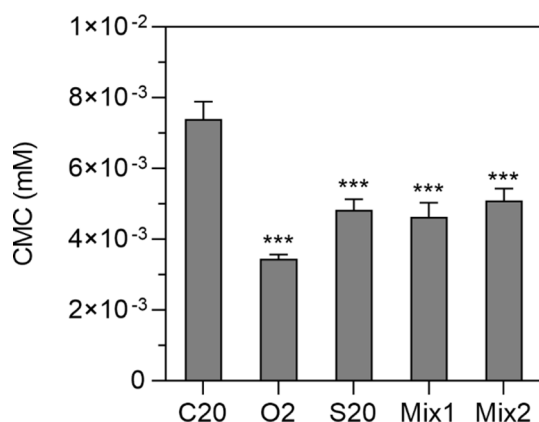

Fig. 6. Comparison of CMC values of investigated emulsifiers and their mixtures. Mixed emulsifier samples include mixtures of C20 with O2 (Mix1) and C20 with S20 (Mix2) in equimolar ratio. The CMC of each emulsifier or emulsifier mixture was compared with the CMC of C20 to determine significant differences. Mean $\pm$ SD, n $\geq$ 3, *** p < 0.001.

be noticed in Fig. 1.

3.7. Spectral comparison of skin samples

To investigate the spectral variations when measuring skin samples with different excitation wavelengths, Fig. 8 depicts the depth plots of keratin signal intensity at 532 nm (orange line) and 785 nm (green line) excitation wavelengths. The skin surface was determined with laser focus moving to the place where the keratin signal intensity firstly reached half maximum. With the laser beam focusing into the deeper layer of SC, the spectral intensity decreased due to signal attenuation. We noticed that the spectrum acquired with 532 nm excitation wavelength has a higher intensity than at 785 nm in the superficial layer of the skin and then reaches a similar intensity level in the deeper layer. We also extracted the spectra from the skin depth of 5 μm (point A), 30 μm (point B), and 70 μm (point C) at both wavelengths to gain more information. The spectral quality and SNR that ensure the data validity were compared. Based on the results, specific spectral signals of skin and procaine can be easily recognized at the depth of 5 μm and 30 μm of both lasers. However, when the laser beam moves to around 70 μm, the excitation wavelength of 532 nm was not able to provide a clear spectrum, thus not enabling the identification of characteristic peaks. On the other hand, using the 785 nm laser, clear spectra were observed from 70 μm depth. The spectral comparison at point C thus evidenced the advantage of using a 785 nm laser for measuring the deeper depth of skin samples.

3.8. Fluorescent skin samples

To investigate the proper laser wavelength in CRS analysis that could overcome the background fluorescence and is more advantageous to evaluate the skin properties, a piece of skin with inherent fluorescence effects was used. Results of SC and skin properties were summarized in Fig. 9. We observed that huge background fluorescence obscures the recorded skin spectrum at 532 nm excitation wavelength (Fig. 9A-B). The switch of different gratings and background subtractions cannot solve this difficulty. Instead, the spectrum obtained at 785 nm displayed a clear skin spectrum without fluorescent background (Fig. 9C). SC sample was also measured at both excitation wavelengths. The separated SC shows minimized fluorescent background at 532 nm laser wavelength (Fig. 9E). Even more intense signals can be recognized from Fig. 9F in the fingerprint region. However, their spectral quality is still worse than the spectrum obtained at 785 nm laser wavelength whose signal-to-noise ratio (SNR) has been obviously improved. Thus, we can sum up that 785 nm excitation wavelength is more appropriate to evaluate fluorescent skin samples.

3.9. Spectral photoluminescence

The photoluminescence effect is commonly found when using CRS configured with a 785 nm excitation wavelength. To perform CRS measurements, SC samples should be placed onto a slide as substrate and covered with a coverslip for the application of the water immersion objective. We summarized the SC spectra using different types of slides and coverslips measured at 785 nm excitation wavelength. We observed that when placing the SC on a glass slide, the spectrum acquired shows a strong and broad peak at around 1400 cm^{-1} covering fingerprint Raman scattering of skin sample (Fig. 10A). It was caused by the photoluminescence detected from the sample substrate when measuring thin and transparent SC samples. Instead, the spectrum obtained at 532 nm excitation wavelength showed no such effect (data not shown). To eliminate the photoluminescence effect, potential substrates such as the quartz slide and aluminum foil were considered whose performances have been confirmed in existing studies of physical and biological samples (Cui et al., 2016; Kerr et al., 2015). Thus, in SC spectra, weak photoluminescence was found at high wavenumber region using quartz
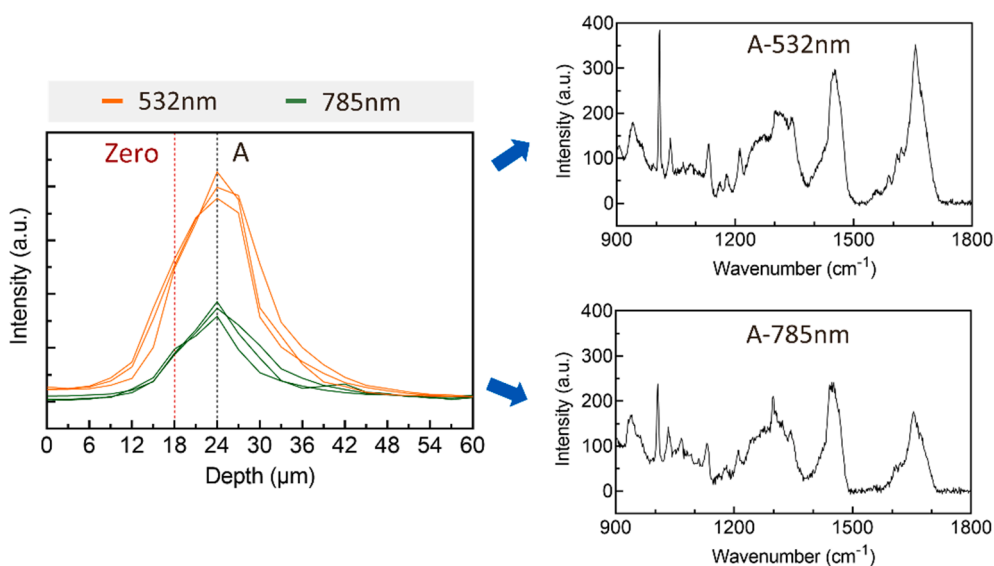
Fig. 7. Depth profiles of isolated SC showing the variation of amide-I signal intensity versus depth obtained at excitation wavelengths of 532 nm (orange line) and 785 nm (green line); two vertical dotted lines presented the skin surface (Zero) by determining the amide-I signal intensity reaches the half maximum for the first time and the highest intensity spot (Point A); two spectra showing at the right side were extracted from profiles at point A obtained from excitation wavelengths of 532 nm and 785 nm.
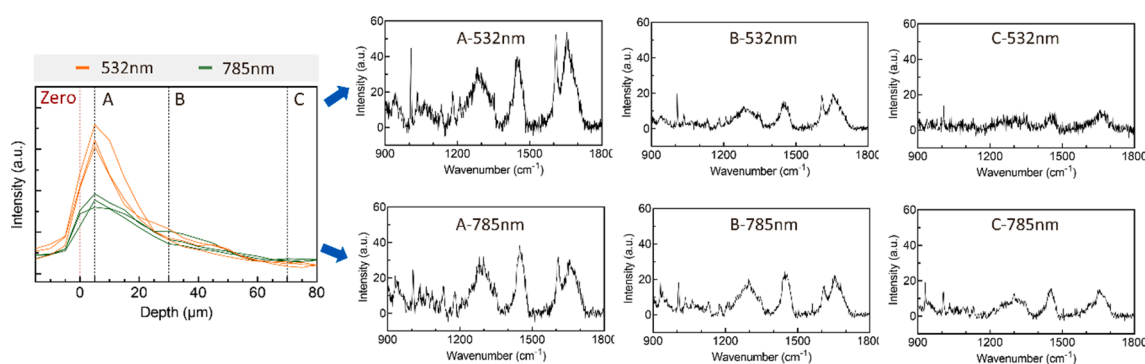
Fig. 8. The profiles of dermatomed skin samples showing the variation of amide-I signal intensity versus depth obtained at excitation wavelengths of 532 nm (orange line) and 785 nm (green line); two vertical dotted lines presented the skin surface (Zero), the skin depth of 5 μm with the highest intensity (Point A), the skin depths of 30 μm (Points B) and 70 μm (Point C); the spectra shown at the right side were extracted from profiles at point A, B and C obtained from excitation wavelengths of 532 nm and 785 nm.
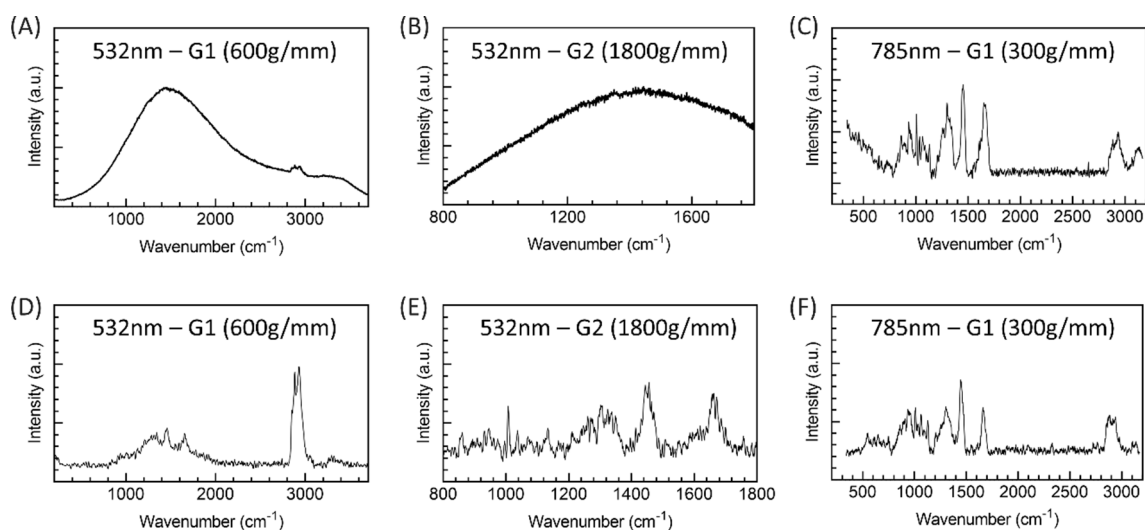
Fig. 9. Representative CRS spectra of dermatomed skin with inherent fluorescence effects and isolated SC; dermatomed skin spectra obtained at 532 nm with 600 g/mm grating (A), 532 nm with 1800 g/mm (B), and 785 nm with 300 g/mm (C); SC spectra obtained at 532 nm with 600 g/mm grating (D), 532 nm with 1800 g/mm (E) and 785 nm with 300 g/mm (F).
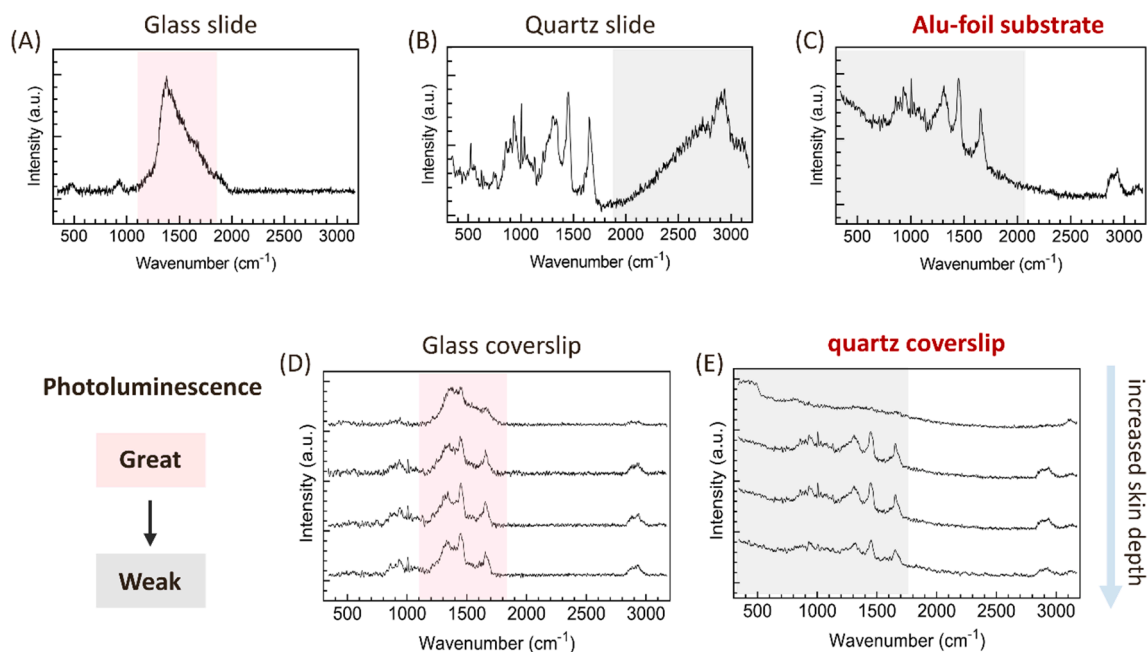
Fig. 10. Representative CRS spectra of isolated SC obtained at 785 nm with the use of different sample substrates including glass slide (A), quartz slide (B), and aluminum foil wrapped glass slide (C), and the application of glass coverslip (D) and quartz coverslip (E) when performing depth scanning analysis.

slide and at fingerprint region using aluminum foil-wrapped glass slide (Fig. 10B-C). Both of their applications overcome the challenge of the photoluminescence effect. Since weak and broad photoluminescence appeared in the fingerprint region can be easily removed after background subtraction, spectrum recorded when placing onto aluminum foil is also capable to analyze SC properties. Thus, considering the number of sample types and sites for repetition (more than 15 pieces of SC), the use of aluminum foil will be more cost-effective.

The depth spectra collected with glass and quartz coverslips were shown in Fig. 10D-E. We observed that the SC Raman scattering interfered with great photoluminescence when applying the glass coverslip. By putting a piece of quartz coverslip (25 × 25 mm) on top of the SC sample, the photoluminescent peak can be eliminated. In this case, the quartz coverslip can be reused for each SC sample in measurement which would be also cost-effective.

4. Conclusion

The effects of emulsifiers and their mixtures on SC properties and skin penetration performances have been investigated in this study. Reduced interactions of emulsifier mixtures with skin components were demonstrated from the results. The improvement of emulsifiers and mixtures acting on drug penetration showed also the same trend. Further, correlations of reduced CMC values of emulsifier mixtures with their relatively reduced SC impairment and skin penetration enhancing abilities were established. To sum up, higher CMC values of emulsifiers or their mixtures may trigger their interactions with skin components, then cause SC lipid extractions, thickness reduction, and enhanced drug penetration. It, thus, suggests monomers existing in emulsifier solutions as the main theory of skin penetration and SC lipids interruption. Although further studies need to be done to gain deeper insights into the interactions between emulsifiers and skin, this finding can still give specific advice in employing PEGylated emulsifiers in mixtures to build milder systems and is also useful as an analogy for other kinds of emulsifiers.

We also demonstrated the use of excitation wavelengths of 532 nm and 785 nm to be suitable in analyzing SC and skin sample properties in this study. Consistent results were obtained in comparing the effects of different emulsifier samples on skin. Thereinto, the limits of 785 nm

wavelength are lower spectral intensity and the interference of coverslips and substrates. The main benefits are the collection of information from deeper skin layers and the elimination of skin fluorescence effects that appear in some skin samples. In conclusion, there is no doubt that both 532 nm and 785 nm wavelengths can be used in skin studies. The preference should be determined based on experimental requirements.

CRediT authorship contribution statement

Yali Liu: Conceptualization, Methodology, Investigation, Data curation, Writing – original draft, Visualization, Funding acquisition. **Dominique Jasmin Lunter:** Conceptualization, Methodology, Resources, Writing – review & editing, Supervision, Project administration.

Declaration of Competing Interest

The authors declare that they have no known competing financial interests or personal relationships that could have appeared to influence the work reported in this paper.

References

Ali, S.M., Bonnier, F., Tfayli, A., Lambkin, H., Flynn, K., McDonagh, V., Healy, C., Clive Lee, T., Lyng, F.M., Byrne, H.J., 2012. Raman spectroscopic analysis of human skin tissue sections ex-vivo: evaluation of the effects of tissue processing and dewaxing. J. Biomed. Opt. 18, 061202 https://doi.org/10.1117/1.jbo.18.6.061202.

Ananthapadmanabhan, K.P., Yu, K.K., Meyers, C.L., Aronson, M.P., 1996. Binding of surfactants to stratum corneum. J. Cosmet. Sci. 47, 185–200.

Arora, A., Kisak, E., Karande, P., Newsam, J., Mitragotri, S., 2010. Multicomponent chemical enhancer formulations for transdermal drug delivery: More is not always better. J. Control. Release 144 (2), 175–180. https://doi.org/10.1016/j.jconrel.2010.02.015.

Azum, N., Rub, M.A., Asiri, A.M., 2014. Experimental and theoretical approach to mixed surfactant system of cationic gemini surfactant with nonionic surfactant in aqueous medium. J. Mol. Liq. 196, 14–20. https://doi.org/10.1016/j.molliq.2014.03.008.

Bae, J., Maurya, A., Shariat-Madar, Z., Murthy, S.N., Jo, S., 2015. Novel redox-responsive amphiphilic copolymer micelles for drug delivery: synthesis and characterization. AAPS J. 17 (6), 1357–1368. https://doi.org/10.1208/s12248-015-9800-2.

Ban, C., Jo, M., Park, Y.H., Kim, J.H., Han, J.Y., Lee, K.W., Kweon, D.-H., Choi, Y.J., 2020. Enhancing the oral bioavailability of curcumin using solid lipid nanoparticles. Food Chem. 302, 125328. https://doi.org/10.1016/j.foodchem.2019.125328.

Belsey, N.A., Garrett, N.L., Contreras-Rojas, L.R., Pickup-Gerlaugh, A.J., Price, G.J., Moger, J., Guy, R.H., 2014. Evaluation of drug delivery to intact and porated skin by coherent Raman scattering and fluorescence microscopes. J. Control. Release 174, 37–42. https://doi.org/10.1016/j.jconrel.2013.11.002.

Binder, L., Klang, V., Sheikh Rezaei, S., Neuer, O., Zhang, Z., Lunter, D.J., Wolzt, M., Valenta, C., 2019. Topical application of highly concentrated water-in-oil emulsions: physiological skin parameters and skin penetration in vivo - a pilot study. Int. J. Pharm. 571, 118694. https://doi.org/10.1016/j.ijpharm.2019.118694.

Blagojević, S.N., Blagojević, S.M., Pejić, N.D., 2016. Performance and efficiency of anionic dishwashing liquids with amphoteric and nonionic surfactants. J. Surfactants Deterg. 19 (2), 363–372. https://doi.org/10.1007/s11743-015-1784-5.

Chen, Y., Qiao, F., Fan, Y., Han, Y., Wang, Y., 2017. Interactions of cationic/anionic mixed surfactant aggregates with phospholipid vesicles and their skin penetration ability. Langmuir 33 (11), 2760–2769. https://doi.org/10.1021/acs.langmuir.6b04093.

Chiappisi, L., 2017. Polyoxyethylene alkyl ether carboxylic acids: an overview of a neglected class of surfactants with multiresponsive properties. Adv. Colloid Interface Sci. 250, 79–94. https://doi.org/10.1016/j.cis.2017.10.001.

Cui, L., Butler, H.J., Martin-Hirsch, P.L., Martin, F.L., 2016. Aluminium foil as a potential substrate for ATR-FTIR, transflection FTIR or Raman spectrochemical analysis of biological specimens. Anal. Methods 8 (3), 481–487.

Darvin, M.E., Fluhr, J.W., Caspers, P., van der Pool, A., Richter, H., Patzelt, A., Sterry, W., Lademann, J., 2009. In vivo distribution of carotenoids in different anatomical locations of human skin: comparative assessment with two different raman spectroscopy methods. Exp. Dermatol. 18, 1060–1063. https://doi.org/10.1111/j.1600-0625.2009.00946.x.

de la Maza, A., Parra, J.L., 1994. Solubilization of unilamellar phospholipid bilayers by nonionic surfactants. Colloid Polym. Sci. 272 (6), 721–730. https://doi.org/10.1007/BF00659286.

dos Santos, L., Tippavajhala, V.K., Mendes, T.O., da Silva, M.G.P., Fávero, P.P., Téllez Soto, C.A., Martin, A.A., 2019. Evaluation of penetration process into young and elderly skin using confocal Raman spectroscopy. Vib. Spectrosc. 100, 123–130. https://doi.org/10.1016/j.vibspec.2018.11.010.

Franzen, L., Windbergs, M., 2015. Applications of Raman spectroscopy in skin research — from skin physiology and diagnosis up to risk assessment and dermal drug delivery ✰. Adv. Drug Deliv. Rev. 89, 91–104. https://doi.org/10.1016/j.addr.2015.04.002.

Ghita, A., Matousek, P., Stone, N., 2016. Exploring the effect of laser excitation wavelength on signal recovery with deep tissue transmission Raman spectroscopy. Analyst 141 (20), 5738–5746.

Hall-Manning, T.J., Holland, G.H., Rennie, G., Revell, P., Hines, J., Barratt, M.D., Basketter, D.A., 1998. Skin irritation potential of mixed surfactant systems. Food Chem. Toxicol. 36 (3), 233–238. https://doi.org/10.1016/S0278-6915(97)00144-0.

Hara, R., Ishigaki, M., Kitahama, Y., Ozaki, Y., Genkawa, T., 2018. Excitation wavelength selection for quantitative analysis of carotenoids in tomatoes using Raman spectroscopy. Food Chem. 258, 308–313. https://doi.org/10.1016/j.foodchem.2018.03.089.

Harris, L.V., Hutchinson, I.B., Ingley, R., Marshall, C.P., Olcott Marshall, A., Edwards, H.G.M., 2015. Selection of portable spectrometers for planetary exploration: a comparison of 532 nm and 785 nm raman spectroscopy of reduced carbon in Archean cherts. Astrobiology 15, 420–429. https://doi.org/10.1089/ast.2014.1220.

James-Smith, M.A., Hellner, B., Annunziato, N., Mitragotri, S., 2011. Effect of surfactant mixtures on skin structure and barrier properties. Ann. Biomed. Eng. 39 (4), 1215–1223. https://doi.org/10.1007/s10439-010-0190-4.

Jiao, J., 2008. Polyoxyethylated nonionic surfactants and their applications in topical ocular drug delivery. Adv. Drug Deliv. Rev. 60 (15), 1663–1673. https://doi.org/10.1016/j.addr.2008.09.002.

Kerr, L.T., Byrne, H.J., Hennelly, B.M., 2015. Optimal choice of sample substrate and laser wavelength for Raman spectroscopic analysis of biological specimen. Anal. Methods 7 (12), 5041–5052.

Kumar, S., Zakrewsky, M., Chen, M., Menegatti, S., Muraski, J.A., Mitragotri, S., 2015. Peptides as skin penetration enhancers: mechanisms of action. J. Control. Release 199, 168–178. https://doi.org/10.1016/j.jconrel.2014.12.006.

Lee, C.H., Kawasaki, Y., Maibach, H.I., 1994. Effect of surfactant mixtures on irritant contact dermatitis potential in man: sodium lauroyl glutamate and sodium lauryl sulphate. Contact Dermatitis 30, 205–209. https://doi.org/10.1111/j.1600-0536.1994.tb00644.x.

Lim, H., Kassim, A., Huang, N., Ambar Yarmo, M., 2009. Palm-based nonionic surfactants as emulsifiers for high internal phase emulsions. J. Surfactants Deterg. 12 (4), 355–362. https://doi.org/10.1007/s11743-009-1138-2.

Liu, Y., Lunter, D.J., 2020a. Systematic investigation of the effect of non-ionic emulsifiers on skin by confocal Raman spectroscopy—a comprehensive lipid analysis. Pharmaceutics 12, 223. https://doi.org/10.3390/pharmaceutics12030223.

Liu, Y., Lunter, D.J., 2020b. Tracking heavy-water-incorporated confocal Raman spectroscopy for evaluating the effects of PEGylated emulsifiers on skin barrier. J. Biophotonics 13, 1–12. https://doi.org/10.1002/jbio.202000286.

Liu, Y., Lunter, D.J., 2021a. Optimal configuration of confocal Raman spectroscopy for precisely determining stratum corneum thickness: evaluation of the effects of polyoxyethylene stearyl ethers on skin. Int. J. Pharm. 597, 120308. https://doi.org/10.1016/j.ijpharm.2021.120308.

Liu, Y., Lunter, D.J., 2021b. Profiling skin penetration using PEGylated emulsifiers as penetration enhancers via confocal Raman spectroscopy and fluorescence spectroscopy. Eur. J. Pharm. Biopharm. 166, 1–9. https://doi.org/10.1016/j.ejpb.2021.04.027.

López-López, M., Vaz, J., García-Ruiz, C., 2015. Confocal Raman spectrocopy for the analysis of nail polish evidence. Talanta 138, 155–162. https://doi.org/10.1016/j.talanta.2015.02.031.

Lu, G., Moore, D.J., 2012. Study of surfactant-skin interactions by skin impedance measurements. Int. J. Cosmet. Sci. 34, 74–80. https://doi.org/10.1111/j.1468-2494.2011.00683.x.

Lunter, D.J., 2016. How confocal is confocal raman microspectroscopy on the skin? Impact of microscope configuration and sample preparation on penetration depth profiles. Skin Pharmacol. Physiol. 29, 92–101. https://doi.org/10.1159/000444806.

Lunter, D., Daniels, R., 2014. Confocal Raman microscopic investigation of the effectiveness of penetration enhancers for procaine delivery to the skin. J. Biomed. Opt. 19 (12), 126015. https://doi.org/10.1117/1.JBO.19.12.126015.

Mahrhauser, D.-S., Nagelreiter, C., Gehrig, S., Geyer, A., Ogris, M., Kwizda, K., Valenta, C., 2015. Assessment of Raman spectroscopy as a fast and non-invasive method for total stratum corneum thickness determination of pig skin. Int. J. Pharm. 495 (1), 482–484. https://doi.org/10.1016/j.ijpharm.2015.09.018.

Mélot, M., Pudney, P.D.A., Williamson, A.-M., Caspers, P.J., Van Der Pol, A., Puppels, G.J., 2009. Studying the effectiveness of penetration enhancers to deliver retinol through the stratum cornum by in vivo confocal Raman spectroscopy. J. Control. Release 138 (1), 32–39. https://doi.org/10.1016/j.jconrel.2009.04.023.

Morris, S.A.V., Ananthapadmanabhan, K.P., Kasting, G.B., 2019. Anionic surfactant-induced changes in skin permeability. J. Pharm. Sci. 108 (11), 3640–3648. https://doi.org/10.1016/j.xphs.2019.06.030.

Park, E.S., Chang, S.Y., Hahn, M., Chi, S.C., 2000. Enhancing effect of polyoxyethylene alkyl ethers on the skin permeation of ibuprofen. Int. J. Pharm. 209, 109–119. https://doi.org/10.1016/S0378-5173(00)00559-7.

Pudlas, M., Koch, S., Bolwien, C., Thude, S., Jenne, N., Hirth, T., Walles, H., Schenke-Layland, K., 2011. Raman spectroscopy: a noninvasive analysis tool for the discrimination of human skin cells. Tissue Eng. Part C Methods 17 (10), 1027–1040. https://doi.org/10.1089/ten.tec.2011.0082.

Seweryn, A., 2018. Interactions between surfactants and the skin – theory and practice. Adv. Colloid Interface Sci. 256, 242–255. https://doi.org/10.1016/j.cis.2018.04.002.

Shiloach, A., Blankschtein, D., 1998. Predicting micellar solution properties of binary surfactant mixtures. Langmuir 14 (7), 1618–1636. https://doi.org/10.1021/la971151r.

Tfaili, S., Josse, G., Gobinet, C., Angiboust, J.F., Manfait, M., Piot, O., 2012. Shedding light on the laser wavelength effect in Raman analysis of skin epidermises. Analyst 137, 4241–4246. https://doi.org/10.1039/c2an16115j.

Trebolazabala, J., Maguregui, M., Morillas, H., De Diego, A., Madariaga, J.M., 2013. Use of portable devices and confocal Raman spectrometers at different wavelength to obtain the spectral information of the main organic components in tomato (Solanum lycopersicum) fruits. Spectrochim. Acta - Part A Mol. Biomol. Spectrosc. 105, 391–399. https://doi.org/10.1016/j.saa.2012.12.047.

Tuschel, D., 2016. Selecting an excitation wavelength for raman spectroscopy. Spectroscopy 31, 14–23.

Vyumvuhore, R., Tfayli, A., Piot, O., Le Guillou, M., Guichard, N., Manfait, M., Baillet-Guffroy, A., 2014. Raman spectroscopy: in vivo quick response code of skin physiological status. J. Biomed. Opt. 19 (11), 111603. https://doi.org/10.1117/1.JBO.19.11.111603.

Wasan, K.M., Choo, E., Sivak, O., Wallis, S., Letchford, K., Burt, H.M., Stewart, D.J., Lukic, T., 2004. Determining the critical micelle concentration of a novel lipid-lowering agent, disodium ascorbyl phytostanyl phosphate (FM-VP4), using a fluorescence depolarization procedure. Drug Dev. Ind. Pharm. 30 (7), 725–730. https://doi.org/10.1081/DDC-120039509.

Zhang, Z., Lukic, M., Savic, S., Lunter, D.J., 2018. Reinforcement of barrier function – skin repair formulations to deliver physiological lipids into skin. Int. J. CosmReinforcement Barrier Funct. – Ski. Repair Formul. Deliv. Physiol. Lipids into Ski. Sci. 40 (5), 494–501. https://doi.org/10.1111/ics.12491.

Zhang, Z., Lunter, D.J., 2018. Confocal Raman microspectroscopy as an alternative method to investigate the extraction of lipids from stratum corneum by emulsifiers and formulations. Eur. J. Pharm. Biopharm. 127, 61–71. https://doi.org/10.1016/j.ejpb.2018.02.006.

Zhou, C., Wang, D., Cao, M., Chen, Y., Liu, Z., Wu, C., Xu, H., Wang, S., Wang, Y., 2016. Self-aggregation, antibacterial activity, and mildness of cyclodextrin/cationic trimeric surfactant complexes. ACS Appl. Mater. Interfaces 8 (45), 30811–30823. https://doi.org/10.1021/acsami.6b1166710.1021/acsami.6b11667.s001.